Contents of issue 5 vol. XLVII

Polish Academy of Sciences
Institute of Fundamental Technological Research

Archives of Mechanics

Archiwum Mechaniki Stosowanej

volume 47 issue 5

Polish Scientific Publishers PWN
Warszawa 1995

ARCHIVES OF MECHANICS IS DEVOTED TO
Theory of elasticity and plasticity • Theory of nonclassical continua • Physics of continuous media • Mechanics of discrete media • Nonlinear mechanics • Rheology • Fluid gas-mechanics • Rarefied gas • Thermodynamics

---

Printed in Poland, Editorial Office: Świętokrzyska 21,
00-049 Warszawa (Poland)

Arkuszy wydawniczych 13,75. Arkuszy drukarskich 11,75
Papier offset. kl. III 70 g. B1. Oddano do składania we wrześniu 1995 r.
Druk ukończono w listopadzie 1995 r.
Druk i oprawa: Drukarnia Braci Grodzickich, Żabieniec ul. Przelotowa 7

Arch. Mech., 47, 5, p. 827, Warszawa 1995

Preface

This issue of the Archives of Mechanics has been devoted to the international colloquium EUROMECH 326 organized in September 1994 in Kielce. The colloquium was named "Experimental and Macroscopic Theory in Crack Propagation". More than 40 prominent scientists from all over the world (representing 14 countries) have gathered together to discuss new ideas and trends in the field of dynamic fracture. Discussions were very stimulating since scientists taking part in the colloquium represented various overlapping fields: mechanics of solids, experimental mechanics, physics of solids and material science.

The rapid development of experimental and numerical techniques that took place recently provided new tools to deal with this very complex problem. New results obtained concerning the structure of the stress fields in front of a rapidly propagating crack tip and crack tip trajectories registered experimentally with a great accuracy forced researchers to reconsider their points of view on this phenomenon. Many new ideas were discussed during the colloquium.

The intention of the organizers was to present some of the results delivered during the conference to those who were not able to participate in this scientific event. This issue of the Archives of Mechanics contains only 11 of the presented lectures. It is very likely that up to six other papers will be published in the next issue. The remaining lectures were published in other journals before or after the colloquium.

The EUROMECH 326 has proved once more that this kind of scientific meeting is the best forum for exchange of the scientific ideas and research experiences.

A. Neimitz
(co-chairman)

Arch. Mech., 47, 5, pp. 829–844, Warszawa 1995

Dynamic crack instability: the "twin-crack" model

N.P. ANDRIANOPOULOS and S.K. KOURKOULIS (ATHENS)

A GEOMETRICAL interpretation of crack instability phenomena is described in the present work. This interpretation is based on the "twin-crack" model according to which random microbranching accompanying propagating crack-tips causes macroscopic instability, when two microbranches dominate over their companions. The future path of such dominating pairs is predicted by means of the T-criterion of fracture. It is shown that all the arbitrary geometrical configurations of pairs of microbranches can be classified to a few macroscopic patterns representing macroscopic branching, kinking, curving and arrest-deceleration, respectively.

1. Introduction

ONE OF THE MOST intriguing aspects of a propagating crack is its directional instability which appears as an either symmetric/asymmetric crack branching or as gradual/abrupt deviation of a single crack-tip from its straight path, under conditions not well-defined. Historically the first approach to this problem was developed by YOFFE [1] who assumed that a running crack splits into two branches, symmetrically placed on both sides of the initial straight path, when a proper mechanical quantity (hoop stress in that case) exhibits two extrema in its polar distribution instead of one. Consequently, the crack is forced to split in order to follow the directions of these extrema. If this is true, then each material must possess a certain crack velocity limit separating a low velocity area where only single crack-tips are allowed to run from a high velocity one where only branched cracks are observed. Such a sharp limit does not exist as it is experimentally concluded. On the contrary, branching is observed in a wide range of crack velocities starting at a lower limit of about $0.30c_2$, c_2 being the distortional stress wave velocity [2]. The same absence of a sharp velocity limit is also observed in case of a single deviating crack.

The same as the above Yoffe-like approach is accompanied by a more fundamental difficulty. Really, it is questionable how a material *suddenly* supplies at the moment of branching at least double amount of mechanical energy to support two running crack-tips instead of a single one. Such an energy-release discontinuity had to be accompanied by an equally sudden remote unloading at the moment of branching, which, however, has not been reported.

There are two alternatives to resolve the situation, i.e. either instability criteria (like the Yoffe one) are inappropriate or they are applied in a wrong way.

If the first alternative is true then how their success to predict crack initiation is explained? Are crack initiation, propagation and instability three completely different phenomena obeying equally different physical laws? If so, only casuistic interpretation of physical phenomena exists depending not only on the phenomenon itself but, perhaps, on the type of material and specimen geometry as well. Such a dark and disappointing situation must be rejected simply because it violates the ultimate goal of Science to interpret and predict the maximum possible number of physical phenomena with the minimum possible number of assumptions. Consequently, any failure of fracture criteria to predict crack instability cannot be directly connected exclusively to them, provided that these criteria explain to some degree relative phenomena and mainly they can be connected with fundamental physical laws. This connection is guaranteed when a criterion can be expressed in words beyond any algebraic equation. For example, an equation obtained through curve fitting procedures on a set of experimental data is not necessarily a criterion in the present sense, because a deterministic relation between cause and result cannot be always established.

The second alternative, i.e. wrong application of a "correct" criterion seems, then, more realistic. The main reason for a possibly wrong application is the unavoidable discrepancy between theoretical assumptions concerning constitutive behaviour and internal structure of materials on the one hand, and reality on the other. Although theoretical descriptions of the constitutive behaviour of materials can be considerably improved by eliminating mathematically friendly (but physically marginal) assumptions like linearity, small scale yielding, plane stress/strain etc., in expenses of simplicity, the same is not true in case of material texture. The exact distribution of random irregularities in the microstructure or inclusions of various mechanical properties, size and severity by no means can be predicted. Existing micro-structural models like arrays of equally spaced circular inclusions of the same radius or a single macroscopic inclusion embedded in a "perfect" canvas are too simple to be realistic. More sophisticated models do not exist or they are too complicated to be manipulated and, eventually, they do not contribute to a considerable improvement of predictions. It is a pity, because such models are intuitively attractive as far as they resemble the "crash" of a running crack on the wall formed by an obstacle and so they carry a physical content.

The conclusion is that a general fracture criterion based on Continuum Mechanics considerations is highly desirable as far as it can be sensitive to structural irregularities in a simple (not detailed) way. Aim of the present work is to describe such a combined model based on a Continuum Mechanics fracture criterion and elementary geometrical assumptions concerning the state of the material in the neighbourhood of a running crack-tip just before macroscopic instability occurs.

2. Theoretical preliminaries

2.1. The "twin-crack" model

It is now confirmed from many different experimental sources (e.g. [3–5]) that in materials where any type of macroscopic crack instability is eventually observed, the supposingly single crack-tip is replaced, even from the early steps of propagation, by a cloud or tuft of many microcracks of arbitrary lengths and orientations. These micro-cracks are created before any macroscopic instabilities are observed. The "shape" of the tuft (i.e. the number of microcracks and their lengths and orientations) reflects, obviously, the microstructural situation at the vicinity of the running crack tip.

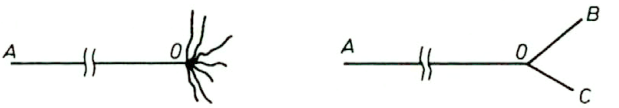

FIG. 1. The "twin-crack" model.

For the sake of simplicity it is assumed that all microcracks are straight lines emanating from the mathematical single crack tip, 0, running with velocity v (Fig. 1). Gradually, two microcracks dominate over their companions. At that time and on, the mathematical single crack-tip, 0, becomes stationary and the two "winners" run towards their initial direction with the velocity, v, of their mother-crack. The future of each one of the two dominant microcracks ($0B$) and ($0C$) is then predicted by applying any suitable fracture criterion as it will be described in the next section. This is the "twin-crack" model which was successfully applied to predict symmetric [4] or asymmetric [6] branching.

A first objection for this model might be connected with the assumption of two winning microcracks instead of one or three. One winner is the mother-crack itself and, so, no instability is expected in general. Three winners resulting in tri- instead of bi-furcation is an extremely rare phenomenon, observed almost exclusively in cases where a large hard inclusion with size comparable to the crack length is artificially implanted ahead of the running crack [7]. So, it is reasonable to work with two winning microcracks.

The question of energy-release discontinuity implied by the Yoffe-like approaches can also be resolved. Namely, according to the present model the apparent energy release is the sum of the respective quantities of the tuft of microcracks. Domination of two microcracks implies that the rest of the tuft dies and, so, small scale local energy transfer to two winners is adequate to support the initial stages of their propagation. Of course, each winning microcrack forms after a while its own tuft which may cause a second order instability, when conditions permit it, and so on. Such procedures do not require any sudden increase of energy-release.

Application of any fracture criterion necessitates exact geometry of the star-shaped configuration of Fig. 1, which cannot be *a priori* known. So, scanning of many arbitrary combinations of lengths and orientations of the winning pair of microcracks is required, to see whether or not these combinations can be classified into a few groups of macroscopic patterns corresponding to the observed types of crack instability.

2.2. The dynamic stress field in star-shaped cracks

The application of the above-described "twin-crack" model necessitates the knowledge of the dynamic stress field around the singular points A, B and C of Fig. 1. The values of the dynamic stress intensity factors (SIFs) K_{I}^{D} and K_{II}^{D}, are obtained, according to KOSTROV [8], as functions of their stationary values, K_{I}^{S} and K_{II}^{S}, and suitable correction factors taking into account dynamic effects:

$$\underset{\mathrm{II}}{K_{\mathrm{I}}^{D}} = \underset{\mathrm{II}}{K_{\mathrm{I}}^{S}} k(v). \tag{2.1}$$

The stationary values of SIFs at the three tips were computed separately adopting the method developed by THEOCARIS [9]. According to this procedure, the three branches of the complex crack configuration of Fig. 1 are considered as three independent cracks. Then applying the DATSHYSHIN–SAVRUK [10] method, the following three complex singular-integral equations are obtained:

$$\int_0^{\alpha_n} \frac{g_n'(t)}{t-s}dt + \sum_{\substack{k=A,B,C \\ k=n}} \int_0^{\alpha_k} \left[M_{nk}(t,s)g'(t) + L_{nk}(t,s)\overline{g_k'(t)}\right] dt = \pi(\sigma_{nk} - i\sigma_{tk}) \tag{2.2}$$

with $0 < s < \alpha_n$ and $n = A, B, C$. In this equation, α_k $(k = A, B, C)$ are respectively the lengths α, b, c of the cracks $0A$, $0B$, $0C$. For the kernels it holds:

$$\begin{aligned} M_{nk}(t,s) &= \overline{S_{nk}(t,s)} + S_{nk}(t,s)\exp[2i(\theta_k - \theta_n)], \\ L_{nk}(t,s) &= S_{nk}(t,s\left\{1 - \frac{S_{nk}(t,s)}{\overline{S_{nk}(t,s)}}\exp[2i(\theta_k - \theta_n)]\right\}, \end{aligned} \tag{2.3}$$

with

$$\begin{aligned} S_{nk} &= \frac{1}{2}\{t - s\exp[i - (\theta_k - \theta_n)]\}^{-1}, \\ \sigma_{nk} - i\sigma_{tk} &= -s[1 + \exp(2i\theta_k)]/2. \end{aligned} \tag{2.4}$$

Further, if the single-valuedness condition for the displacements around the composite crack is considered, the following equation is obtained:

$$\sum_{k=A,B,C} \left[\exp(i\theta_k)\int g_k'(t)\,dt\right] = 0. \tag{2.5}$$

The unknown functions $g'(t)$ are proportional to the density of the dislocations along the three branches. They are related to the complex SIFs, K_k ($k = A, B, C$), through the relations:

$$K_k = \sigma(2\pi\alpha_k)^{1/2} \lim_{s\to\alpha_k} \left[(\alpha_k - s)^{1/2}\overline{g}'_k(s)\right]. \tag{2.6}$$

Writing $\overline{g}'_k(s)$ as:

$$\overline{g}'_k(s) = (\alpha_k - s)^{1/2}[h_{k1}(s) + ih_{k2}(s)], \tag{2.7}$$

where the real, $h_{k1}(s)$ and the imaginary, $h_{k2}(s)$, parts of it have no singularities in $s = \alpha_k$, the complex SIFs are, finally, written as:

$$K_k = \sigma(2\pi\alpha_k)^{1/2}\,[h_{k1}(\alpha_k) - ih_{k2}K(\alpha_k)]\,, \qquad k = A, B, C. \tag{2.8}$$

The solution of the obtained complex singular integral system was achieved numerically by applying the Gauss-Legendre and Gauss-Lobatto integration rules. The Gauss-Lobatto rule was applied to the integral equation for the branch $0A$ with $N = 30$ points of integration, and the Gauss-Legendre rule to the integral equations of branches $0B$, $0C$ with the same number of integration points. Since the Gauss-Lobatto method has $(N-1)$ collocation points arising from the linear system of $6N$ real unknowns, two real equations are missing, which are supplied by the condition of single-valuedness of the displacements in complex form (Eq. (2.5)).

The main advantage of the procedure described above is that it permits the direct calculation of SIFs at the tips of the branches without any extrapolation. Also, the method is found to be very accurate and stable for extreme geometries (small angles φ_i ($i = B, C$) and strongly unequal lengths b and c), which are of special importance for the present study.

The values of the stationary SIFs, after being corrected through Eq. (2.1), are introduced into the dynamic stress field given by FREUND and CLIFTON [11].

2.3. The T-criterion of fracture

The stress field being known, a fracture criterion can be applied to predict the behaviour of each one of the three tips A, B and C. A suitable criterion was judged to be the T-criterion [12, 13] and this criterion was applied. It states that a crack starts to propagate when the maximum value, T_V^*, of the dilatational component of the elastic strain energy density takes a critical value, $T_{V,0}$, which is considered as a material constant, provided that the computation of the dilatational strain energy density is performed along the Mises elastic-plastic boundary, where the distortional part, T_D, of the strain energy density equals to another material constant, $T_{D,0}$.

For the plane stress conditions, assumed here, the T-criterion is expressed as follows:

$$T_D(r,\theta)\Big|_{r=r(\theta)} = \frac{(1+\nu)}{3E}(\sigma_{11}^2 + \sigma_{22}^2 - \sigma_{11}\sigma_{22}) = T_{D,0}\,, \tag{2.9}$$

$$\frac{\partial T_V(r(\theta),\theta)}{\partial\theta}\Big|_{\theta=\theta_0} = 0 \quad \text{and} \quad \frac{\partial^2 T_V(r(\theta),\theta)}{\partial\theta^2}\Big|_{\theta=\theta_0} < 0, \tag{2.10}$$

$$T_V^*(r(\theta_0),\theta_0)\Big|_{\theta=\theta_0} = \frac{(1-2\nu)}{6E}(\sigma_{11}+\sigma_{22})^2 = T_{V,0}\,. \tag{2.11}$$

The T-criterion was selected because its physical content is clear. Namely, its first statement (Eq. (2.9)) is the Mises yield condition connecting yielding with shear stresses and the second one (Eq. (2.11)) is a natural expansion of the Mises condition, connecting brittle fracture with normal stresses. Its strong physical basis allows for the T-criterion a wide range of successful applications from crack initiation in brittle or ductile materials [14] to crack nucleation in initially uncracked materials subjected to metal-forming processes [15] which lie outside Fracture Mechanics.

3. Application of the "twin-crack" model

The crack geometry according to the "twin-crack" model is shown in Fig. 2 where various geometrical quantities are indicated. In general, $\varphi_B \neq -\varphi_C$ and $b \neq c \ll a$. Referring to Fig. 2 we define $\theta_{p,i}$ $(i = B, C)$ as the angle of microbranch propagation measured with respect to its initial direction and $\theta_{b,i}$ $(i = B, C)$ as the respective quantity measured with respect to mother-crack axis. Elementary geometrical considerations show that

$$\theta_{b,i} = \varphi_i + \arcsin\left\{\sin\theta_{p,i}\left[\sqrt{1 - l_i^2\sin^2\theta_{p,i}} - l_i\cos\theta_{p,i}\right]\right\}, \tag{3.1}$$

with $l_i = \left\{\frac{b}{l}, \frac{c}{l}\right\}$, $i = B, C$. In Eq. (3.1) l is the distance from tip 0 to the point where angle measurements are performed. Usually, l is much larger than b and c, so that Eq. (3.1) reduces to:

$$\theta_{b,i} \cong \varphi_i + \theta_{p,i}\,, \qquad i = B, C \tag{3.2}$$

which overestimates $\theta_{b,i}$ by less than 2%.

For a given geometry $(\varphi_B, \varphi_C, b, c)$ and crack velocity v, at each one of the three tips A, B, C of Fig. 2 there exists a direction with maximum value of dilatational strain energy density $T_{V,i}^*$ $i = A, B, C$. In order for a certain crack-tip to

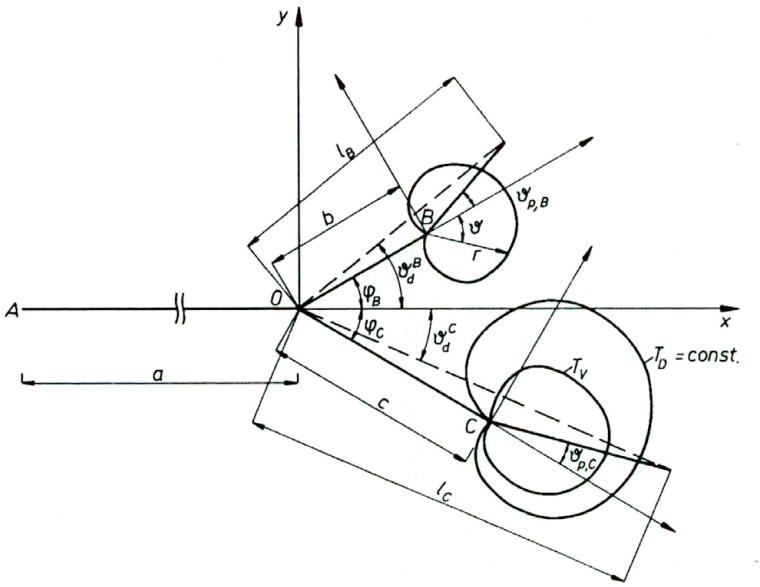

FIG. 2. The "twin-crack" model. Definition of various geometrical quantities.

propagate, the respective $T^*_{V,i}$ must be at least equal to a material property (say $T_{V,0}$) according to the T-criterion. In addition, double pattern (tip 0) is preferred in comparison to a single pattern (tip A) when the sum of maximum values of dilatational strain energy density at this tip is larger than the respective quantity at A. Consequently, the necessary condition for instability to occur are both:

$$\begin{cases} T^*_{V,i} > T_{V,0}\,, & \text{for at least one of the microbranches,} \\ T^*_{V,B} + T^*_{V,C} > T_{V,A}\,. \end{cases} \tag{3.3}$$

Obviously $T^*_{V,A} = T_{V,0}$ when the mother-crack is running with constant velocity.

Some examples will clarify the procedures required for the application of the present model. For that a family of winning microcracks with length-symmetry ($b = c$) and variable orientations ($\varphi_B \neq -\varphi_C$) and a second one preserving initial direction-symmetry ($\varphi_B = -\varphi_C$) and varying lengths ($b \neq c$) are selected. In Fig. 3a the ratio $T^*_{V,i}/T_{V,A}$ ($i = B, C$) is plotted versus φ_B for $\varphi_C = -5°$, $b = c = a/40$ and various velocities v. Any combination (φ_B, v) corresponding to $T^*_{V,i}/T^*_{V,A} > 1$ indicates a microcrack satisfying the first of conditions (3.3) and, consequently, able to propagate. In Fig. 3b the ratio $(T^*_{V,B} + T^*_{V,C})/T^*_{V,A}$ is also plotted for the same as in Fig. 3a combinations to check whether or not the second condition is satisfied. It must not be misinterpreted that in the present example all combinations satisfy the second condition. It is due to the assumption of equal velocity of mother-crack and winning microbranches. In Fig. 3c the

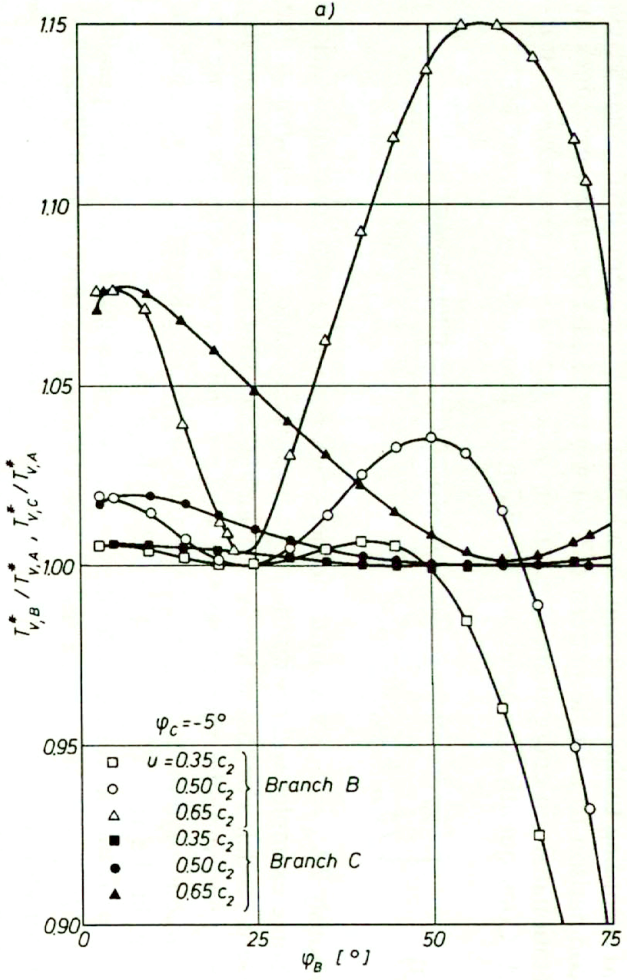

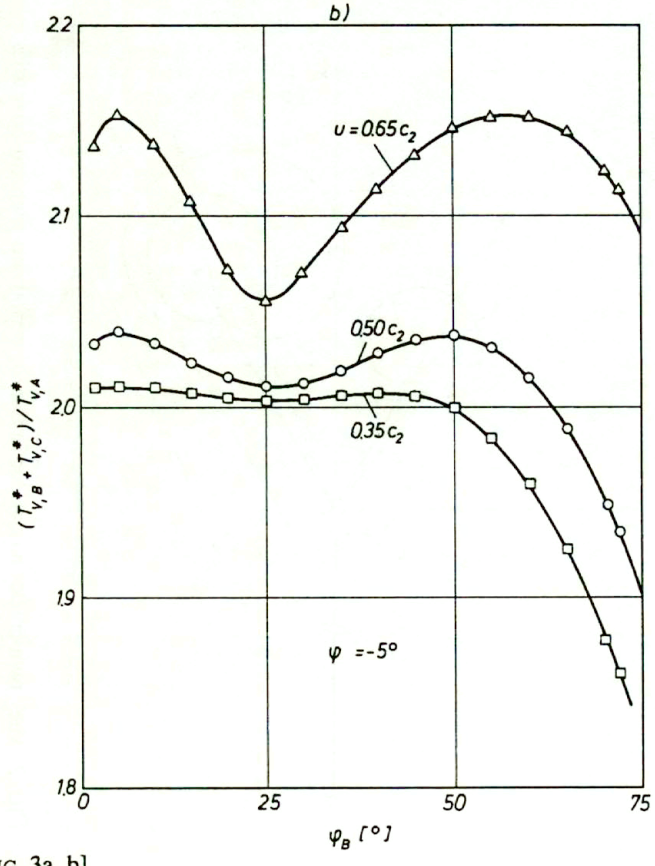

[FIG. 3a, b]

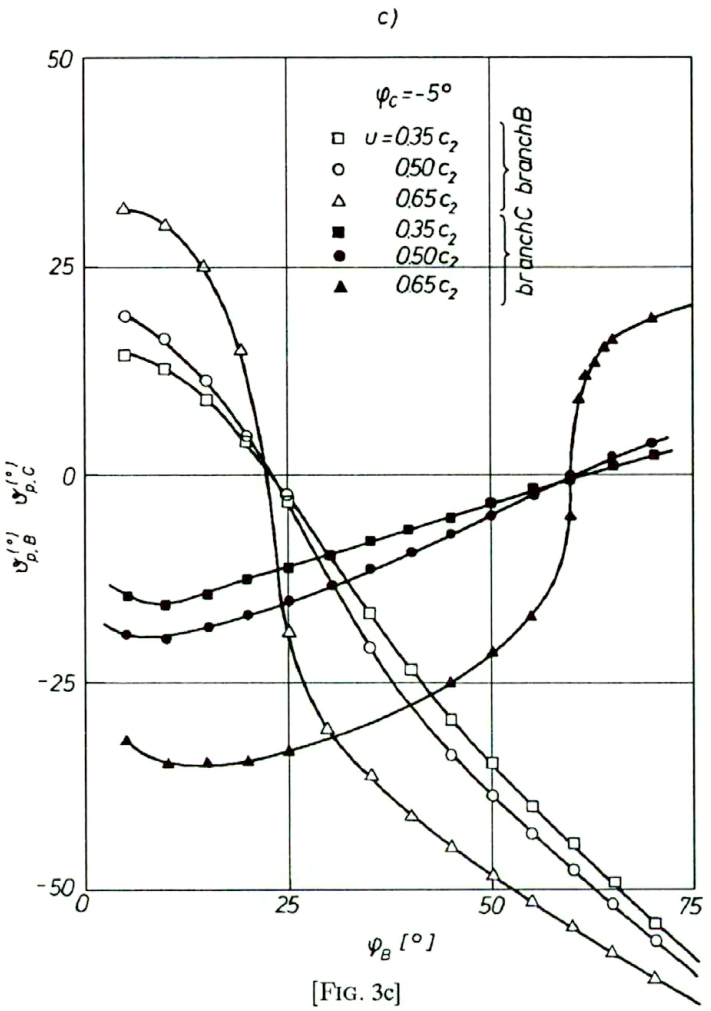

[FIG. 3c]

FIG. 3. a. Maximum values of dilatational strain energy density at branch tips B and C reduced to the corresponding quantity at tip A for $v = 0.35c_2$, $v = 0.50c_2$, $v = 0.65c_2$. b. Sum of the maximum values of dilatational strain energy densities at branch tips B and C reduced to the corresponding quantity at tip A for $v = 0.35c_2$, $v = 0.50c_2$, $v = 0.65c_2$. c. Propagation direction $\theta_{p,i}$ $(i = B, C)$ for the two microbranches $0B$ and $0C$ for $v = 0.35c_2$, $v = 0.50c_2$, $v = 0.65c_2$ and $\varphi_C = -5°$.

expected angles of branch propagation $\theta_{p,i}$ $(i = B, C)$ are plotted for the same combinations.

Similarly, in Figs. 4a, b the variation of $T^*_{V,i}/T^*_{V,A}$ for $i = B, C$, respectively, are plotted for the directionally symmetric microcracks. In this case, $\varphi = \varphi_B = -\varphi_C$, $r = c/b$ and $v = 0.5c_2$. Finally in Fig. 4c, the expected propagation angles $\theta_{p,B}$, $\theta_{p,C}$ are plotted versus φ $(= \varphi_b = -\varphi_C)$.

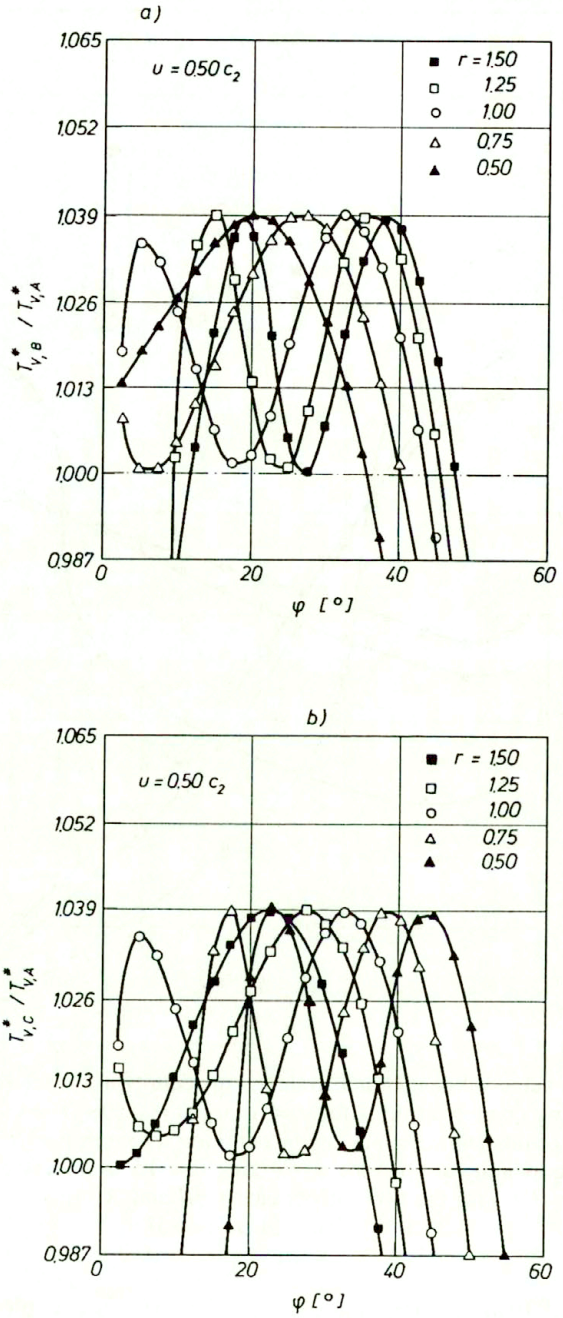

[FIG. 4a, b]

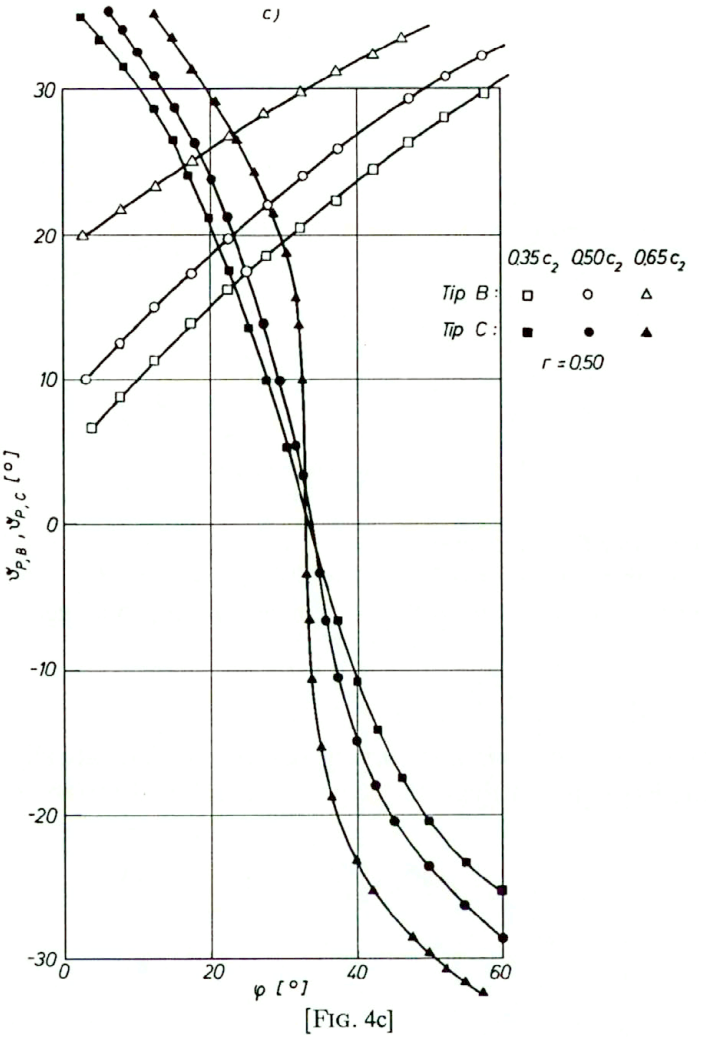

[FIG. 4c]

FIG. 4. a. The variation of $T^*_{V,B}$ vs angle φ for $v = 0.5c_2$ and various r-values. b. The variation of $T^*_{V,C}$ vs angle φ for $v = 0.5c_2$ and various r-values. c. The variation of angles $\theta_{p,B}$ and $\theta_{p,C}$ vs angle φ and for $v = 0.35c_2$, $v = 0.50c_2$, $v = 0.65c_2$.

3.1. Branching

A typical macroscopic branching pattern, shown in Fig. 5, can be obtained from many arbitrary microscopic combinations. For example, when $v = 0.5c_2$ and $\varphi_B = -\varphi_C = 5°$, from Fig. 3a it is obtained that both branches satisfy the first of conditions (3.3), as well as the second one as it can be seen in Fig. 3b. Then, the two microbranches are expected to run independently to directions $\theta_{p,B} = -\theta_{p,C} \cong 18°$, according to Fig. 3c. According to Eq. (3.2) this combination

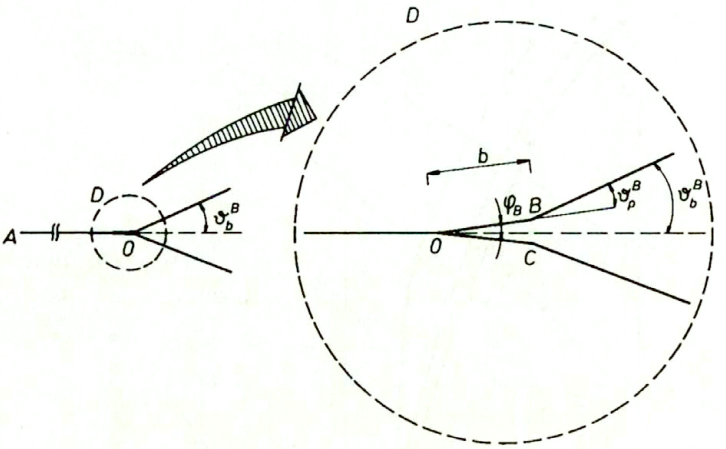

FIG. 5. A typical branching pattern.

corresponds to macroscopic branching angles $\theta_{b,B} = -\theta_{b,C} \cong 23°$. A similar combination is given by: $v = 0.5c_2$, $\varphi_B = 50°$, $\varphi_C = -5°$, $\theta_{p,B} \cong -38°$, $\theta_{p,C} \cong -5°$ resulting to $\theta_{b,B} \cong 12°$, $\theta_{b,C} \cong -10°$ corresponding to a slightly asymmetric branching.

3.2. Kinking-curving

A typical macroscopic kinking-curving pattern is schematically indicated in Fig. 6. Distinction between these two types of directional instability is based on

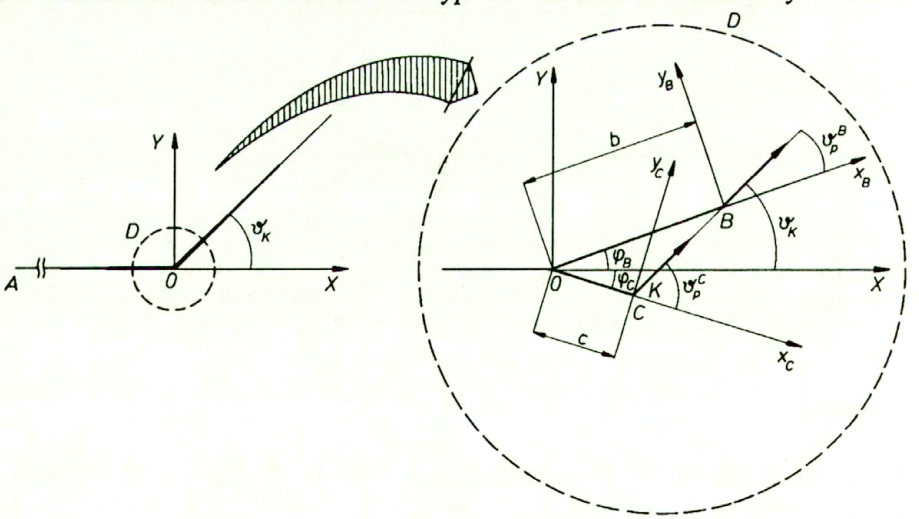

FIG. 6. A typical kinking-curving pattern.

the macroscopical *impression* given by the pattern. Big values of deviation – angles θ_k – correspond to kinking, while small ones to curving. Peculiarly enough, this

distinction is helped by the lack of intermediate values (say $15° < \theta_k < 30°$) of θ_k. However, numerical results obtained through the present model indicate that both instabilities require asymmetric geometry of microbranch and relatively high velocities ($v \geq 0.48c_2$).

An example: For $v = 0.5c_2$, $b = a/40$, $c = a/80$ (i.e. $r = 0.5$), $\varphi = \varphi_B = -\varphi_C = 7.5°$, it is concluded from Fig. 4a that $T^*_{V,B} > T^*_{V,A}$ $(= T_{V,0})$ and $T^*_{V,C} < T^*_{V,A}$ implying that only tip B is allowed to propagate in a direction $\theta_{p,B} \cong 34°$ according to Fig. 4c, which through Eq. (3.2) corresponds to a kinking angle $\theta_k = \varphi + \theta_{p,B} \cong 7.5° + 34° = 41.5°$.

3.3. Crack arrest-deceleration

Crack arrest-deceleration is macroscopically manifested when both microcracks run toward paths intersecting, after a while, the mother-crack path. Such a pattern is represented in Fig. 7. As it is shown, the "apparent" macroscopically observable crack-tip moves from point $0'$ to point $0''$, although the real path is $(B0'') \cong (C0'') > (0'0'')$. This elongation of the crack-path is macroscopically interpreted as reduction of the (single-tip) crack velocity. Elementary geometrical considerations in Fig. 7 show that:

$$v_{\text{arrest}}/v \cong \sin(90° + \varphi_B - \theta_{p,B}) \cong \sin(90° - \varphi_C + \theta_{p,C}) \tag{3.4}$$

indicating that the apparent crack velocity v_{arrest} may take low values or even be momentarily zero when $\varphi_B - \theta_{p,B} = -(\varphi_C - \theta_{p,C}) = -90°$.

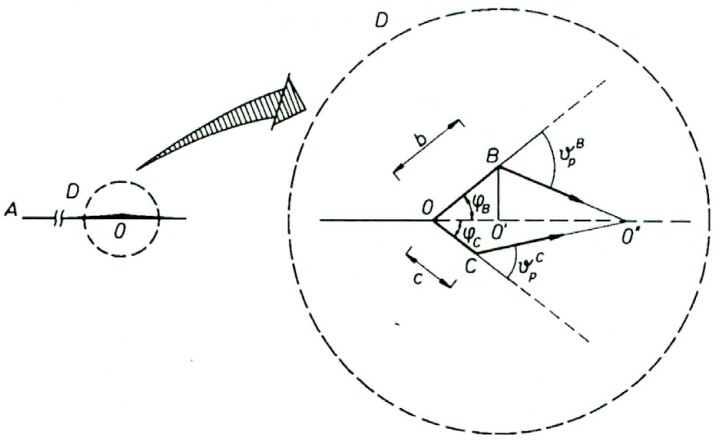

FIG. 7. A typical crack arrest-deceleration pattern.

However, such combinations are rare, appearing at high velocities and strongly asymmetric geometries of microcracks.

4. Results and conclusions

A detailed scanning of many arbitrary initial microbranch combinations belonging to either equal lengths and unequal angles or equal angles and unequal lengths, was performed to locate configurations corresponding to the above-mentioned crack instabilities. Examination of the fully asymmetric case with respect to both lengths and orientations of the winning pair is not yet completed. The results of scanning are gathered in Fig. 8. In this figure the half sum of branching angles $(|\theta_{b,B}| + |\theta_{b,C}|)/2$ in case of branching and kinking-curving angle θ_k in case of kinking-curving are plotted versus mother-crack velocity v reduced to shear waves velocity c_2. Typical branching angles form two rather narrow bands. The upper one corresponds to the first maximum of $T_{V,i}$ $(i = B, C)$ in Fig. 3a, and the lower one to the second maximum of the same quantity versus angle φ_B.

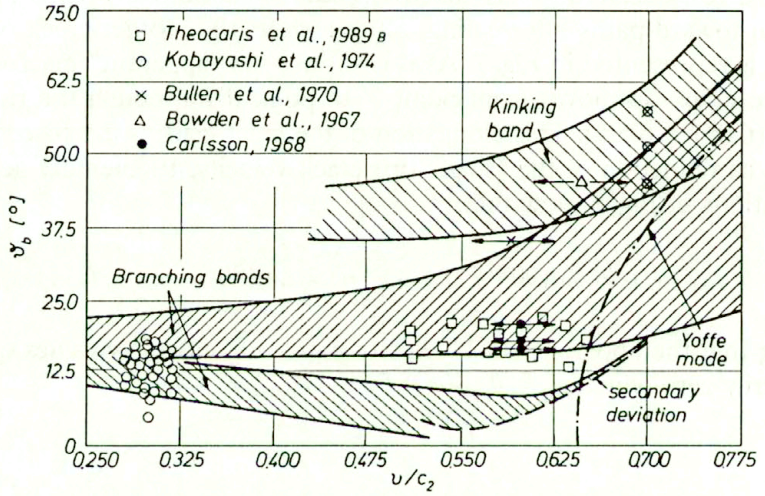

FIG. 8. Map of dynamic crack instability predictions.

Another band appears at the upper right corner, corresponding to kinking angles, while the dashed line at the lower right corner of the same figure represents smooth curving angles. In the same figure, predicted branching half-angles according to the T-criterion applied in the Yoffe-like way of a single tip are indicated for comparison purposes.

Experimental points gathered from various sources [2, 16-20] agree well with the predictions of the twin-crack model. It is also clear that the Yoffe-like application of the same criterion of fracture fails to give acceptable predictions, especially for branching under relatively low velocities, and it cannot give any prediction for kinking-curving.

It is then allowable to conclude that:

i. Crack-path instabilities occur when the "twin-crack" pattern offers more advantages over the "single-tip" pattern, in terms of strain energy release.

ii. In spite of the completely arbitrary initial "twin-crack" configurations, instability predictions in macroscopic terms (velocity, angle of instability) belong to rather narrow bands (or even single lines) for each type.

iii. The *a priori* unknown lengths and orientations of the two microbranches act as a stochastic (random) factor to the whole instability phenomenon. However, its effect is bounded by macroscopic (deterministic) factors like crack velocity, stress intensity etc.

iv. The double (stochastic – deterministic) character of crack instability does not allow for sharp velocity (or any other mechanical quantity) thresholds for instability to appear. In reality, the whole instability surface is an eight-dimensional function of the form:

$$f(\theta_B, \theta_C, b/a, c/a, \varphi_B, \varphi_C, v, \sigma_\infty) = \text{const.}$$

v. Experimental evidence shows clear preference to the "twin-crack" model. Yoffe-mode approaches lead to predictions far away from reality, especially for low velocities.

vi. The present model is a tool to obtain predictions. In that sense this is "true" but not necessarily "real", whatever "reality" means.

Acknowledgements

This work was partly presented in EUROMECH-326 colloquium on *"Experiment and Macroscopic Theory in Crack Propagation"*, held in Kielce, Poland in September 25-28, 1994.

References

1. E.H. YOFFE, *The moving Griffith crack*, Phil. Mag., **42**, 739–750, 1951.
2. A.S. KOBAYASHI, B.G. WADE, W.B. BRADLEY and S.T. CHIU, *Crack branching in homalite 100 sheets*, Engng. Fract. Mech., **6**, 81–82, 1974.
3. K. RAVI-CHANDAR and W.G. KNAUSS, *An experimental investigation into dynamic fracture: II. Microstructural aspects*, Int. J. Fracture, **26**, 65–80, 1984.
4. P.S. THEOCARIS, N.P. ANDRIANOPOULOS and S.K. KOURKOULIS, *Crack branching – A "twin-crack" model based on macroscopic energy fracture criteria*, Engng. Fract. Mech., **34**, 1097–1107, 1989.
5. P.S. THEOCARIS, *Blunting phenomena in cracked ductile plates under mixed mode conditions*, Engng. Fract. Mech., **31**, 255–270, 1988.
6. P.S. THEOCARIS, N.P. ANDRIANOPOULOS and S.K. KOURKOULIS, *The "twin-crack" model and the T-criterion in predicting dynamic instability for asymmetric cracks*, Engng. Fract. Mech., **43**, 137–146, 1992.
7. P.S. THEOCARIS and C.B. DEMAKOS, *Crack bifurcation modes in composite plates under impact*, Int. J. Fracture, **32**, 71–92, 1986.
8. B.V. KOSTROV, *On the crack propagation with variable velocity*, Int. J. Fracture, **11**, 47–56, 1975.
9. P.S. THEOCARIS, *Asymmetric branching of cracks*, J. Appl. Mech., **44**, 611–618, 1977.
10. A.P. DATSYSHIN and M.P. SAVRUK, *A system of arbitrarily oriented cracks in elastic solids*, J. Appl. Math. Mech. (PMM), **37**, 306–313, 1973.

11. L.B. FREUND and R.J. CLIFTON, *On the uniqueness of plane elastodynamic solutions for running cracks*, J. Elasticity, **4**, 293–299, 1974.
12. P.S. THEOCARIS and N.P. ANDRIANOPOULOS, *The T-criterion applied to ductile fracture*, Int. J. Fracture, **20**, R125–R130, 1982.
13. N.P. ANDRIANOPOULOS and P.S. THEOCARIS, *The Griffith–Orowan fracture theory revisited: The T-criterion*, Int. J. Mech. Sci. **19**, 793–801, 1985.
14. N.P. ANDRIANOPOULOS and P.S. THEOCARIS, *LEFM brittle and ductile fracture as described by the T-criterion*, Engng. Fract. Mech., **30**, 5–12, 1988.
15. N.P. ANDRIANOPOULOS, *Metalforming limit diagrams according to the T-criterion*, J. Mat. Processing Technology, **39**, 213–226, 1993.
16. P.S. THEOCARIS, N.P. ANDRIANOPOULOS and S.K. KOURKOULIS, *Brittle curving and branching under high dynamic loading*, Int. J. Press. Vess. & Piping, **46**, 149–166, 1991.
17. F.P. BOWDEN, J.H. BRUNTON, J.E. FIELD and A.P. HEYES, *Controlled fracture of brittle solids and interruption of electric current*, Nature, **216**, 38–42, 1967.
18. F.P. BULLEN, F. HENDERSON and L. WAIN, *Crack branching in heavily drawn chromium*, Phil. Mag., **21**, 689–699, 1970.
19. A.J. CARLSSON, *On the mechanism of brittle fracture propagation*, Trans. Royal Inst. Technol., Stockholm, **205**, 1–39, 1963.
20. P.S. THEOCARIS, *Secondary afterfailure fractures due to transversely reflected waves*, Engng. Fract. Mech., **15**, 283–290, 1981.

NATIONAL TECHNICAL UNIVERSITY OF ATHENS
DEPARTMENT OF ENGINEERING SCIENCE, ATHENS, GREECE.

Received September 16, 1994.

Arch. Mech., 47, 5, pp. 845–857, Warszawa 1995

Theoretical analysis of the cutting method for the measurement of crack bridging tractions

H. BASOALTO, F. GUIU and R.N. STEVENS (LONDON)

THIS PAPER is concerned with the determination of the bridging stress field that arises from the existence of bridging ligaments on the crack faces. The method presented here is based on a cutting procedure, in which the displacements at the edge or mouth of the crack are maintained constant by reduction of the external load as the bridging ligaments are progressively removed. It provides a means of calculating the entire closure force due to bridging. The closure force was assumed to be composed of a discrete distribution of tractions, so that we are not forced to solve an integral equation in the displacements. The ratio $R(x)$ of the bridging load, P_2, removed by making a cut from x to $x + \Delta x$ and the change in the external load required to keep the crack mouth displacements constant, is found as a function of x. The $R(x)$ was calculated using weight functions. From this, the bridging stress intensity factor can be determined for each removed traction so that the total K can be obtained by summation of individual values of K. However, the calculations can be greatly simplified if the assumption of straight crack faces is made, which allows the equality of the stress intensity factors of two non-identical stress systems to be assumed.

Notations

A	measured crack length,
a	normalised crack length ($= A/W$),
$K(a)$	stress intensity factor,
$f(a)$	normalised stress intensity factor ($= K(a)/(\sigma\sqrt{\pi A})$),
$m(x, a)$	weight function,
$R^w(x)$	load ratio obtained by weight functions,
$R^s(x)$	load ratio obtained by straight crack approximation,
$t^{(1)}(x)$	externally applied tractions,
$t^{(2)}(x)$	bridging stress field acting on crack faces,
$U_i(x, a)$	crack displacement field ,
$u_i(x, a)$	normalised crack displacement field corresponding to the i-th stress system ($= U_i(x, a)/W$)),
X	measured position from the crack mouth,
x	normalised distance from the crack mouth (X/W),
W	relevant linear dimensions of body (e.g., width in the case of a compact tension specimen).

1. Introduction

THE PROBLEM of crack bridging deals with material systems in which there exist ligaments that bridge the crack faces, thereby opposing the opening effect that an external load has on the crack displacements. The nature of this closure force depends on the microstructure of the material in question. For the case of lead

particles dispersed in a glass matrix, it is intact individual particles intersected by the crack that provide a negative pressure [2], while in matrix-fiber composites it is unbroken fibers bridging the crack that give rise to such a force [18]. Non-transforming ceramics such as alumina have been found to be bridged by unbroken grains under static and cyclic loading conditions, as well as topological mismatch between the crack faces [10, 23, 25]. The effect of these bridging ligaments is to shield the crack tip from the influence of an external load. In other words, they result in a net stress intensity factor at the tip less than that obtaining were the crack to be totally free of bridging ligaments. Bridging ligaments are therefore a significant source of toughness to such materials and it is of great importance to be able to understand the mechanism of bridging.

In order to calculate the contribution of the bridging ligaments to the net stress intensity factor, one must know exactly how the bridging tractions are distributed along the crack, since the bridging stress intensity factor, $K_b(a)$, is determined by [5]

$$K_b = \sqrt{W} \int_{x_0}^{a} t(x) m(x, a)\, dx, \tag{1.1}$$

where $t(x)$ is the distribution of stress provided by the ligaments, $m(x, a)$ is the weight function, x_0 is the end of the bridging zone, and W is the width of the body if it is finite. Upper case letters are used herein to designate quantities (such as crack length A) with physical dimensions, and lower case letters for the corresponding normalised quantity, e.g., $x = X/W$, $a = A/W$. However, the problem is not so clear-cut, since physically the traction acting upon the crack faces is some general function of the displacements, $U(x, a)$. This means that the functional dependence of the closure force on position, x, along the crack is a result of the functional composite $t[U(x)]$. The total crack opening displacement field is given by

$$U(x, a) = U_e(x, a) - \frac{\sqrt{W}}{E'} \int_{a_0}^{a} \int_{x_0}^{s} t[U(\xi)] m(\xi, s) m(x, s)\, d\xi ds, \tag{1.2}$$

where $U_e(x, a)$ is the crack displacement due to the external load and E' is Young's modulus, E for plain stress and $E/(1-\nu^2)$ for plain strain. Equation (1.2) is a nonlinear integral equation of the second kind and has received considerable attention with the aim of finding solutions appropriate for the problem of bridging [1, 6, 7]. In order to use Eq. (1.2) and determine $K_b(a)$, the $t[U]$ relationship must be known. A number of empirical expressions have been used for the $t[U]$ relationship [8, 17, 21]. Most of these give $t[U]$ increasing rapidly with U to a maximum, then declining more slowly to zero at a characteristic displacement.

This paper is concerned with a theoretical analysis of an experimental technique for the determination of the bridging traction and the bridging stress intensity factor. The experiments consist of making a series of cuts into the crack from the mouth to progressively remove bridging tractions by cutting ligaments. This causes the crack mouth displacements to increase. The decrease in external load required to return the crack mouth displacement to its original value is then measured, and the analysis relates this change in load to the traction removed by cutting. The crack length is divided into segments of length Δx (equal to the depth of a single cut) and the traction on each segment is regarded as being constant. Essentially this constant traction in the model is the average traction exerted on the segment of the real crack.

Theoretical analysis of the cutting procedure is nothing new and much of the literature on the subject derives from the general framework laid down by HU and WITTMANN [13]. To simplify the theory, the assumption of linear crack faces is usually made. This assumption does not allow the closure force to alter the shape of the crack in any way, so that the crack displacement fields can be approximated by parabolas [21]. Use of a straight crack approximation leads to workable analytical solutions which are much easier to use than the integral equation [16]. For example, Reichl and Steinbrech used the straight crack assumption to calculate the average load of the bridging ligaments in alumina under static loading from which the $K_b(a)$ is obtained [19]. A similar approach has been used by LI and GUIU [15] on alumina under cyclic conditions.

The question "how good is the straight crack approximation?" is clearly very important. To investigate the validity of the straight crack approximation, a relationship $R(x)$ between the change in the external load and the removed bridging traction is obtained under the assumption and compared to that determined by weight functions.

2. General formalism

Consider an elastic body containing an edge crack and subject to an externally applied traction, $t^{(1)}$, and some distribution of closure tractions, $t^{(2)}$, on the crack faces. The closure force is assumed to be a discrete distribution of tractions of the form

$$t^{(2)}(x) = \sum_{i=1}^{N} T_i H(x - \eta_i), \qquad x_0 \leq x \leq a,$$

$$\Delta x \ll 1.0, \qquad T_i = P_i/\Delta X, \qquad H(x - \eta_i) = \begin{cases} 1 & \eta_i \leq x \leq \eta_i + \Delta x, \\ 0 & \text{otherwise}, \end{cases} \tag{2.1}$$

where P_i is a force per unit length of constant magnitude over the interval $\eta_i \leq x \leq \eta_i + \Delta x$. The problem is, given information about the external stress system,

how does one proceed to calculate K_b? The total crack opening displacement field is given by superposition as

$$U_0(x,a) = u_0(x,a)W,$$

$$u_0(x,a) = u_{e1}(x,a) - \frac{1}{E'}\int_{a_0}^{a}\int_{x_0}^{s} t^{(2)}(\xi)m(\xi,s)m(x,s)\,d\xi ds\,, \tag{2.2}$$

where $u_{e1}(x,a)$ is the normalised displacements produced by the external load. Substitution of $t^{(2)}$ into Eqs. (2.2) gives

$$u_0(x,a) = u_{e1}(x,a) - \frac{1}{E'}\sum_{i=1}^{N} T_i \int_{a_0}^{a}\int_{\xi_i}^{\xi_i+\Delta x} H(\xi-\eta_i)m(\xi,s)m(x,s)\,d\xi ds\,.$$

Note that the position variable x is fixed and corresponds to that point where the displacements are experimentally measured. Suppose that a *perfect* cut is made into the crack removing the traction T_1 furthest from the crack tip, while keeping the external load fixed. The net displacement at the mouth will increase as a result giving a new measurable value $u_1(x,a) > u_0(x,a)$. At this point it is assumed that simultaneously with the removal of the traction by cutting, the load is reduced so as to maintain the displacement at some chosen point (e.g., the crack mouth) constant. Therefore, the displacement $u_1(x,a)$ must be decreased by relaxing the magnitude of the external load until the original value, $u_0(x,a)$, at the chosen point is achieved,

$$u_0(x,a) = u_{e2}(x,a) - \frac{1}{E'}\sum_{i=2}^{N} T_i \int_{a_0}^{a}\int_{\xi_i}^{\xi_i+\Delta x} H(\xi-\eta_i)m(\xi,s)m(x,s)\,d\xi ds\,.$$

It follows immediately that the displacement of the chosen point caused by the removed traction must equal that brought about by the change in the external load, i.e.,

$$\Delta u_e(x,a) = u_{e2}(x,a) - u_{e1}(x,a) = \frac{P_1}{E'}\int_{a_0}^{a} m(\xi,s)m(x,s)\,ds. \tag{2.3}$$

The change in displacement at the crack mouth due to the decrease in load ΔP_e is given by

$$\Delta u_e(0,a) = \frac{\Delta P_e}{E'} = \int_0^a f_e(s)m(0,s)\,ds\,, \tag{2.4}$$

where K is written in terms of the normalised stress intensity factor, $f_e(a)$, as

$$K(a) = \Delta P_e f_e(a)\sqrt{\pi a W}\,.$$

Hence, we find the ratio $R(x)$ of the change in the external load required to maintain constant crack mouth displacement and the bridging traction removed by the cutting, to be

$$R^w(\xi) = \frac{\Delta P_e}{P_i} = \frac{\int_{a_0}^{a} m(\xi, s)m(x, s)\, ds}{\int_{0}^{a} f_e(s)m(x, s)\, ds}. \tag{2.5}$$

To evaluate the displacements, the weight function for a given body geometry must be known, and for details of finding such functions refer to GLINKA and SHEN [9], FETT *et al.* [12], WU and CARLSSON [27]. Thus, for the case when $\Delta x \ll 1.0$ equation (2.5) is independent of the traction size resulting in a unique $R^w(\xi)$ for a given elastic body. If ΔP_e is known then the magnitude of the bridging traction can be calculated, and from this the corresponding contribution to the stress intensity factor is obtained. ΔP_e is the change in the external load required to maintain the same crack mouth displacement as the removed traction and is therefore referred to as the *equivalent load* [11]. Thus, for a fully bridged crack, repeating the cutting procedure until it is totally traction free allows the distribution of tractions to be found and the shielding stress intensity factor to be calculated by summation of the individual values of K.

3. Straight crack approximation

From the last section the determination of the closure force requires knowledge of the weight function for a given body geometry. However, this can be avoided if the non-physical assumption of linear crack faces is made. Such an approximation has been made by many workers in the past [13, 14, 21, 24] in order to simplify the calculation of the closure force. Suppose that the displacements produced by the equivalent load and the bridging force are made equal as in the last section; this will in effect be the same as equating moments since the axis of rotation of the body will now coincide with the crack tip. Let the moment due to the equivalent load be $M^{(1)}$. The moment of the bridging traction about the tip is

$$M^{(2)} = \int_{x_1}^{x_2} t^{(2)}(x)(a - s)\, dx; \tag{3.1}$$

then, equating displacements requires that

$$M^{(1)} = \int_{x_1}^{x_2} t^{(2)}(x)(a - s)\, dx. \tag{3.2}$$

Take the case when the external load is a point force and extrapolate its point of application to the crack surfaces, a non-physical approximation carried for the compact tension specimen, see [14, 20]. Equation (3.2) gives

$$\Delta P_e = \int_{x_1}^{x_2} t^{(2)}(x)(1 - x/a)\,dx\,. \tag{3.3}$$

Suppose that $t^{(2)}(x) = P_2\delta(x - \xi)$, where $\delta(x - \xi)$ is the Dirac delta function and represents a unit point force at $x = \xi$; then,

$$\begin{aligned} P_e &= P_2 R^s(\xi), \\ R^s(\xi) &= (1 - \xi/a), \end{aligned} \tag{3.4}$$

which gives a linear relationship between the equivalent load and load P_2. Note that $R^s(\xi)$ contains no terms that are dependent in any way on the external boundaries of the body and therefore applies to all geometries, in contrast with the load ratio obtained via weight functions. If $t^{(2)}(x)$ is taken as a traction of length Δx, we have a ratio $R'^s(\xi)$ related to that of equation (10) as

$$R'^s(\xi) = R^s(\xi) - \Delta x^2/2a\,, \tag{3.5}$$

and this reduces to $R'^s(\xi) = R^s(\xi)$ for $\Delta x \ll 1.0$, which was the same result found in the last section when using weight functions. Thus, the assumption of straight crack faces leads to a simple approximate relation for determining the closure force, a result that is independent of the body geometry.

However, the assumption of zero crack curvature has much deeper implications than just allowing the equality of displacement fields as a whole of two non-identical stress systems. Enforcing such a condition results in the equality of stress intensity factors for the two loading systems under question, which under normal circumstances can not be done. To show that the stress intensity factors for the two loading systems under question, we must look at the asymptotic behaviour of the displacements in the vicinity of the crack tip. In real elastic bodies, were the assumption of linear crack faces does not hold, the displacements near the tip are

$$\lim_{x \to a}(a - x)^{-1/2}U^* = \frac{2\sqrt{2}}{E'}K(a), \tag{3.6}$$

and the crack displacement field has the form

$$U(x, a) = U^* g(x, a), \tag{3.7}$$

where $g(x, a)$ is a function describing the shape of the crack faces away from the tip and is such that it is unity at $x = a$. If the crack faces are assumed to

be straight, then the singular behaviour of Eq. (3.6) will not be appropriate and instead one must use

$$\lim_{x \to a} (a - x)^{-1} U^* = \frac{2\sqrt{2}}{E'} K(a); \tag{3.8}$$

the displacement field will require that $g(x, a)$ be unity for all x. Thus, if two stress systems produce the same displacement field, then according to equation (3.8) their stress intensity factors must also be the same. The consequence of this with regard to bridging is that the shielding stress intensity factor can be calculated without having to know anything of the way the crack is bridged. All that is needed is to be able to measure the equivalent load and compute the associated stress intensity factor using well-known empirical formulas, and according to the straight crack approximation, this leads to the bridging stress intensity factor.

4. Application

The above analysis can be used to calculate the magnitude of the bridging tractions once the relationship between the change in the applied load and the removed traction, i.e. the loading ratio is known. The change in the applied load (or equivalent load ΔP_e) is obtained experimentally by the methods described in [14, 15]. In Sec. 5, we present the loading ratio graphically for the compact tension specimen with different crack lengths. Thus, for a given crack length, equivalent load and location where the cut has been made, the value of the loading ratio is read from the graph, and the magnitude of the removed traction is obtained by the simple relation

$$T_i = \frac{\Delta P_e}{\Delta X B} \frac{1}{R(\xi_i)}, \tag{4.1}$$

where T_i is the traction at location ξ_i along the crack length, ΔX is the cut length and B the specimen width.

5. Results and discussion

It is important to know how accurate the straight crack approximation is in calculating the closure force. This has been done by calculating both the $R^w(\xi)$ and $R^s(\xi)$ for the compact tension specimen and comparing the two results. The specimen geometry with the appropriate loading configuration is shown in Fig. 1. The weight function for this geometry was calculated using the formalism of WU and CARLSSON [27], where the reference load was taken as a uniform crack face pressure. The weight function was then used to calculate the displacements at the loading line ($x = 0$) produced by the external pin load and a closure traction. In practise the cutting experiments are performed by equating displacements at

the back of the specimen, behind the loading line at $x = -0.25$. However, to calculate the $R(\xi)$ at the back requires expressions for the displacements there, and it is not possible to use the weight functions to do so as they are defined for the interval between the loading line and the crack tip.

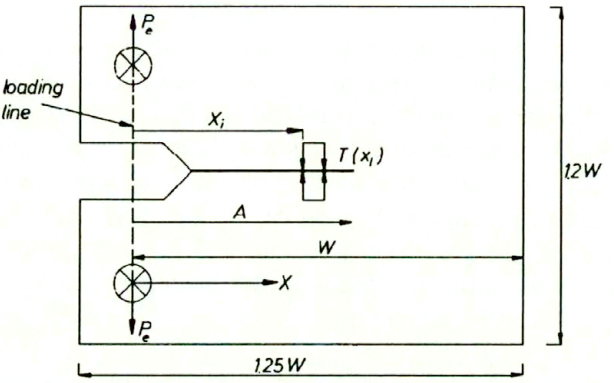

FIG. 1.

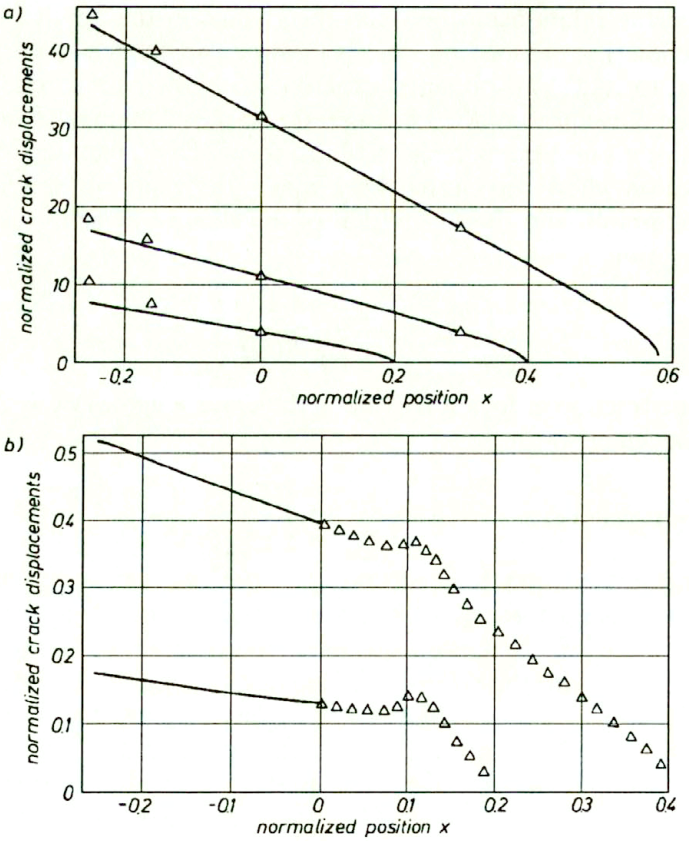

FIG. 2.

To overcome this difficulty, an approximation has to be made. It was assumed that the displacements at the back of the specimen can be obtained by linear extrapolation. The crack displacements were calculated at two points, namely at $x = 0$ and 0.03, through which a line passed and was extrapolated to the back of the specimen. The assumption was tested by comparing the displacements produced by the pins with the empirical results of SAXENA and HUDAK [22]. Figure 2a shows the result and it is observed that such an approximation is a justifiable one for this case. For the traction, linear extrapolation can still be used with the condition that they are not too close to the loading line, see Fig. 2b. In practice there will be no bridging tractions in the near vicinity of loading line because of the presence of a notch.

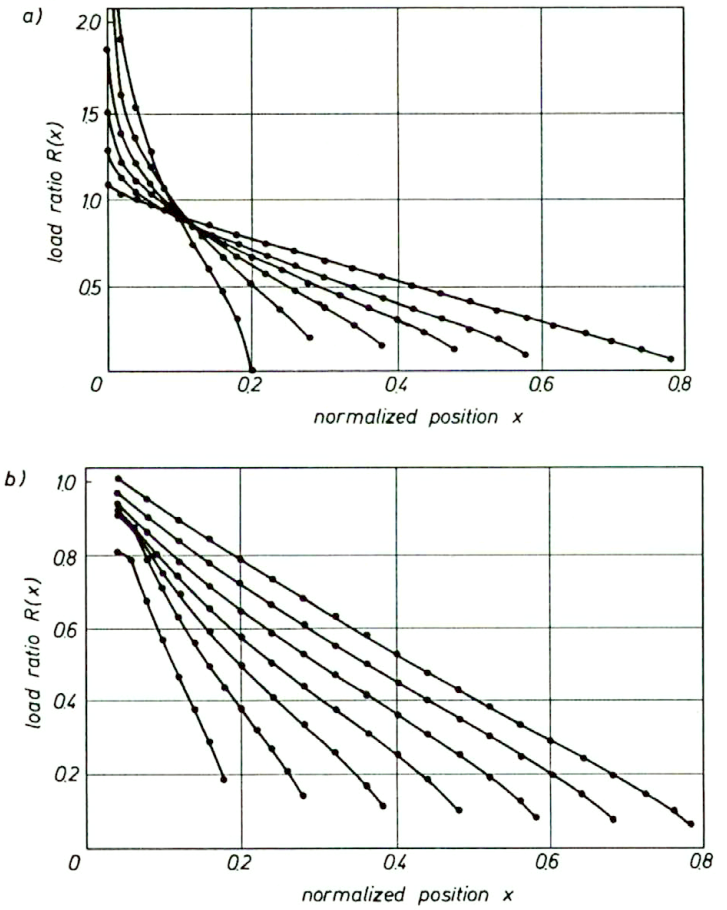

FIG. 3.

The $R(\xi)$ for the compact tension specimen was evaluated by equating displacements at the loading line and at the back of the specimen; the results are shown in Fig. 3. In both cases it is observed that the load ratio is a monotonically

decreasing function, having a maximum value at the loading line and falling off to zero at the crack tip. If $R^w(\xi)$ is viewed as a normalised displacement produced by a point force, then the measured displacements will be greatest when the traction is applied directly on the loading line and continuously decrease as it is made to approach the crack tip, and becomes less effective in opening the crack at the point of measurement. The crack displacement field of a traction at different locations along the crack length maintaining a constant displacement at the loading line is shown in Fig. 4. It is observed that displacement field for a short crack is highly distorted, especially when the traction is close to the tip, whereas for the large crack the displacements are approximately linear. Therefore, one would expect the errors in determining the closure force to be greatest when dealing with short cracks.

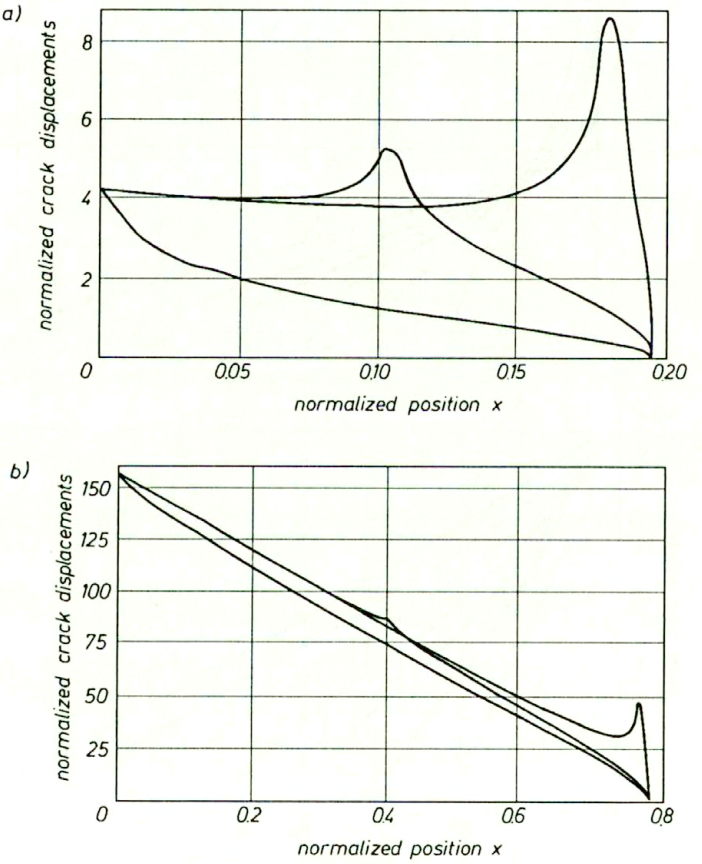

FIG. 4.

In Figs. 5 and 6 the relative error $E(x)$ beetween $R^w(\xi)$ and $R^s(\xi)$ is given. For a given crack length the error made in the magnitude of the bridging force is seen to increase, the closer it is to the crack tip. Large errors are made if

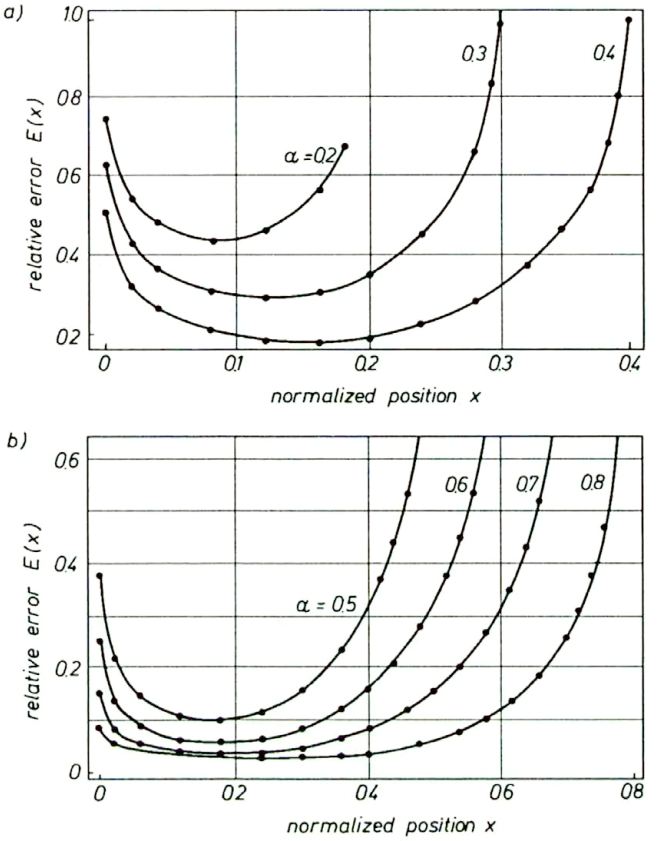

FIG. 5.

the displacements are equated at the loading line, requiring normalised crack lengths $a \geq 0.5$ to produce an error $E(x) < 10\%$ with the tractions not too close to the crack tip and on the interval I, $09 \leq x/a \leq 0.75$. Thus, in this case if the approximation of linear crack faces is to be assumed, then the minimum normalised crack length that can be used to measure $t^{(2)}(x)$ is 0.5. However, in practise it is not possible to use such large cracks to measure experimentally the closure force. Equating displacements at the back of the specimen results in decreasing the minimum crack length required to give an error $E(x) < 10\%$ from $a \geq 0.5$ to $a \geq 0.3$, for tractions lying in the interval I and not too close to the tip.

From the results the straight crack approximation does provide a good means of computing the magnitude of the bridging tractions, as long as they are not too close to the crack tip. However, in real materials the greatest contribution to the closure force, and therefore to the $K_b(a)$, comes precisely from those ligaments near the tip. Thus, the shield stress intensity factor obtained by the straight crack method may differ considerably from its actual value.

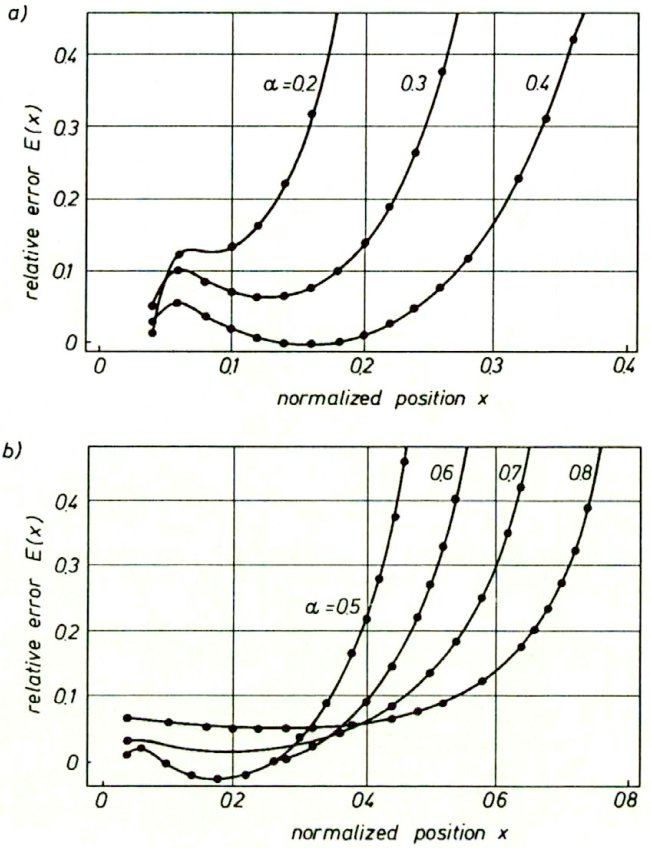

FIG. 6.

References

1. C. ATKINSON, *An iterative scheme for solving problems relating to cracks opening under a displacement-dependent internal stress*, Int. J. Frac. Mech., **6**, 2, 1970.
2. M.F. ASHBY, F.J. BLUNT and M. BANNISTER, *Flow characteristics of highly constrained metal wires*, Acta Metall., **37**, 7, pp. 1847–1857, 1989.
3. M. BANNISTER, H. SHERCLIFF, G. BAO, F. ZOK and M.F. ASHBY, *Toughening in brittle systems by ductile bridging ligaments*, Acta Metall. Mater., **40**, 7, pp. 1531–1537, 1992.
4. S.J. BENNISON and B.R. LAWN, *Role of interfacial grain-bridging sliding friction in the crack-resistance and strength properties of nontransforming ceramics*, Acta Metall., **37**, 10, pp. 2659–2671, 1989.
5. H.F. BUECKNER, *A novel principle for the computation of stress intensity factors*, ZAMM, **50**, 9, 529–546, 1970.
6. B.N. COX and D.B. MARSHALL, *Stable and unstable solutions for bridged cracks in various specimens*, Acta Metall. Mater., **39**, 4, pp. 579–589, 1991.
7. B.N. COX and D.B. MARSHALL, *Concepts for bridged cracks in fracture and fatigue*, Acta Metall. Mater., **42**, 2, pp. 341–363, 1994.
8. B.N. COX, D.B. MARSHALL and M.D. THOULESS, *Influence of statistical fiber strength distribution on matrix cracking in fiber composites*, Acta Metall., **37**, 7, pp. 1933–1943, 1989.
9. G. GLINKA and G. SHEN, *Universal features of weight functions for cracks in Mode I*, Engng. Frac. Mech., **40**, 6, pp. 1135–1146, 1991.

10. F. GUIU, M.J. REECE and D.A.J. VAUGHAN, *Cyclic fatigue of ceramics*, J. Mat. Sci., **26**, 3275–3286, 1991.
11. F. GUIU, M. LI and M.J. REECE, *The role of crack bridging ligaments in the cyclic fatigue behaviour of alumina*, J. Am. Ceram. Soc., **75**, 2976, 1992.
12. T. FETT, C. MATTHECK and D. MUNZ, *On the calculation of crack opening displacement from stress intensity factor*, Engng. Frac. Mech., **27**, 6, pp. 697–715, 1987.
13. X. HU and H. WITTMANN, *An analytical method to determine the bridging stress transferred within the fracture process zone. I. General theory*, Cement and Concrete Research, **21**, pp. 1118–1128, 1991.
14. M. LI and F. GUIU, *Subcritical fatigue crack growth in alumina. Part I. Effects of grain size, specimen size and loading mode*, Acta Metall., [in press].
15. M. LI and F. GUIU, *Subcritical fatigue crack growth in alumina. Part II. Crack bridging and cyclic fatigue mechanisms*, Acta Metall., [in press].
16. Y.W. MAI, B. BARAKAT, B. COTTERELL and M.V. SWAIN, *R-curve behaviour in a macro-defect-free cement paste*, Philosophical Magazine A, **62**, 3, 347–361, 1990.
17. Y.W. MAI and B.R. LAWN, *Crack-interface grain bridging as a fracture resistance mechanism in ceramics. II Theoretical fracture mechanics model*, Am. Ceram. Soc., **70**, 4, 289–94, 1987.
18. D.B. MARSHALL, B.N. COX and A.G. EVANS, *The mechanics of matrix cracking in brittle-matrix fiber composites*, Acta Metall., **33**, 11, pp. 2013–2021, 1985.
19. A. REICHL and R.W. STEINBRECH, *Determination of crack-bridging forces in alumina*, J. Am. Ceram. Soc., **71**, 6, C-299-c-301, 1988.
20. J.R. RICE, *Some remarks on elastic crack-tip stress fields*, Int. J. Solids Structures, **8**, 751–758, 1972.
21. RODEL, J.F. KELLY and B.R. LAWN, *In situ measurements of bridged crack interfaces in the scanning electron microscope*, J. Am. Ceram. Soc., **73**, 11, 3313–18, 1990.
22. A. SAXENA and S.J. HUDAK, *Review and extension of compliance information for common crack growth specimens*, Int. J. Frac., **14**, 5, 1978.
23. R. STREINBRECH, R. KHEHANS, W. SHAARWACHTER, *Increase of crack resistance during slow crack growth in Al_2O_3 bend specimens*, J. Mater. Sci., **18**, 265–270, 1983.
24. R.W. STEINBRECH, A. REICHL and W. SCHAARWACHTER, *R-curve behaviour of long cracks in alumina*, J. Am. Ceram. Soc., **73**, 7, 2009–2015, 1990.
25. M.V. SWAIN, *R-curve behaviour in a polycrystalline alumina material*, J. Mater. Sci., **5**, 1313–1315, 1986.
26. G. VEKINIS, M.F. ASHBY and P.W.R. BEAUMONT, *R-curve behaviour of Al_2O_3 ceramics*, Acta Metall. Mater., **38**, 6, pp. 1151–1162, 1990.
27. X.R. WU and A.J. CARLSSON, *Weight function and stress intensity factor solutions*, Pergamon, New York 1991.

DEPARTMENT OF MATERIALS, QUEEN MARY AND WESTFIELD COLLEGE,
UNIVERSITY OF LONDON, LONDON, ENGLAND.

Received December 2, 1994.

Arch. Mech., 47, 5, pp. 859–871, Warszawa 1995

Intersonic mode II crack expansion

K.B. BROBERG (DUBLIN)

EXPANSION OF A CRACK with constant velocity in an infinite, linearly elastic plate, starting from zero length, is one example of a self-similar problem. A method for solving such problems, using double Laplace transforms, is discussed and applied to a Mode II crack expanding at intersonic velocity. The usual assumption for sub-Rayleigh crack speeds, point-sized process regions, leads to a stress singularity which is too weak to allow energy flow into the process region. This complication is, for simplicity, overcome by a combination of two problems, one assuming a point-sized process region, and the other one assuming a finite process region, according to the Barenblatt model, but regarding only the neighbourhood of a crack edge. The result shows a substantial energy flux into the process region, except at intersonic velocities close to either the S or the P-wave velocity. Intersonic Mode II propagation should therefore be possible for a crack that succeeds to accelerate through the forbidden interval between Rayleigh and S-waves. Possible mechanisms for such acceleration are discussed.

1. Introduction

A PURELY MATHEMATICAL treatment of the problem of a Mode I crack propagating at super-Rayleigh velocity leads to the physically unacceptable result that energy flows away from the process region, i.e. the process region generates, rather than dissipates, energy. For Mode II the same result is obtained for super-Rayleigh, subsonic velocities, but not for intersonic velocities (FREUND [16], BURRIDGE *et al.* [14], BROBERG [9, 11]). However, a complication arises if the convenient assumption of a point-sized process region is made: this results in zero energy flow to the process region, except at the curious velocity $\sqrt{2}c_s$, where c_s is the velocity of S-waves. This result depends on the fact that the familiar square-root singularity at subsonic velocities is changed to a weaker singularity, except at $\sqrt{2}c_s$.

A square-root singularity in the idealization of a point-sized process region implies a non-zero energy flux to this region at crack growth, and it can be shown that this energy flux is, in the first approximation, the same as for a finite process region (BROBERG [6]). On the other hand, as it will be shown here, a weaker singularity, r^{-q}, where $0 < q < 1/2$, leads to an energy flux which is proportional to $(d/a)^{1-2q}$, where d expresses the linear extension of the process region and a is a measure of the crack length. Thus it is zero for $d = 0$.

The self-similar problem of a Mode I crack, expanding at sub-Rayleigh velocity was studied by BROBERG [5] using an integral equation approach. It was later solved also by CRAGGS [15], who took immediate advantage of the self-similarity by reducing the number of independent variables from three (r, φ, t) to two $(r/t$

and φ), and then applied the Chaplygin transformation

$$\operatorname{sech}^{-1}\left(\frac{r}{c_p t}\right) = -\varrho_p\,, \tag{1.1}$$

$$\operatorname{sech}^{-1}\left(\frac{r}{c_s t}\right) = -\varrho_s\,, \tag{1.2}$$

where c_p is the propagation velocity of P-waves and t is time, to obtain the Laplace equations for the displacement potentials ϕ and ψ

$$\frac{\partial^2\phi}{\partial\varrho_p^2} + \frac{\partial^2\phi}{\partial\varphi^2} = 0, \tag{1.3}$$

$$\frac{\partial^2\psi}{\partial\varrho_s^2} + \frac{\partial^2\psi}{\partial\varphi^2} = 0. \tag{1.4}$$

A similar method was devised by Smirnov and Sobolev for self-similar problems in general, see SMIRNOV [24]. General methods have also been discussed by WILLIS [25]. Here a different approach to self-similar problems will be applied, using double Laplace transforms. It is based on a general feature of self-similarity: homogeneous expressions, which prevail, not only in the physical region, but also in the Laplace transform region.

2. Double Laplace transforms for self-similar problems

Laplace transforms are here defined in dimension-true way, as in van der POL and BREMMER [25], so that the one-sided Laplace transform of a function $h(\tau)$, where $\tau = c_p t$, is

$$\mathcal{L}_{p\tau}h(\tau) = p\int_0^\infty e^{-p\tau}h(\tau)\,d\tau\,, \tag{2.1}$$

and the two-sided Laplace transform of a function $g(x)$ is

$$\mathcal{L}_{qx}g(x) = q\int_{-\infty}^{\infty} e^{-qx}g(x)\,dx. \tag{2.2}$$

With the representation

$$u = \frac{\partial\phi}{\partial x} + \frac{\partial\psi}{\partial y}\,, \tag{2.3}$$

$$v = \frac{\partial\phi}{\partial y} - \frac{\partial\psi}{\partial x}\,, \tag{2.4}$$

where u is the displacement in the x direction, v the displacement in the y direction, the equations of motion take the form

$$\Delta\phi = \frac{\partial^2\phi}{\partial\tau^2}, \tag{2.5}$$

$$\Delta\psi = \frac{1}{k^2}\cdot\frac{\partial^2\psi}{\partial\tau^2}, \tag{2.6}$$

where $k = c_s/c_p$. After double Laplace transformation,

$$\Phi = q\int_{-\infty}^{\infty} e^{-qx}p\int_{0}^{\infty} e^{-p\tau}\phi\, d\tau dx, \tag{2.7}$$

$$\Psi = q\int_{-\infty}^{\infty} e^{-qx}p\int_{0}^{\infty} e^{-p\tau}\psi\, d\tau dx, \tag{2.8}$$

the equations

$$q^2\Phi + \frac{d^2\Phi}{dy^2} = p^2\Phi, \tag{2.9}$$

$$q^2\Psi + \frac{d^2\Psi}{dy^2} = \frac{p^2}{k^2}\Psi \tag{2.10}$$

are obtained.

For a self-similar problem within linear elasticity, stresses and strains are functions of x/τ and y/τ. It is easy to show that the corresponding double Laplace transforms are functions of p/q and py. It can then be concluded that the solution of (2.9) and (2.10) for $y > 0$ must be of the form

$$\Phi = \frac{1}{q^2}A\left(\frac{p}{q}\right)e^{-(p^2-q^2)^{1/2}y}, \tag{2.11}$$

$$\Psi = \frac{1}{q^2}C\left(\frac{p}{q}\right)e^{-(p^2/k^2-q^2)^{1/2}y}, \tag{2.12}$$

and that transforms of the type

$$q^n F^{(P)}\left(\frac{p}{q}\right)e^{-(p^2-q^2)^{1/2}y}, \tag{2.13}$$

$$q^n F^{(S)}\left(\frac{p}{q}\right)e^{-(p^2/k^2-q^2)^{1/2}y} \tag{2.14}$$

will appear, where the integer n depends on the quantity represented. Such transforms can be directly inverted. Since a multiplication by q corresponds simply to

a differentiation with respect to x in the physical plane, it is sufficient to establish the inversion for one value of n only. The simplest choice, $n = 1$, will be used here, corresponding to the double Laplace transform of a stress gradient or a mass acceleration. For S-waves, radiating from $y = 0$ into the half-space $y \geq 0$, such a transform will have the form:

$$\mathcal{L}_{p\tau}\mathcal{L}_{qx} f^{(S)}(x, y, \tau) = qF^{(S)}\left(\frac{q}{p}\right) e^{-(p^2/k^2 - q^2)^{1/2} y}. \tag{2.15}$$

Branch points are usually found only on the real axis in the ζ-plane, where $\zeta = \xi + i\eta = q/p$, and inversion with respect to q is then possible by deformation of the integration path in the formal inversion

$$\mathcal{L}_{p\tau} f^{(S)}(x, y, t) = \frac{1}{2\pi i} \int_{-i\infty}^{i\infty} e^{qx - (p^2/k^2 - q^2)^{1/2} y} F^{(S)}\left(\frac{q}{p}\right) dq \tag{2.16}$$

$$= \frac{1}{2\pi i} \int_{-i\infty}^{i\infty} p e^{p[\zeta x - (1/k^2 - \zeta^2)^{1/2} y]} F^{(S)}(\zeta) d\zeta$$

to the hyperbola branch Γ, given by (cf. BRODERG [4])

$$\frac{\xi^2}{x^2} - \frac{\eta^2}{y^2} = \frac{1}{k^2 r^2}, \qquad r^2 = x^2 + y^2, \qquad \frac{\xi}{x} < 0, \tag{2.17}$$

i.e. the left-hand branch if $x > 0$, and the right-hand branch if $x < 0$. Then $s = \zeta x - (1/k^2 - \zeta^2)^{1/2} y$ is real on Γ, and such that s decreases from $-r/k$ to $-\infty$ as ζ goes from $-x/(kr)$ to infinity either along branch Γ_+ (the part of Γ for $\eta > 0$) or along branch Γ_- (the part of Γ for $\eta < 0$). During this procedure it helps to regard p as a real and positive number, which can be done without affecting the generality, cf. LERCH [20]. The remaining inversion with respect to p is reduced to inversion of pe^{sp}, giving $\delta(\tau + s)$, where $\delta(\cdot)$ is the Dirac delta function, and the result is

$$f^{(S)}(x, y, \tau) = -\frac{U\left(\tau - \frac{r}{k}\right)}{2\pi i} \Big\{ g_+^{(S)}(-\tau)[F_+^{(S)}(\zeta)]_{\zeta = \zeta_+^{(S)}(-\tau)} \tag{2.18}$$

$$- g_-^{(S)}(-\tau)[F_-^{(S)}(\zeta)]_{\zeta = \zeta_-^{(S)}(-\tau)} \Big\},$$

where $U(\cdot)$ is the unit step function, index plus refers to the part of the hyperbola on $\Im\zeta > 0$, index minus to the part on $\Im\zeta < 0$, and

$$\zeta_\pm^{(S)}(s) = \frac{xs}{r^2} \pm \frac{iy}{kr^2}\sqrt{k^2 s^2 - r^2} \quad \text{on } \Gamma_\pm, \tag{2.19}$$

$$g_\pm^{(S)}(s) = \frac{d\zeta_\pm^{(S)}}{ds} = \frac{x}{r^2} \pm \frac{iky s}{r^2\sqrt{k^2 s^2 - r^2}}. \tag{2.20}$$

For P-waves (superscript P) the inversions are given by the same formulae, but k should be substituted by 1 everywhere, i.e. in the unit step function, in the equation for the hyperbola and in the definitions of $\zeta_{\pm}^{(P)}(s)$ and $g_{\pm}^{(P)}(s)$.

For $y = 0$ the inversion formula can be applied for P and S-waves together, and it reads

$$f(x,0,\tau) = -\frac{1}{2\pi i x}[F_+(\xi) - F_-(\xi)]_{\xi=-\tau/x}, \tag{2.21}$$

where $qF(q/p)$ is the Laplace transform of $f(x,0,\tau)$ and indices plus and minus refer, respectively, to the upper and the lower side of the negative (positive) real axis if $x > 0$ ($x < 0$).

3. Intersonic Mode II crack expansion, assuming a point-sized process region

The crack is assumed to expand symmetrically with velocity V from $x = 0$ in the plane $y = 0$, so that the crack edges are at $|x| = Vt = \beta\tau$ for $t > 0$. The remote load is a shear stress $\tau_{xy} = \tau_{xy}^{\infty}$. It is assumed that $\sigma_y = 0$ everywhere, but, if so desired, a compressive stress $\sigma_y < 0$ can be superposed, combined with Coulomb friction on the crack faces. The upper half-plane, $y \geq 0$, is studied. The boundary conditions for $y = 0$ consist of $\sigma_y = 0$ for all x, $\tau_{xy} = 0$ for $|x| < \beta\tau$ and $u = 0$ for $|x| > \beta\tau$.

Put

$$\mathcal{L}_{p\tau}\mathcal{L}_{qx}(\tau_{xy})_{y=0} = \zeta H(\zeta), \tag{3.1}$$

$$\mathcal{L}_{p\tau}\mathcal{L}_{qx}(u)_{y=0} = \frac{k^2}{\mu p} G(\zeta), \tag{3.2}$$

where μ is the modulus of rigidity. Then, after straightforward application of the transformed Laplace boundary conditions and use of the inversion formula (2.21), the following relations emerge:

$$G(\zeta) = \frac{(1/k^2 - \zeta^2)^{1/2} H(\zeta)}{\zeta^3 R(1/\zeta)}, \tag{3.3}$$

$$\left(\frac{\partial \tau_{xy}}{\partial \tau}\right)_{y=0} = -\frac{1}{2\pi i x}[H_+(\xi) - H_-(\xi)]_{\xi=-\tau/x} \quad \text{for } \xi^2 > \frac{1}{\beta^2}, \tag{3.4}$$

$$\left(\frac{\partial^2 u}{\partial \tau^2}\right)_{y=0} = -\frac{k^2}{2\pi i \mu x}[G_+(\xi) - G_-(\xi)]_{\xi=-\tau/x} \quad \text{for } \xi^2 < \frac{1}{\beta^2}, \tag{3.5}$$

where $R(z) = 4k^3(1 - z^2)^{1/2}(k^2 - z^2)^{1/2} - (z^2 - 2k^2)^2$ is the Rayleigh function, defined through branch cuts on $\Im z = 0$ along the portions $-1 \leq z \leq -k$, $k \leq z \leq 1$ and branch choice such that $R(z) \to 2k^2(1 - k^2)z^2$ as $z \to \infty$. The

two last equations constitute a Hilbert problem. With regard to (3.3), the second equation can be written as

$$H_+(\xi) - C(\xi)H_-(\xi) = 0 \qquad \text{for} \quad \xi^2 < \frac{1}{\beta^2}, \tag{3.6}$$

where

$$C(\xi) = \frac{(1-\xi^2)_+^{1/2}[\xi^4 R(1/\xi)]_-}{(1-\xi^2)_-^{1/2}[\xi^4 R(1/\xi)]_+} \tag{3.7}$$

which, with extension of the definition of $C(\xi)$, so that (3.6) is valid for all ξ, can be written as

$$C(\xi) = \begin{cases} 1 & \text{for} \quad \xi^2 < 1, \\ e^{2\pi i g(\xi)} & \text{for} \quad -1/\beta < \xi < -1, \\ e^{-2\pi i g(\xi)} & \text{for} \quad 1 < \xi < 1/\beta, \\ 1 & \text{for} \quad 1/\beta^2 < \xi^2, \end{cases} \tag{3.8}$$

where

$$g(\xi) = \frac{1}{\pi}\operatorname{atan}\frac{4k^3\sqrt{1-1/\xi^2}\sqrt{1/\xi^2-k^2}}{(1/\xi^2-2k^2)^2}. \tag{3.9}$$

In a logarithmic form equation (3.6) reads

$$[\ln H(\xi)]_+ - [\ln H(\xi)]_- = \ln C(\xi), \tag{3.10}$$

and then Plemelj's formulae give the solution which, with regard to the physical condition of bounded stress-strain energy in the crack edge neighbourhood, is

$$H(\zeta) = \frac{D}{1/\beta^2 - \zeta^2} \cdot e^{-I(\zeta)}, \tag{3.11}$$

where

$$I(\zeta) = 2\int_1^{1/\beta} \frac{w g(w)}{w^2 - \zeta^2} dw \tag{3.12}$$

and D is a constant, which is determined by using the condition that $\tau_{xy} \to \tau_{xy}^{\infty}$ as $|\xi| \to \infty$. The stress τ_{xy} is obtained by integrating the expression

$$\frac{\partial(\tau_{xy})_{y=0}}{\partial \tau} = -\frac{1}{2\pi i x}[H_+(\xi) - H_-(\xi)]_{\xi=-\tau/x} \tag{3.13}$$

giving

$$(\tau_{xy})_{y=0} = \tau_{xy}^{\infty} + \frac{1}{2\pi i}\int_{\Gamma} H(\zeta)\, d\zeta, \tag{3.14}$$

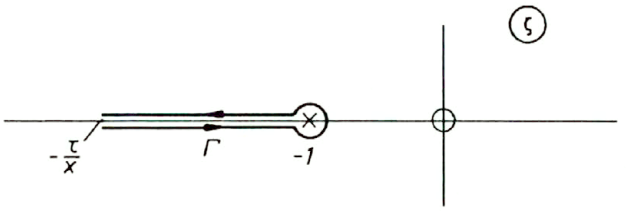

FIG. 1. Path of integration for determination of $(\tau_{xy})_{y=0}$ at arbitrary $x > 0$.

where, assuming $x > 0$, Γ is the path shown in Fig. 1. By letting $\tau/x \to \infty$, corresponding to the extension of the path to $\zeta = -\infty$, i.e. to the path Γ_∞ in Fig. 2, the stress becomes zero, so that

$$\tau_{xy}^{\infty} + \frac{1}{2\pi i} \int_{\Gamma_\infty} H(\zeta)\, d\zeta = 0. \tag{3.15}$$

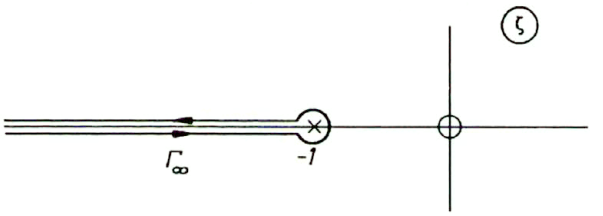

FIG. 2. Path of integration for determination of $(\tau_{xy})_{y=0}$ for $0 \le x < Vt$.

It might be convenient to deform this path to the imaginary axis, giving the equation

$$\frac{1}{2\pi} \int_{-\infty}^{\infty} H(\eta)\, d\eta = -\tau_{xy}^{\infty} \tag{3.16}$$

for determination of D. Details are found in BROBERG [12]. Of special interest is the displacement $u_{y=0}$ and the stress $(\tau_{xy})_{y=0}$. Both result in rather complicated expressions. The displacement can be obtained from the expression for the mass acceleration,

$$\left(\frac{\partial^2 u_+}{\partial \tau^2}\right)_{y=0} = \begin{cases} \dfrac{1}{4\pi\mu|x|} \cdot \dfrac{\sin^2 \pi g}{k^2 \xi^2 \sqrt{\xi^2 - 1}} H(\xi) \\ \qquad \text{for} \quad 1/\beta < \xi = \tau/|x| < 1/k\,, \\ -\dfrac{k^2}{\pi\mu|x|} \cdot \dfrac{\sqrt{\xi^2 - 1/k^2}}{\xi^4 R(1/\xi)} H(\xi) \\ \qquad \text{for} \quad \xi = \tau/|x| > 1/k\,, \end{cases} \tag{3.17}$$

where $g = g(1/\beta)$. Note the singular behaviour both at $|x| = c_R t$, where c_R is the Rayleigh speed, and at $|x| = c_s t$, in contrast to the very simple elliptic shape of the crack face displacement in the sub-Rayleigh case.

For the crack edge vicinity, $x \approx \beta\tau = a$, the shear stress on $y = 0$,

$$\tau_{xy} \to \frac{\tau_{xy}^{\infty}}{N} \cdot \frac{\beta \sin \pi g \cdot e^{-I_0(1/\beta)}}{2^{1-g} g} \cdot \left(\frac{1-\beta}{1+\beta}\right)^g \cdot \left(\frac{a}{x-a}\right)^g \qquad \text{as } x \to a+0, \tag{3.18}$$

where $N = -\pi\tau_{xy}^{\infty}/D$, and

$$I_0(\xi) = 2 \int_1^{1/\beta} \frac{wg(w) - 1/\beta \cdot g(1/\beta)}{w^2 - \xi^2} dw\,. \tag{3.19}$$

Constant N is approximately 1.182 for $k^2 = 1/3$, corresponding to Poisson's ratio $\nu = 1/4$ at plane strain.

The displacement gradient on the upper crack face,

$$\frac{\partial u_+}{\partial x} \to -\frac{Y_{II}(\beta)}{2(1-k^2)\mu} \cdot \frac{\tau_{xy}^{\infty}}{N} \cdot \frac{\beta \sin \pi g \cdot e^{-I_0(1/\beta)}}{2^{1-g} g} \cdot \left(\frac{1-\beta}{1+\beta}\right)^g \cdot \left(\frac{a}{a-x}\right)^g \tag{3.20}$$

as $x \to a - 0$, where

$$Y_{II}(\beta) = \frac{(1-k^2)\beta^2 \sin \pi g}{2k^2\sqrt{1-\beta^2}}\,. \tag{3.21}$$

4. The energy flux into the process region at intersonic crack velocities

A Barenblatt Model of a process region with length $d \ll Vt$ is assumed, see Fig. 3. Using the same procedure as in BRODERG [6], which allows for a process

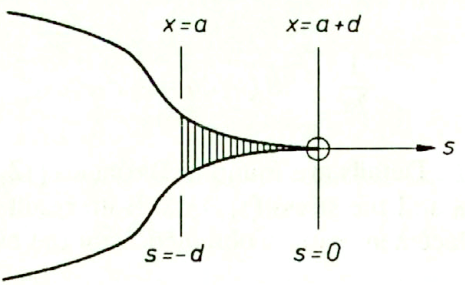

FIG. 3. Barenblatt model of a process region. Cohesive forces act across the shaded region.

region of a finite size (repeated in a more general way in BRODERG [7]), the energy flux into this process region is calculated as

$$\mathcal{G}(V) = 2 \int_{-d}^{0} \tau_{xy}^{0}(s) \frac{\partial u}{\partial s}\, ds\,. \tag{4.1}$$

Here s is a length coordinate measured from the front of the process region, increasing in positive x direction, and d is the length of a Barenblatt model of the process region, for which the stress distribution τ_{xy}^0 is assumed to be a known function,

$$\tau_{xy} = \tau_D \cdot D(s/d), \tag{4.2}$$

where τ_D is the cohesive strength. Such a stress distribution is obtained from the solution for the crack with point-sized process regions by suitable superpositions of such cracks, running at different speeds, from β to $\beta + d/\tau$, where $d \ll \beta\tau$, cf. BROBERG [6, 7]. By using (3.18) and (3.20), the energy flux is found to be

$$\mathcal{G}(V) = \frac{\pi(\tau_{xy}^{\infty})^2 a}{\mu} B(\beta) \Gamma_D(g) \left(\frac{d}{a}\right)^{1-2g}, \tag{4.3}$$

where

$$B(\beta) = \frac{\beta^4 e^{-2I_0(1/\beta)} \sin^2 \pi g}{2^{2(2-g)} k^2 N^2 g^2 \sqrt{1-\beta^2}} \cdot \left(\frac{1-\beta}{1+\beta}\right)^{2g}, \tag{4.4}$$

$$\Gamma_D(g) = \frac{2 w_D(g)}{\sin \pi g \left[\int_0^1 \frac{D(-w)}{w^{1-g}} dw\right]^2}, \tag{4.5}$$

$$w_D(g) = \int_0^1 D(-v) v^{1-g} \left[\int_0^1 \frac{D(-v) - D(-w)}{w^{1-g}(w-v)} dw + D(-v) \int_1^{\infty} \frac{dw}{w^{1-g}(w-v)}\right] dv. \tag{4.6}$$

Note that both integrands of the inner integrals are positive.

The expression for $\mathcal{G}(V)$ consists of four factors. The first one expresses the dependence of load and crack length, as in the subsonic case, the second one, $B(\beta)$, is a function of β only, the third one, $\Gamma_D(g)$, depends on the crack velocity and the relation (4.2), and the fourth one, $(d/a)^{1-2g}$, as already mentioned in the Introduction, expresses the dependence on the size of the process region.

Numerical calculations have been performed, assuming the form

$$D(s/d) = 1 + s/d, \qquad -d \le s \le 0. \tag{4.7}$$

The result, expressed as $\mathcal{G}(V)/\mathcal{G}(0)$ is shown in Fig. 4 for some values of the Poisson ratio. Note that $\mathcal{G}(V)/\mathcal{G}(0)$ is the ratio between the energy flux at velocity

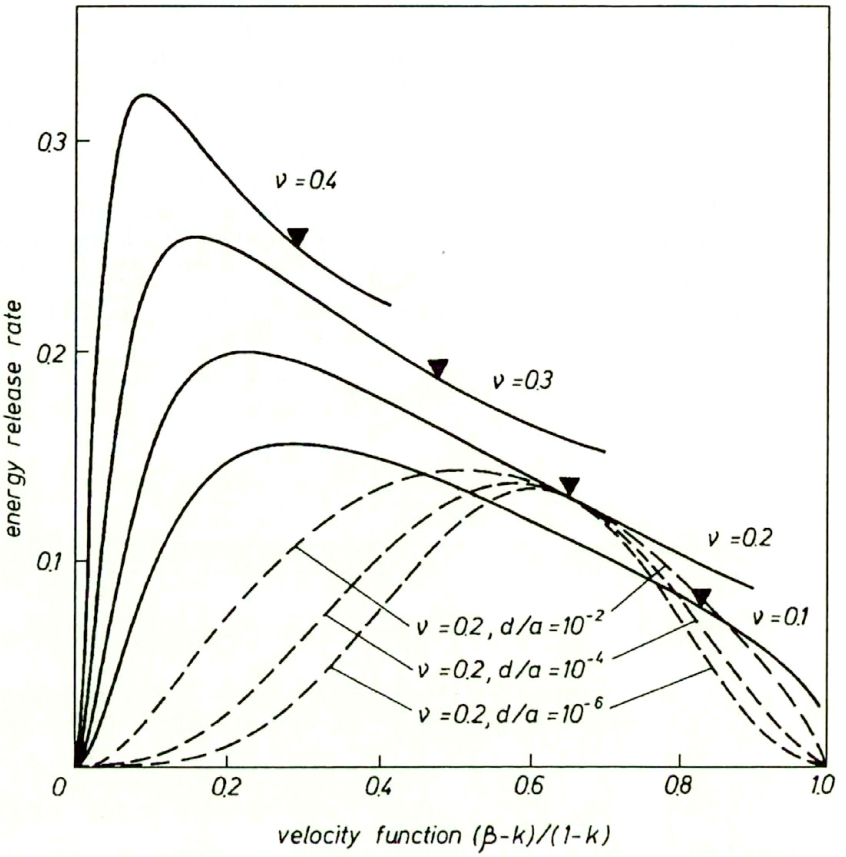

FIG. 4. Dependence of normalized energy flux, $\mathcal{G}(V)/\mathcal{G}(0)$, on crack velocity β in the intersonic region. Plane strain is assumed. The solid line curves for Poisson's ratio $\nu = 0.1$, 0,2, 0.3 and 0.4 are drawn from numerical calculations, after putting $d/a = 1$. From these curves the energy flux for realistic values of d/a is found by multiplication with $(d/a)^{1-2\gamma}$. Three examples are shown for $\nu = 0.2$: $d/a = 10^{-2}$, 10^{-4} and 10^{-6}. Filled triangles point to the velocity $\beta = 2^{1/2}k$ for each value of Poisson's ratio.

V and the energy flux at infinitesimally small velocity, both at the same current crack length a. Figure 5 (sketched) shows this relative energy flux into the process region for all velocities between zero and the P-wave velocity.

In the middle part of the figure also the assumed absolute energy flux $\mathcal{G}(V)$, for a hypothetical crack acceleration from a stationary state, is shown, and the lower part shows an assumed relation between the crack length and velocity. If the energy flux required were independent of the crack velocity, the dashed line in the middle part of the figure, then the development of the crack length would be as shown by the dashed curve in the lower part of the figure.

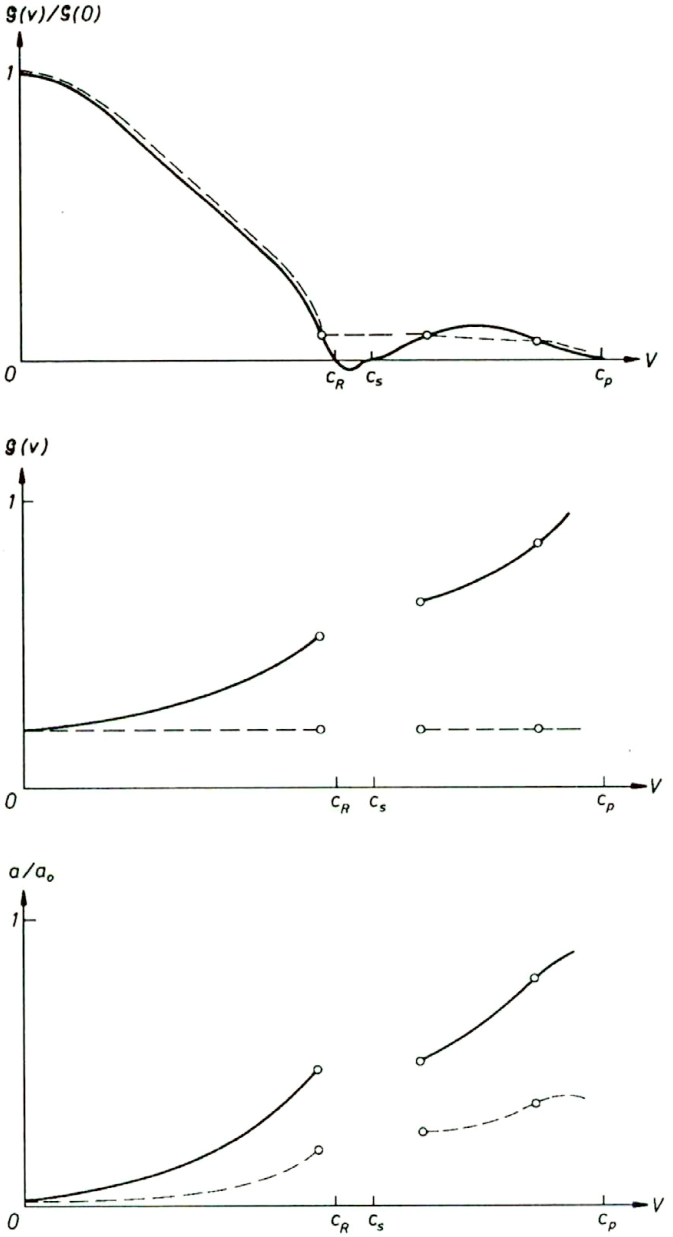

FIG. 5. Normalized energy flux into the process region as a function of the crack velocity (upper figure), total energy flux into the process region for a hypothetical case of crack acceleration (middle figure), and the crack growth (lower figure). In the upper figure the dashed line indicates a possible acceleration event. In the two lower figures the dashed lines indicate the acceleration event which would result if the energy dissipation in the process region were independent of the crack velocity; the solid lines assume a probable realistic dependence.

5. Discussion

The investigation shows that intersonic Mode II crack propagation is possible from the energy point of view. Whether it will take place in reality, depends therefore on other requirements, such as a high ambient pressure to prevent Mode I growth through kinking (cf. MELIN [21]), a material which is not prone to branching – or a weak layer to prevent branching, or a mechanism by which the forbidden super-Rayleigh, subsonic region can be bypassed. The latter requirement might be satisfied by opening of cracks ahead of the main crack, due to a stress peak, travelling with S-wave speed (BURRIDGE [13]), and becoming more and more pronounced when the velocity of the main crack approaches the Rayleigh speed (cf. BROBERG [10]). Another possibility for a "jump" to a higher velocity is the rupture of a weak inhomogeneity in front of the crack or some other action of an inhomogeneity.

Experimental evidence of intersonic Mode II crack growth is presently scarce. There are some indications of intersonic velocities from the Imperial Valley earthquake 1982 (ARCHULETA [3]), and intersonic crack growth along an interface between dissimilar media has been reported by LAMBROS and ROSAKIS [19]. Some numerical calculations show acceleration through the forbidden region to intersonic velocities (ANDREWS [1, 2], JOHNSSON [17, 18]), presumably due to the finiteness of the finite element mesh in their simulations.

The energy flux into the process region is clearly dependent on the size of this region. If the size of the process region is not uniquely correlated to the crack speed, then a unique relation between energy flux and crack speed does not exist, as has been demonstrated experimentally for Mode I by RAVI-CHANDAR [22], see also RAVI-CHANDAR and KNAUSS [23]. It is a consequence of the loss of a significant intrinsic length parameter at very high velocities (cf. BROBERG [8]) and it can be expected also for Mode II.

References

1. D.J. ANDREWS, *Rupture velocity at plane strain shear cracks*, J. Geophys. Res., **81**, 5679–5687, 1976.
2. D.J. ANDREWS, *Dynamic plane-strain rupture with a slip-weakening friction law calculated by a boundary-integral method*, Bull. Seism. Soc. Am., **75**, 1–22, 1985.
3. R.J. ARCHULETA, *Analysis of near source static and dynamic measurements from the 1979 Imperial Valley earthquake*, Bull. Seism. Soc. Am., **72**, 1927–1956, 1982.
4. K.B. BROBERG, *A problem on stress waves in an infinite elastic plate*, Transactions Roy. Inst. Techn., Stockholm, Sweden, **139**, 1–27, 1959.
5. K.B. BROBERG, *The propagation of a brittle crack*, Arkiv för Fysik, **18**, 159–192, 1960.
6. K.B. BROBERG, *On the speed of a brittle crack*, J. Appl. Mech., **31**, 546–547, 1964.
7. K.B. BROBERG, *Discussion of fracture from the energy point of view*, Recent Progress in Applied Mechanics, B. BROBERG, J. HULT and F. NIORDSON [Eds.]., Almqvist and Wiksell, Stockholm, 125–151, 1967.
8. K.B. BROBERG, *On the behaviour of the process region at a fast running crack tip*, [in:] High Velocity Deformation of Solids, K. KAWATA and J. SHIOIRI [Eds.], Springer-Verlag, Berlin-Heidelberg, 182–194, 1979.

9. K.B. BROBERG, *Velocity peculiarities at slip propagation*, Report from the Division of Engineering, Brown University, Providence, R.I. 1980.
10. K.B. BROBERG, *Irregularities at earth-quake slip*, J. Tech. Phys., **26**, 275–284, 1985.
11. K.B. BROBERG, *The near-tip field at high crack velocities*, Int. J. Fracture, **39**, 1–13, 1989.
12. K.B. BROBERG, *Intersonic bilateral slip*, Geophys. J. Int., **119**, 706–714, 1994.
13. R. BURRIDGE, *Admissible speeds for plane-strain self-similar shear cracks with friction but lacking cohesion*, Geophys. J. Roy. Astr. Soc., **35**, 439–455, 1973.
14. R. BURRIDGE, G. CONN and L.B. FREUND, *The stability of rapid Mode II shear crack with finite cohesive traction*, J. Geophys. Res., **85**, 2209–2222, 1979.
15. J.W. CRAGGS, *Fracture criteria for use in continuum mechanics*, [in:] Fracture of Solids, D.C. DRUCKER and J.J. GILMAN [Eds.], Interscience Publishers, N.Y., 51–63, 1963.
16. L.B. FREUND, *The mechanics of dynamic shear crack propagation*, J. Geophys. Res., **84**, 2199–2209, 1979.
17. E. JOHNSON, *On the initiation of unidirectional slip*, Geophys. J. Int., **101**, 125–132, 1990.
18. E. JOHNSON, *The influence of the lithospheric thickness on bilateral slip*, Geophys. J. Int., **108**, 151–160, 1992.
19. J. LAMBROS and A.J. ROSAKIS, *Shear dominated transonic crack growth in bimaterials. Part I. Experimental Observations*, SM Report 94-14, Graduate Aeronautical Laboratories, California Institute of Technology, Pasadena, California 91125, 1994.
20. M. LERCH, *Sur un point de la théorie des fonctions génératrices d'Abel*, Acta Mathematica, **27**, 339–351, 1903.
21. MELIN, SOLVEIG, *When does a crack grow under Mode II conditions?*, Int. J. Fract., **30**, 103–114, 1986.
22. K. RAVI-CHANDAR, *An experimental investigation into the mechanics of dynamic fracture*, Ph.D. Thesis, California Institute of Technology, Pasadena, California 1982.
23. K. RAVI-CHANDAR and W.G. KNAUSS, *An experimental investigation into dynamic fracture, in four parts*, Int. J. Fract., *I. Crack initiation and arrest*, **25**, 247–262, *II. Microstructural aspects*, **26**, 65–80, *III. On steady-state crack propagation and crack branching*, **26**, 141–154, *IV. On the interaction of stress waves with propagating cracks*, **26**, 189–200, 1984.
24. V.I. SMIRNOV, *A Course of Higher Mathematics*, **III**, Addison-Wesley, Reading, Mass 1964.
25. B. VAN DER POL and H. BREMMER, *Operational calculus based on the two-sided Laplace integral*, Cambridge University Press, Cambridge 1959.
26. J.R. WILLIS, *Self-similar problems in elastodynamics*, Phil. Trans. Roy. Soc. (London), **274**, 435–491, 1973.

DEPARTMENT OF MATHEMATICAL PHYSICS,
UNIVERSITY COLLEGE DUBLIN, BELFIELD, DUBLIN, IRELAND.

Received December 2, 1994.

Arch. Mech., 47, 5, pp. 873–887, Warszawa 1995

A model for dynamic ductile crack growth

R.M. CURR and C.E. TURNER (LONDON)

A MODEL for ductile crack growth consistent with the behaviour of real elastic-plastic material is expressed for quasi-static behaviour, firstly in terms of energy dissipation rate and then in terms of crack tip opening angle. It is then proposed that, since the energy dissipation rate is but a statement of conservation of energy, dynamic ductile crack growth should also be seen in the same terms, with a critical crack tip opening angle being also a function of crack speed or local strain rate. Some recent three-dimensional finite element computations of a crack running in a large plate are re-examined satisfactorily in this light.

Nomenclature

- a, a_0 crack length, original crack length,
- b ligament, $W - a$,
- B thickness,
- C energy rate available to drive the crack, per unit crack area,
- da increment in crack length, but not implying $da \to 0$,
- D energy dissipation rate, per unit crack area,
- E' effective modulus depending on the degree of plane stress or strain,
- G the classical energy release rate,
- I the elastic energy exchange rate in the presence of plasticity,
- J the classical J-contour integral (but evaluated from the area under a loading diagram in experimental work),
- K the classical stress intensity factor,
- L a normalisation factor for load, equal to the plastic constraint factor at limit load,
- q load point displacement,
- Q load,
- r^* a factor that defines the position of the instantaneous centre of rotation in a deep notch bend test during crack growth,
- R resistance to crack growth after initiation,
- S span of a bend test piece,
- U work done,
- w internal strain energy, not necessarily recoverable,
- W width of a test piece,
- α crack tip opening angle,
- $\alpha_{g,\mathrm{pl}}$ a measure of α based on the global plastic displacement rate,
- Γ surface energy,
- Δa accumulated crack growth,
- η a geometric factor relating J to work per unit area,
- σ_0 a reference yield or proof stress.

1. Introduction

TWO-DIMENSIONAL finite element computation of dynamic crack growth in essentially elastic systems was established as a feasible procedure some twenty years ago. Programs for elasto-plastic dynamic behaviour in either two or three dimensions now exist and have been used, for example, to study high-speed cleavage fracture in steels, fracture of pipe-lines and crack tunnelling. Correlation with experimental data has proved difficult, partly because of uncertainty in the interpretation of experimental data, and partly because of uncertainty in the correctness of the computational models used. Some examples of recent dynamic studies are given [1–4].

In lefm models with well contained yield, a critical K or G criterion is generally used for crack advance, perhaps taken as a function of crack speed. It is believed that representing the energy loss, G, by "hold-black" forces that reduced to zero as the crack tip node was allowed to separate and then subtracting that energy from the remaining system, was first implemented in [5]. An appropriate criterion for growth with appreciable plasticity is less well agreed, even for quasi-static behaviour. The inadequacy of a "hold-back" model for static growth in an elastic plastic system was pointed out, [6, 7]. The present work relates to ductile crack growth following initiation by impact or other dynamic loading. The speed of crack advance, perhaps some two to six hundred meters per second, does not seem to merit complicated models of the mechanical properties of the metal at high strain rates other than a direct dependence of yield stress on strain rate. A brief description is therefore given of a recent model for static crack growth, followed by its relation to the dynamic case. The modelling of crack advance in a certain three-dimensional program is then described and outlines given of some particular results.

2. Quasi-static crack growth

The objective here is to provide an analysis for a conventional small test piece from which data for stable crack growth can be obtained and then transferred to other situations such as a structure in contained yield. The test piece considered in detail is the deep notch bend (DNB) configuration.

2.1. A macro-scale model

In the presence of appreciable plasticity, toughness is usually described in terms of either crack opening displacement (COD) or the J-integral and crack growth toughness plotted as R-curves of COD or J versus crack growth, Δa. The definition of COD, with growth, is uncertain. In some test data it is represented as the opening at the original crack tip whereas in others, it is taken at the advancing tip. In this latter case, COD may be translated into crack tip opening

angle, CTOA. The J-integral is known to become path-dependent with growth. Initial studies, [8], suggested it might remain path-independent for growth up to about 6% of the ligament but recent studies, [9–11], show it is path-dependent from the first step of growth.

An alternative approach is to describe stable crack growth through the energy dissipation rate, D, for growth in real elastic-plastic (rep) material, i.e. incremental plasticity for loading and linear elasticity for unloading, [12–15]. The term D relates to the dissipation of energy by fracture and plasticity, although any plasticity not connected to the crack tip field (e.g. at remote loading points) should not be included. For stable growth, the crack driving force, C, must be equal to the dissipation rate, D, so that for a two-dimensional model, thickness, B, crack advance, da,

$$C = d(U - w_{el})/B\,da = d(w_{pl} + \Gamma)/B\,da = D,$$

where U is work, dw_{el} is the recoverable elastic energy, w_{pl} is the energy dissipated in plasticity and Γ is the energy dissipated in fracture. The dissipation is mainly into heat. The energy associated with the residual stresses during unloading has not been separately identified. It is shown, [15], that for strict lefm, $C = G$ and $d\Gamma/Bda = 2\gamma_0$, the real surface energy. For the conventional engineering application of lefm, $C \approx G$ and $d\Gamma/Bda = 2\gamma_{eff}$ in the Irwin–Orowan sense. With appreciable plasticity, there is no direct relationship between D and the conventional terms.

Since $C = D$ expresses conservation of energy, it must be applicable to any description of stable growth but will not in itself provide a criterion for growth. Some exploration was made with fully plastic cases, [13, 14], of splitting D into areal and volumetric components for fracture, shear-lips and general (slip-line) plasticity, each with a specific intensity and associated area or volume. However, a more fruitful analysis was seen, [14] in terms of crack opening angle and it was shown, [15], that D could be re-expressed as

$$D = G + Qdq_{pl}/B\,da,$$

where Q is load, q is load point displacement and subscript pl implies the plastic component. This expression holds for any degree of plasticity and any (two-dimensional) configuration. The term G is the conventional lefm term. The non-dimensional term dq_{pl}/da invites treatment as some global measure of CTOA. For deep notch bend (DNB) pieces, experiment showed that dq_{pl} was proportional to $1/b$ [14, 16], where b is the width of the current ligament, $\{W - (a_0 + \Delta a)\}$. An example is shown, Fig. 1. This linearity allowed a global crack opening angle (COA), $\alpha_{g,pl}$, to be defined as

$$dq_{pl}/da = S\alpha_{g,pl}/4r^*b, \tag{2.1}$$

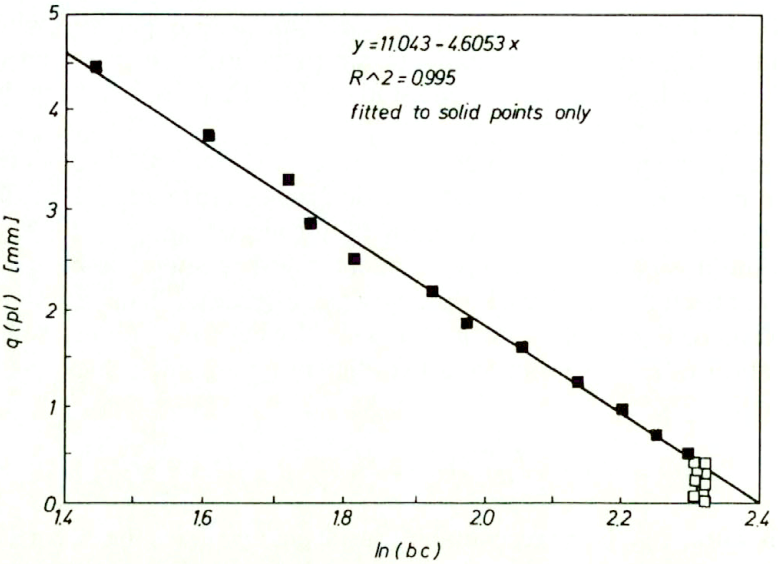

FIG. 1. An example of the linearity of q_{pl} with $\ln b$, relevant to the interpretation of (2.1); after [14].

where S is span and r^* was at first taken to be the rotational constant, $r = 0.4$, as in the standard COD test. It was then realised, [16, 17], that r^* should be defined incrementally for the position of the instantaneous centre of rotation. This was found to be at $(r^*b, -c)$ with $r^* \approx 0.8$ or 0.9 for the high strength low hardening metals of [14, 16], with c being a small negative distance proportional to Δa, implying the instantaneous centres were rather near the "back" face of the specimen and slightly into the "other" half of the piece. The value of r^* was constant with growth for these fully plastic data so that, taken together with (2.1), $\alpha_{g,\mathrm{pl}}$ was also constant with growth. For a centre cracked plate in tension, $dq_{\mathrm{pl}}/da = \alpha_{g,\mathrm{pl}}$. This analysis and that of (2.1) are rigid-plastic, so some uncertainty remains on whether the global COA, $\alpha_{g,\mathrm{pl}}$, is indeed identical to the true tip CTOA, α. Until that is resolved, the relationship is written

$$\alpha_{g,\mathrm{pl}} = \kappa\alpha,$$

where κ is a constant of the order of unity.

2.2. A micro-scale model

In [15] this analysis was associated with a model for micro-void growth and coalescence (mvc) in which CTOA, α, was seen as the consequence of a final crack opening stretch, δ_t, of the micro-ligament between the current tip and a void at distance, d, ahead of it, as suggested by WNUK [18]. Thus

$$\alpha = \delta_t/d.$$

One consequence of that model is that each step of crack advance, written as da, is for a finite distance, d (the spacing of the inclusions on which the void grows). Nevertheless, the conventional differential notation is retained as a convenience despite the clear physical statement that da does not tend to a limit of zero. Another consequence is that the CTOA does not exist until after the micro-ligament has separated. In short, the true local CTOA must either be formed in the increment, as in (2.1) or, if by differentiation of COD, then that must be conducted at constant ligament size, b.

Support for this micro-model was taken from works such as [19, 20], where direct measurement by a variety of techniques had shown that CTOA was indeed constant with growth. The CTOA was however a function of both the position through the thickness and of the overall configuration, the former no doubt due to degree of out-of-plane constraint and the latter, of in-plane constraint. In [15] a more detailed description of this model is given in terms of two stages of growth. The first event in each step of growth is the formation and then expansion of voids ahead of the crack tip, thereby forming a micro-ligament between the tip and the void ahead of it; this micro-ligament is then separated by a micro-scale instability. For application, this model is formalised into two stages. The first is seen as "damage" in which the voids form and expand during plastic flow at fixed crack length; the second is seen as actual crack growth with an apparent fracture energy, in the Irwin - Orowan sense. In this formalised model, the first stage is driven by increments in work, $dU = Q\,dq$, and the scond by changes in elastic energy at fixed displacement, $\partial w_{\mathrm{el}}/B\partial a|_q$.

There are several features of the physical model that are not carried over correctly into this practical model, but that is accepted at the present stage of the work. Thus, in the physical model, most of the surface energy is used in the formation and expansion of the voids in the first or "damage" stage of each step, but there is no advance, da, of the crack tip. As in the conventional use of plasticity in metal working, such as rolling or extrusion, the formation of new surfaces is not distinguished from the dissipation of energy in general plastic flow. With work hardening, there will be an increase in load and thus in elastic strain energy during this stage. In the absence of a detailed crack tip model with large deformations at the tip itself, the separation stage, taken as a micro-instability, must contain the energy both to stretch the micro-ligament plastically and then to drive the instability. There must therefore be plastic flow around the tip during this second stage, which, since the process is taken at fixed displacement, must be driven by "release" of elastic energy. In short, the second stage is akin to the Irwin - Orowan model for engineering lefm and contains a much larger change in elastic energy than just that to drive the instability itself. However, despite that working picture, it is not clear in reality how much, if any, new crack surface is formed in this stage, since the micro-ligament might neck to a point or to some void growth and separation on a finer scale. In three dimensions, these two stages of growth will, of course, be merged by random variations of micro-structure through the thickness.

2.3. Some features of the model; R-curves, initiation and instability

2.3.1. R-curves. The energy dissipation rate, D, is seen as the true mechanical meaning of crack growth resistance. It is identical to G for strict lefm, where G and D must be constant with crack growth. In engineering lefm, where some amount of yielding is implied, J is usually taken to be similar to G as enhanced by a correction for plastic zone size. D is conceptually the same as the enhanced value of G but differs slightly according to the a/W ratio as the plastic zone correction becomes larger. In full plasticity, D differs from J very significantly, as shown Fig. 2. After initiation, J is usually represented by a so-called J_R-curve

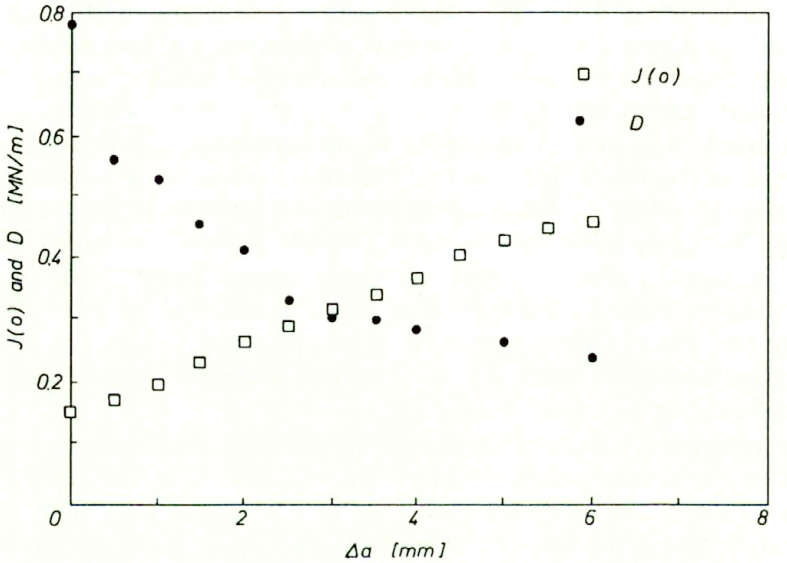

FIG. 2. An example of a conventional rising J-R-curve and of the energy dissipation rate, D, for quasi-static fully plastic ductile crack growth, after [14].

that rises with growth. In general, D reduces rapidly with growth as the load on the remaining fully plastic ligament gets smaller, although for high hardening materials, there is sometimes a region of rising D where the increase in load, due to hardening, more than offsets the reduction in remaining width. It is clear that D/b is akin to dJ/da in that both are d/Bda rates, whereas the only energetic meaning of an experimental J derived from the area of the loading diagram is a normalised cumulative energy, not a d/Bda rate. These relationships, together with discussion on a characterising rather than energetic meaning of J_R (where the former retains the factor η in the normalisation of area whereas the latter does not) are discussed more fully in [21].

2.3.2. Initiation. Initiation has not been closely studied. Conceptually it is seen as the first occurence of damage leading to void growth followed by micro-instability, but all the relevant values are different from later steps in growth because there

has been no prior region of intense crack tip damage. Despite the recent Two Parameter models for initiation, such as [22, 23], data shown in [22] present no effect of constraint on COD for "zero" growth. The effect of constraint is seen when COD is defined at some small amount of growth, here interpreted as CTOA, albeit in the transient regime before a steady state of growth becomes established. In [19] the COD at "zero" growth was also near independent of configuration, but after a small transient regime the steady state CTOA was clearly configuration-dependent (about twofold higher for centre cracked tension than for deep notch bend or compact tension for the low strength steel used). Any conflict between the present and Two Parameter models over the constraint dependency of initiation is thus apparent rather than real, according to the terminology used, COD or CTOA, to characterise small amounts of growth. A simple CTOA model for the transient regime, to connect a known initiation COD and steady state CTOA, is given [24].

2.3.3. Final ductile instability. With plasticity, the change in elastic energy during each step in growth is larger than $GBda$ but less than $BJda$, since the "release" cannot be less than the linear case nor more than the nonlinear elastic case. For the elastic-plastic case the "release" written [25] as $BI\,da$, is

$$I = G + G^*.$$

The energy rate G is the lefm term that drives fracture in the Irwin–Orowan sense. The energy rate G^* passes to plasticity, perhaps such as in the plastic wake, additional to the plasticity of general plastic flow and damage in the first stage of growth. The source of the extra elastic change is that at fixed displacement, q, there is an interchange of movements, $dq_{\mathrm{pl}} = -dq_{\mathrm{el}}$, that cannot of course occur in the strict lefm case. This G^* term is dependent on the compliance of the whole system over which the fixity is taken for the separation stage and leads to the system dependence of final ductile instability, as discussed [26].

3. Dynamic crack growth

3.1. The model used

The availability of the energy in the system, and indeed in the more remote parts of a test specimen, depends on the crack speed so that if applied to other than ductile growth, the present concepts must be treated with caution; they were developed explicitly for the micro-ductile situation. If they were to be applied to brittle fracture, not only is the micro-model described above inappropriate, but the crack speeds would have to be limited to some small fraction of the Rayleigh wave speed to minimise inertia effects in the specimen. Perhaps more significantly, inertia in the testing system might also be relevant, since any sustained force on the system might not be transmitted to the test section during crack growth. In

the limit of high speed fracture only the length-independent G term is available to drive the crack, as in lefm.

In reality, the development of the dynamic treatment outlined below took place quite separately from the quasi-static model just described. As a matter of routine, in all uses of the two-dimensional elasto-dynamic program, [5], conservation of energy was monitored. The only terms were the strain and kinetic energies and the energy dissipated through the "hold-back" force, applied as the tip node was released. A three-dimensional program became available, based on WHAMSE, [27]. It encompassed elasto-plastic dynamic growth with finite displacements and used plate and shell elements of "hour-glass" type. A constant strain 8-node hexahedral "brick" element is well known but a number of unsatisfactory features exist, [4], for example zero bending and torsional stiffness. These features were rectified as suggested in [28] and the improved elements with realistic stiffnesses incorporated into a modified program, WHAMSE2. Application was then made to various dynamic crack problems. The program can be run in either "generation" or "application" mode. In the latter, one of a variety of parameters such as J, U (work), CTOA and so on is specified as a function of crack growth. The crack speed is then the output. The program has been used mainly in the "generation" mode where a crack speed is specified and a toughness parameter generated. In two-dimensional studies, its value was derived from the sum of the nodal "hold-back" work and the local plastic dissipation, divided by the area of crack growth. Any plasticity not connected to the crack tip was excluded from the sum. The use of this sum as the measure of toughness is clearly consistent with the energy dissipation rate, D, as described for quasi-static crack growth. In the studies made, it is independent of element size, although the "hold-back" work itself is not. The limited amount of plasticity in many cases allowed the toughness to be seen as a dynamic value of G so that a more general interpretation for extensive plasticity did not arise.

3.2. An application to the double tension test

3.2.1. A two-dimensional analysis. In the double tension test, a small secondary piece extends from the side of a conventional tension plate, connected by a small neck of material. The secondary piece is then loaded by tension or split by a wedge to introduce a running crack into the edge of the main test plate, Fig. 3. Experimental data on several different structural steels had been reported, [29a], for a series of tests on plates about 1 m wide by 1.5 m long. The starter tab had side grooves that extended some 100 mm into the main plate. In some tests a complete fracture occurred whilst in others, under slightly less arduous conditions of temperature and tension, crack arrest occurred. In certain 50 mm thick plate the arrested cracks stopped almost at the end of the side grooves but showed appreciable tunnelling in which the centreline of the crack was from 27 to 42 mm in advance of the surface length.

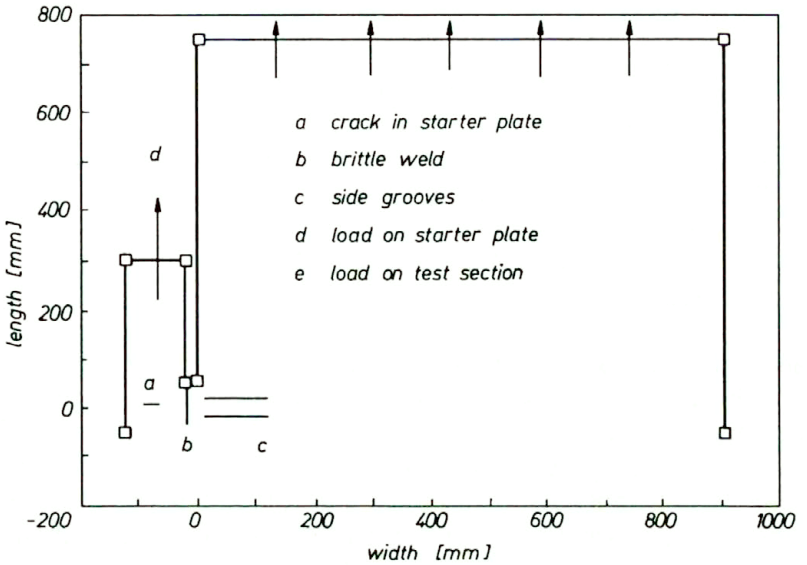

FIG. 3. The double tension test arrangement as used in [29a].

Results of a two-dimensional elasto-dynamic analysis using the program in [5] were reported [29b]. The input data was the nominal crack speed as reported from breaking wires attached to the surface of the plates, about 500 m/s. For the first series at 50 mm thick, the crack speed wires embraced crack lengths of only about 300 mm. Dynamic analyses were made for the completely broken plate with boundary conditions of either fixed displacement or fixed load; a static analysis was also made. It was observed that the nodal forces in the "fixed load" case started to differ from those in the fixed "displacement case" at about 300 μs, a time almost exactly that estimated for the irrotational wave to reach and return from the loaded boundary. The two dynamic estimates, expressed as K_D, were similar and about 10% below the static estimates for the first 200 mm growth, but thereafter the computation for the "constant load" case reached and appreciably exceeded the static value, whilst for the "fixed displacement" case, it converged to the value in the static case. The value of K_D by any of these measures for the 50 mm thick plate, appeared to increase from about 100 MPa$\sqrt{\text{m}}$ at the start of the crack run to about 200 Mpa$\sqrt{\text{m}}$ towards the end of the input data at about 300 mm growth. In short, in so far as estimating G_D was an objective, the analysis appeared reasonable and indeed showed little need for dynamic treatment.

Analysis of the arrested crack cases and of other tests on different steels and thicknesses where the crack wire data embraced nearly all the plate width, were less promising. For the arrested crack cases, K_D oscillated around the static value by about ±15% but both the static and mean dynamic values were uncertain at about the same level because of the uncertainty in the effective crack length with tunnelling. The dynamic data in some tests showed much scatter corresponding

to very erratic input crack speeds from the breaking of the timing wires. Records of strain gauges placed near the crack path allowed a reasonably smoothed crack speed history to be constructed, from which smoothed input a reasonable dynamic analysis was made. The overall pattern was of K_D rising with crack growth from about 100 MPa$\sqrt{\text{m}}$ to about 280 MPa$\sqrt{\text{m}}$ for a particular steel over a crack growth of about 350 mm, and then remaining substantially constant until the end of the run at 700 mm growth. This was interpreted as a growth of shear-lips and tunnelling over the first part of the history, followed by a near steady state of growth for the second part.

3.2.2. A three-dimensional model. The main uncertainty in the results just outlined, lies in the enforced lack in two dimensions of a model of crack tunnelling and shear-lip formation, [3]. When the modified WHAMSE2 program came into use, it became possible to model three-dimensional features, such as side-grooves, shear-lips and crack-front curvature, given an adequate experimental description. In fact, only side grooves (where appropriate) and crack front curvature were incorporated. The shear-lip shapes were not known and it was also reasoned that the difference in energy dissipation between flat and oblique shear modes, both ductile, would be rather small. Comparison of predicted surface strains with strain gauges records of the passing crack, was very satisfactory, Fig. 4, for two estimates

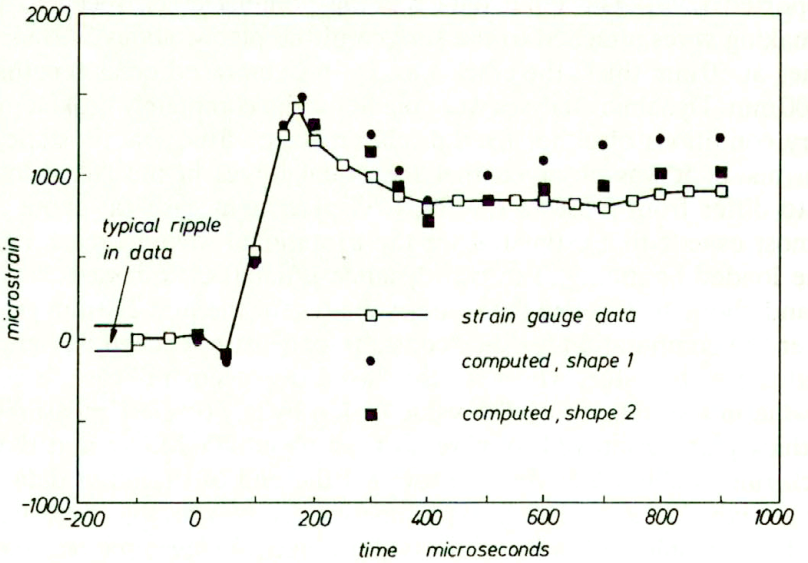

FIG. 4. A comparison of a strain gauge record during dynamic crack growth, from [29a], and the strains computed using the three-dimensional tunnelling model described here.

of the crack front profile. With such an estimated shape, the three-dimensional dynamic calculations showed a virtually constant value of $K_D \approx 155\,\text{MN}\sqrt{\text{m}}$ for crack growth from about 100 mm at entry to the plate to 140 mm before arrest,

whilst the velocity reduced from 370 m/s at the entry of the crack into the main plate to zero at arrest.

For the case of complete fracture in the same material, the crack speed at entry to the plate (still side-grooved) was about 600 m/s. It fell to about 380 ± 20 m/s at a length of about 150 mm (corresponding to where arrest occurred in the other test) and then accelerated to about 500 m/s at 300 mm growth, after which there was no crack speed available. Thereafter the results depend upon uncertain assumptions. Assuming little increase in crack speed, consistent with a nearly constant extent of tunnelling, K_D showed an appreciable increase with further growth, just as in the two-dimensional computations described in Sec. 3.2.1. Allowing for a further degree of tunnelling (up to about 88 mm) caused crack speeds up to about 800 m/s with a modest increase in K_D from 150 MPa$\sqrt{\text{m}}$ at 300 m/s (consistent with the data from the arrested crack case) to about 180 MPa$\sqrt{\text{m}}$ at 800 m/s. But in the absence of more detailed experimental data, there is no guidance on where between the two limits of constant extent of tunelling or constant K_D, these particular tests should fall.

4. Discussion

The computations just discussed show that the WHAMSE2 program, as now developed, gives a very plausible interpretation of certain dynamic experimental data for ductile crack growth and arrest but also shows that this work is a long way from being able to predict the behaviour of a dynamic crack, *a priori*. Nevertheless, a selfconsistent interpretation of experimental data and extraction of effective K_D values seems quite possible for the ductile behaviour and crack speeds investigated, to a level set by the accuracy and detail of the input data available.

In the two-dimensional or straight crack front case, an effective G based on energy dissipated in both nodal release and plastic zone, has been used. To obtain a useful K or G in the three-dimensional case, the mid-section nodal stresses and displacements at the tip, in the y direction perpendicular to the crack plane, were averaged for a pair of crack face nodes in the thickness direction and then multiplied to give, in effect, a local dissipation rate. This was calibrated as an effective G by comparison with the G based on energy dissipation rate for a straight crack front solution of the same problem with the same element size, d_x by d_y, to give

$$G_D = c\sigma_{yy}\delta_y d_x/d_y.$$

Such a calibration constant, c, is no doubt a function of the degree of plasticity, the proportions of the element and perhaps the ratio of kinetic to strain energy.

In the light of the more recent static model described, an interpretation through CTOA would now be explored but in the double tension computations described no attempt was made to do so. Nevertheless, the nodal displacements

used (albeit not based on just the plastic component of opening as seen for the physical model) when divided by the nodal spacing, give a CTOA measure of toughness. In a steady state condition, where the local crack tip stress, σ_{yy}, is constant, the CTOA criterion would be identical to the effective G or K criterion actually used.

In general, where local crack tip stress may vary due to oscillations in kinetic energy and to work hardening, it is not clear whether an energetic view is preferable to the kinematic view implied by CTOA taken as CTOD over a nodal distance. The latter is much more easily applied to curved crack fronts than is an energy rate and is compatible with the conservation of energy statements for the two-dimensional quasi-static treatment of rep material, made in Sec. 2. Arrest would be seen when the applied CTOA did not reach the critical CTOA, but on arrest, large oscillations are seen in elastic energy rather than in CTOA. Reverting to the micro-arguments of Sec. 2.2, it will be recalled that a key feature was that the final stretch, δ_t, was essentially plastic in nature. In the lefm model there is no opening at the tip and the $\sqrt{r}$ dependence of the elastic opening implies that an apparent elastic CTOA modelled by elements of size d would increase according to $1/\sqrt{d}$. In the type of modelling used in this and most other crack growth programs, there appears to be an elastic component of opening (at the nodal distance, d, behind the tip) which does not have a counterpart in the physical model of CTOA described here. Prior to initiation, COD has been modelled in finite element studies by use of the collapsed node element whereby, on loading, an actual displacement occurs at the crack tip. That model was extended to certain problems of crack growth in two dimensions, [30], but has not yet been applied to the study of dissipation rate, CTOA or R-curves, still less to dynamic growth.

5. Conclusions

A recently developed energy dissipation rate model of stable static growth, also expressed in terms of G and a global measure of crack tip opening angle, has been summarised.

A three-dimensional elasto-plastic dynamic finite element program has been outlined and an application given to a ductile crack running and/or arresting in a double tension test.

Despite a number of reservations on the details of how the physical model seen for ductile crack growth is best interpreted for analytical or computational studies, the treatment of dynamic toughness described is consistent with the energy dissipation rate, D, and thus the CTOA model developed for static crack growth, although there is no doubt a critical CTOA is a function of constraint and, in the dynamic case, of crack speed.

The results also show the importance of modelling the essentially three-dimensional feature of crack tunnelling. But the factors of crack speed, crack front profile and variation of toughness with crack speed are all interlinked. To get a full interpretation of a test, a rather detailed set of input data is required, such as of crack speed history together with a number of strain gauge records as the crack passes, because the crack front profile is an unknown shape both as a function through the thickness at any instant of its development with crack advance.

At the present time no *a priori* prediction of dynamic ductile crack growth and arrest can be made beyond a rather general pattern of behaviour.

6. Appendix. Some features of WHAMSE2

Many details of the modified WHAMSE program have not been detailed here. A few remarks are now given.

Work hardening is incorporated in a linear piece-wise manner, although in some experimental data even a dynamic stress-strain curve may not be available. Incorporation of a model of variation of properties with strain rate is quite possible but, as already noted, for the crack speeds in question here, none has been used.

A general validation of the program has been made by comparing results with certain published data, notably the method of caustics data in [31], and with in-house experimental data on cracks running in araldite and impact tests on steel pieces. A static capability has been introduced into what is essentially a dynamic method of solution by allowing the inertia of selected elements to be increased during early stages of loading and then setting the residual velocity components to zero. A very modest degree of damping is also introduced to eliminate spurious oscillations that otherwise develop from numerical round off errors. Checks have then been made with various known two and three-dimensional static solutions.

In the double tension work described, an element of size 6.25 mm along the crack path (about 0.06% of the width) was used in several studies. For that element size, a time step of 0.5 μs was used, about 80% of the critical time step, but of course much smaller element sizes and time steps might be required in other problems. For some of the computations described, using a mesh of 4742 nodes and 2787 elements, the execution time on an IBRM RS6000 work station was just under 30 mins per 1000 time steps or 1 hr per millisecond of real time. For comparison with another program detailed in the literature, [32], a similar dynamic three-point bend test was run. In [32], a running time of 5hr per millisecond of real time was quoted using a CRAY-XMP computer. The present program showed a similar running time when run on a SUN work station of about one tenth of the operational speed of the CRAY.

References

1. H. HOMMA, D.A. SHOCKEY and G. YAGAWA [Eds.], *Dynamic fracture mechanics for the 1990's*, ASME, P.V.P., **160**, 1989.
2. M. KANNINEN and colleagues, G. BUZZICHELLI, G. DEMOFONTI, L. RIZZI, S. VENZI and S. CINQUETTI, *Dynamic fracture mechanics analysis and experimentation for the arrest of ductile fracture propagation in gas pipelines*, [in:] Pipeline Technology Confrence, K.VIV, Antwerpe 1990.
3. C.H. POPELAR, *A quasi-three-dimensional model for crack propagation in materials that exhibit extensive crack tunelling*, [in:] Proc. of the Fourth International Conference on Numerical Methods, A.S.T.M, Philadelphia, 753–766, 1987.
4. P.M. VARGAS and R.H. DODDS Jr, *Three-dimensional inelastic reponse of single-edge notch bend specimens subjected to impact loading*, Report UILU-ENG-**93-2006**, University of Illinois, 1993.
5. P.N.R. KEEGSTRA, *A transient finite element propagation model for nuclear pressure vessel steels*, J. Inst. Nucl. Engngs., **17**, 89–96, 1976.
6. A.P. KFOURI and K.J. MILLER, *Crack separation energy rates in elastic-plastic fracture mechanics*, Proc. Inst. Mech. Engngs., **190**, 48, 571–584, 1976.
7. J.R. RICE, *Some computational problems in elastic-plastic crack mechanics*, [in:] Numerical Methods in Fracture Mechanics, A.R. LUXMOORE and R.J. OWEN [Eds.], Pineridge Press, Swansea, 434–449, 1978.
8. C.F. SHIH, H.G. de LORENZI and W.R. ANDREWS, *Studies on crack initiation and stable crack growth*, ASTM, **668**, 65–120, 1979.
9. H. YUAN and W. BROCKS, *On the J-integral concept for elastic-plastic crack extension*, Nucl. Engng. and Design, **131**, 157–173, 1991.
10. X.J. XIN and M.R. GOLDTHORPE, *Finite element analysis of stable crack growth in compact specimens of A508 steel*, Fat. Fract. Engng. Mater. and Struct., **16**, 1309–1327, 1993.
11. C.E. TURNER, *Energy dissipation rate, CTOA and J-integral models of R-curves*, [in:] Pressure Vessel Integrity, 1993, ASME, P.V.P., **250**, 19–34, 1993.
12. C.E. TURNER, *A re-assessment of ductile tearing resistance*, [in:] Fracture Behaviour and Design of Materials and Structures, Proc. ECF8, D. FIRRAO [Ed.], EMAS, Warley, U.K., vol. II, 933–949 and 951–968, 1990.
13. S. JOHN and C.E. TURNER, *Alternative representations for scaled R-curves in a titanium alloy*, [in:] Defect Assessment in Components: Fundamentals and Applications, ESIS/EGF Pub. 9, J.G. BLAUEL and K.-H. SCHWALBE [Eds.], MEP, London, 299–318, 1991.
14. L. BRAGA and C.E. TURNER, *Energy dissipation rate and crack opening angle analyses of fully plastic tearing*, A.S.T.M. STP, **1171**, 1578–175, 1993.
15. C.E. TURNER and O. KOLEDNIK, *A micro and macro approach to the energy dissipation rate model of stable ductile crack growth*, Fat. Fract. Engng. Mater. and Struct., **17**, 9, 1089–1107, 1994.
16. M. DAGBASI and C.E. TURNER, *Fully plastic ductile tearing of HY 130 steel; an analysis by J, COD, energy rate and crack opening angle*, J. Strain Anal., **30**, 4, 257–289, 1995.
17. L. BRAGA and C.E. TURNER, *Analysis of crack opening angle for large amounts of growth*, Int. J. Frac., **65**, R43–R48, 1994.
18. M.P. WNUK, *Occurrence of catastrophic fracture in fully yielded components; stability analysis*, Int. J. Fract. Mech., **15**, 533–581, 1979.
19. O. KOLEDNIK and H.P. STÜWE, *The stereophotogrammetric determination of the critical crack tip opening displacement*, Engng. Frac. Mech., **21**, 145–155, 1985.
20. G.P. GIBBSON and S.G. DRUCE, *An assessment of various crack tip displacement based elastic-plastic fracture parameters to characterise ductile crack growth resistance*, Int. J. Fract., **35**, 139–151, 1987.
21. C.E. TURNER and O. KOLEDNIK, *Applications of energy dissipation rate arguments to stable crack growth*, Fat. Fract. Engng. Mater and Struct., **17**, 10, 1109–1129, 1994.
22. J. HANCOCK, W.G. REUTER and D.M. PARKS, *Constraint and toughness parameterised by T*, A.S.T.M, STP, **1171**, 21–40, 1993.
23. N. O'DOWD and C.F. SHIH, *Family of crack-tip fields characterised by a triaxiality parameter*, J. Mech. Phys. Solids., **39**, 989–1015, 1991.
24. C.E. TURNER, *Size effects in the ductile crack growth of metals*, [in:] Size-Scale Effects in the Failure Mechanisms of Materials and Structures, IUTAM Conference, [to be published, E. and F.N. Spon, Oct. 1994].

25. M.R. ETEMAD and C.E. TURNER, *An investigation of the I and dJ/da concepts for ductile tearing instability*, A.S.T.M. STP, **905**, 485–502, 1986.

26. O. KOLEDNIK and C.E. TURNER, *Applications of energy dissipation rate arguments to ductile instability*, Fat. Fract. Engng. Mater. and Struct., **17**, 10, 1129–1145, 1994.

27. *WHAMSE: a program for three-dimensional structural dynamics*, Computer Code Manual, Northwestern University Dept. of Civil Enginering, principal authors T. BELYTSCHKO and C.S. TSAY, E.P.R.I. Palo Alto, Report NP-2250, 1982.

28. D. KOSLOFF and G.A. FRAZIER, *Treatment of hourglass patterns in low order finite element codes*, Int. J. for Numerical and Analytical Methods in Geomechanics, **2**, 57–72, 1978.

29. B. HAYES and A.A. WILLOUGHBY, a) *Crack arrest in modern carbon-manganese steels-final report*, b) R.M. CURR and C.E. TURNER, *Appendix A; The numerical analysis of crack propagation and crack arrest in wide plates of C-MN steel*, The Welding Institute, Cambridge, **5554**, 1987.

30. L. XIA and C.E. TURNER, *An improved model for an advancing crack*, [in:] Numerical Methods in Fracture Mechanics, LUXMOORE and OWEN [Eds.], Pineridge Press, Swansea, 79–90, 1990.

31. J.K. KALTHOFF, J. BEIMERT, S. WINKLER and W. KLEMM, *Experimental analysis of dynamic effects in different crack arrest test specimens*, A.S.T.M. STP **711**, 109–127, 1980.

32. T.N. NAKAMURA, C.F. SHIH and L.B. FREUND, *Three-dimensional transient analysis of a dynamically loaded three-point bend ductile fracture specimen*, Office of Naval Research, U.S.A, Report ONR, **0365/3**, Sept. 1986.

MECHANICAL ENGINEERING DEPARTMENT
UNIVERSITY OF LONDON, LONDON, ENGLAND.

Received December 2, 1994.

Arch. Mech., 47, 5, pp. 889–897, Warszawa 1995

Nonlinear effects around the fast running crack tip

M. DRŽÍK (BRATISLAVA)

EXPERIMENTAL INVESTIGATION of stress-strain field around a fast running crack tip in polymer material is decribed. The stress-strain field during the cracking changes rapidly so that viscoelastic properties of polymers have to be taken into account. The analysis of influence of the viscoelastic behaviour of the material on the real values of dynamic stress intensity factor was performed on the basis of the holographically measured near-tip deformation. Although the deformation remains almost the same including high crack tip velocities, the stress intensity factor grows considerably.

1. Introduction

FRACTURE OF THE PROPAGATING CRACK from the point of view of mechanics is a highly complicated phenomenon influenced by a number of factors. Theoretical solutions cannot completely explain some of the effects, such as non-elastic deformation, accumulation of micro-defects, continuity of the cracking process etc. Most of the experimental works aimed at the observation of this dynamic fracture process give an information from the macroscopical standpoint. However, occurence of local flaws in the fracture process zone as well as the properties of material also play a significant role. In this respect, the frequently used optical method of caustics collects its shadow patterns from the region nearest to the crack tip but, due to its nature, the data are limited to some points. The whole field of detailed information about the deformation near the crack tip can be reached by using the holographic interferometry. HOLLOWAY *et al.* [1], ROSSMANITH [2] and also KHESIN *et al.* [3] were the first who studied the fast propagating cracks by means of holography. Their experiments were aimed at the investigation of the dynamic fracture toughness and evaluation of these data from the interference fringes obtained.

In the present paper the holographic interferometry with a high spatial resolving power is used for the measurement of dynamic interference pattern in close vicinity of the running crack tip. The specimens are made of polymeric material, so the viscoelastic behaviour of the material is taken into account. Also a considerable distortion of the fringes close to the moving crack tip was observed.

2. Experiment

In order to obtain the isopachic interference fringes, the experiments have been carried out by the experimental set-up of a holographic interferometer designed for clear transparent objects. In the optical arrangement, the image plane holographic technique is used where the diffusor screen is not included. That is

why the recorded interference pattern can be photographically magnified without any appearance of speckle noise. The holograms were taken by a pulsed ruby laser (694.3 nm), with output power of ~ 50 mJ.

Catastrophic propagation of the cracks has been observed on the three-point bend specimens. These slender beams (220 × 50 × 4 mm) were cut from the sheets of polymethylmetacrylate (PMMA) commercially available as Acrylon. Crack movement starts from an initially short notch by the loading force. This was created by a preliminarily compressed strong coil spring which was gripped tightly by means of a steel wire before start. Mechanical wire breaking produces not only the external load, but also triggers the countdown in the synchronisation block of the laser. Before that, the first exposure of the hologram is carried out with unloaded specimen. After the wire breaking, the external load increases as shown in Fig. 1, where the time history of the load for the whole cracking process, together with the evaluated values of stress intensity factor, is drawn. It can

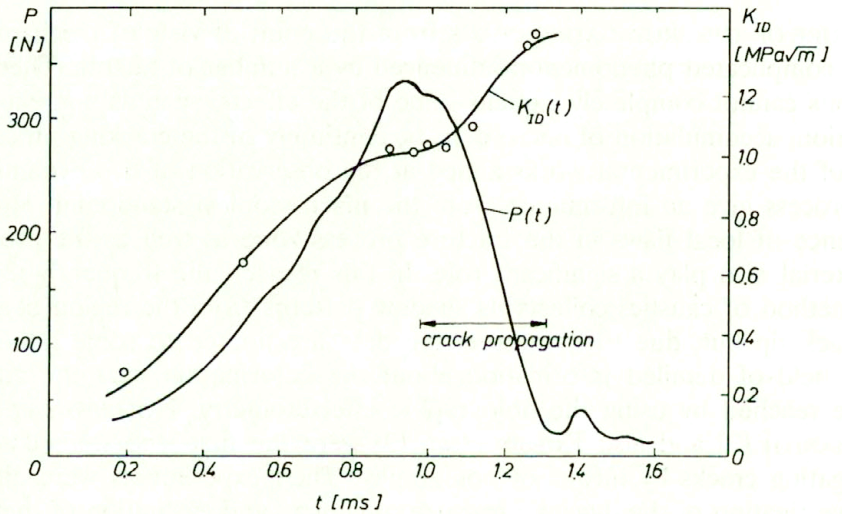

FIG. 1. Experimentally determined values of dynamic stress intensity factor vs. loading force history.

be seen that the loading force (measured by strain gauge) grows monotonically and passes a certain critical region when the crack starts to propagate. In the experiment the loading time to initiation of the fracture took about 1 ms. In this manner the quasi-static conditions of the crack propagation process are secured and the influence of waves reflected from free boundaries of the specimen is negligible. After the lapse of the time interval, the crack tip reaches a position at which the second laser light pulse is flashed. At this second exposure, interference fringes of the instantaneous deformation around the crack are recorded. Crack tip speed at that moment was determined from time intervals between the breakings of graphite conductive lines drawn on the specimen surface, and also from the characteristic microstructure of the fractured surfaces.

An example of the interference pattern obtained at the moment of a fast moving crack is shown in Fig. 2. In the figure the whole field of vision of interferometer is shown.

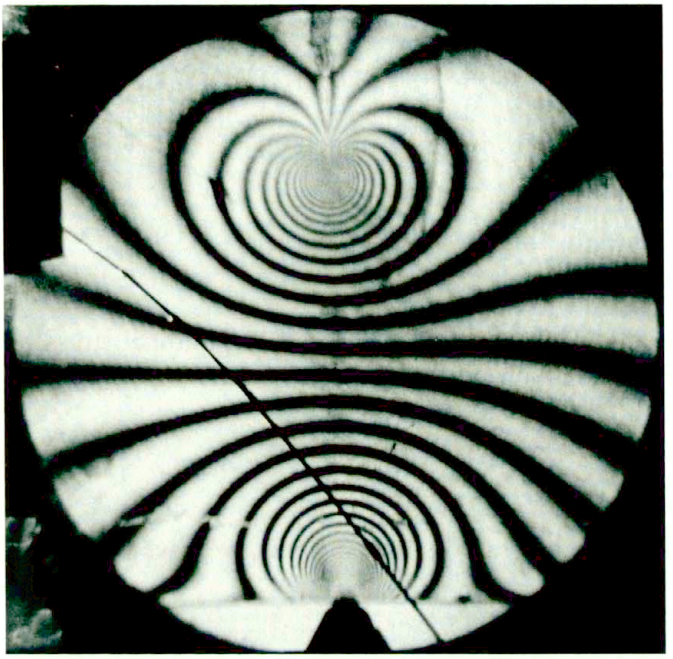

FIG. 2. Isopachic interference pattern in a beam made of PMMA transparent material at the moment of cracking.

3. Evaluation of the dynamic stress field

The interference fringes in Fig. 2 are the so-called isopachics. Procedure of their evaluation is based on the fact that interference fringes visible on the transparent specimen under plane stress conditions are the curves of equal changes of specimen thickness between the unloaded and loaded state. These changes are proportional to the sums of principal stresses, $\sigma_x + \sigma_y$, so we can write

$$\sigma_x + \sigma_y = c_t \frac{N}{h}, \tag{3.1}$$

where N is the fringe order, h is the thickness of the specimen, and c_t is the fringe value. Besides the mechanical parameters, in the case of light propagating through the transparent material, the optical response c_t depends also on the optical properties of the material.

Catastrophic crack growth is a fast dynamic process. In order to evaluate the spatial distribution of the stresses, two main factors have to be taken into account.

If the crack propagates very fast, the velocity of stress wave cannot be regarded as infinite. Thus we have to study the dynamic behaviour of a linear elastic body. The value of the first invariant, under the assumption of constant crack tip velocity, is found by FREUND [4], ABERSON *et al.* [5] from the relationship

$$\sigma_x + \sigma_y = (s_2^2 - s_1^2)\left[\phi_1(z_1) + \overline{\phi_1(z_1)}\right], \tag{3.2}$$

where $\phi_1(z_1)$ is the complex potential function, and

$$s_j = \left[1 - \left(\frac{\dot{a}}{c_j}\right)^2\right]^{-1/2}, \qquad j = 1, 2, \tag{3.3}$$

where c_2, c_1 are the velocities of shearing and longitudinal stress waves, $\dot{a}$ is the crack tip velocity. Assuming the complex stress function $\phi_1(z_1)$ as

$$\phi_1(z_1) = \sum_{n=1}^{\infty} \left(A_{2n-1}\, z^{n-\frac{3}{2}} + A_{2n}\, z^{n-1}\right), \tag{3.4}$$

where A_{2n-1}, A_{2n} are arbitrary real coefficients, we have

$$\sigma_x + \sigma_y = 2(s_2^2 - s_1^2) \sum_{n=1}^{\infty} \left[A_{2n-1}\, \varrho^{n-\frac{3}{2}} \cos\left(n - \frac{3}{2}\right)\vartheta + A_{2n}\, \varrho^{n-1} \cos(n-1)\vartheta\right]. \tag{3.5}$$

In this expression ϱ, ϑ are the polar coordinates which are following the running crack tip. The dynamic stress intensity factor K_{ID} was defined by FREUND [4] as

$$K_{ID} = -\frac{4 s_1 s_2 - (1 + s_2^2)^2}{(1 + s_2^2)} \cdot \sqrt{2\pi} \cdot A_1 . \tag{3.6}$$

After a short analysis of this expression, when real values of maximum crack tip velocities are considered (i.e. the value of $\dot{a}/c_R$ does not exceed 0.2 – 0.3), a very small dynamic correction factor (a few percent) can be found. As a rule, such small correction is of the order of experimental uncertainty and of the measurement errors.

The viscoelastic properties of polymers is a much more important factor. It is well known that all polymers creep under the load. In particular, such polymer as PMMA presents high strain-rate dependence. An assessment of the influence of viscoelasticity on the strain field pattern can be made by comparison of the experimentally obtained interference fringes with the results computed theoretically for viscoelastic environment at different values of the viscoelastic parameters.

However, the complete solution including many parameters of real material may be complicated. The determination of differences between the theoretical solution for a linear elastic material and the results of experiments carried out on the specimens made of viscoelastic polymer material may be an easier way.

The problem under consideration is as follows. The loading force is quasi-statically increasing (Fig. 1), and the deformation around the crack is growing, too. Then the crack starts to propagate and this propagation is rapidly accelerating to the crack tip velocities of about 400 m/s and, at the end of the path, it remains nearly constant. Due to viscoelastic behaviour of the material, the crack tip is situated in a medium which seems to be increasingly stiff.

The concept of linear viscoelasticity is based on the following approximate assumption. For a stress gradient of amplitude σ_0 which rises sinusoidally with a constant angular frequency ω

$$\sigma(t) = \sigma_0 \exp(i\omega t), \tag{3.7}$$

the material response can be written in the form

$$\varepsilon(t) = \varepsilon_0 \exp[i(\omega t - \varphi)], \tag{3.8}$$

where φ is phase angle of time delay of $\varepsilon(t)$ after $\sigma(t)$. The effective complex modulus of the material is defined as

$$E^* = E_1 + iE_2 = \frac{\sigma_0}{\varepsilon_0} \exp(i\varphi). \tag{3.9}$$

If the stress is an independent variable, the deformation at any time t is determined by the expression

$$\varepsilon = \frac{\sigma}{E} + \frac{1}{E} \int_0^t \psi(t - \tau) \frac{d\sigma}{d\tau} d\tau, \tag{3.10}$$

where $\psi(t)$ is the creep function and E is the relaxation modulus of elasticity.

As a result, the constant phase shift over the whole field causes that the strain field will be followed by the same spatial stress distribution. However, the quantitative stress-strain relation will be described by the complex modulus of material for the given frequency of the loading pulse.

The analysis of the shape and distribution of isopachic fringes obtained experimentally was performed. An example of comparison of the fringes with a theoretical solution is shown in Fig. 3. This is the case of the crack tip neighbourhood at the moment of velocity of about 400 m/s. The quasi-static singular solution is drawn by dashed line. As we are proceeding from the crack tip, the layout of separate fringe curves on the whole pattern shows the shift of the curves one after the other in the direction of crack propagation. The curves, and consequently the deformation, further away from the point of the crack tip remain

behind those close to the crack tip. The extent of the zone is limited by the dimension < 2.0 mm (for $r/h < 0.5$) as it is known from the analysis of ROSAKIS and RAVI-CHANDAR [6]. On the other hand, the outside contour of the transient zone ends at points where the influence of non-uniform beam-like farfield loading stress distribution becomes noticeable.

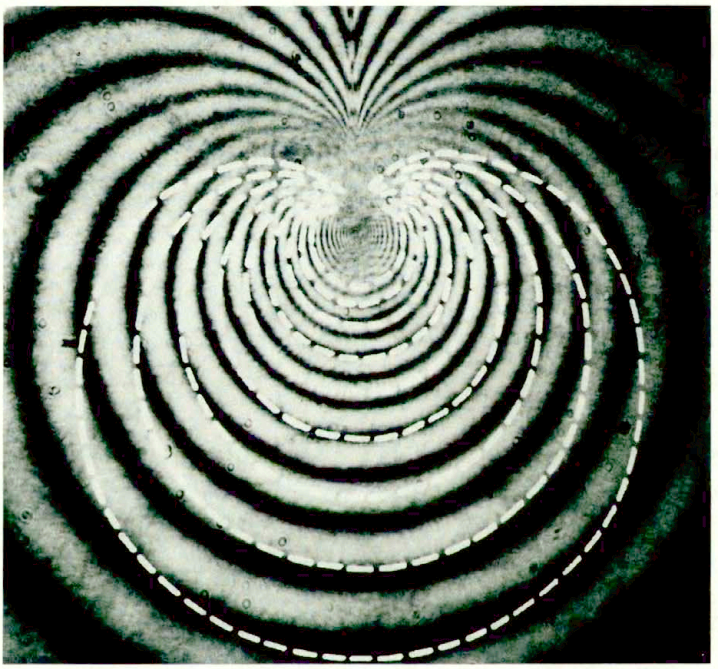

FIG. 3. Comparison of experimental isopachic fringe pattern around the crack tip moving at the velocity of about 400 m/s with that calculated from quasi-static singular solution.

The distortion of fringes visible in the part of the pattern in the near vicinity of the crack tip is caused by the three-dimensionality of the stress field. This shape of the fringes can be observed also in the case of static loading conditions. However, in the transient zone, where the singular term is dominating and 3-D effects are reduced, there is a certain similarity between the shape of curves experimentally obtained and the curves calculated from the quasi-static singular solution. This phenomenon could be explained by the extent of the stress intensity factor field under transient conditions as it is described below. A higher order asymptotic expansion of the crack tip field was obtained for transient crack growth by FREUND and ROSAKIS [7]. The leading term is the stress intensity factor contribution, and the higher order terms take into account the history of the stress intensity factor and the crack motion. At the increasing slope of the time dependence of the stress intensity factor, the transient solution provides a similar pattern of deformation, as it can be seen in Fig. 3.

However, this reasoning may exclude the possibility of non-linearities in the viscoelastic behaviour of the material. A real PMMA material does not exactly obey the linear viscoelasticity theory as that described above. In fact, a considerable residual deformation may occur due to a long-lasting period of creep. This effect is probably observable behind the crack tip, near the crack faces. Obviously, to separate exactly these phenomena, new investigations will be needed.

Another important question which deserves attention is the evaluation of the real value of the dynamic stress intensity factor. As it was mentioned above, at higher loading rates the material parameters change, so the fringe value in expression (3.1) also changes. An expression for the optically inert transparent material such as PMMA may be derived from the optical path difference of interfering light wavefronts before and after deformation of the specimen

$$\sigma_x + \sigma_y = \frac{\lambda}{c_0 - \frac{\nu}{E}(n_0 - 1)} \cdot \frac{N}{h}, \tag{3.11}$$

where λ is wavelength, c_0, n_0 are the optical constant and index of refraction of the optically inert material, respectively, and E, ν are the material parameters: instantaneous modulus of elasticity and Poisson's ratio. On the basis of experiments under dynamic conditions for such a material as PMMA, we can assume negligible changes of the parameters λ, n_0 and small changes of the optical constant c_0 and Poisson's ratio [9]. Thus, modulus E is the most important parameter which influences the fringe value c_t. It must be noted that holography of transparent specimens measures mainly the deformation changes. By our experience, about 70 percent of all the path difference is due to transversal changes of the specimen thickness, and the rest – to the changes of the index of refraction caused by the stress.

Since the dynamic value of Young's modulus depends on the loading frequency, it was necessary to find the relation between the crack velocity and the time history of deformation near the crack path. An assessment of this relation was performed on the assumption that for the material near the path of a moving crack, passing of a crack tip as a function of time appears as a stress pulse [8]. The amplitude of such stress pulse and the point under consideration may be given by the sum of principal stresses (Fig. 4). Assuming that the crack speed is nearly constant, the deformation around the fast running crack tip may be used to determine the time-dependence of the stress sums (see upper right-hand corner of Fig. 4). The typical frequency of this pulse can be obtained using the Fourier analysis. An example of such frequency spectrum is shown in Fig. 5 for the crack tip velocity of about 400 m/s. As it can be seen, the maximum of the spectrum is situated close to the frequency of about 40 kHz. The value of the modulus of elasticity for PMMA Acrylon in the region of such frequencies exceeds 6300 MPa, in comparison with its static value of 3400 MPa [10]. Then, the dynamic fringe value for isopachic evaluation will exceed its static counterpart by 45 percent.

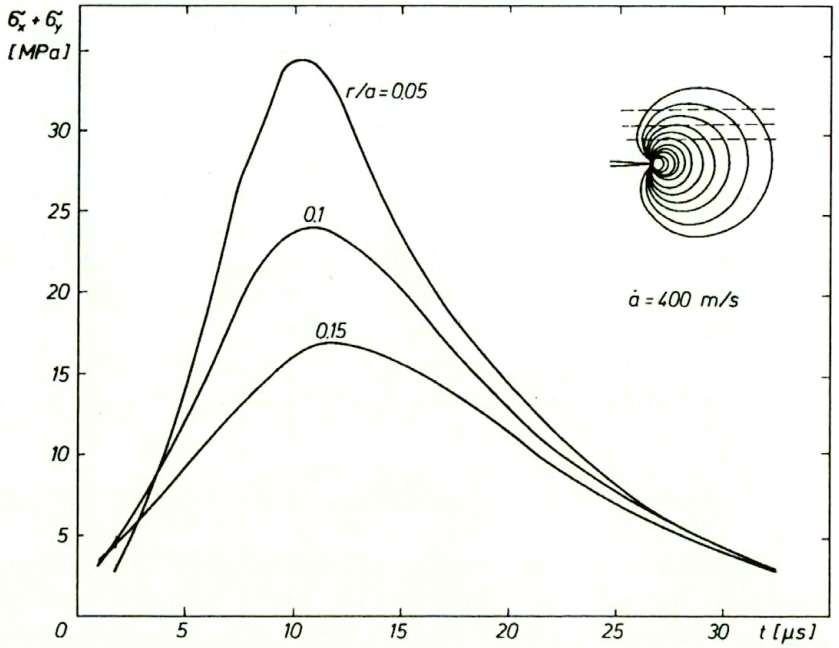

FIG. 4. Stress pulse at three points near the crack path produced by a passing by crack tip.

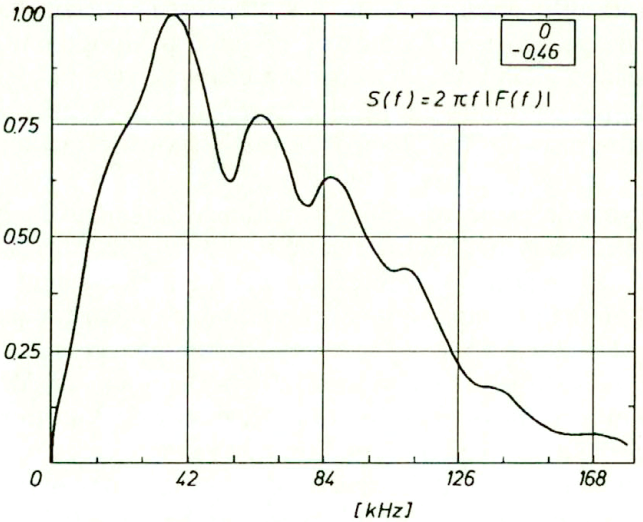

FIG. 5. Frequency spectrum of the stress pulse created by a fast moving stress field around the crack tip.

Using this procedure, true values of dynamic stress intensity factor were obtained for different velocities of the propagating crack. These results are drawn in Fig. 1, where also dependence of that factor on the applied loading force can

be deduced. As it can be seen, the dynamic stress intensity factor does not remain constant but it grows substantially with increasing crack tip velocity.

4. Conclusions

Taking into account the viscoelastic properties of the specimen material, the important corrections to the actual values of the stress intensity factor obtained from experimental data, as well as to the time-dependences must be realized. These corrections are substantial and may reach some tens of percents.

It has been shown that the field of transversal deformation on the cracking specimen under plane stress conditions is retarded with respect to the field of sums of principal stresses, in accordance with the theory of viscoelasticity. Moreover, around the crack tip moving with higher velocities, certain irregularities in the deformation were observed which cannot be explained within the framework of linear viscoelasticity.

References

1. D.C. HOLLOWAY, V.K. DER, W.L. FOURNEY, *Dynamic fracture toughness determination from isopachics of a running crack*, Proc. 6-th Int. Conf. Exp. Stress Anal., VDI - Berichte Nr. 313, München, pp. 71–76, 1978.
2. H.P. ROSSMANITH, *Dynamic stress-intensity-factor determination from isopachics*, Exp. Mech., **19**, 281–285, 1979.
3. G.L. KHESIN, V.N. SACHAROV, I.V. ZHAVORONOK, A.A. DIAROV, V.I. KHE, *Investigation of dynamics of crack growth by photoelasticity and the polarising holographic interferometry* [in Russian], Proc. Statics, Kinetics and Dynamics of Cracks, G.L. KHESIN [Ed.], Moskva, pp. 169–190, 1988.
4. L.B. FREUND, *Crack propagation in an elastic solid subjected to general loading – I, II*, J. Mech. Phys. Solids, **20**, 129–140, 1972.
5. J.A. ABERSON, J.M. ANDERSON, W.W. KING, *Dynamic analysis of crack propagation in elastic solids*, [in:] Elastodynamic Crack Problems, G.C. SIH [Ed.], pp. 72–85, 1977.
6. A.J. ROSAKIS, K. RAVI-CHANDAR, *On crack-tip stress state: An experimental evaluation of 3-D effects*, Int. J. Solids and Struct., **22**, 121–134, 1986.
7. L.B. FREUND, A.J. ROSAKIS, *The structure of the near tip field during transient elastodynamic crack growth*, J. Mech. Phys. Solids, **40**, 699–712, 1992.
8. R. SCHIRRER, *The effects of strain-rate-dependent Young's modulus upon the stress and strain fields around a running crack tip*, Int. J. Fracture, **14**, 265–279, 1978.
9. D.D. RAFTOPOULOS, D. KARAPANOS, P.S. THEOCARIS, *Static and dynamic mechanical and optical behaviour of high polymers*, J. Phys.D.: Appl. Phys., **9**, 869–877, 1976.
10. G. MARTINCHEK, *Some problems of dynamics of viscoelastic bodies* [in Slovak], Report SPZV III-6-8/18, USTARCH SAV, Bratislava 1974.

INSTITUTE OF CONSTRUCTION AND ARCHITECTURE
SLOVAK ACADEMY OF SCIENCES, BRATISLAVA, SLOVAK REPUBLIC.

Received December 2, 1994.

Arch. Mech., 47, 5, pp. 899–914, Warszawa 1995

On fast crack propagation in viscoplastic materials

S. HEIMER, J. HOHE and D. GROSS (DARMSTADT)

A FAST PROPAGATING semi-infinite crack in an infinite body is examined by two different models using a Perzyna-type viscoplastic constitutive equation. In the first part, the crack tip fields of a fast crack in a viscoplastic power law hardening material are investigated. Application of a separation technique leads to a system of ordinary differential equations which is solved by a multiple shooting method. In the second part, a damage yield strip model for fast stationary crack growth based on Gurson's continuum damage model is developed. The obtained system of integral equations is solved by a finite difference scheme. Both approaches are illustrated by some examples.

1. Introduction

IF INELASTIC MATERIAL behaviour is considered in conjunction with rapid deformation, rate effects cannot be neglected. Therefore, in many cases the use of viscoplastic material models is necessary.

The importance of calculating the crack tip fields for moving cracks in such materials has established numerous methods to solve the field equations for power law hardening material models. A lot of work has been done to investigate creep crack growth by HUI and RIEDEL [6], RIEDEL [15], STAMM and WALZ [16, 17], CHANG, POPELAR and STAAB [1], LI and NEEDLEMAN [8], HUI and WU [7]. In comparison, there exist only few works on rapid crack propagation. Some analytical results can be found in [9], while purely numerical treatments based on the finite element method are given by ÖSTLUND [12] and DENG and ROSAKIS [3].

In the first part of this study the "classical" multiple shooting method is used to solve the problem of dynamic crack growth. Use of a special optimization routine that doesn't calculate any derivatives leads, in conjunction with a Runge–Kutta-method, to a very stable numerical scheme. It allows the solution of problems with arbitrary material parameters for plane stress, plane strain and antiplane shear. After calculation of stresses and strains, further investigations can be carried out to draw some conclusions about the direction of crack propagation, the unloading zone, the viscoplastic part of the strains and the relation between the applied load and the crack tip velocity.

Another relatively new approach to consider fracture problems is the description of the fracture process by a damage model. Thus, the fracture process is described by the material constitutive equation itself. Consequently, no external fracture criterion is needed. In the range of damage models available in literature, the model proposed by GURSON [5] has been very successful. It describes the damage process by nucleation, growth and coalescence of microvoids and uses

the void volume fraction f as a damage parameter. Compared with other models, Gurson's model has the advantage of being founded very well on a physical consideration. In the present study, this model has been employed in modified form as given by TVERGAARD and NEEDLEMAN [19, 20, 21].

The direct application of the modified Gurson model yields a very complicated boundary value problem. To avoid the resulting difficulties, ZHANG and GROSS [22] presented a simple Dugdale - Barenblatt - type yield strip model based on Gurson's model. In [22] it was used to consider stable crack growth and nonrate-dependent plasticity. A similar model for rate dependent plasticity which does not include any damage effects was used by NILSSON *et al.* [11].

In the present study, a damage yield strip model is developed to describe viscoplastic behaviour of the matrix material given by a Perzyna - type constitutive equation [13, 14]. The application of this yield strip model to the rapid crack propagation problem leads to a system of nonlinear integral equations, which is solved numerically by a finite difference scheme.

2. Crack tip fields

2.1. General formulation

To investigate the field quantities at a crack tip we start with the governing equations, the equation of momentum balance

$$\sigma_{ij,j} = \varrho\, \ddot{u}_i\,, \tag{2.1}$$

the kinematics

$$\varepsilon_{ij} = \frac{1}{2}(u_{i,j} + u_{j,i}) \tag{2.2}$$

and the material law

$$\dot{\varepsilon}_{ij} = \dot{\varepsilon}^{e}_{ij} + \dot{\varepsilon}^{vp}_{ij}\,. \tag{2.3}$$

As can be seen, it is postulated that in this case the total strain rate can be split up into an elastic and a viscoplastic part, which is given by a Perzyna-type constitutive equation:

$$\dot{\varepsilon}^{vp}_{ij} = \frac{1}{\eta}\left\langle \frac{\sqrt{J_2'}}{k} - 1 \right\rangle^{n} \frac{1}{\sqrt{J_2'}}\sigma'_{ij}\,, \qquad n \geq 1. \tag{2.4}$$

Here k is the yield stress in shear, η is a viscosity parameter and n is a hardening exponent. The deviatoric part of the stress tensor is given by σ'_{ij} and its second invariant by J_2'.

If stresses and strains are expected to be singular at the crack tip, it is possible to eliminate time as an independent variable. This is done by Galilean transformation into a special coordinate system which is fixed at the tip and moves with the crack velocity $\dot{a}$ (Fig. 1 a):

$$\frac{\partial}{\partial \bar{x}} = \frac{\partial}{\partial x}, \qquad \frac{\partial}{\partial \bar{y}} = \frac{\partial}{\partial y}, \qquad \frac{\partial}{\partial t} = -\dot{a}\frac{\partial}{\partial x}. \tag{2.5}$$

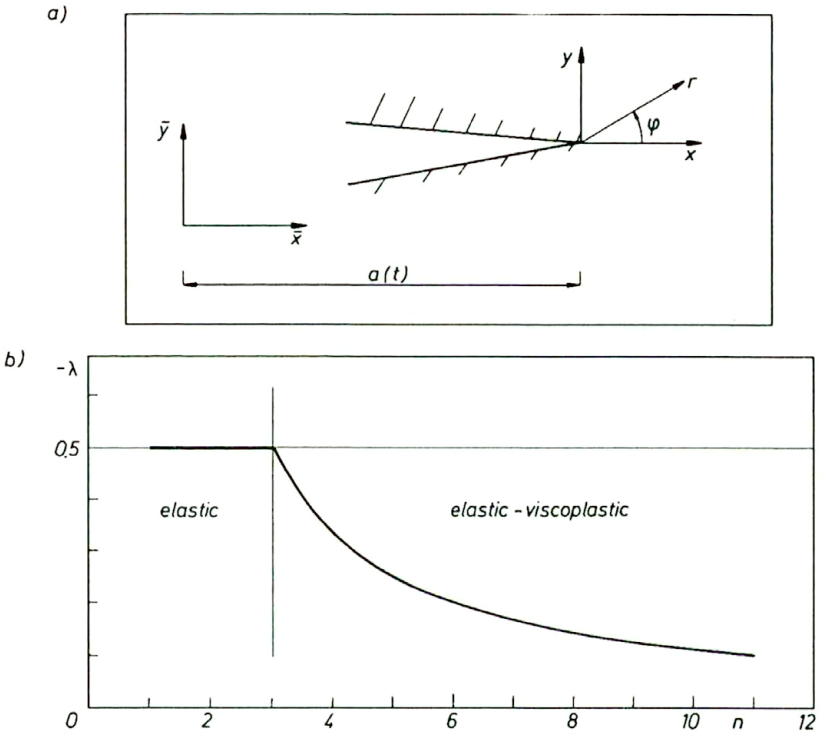

FIG. 1. a) Galilean transformation, b) strength of singularity.

Next, it is assumed that the field quantities can be written in separated form as power series in r. Because of the singularity, only the first term of the series must be considered. This yields the following ansatz for the crack tip field:

$$\sigma_{ij}(r,\varphi) = r^{\lambda}\tilde{\sigma}_{ij}(\varphi), \qquad -\frac{1}{2} \leq \lambda \leq 0. \tag{2.6}$$

The lower limit for λ is a consequence of the postulate that the energy in a small region around the crack tip must be bounded, the upper one guarantees singular stresses. The strength of singularity is directly given by Eqs. (2.1)–(2.4). Following HUI and RIEDEL [6] it is simply found out that the viscoplastic part of the strain rates can never dominate the elastic one. Hence, either the crack tip

fields are described as purely elastic, or both parts of the strain rates have the same singularity. However, λ is a function of the hardening exponent n (Fig. 1 b):

i) $\dot{\varepsilon}^e$ dominates: $\lambda = -\frac{1}{2}, \qquad 1 \leq n < 3,$

ii) otherwise: $\lambda = \frac{1}{1-n}, \qquad n > 3.$

This result leads to the introduction of new dimensionless field quantities:

$$\sigma_{ij}(r,\varphi) = \left(\frac{\eta\,\dot{a}\,k^n}{r\mu^n}\right)^{1/(n-1)} \mu\tilde{\sigma}_{ij}(\varphi),$$

(2.7)

$$u_i(r,\varphi) = \left(\frac{\eta\,\dot{a}\,k^n}{r\mu^n}\right)^{1/(n-1)} r\tilde{u}_i(\varphi),$$

where μ is the shear modulus.

Substitution of (2.7) into (2.1)–(2.4) yields a system of nonlinear differential equations for the angular distribution of stresses and displacements:

$$\mathbf{M}\frac{d\mathbf{Y}}{d\varphi} = \mathbf{f}(\mathbf{Y},\varphi), \tag{2.8}$$

e.g. in case of plane stress

$$\mathbf{Y}(\varphi) = \left(\frac{d\tilde{u}_r}{d\varphi}, \frac{d\tilde{u}_\varphi}{d\varphi}, \tilde{\sigma}_r, \tilde{\sigma}_\varphi, \tilde{\tau}_{r\varphi}, \tilde{u}_r, \tilde{u}_\varphi\right)^T.$$

The solution depends only on the hardening exponent n, Poisson's ratio ν and the Mach number $m = \dot{a}/c_s$, where c_s is the shear wave velocity.

2.2. Numerical solution

Equation (2.8) describes a nonlinear boundary value problem which has some properties that make the solution more difficult. Because matrix **M** is singular at $\varphi = 0$ and $\varphi = \pi$, some differential equations change to algebraic ones. Moreover, very steep gradients can occur in the solution what demands a special integration routine.

First, the problem is transformed into a nonlinear optimization problem by introducing a residuum describing the condition of stress-free crack faces

$$R = \tilde{\sigma}_\varphi^2(\varphi = \pi) + \tilde{\tau}_{r\varphi}^2(\varphi = \pi) \longrightarrow 0. \tag{2.9}$$

Now, (2.8) is solved like an initial boundary value problem by using a suitable starting approximation $\mathbf{Y}_0 = \mathbf{Y}(\varphi = 0)$. The integration is carried out by a Runge-Kutta method of fifth order using an automatic step control. The boundary conditions at $\varphi = \pi$ are controlled by (2.9) and the same procedure is repeated

with a better Y_0 until $R < \varepsilon$. To make the scheme more efficient, the optimization algorithm will be combined with Newton's method, if ε is small enough. This leads to a very stable and powerful multiple shooting algorithm to solve the boundary value problem described above.

2.3. Results

The system of differential equations has been solved for different combinations of parameters n, ν, m. For example, Fig. 2 a shows the angular distribution of the dimensionless circumferential stress $\tilde{\sigma}_\varphi$ in plane stress for $n = 9$. If it is assumed that the direction of crack propagation is determined by Erdogan's and

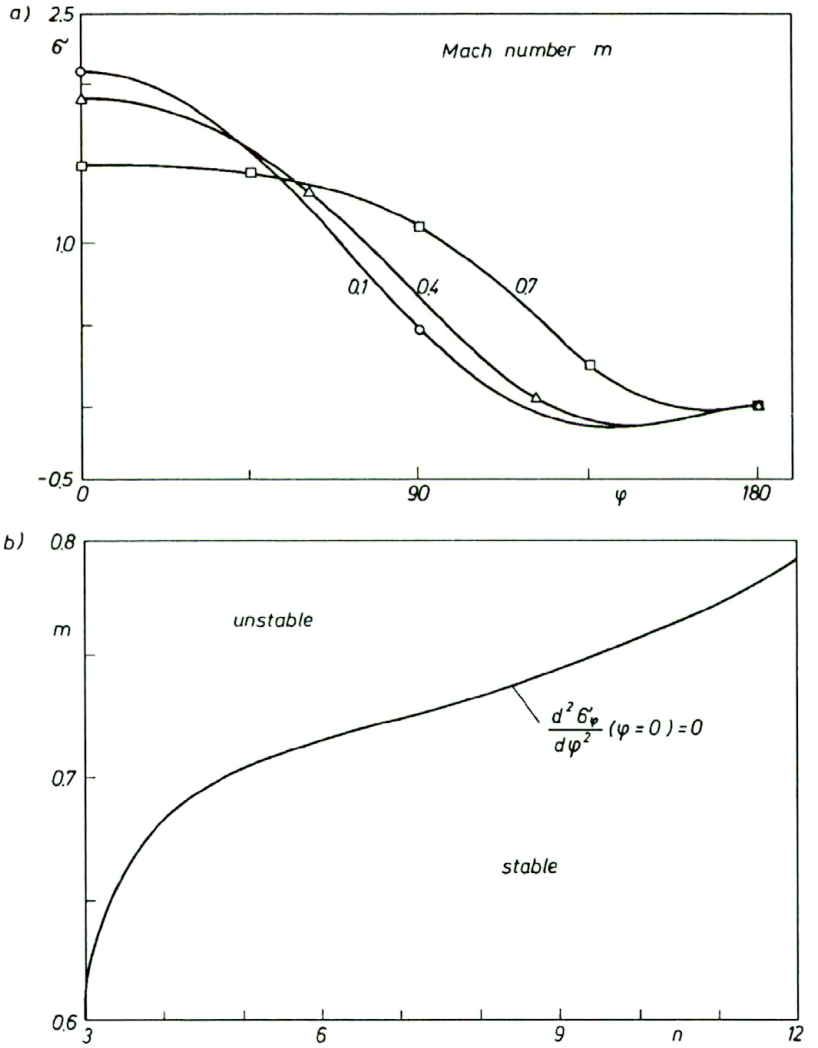

FIG. 2. a) Circumferential stress, b) stability of direction of crack propagation.

Sih's hypothesis of maximum circumferential stress [4], its stability is given by the second derivative of $\tilde{\sigma}_\varphi$ with respect to φ (Fig. 2 b). As can be seen, the assumption of straight crack propagation (2.5) was correct because the crack velocity usually does not exceed $0.6 \cdot m$.

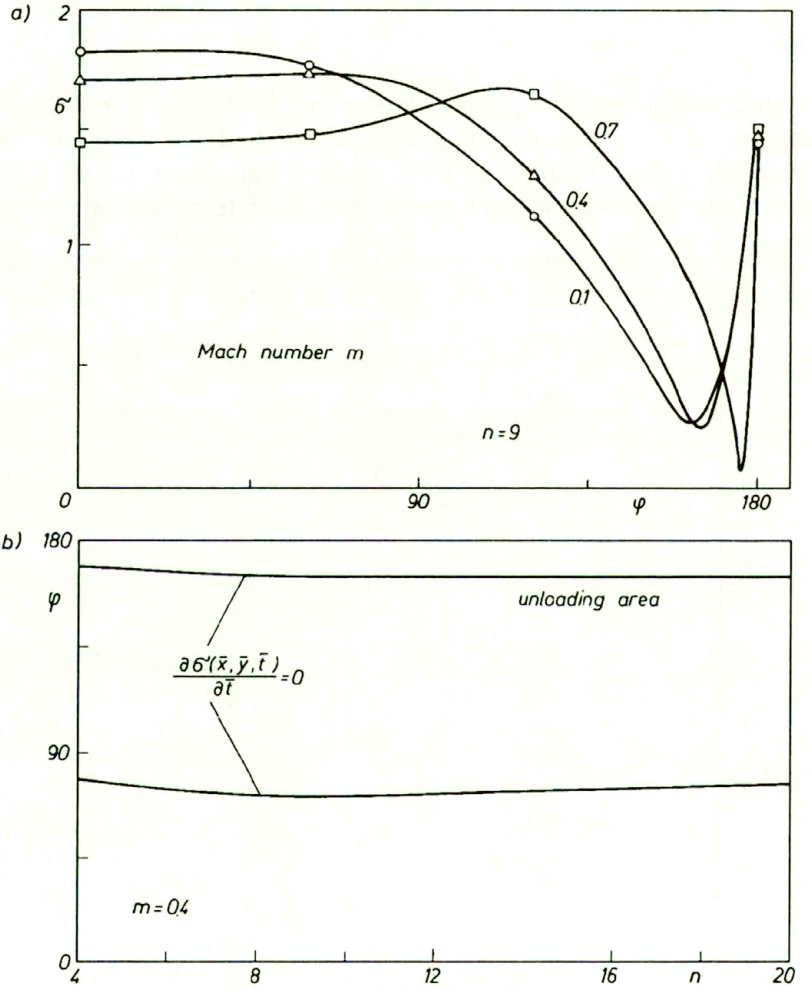

FIG. 3. a) Equivalent stress, b) unloading area.

In Fig. 3 a the angular distribution of the equivalent stress is plotted versus the angle φ again for $n = 9$. The picture clearly shows loading, unloading and reloading areas for different Mach numbers m. The boundaries between the three zones can easily be calculated by

$$\frac{\partial \tilde{\sigma}_e(\bar{x}, \bar{y}, \bar{t})}{\partial \bar{t}} = 0 \tag{2.10}$$

and are represented in Fig. 3 b as functions of the hardening exponent n.

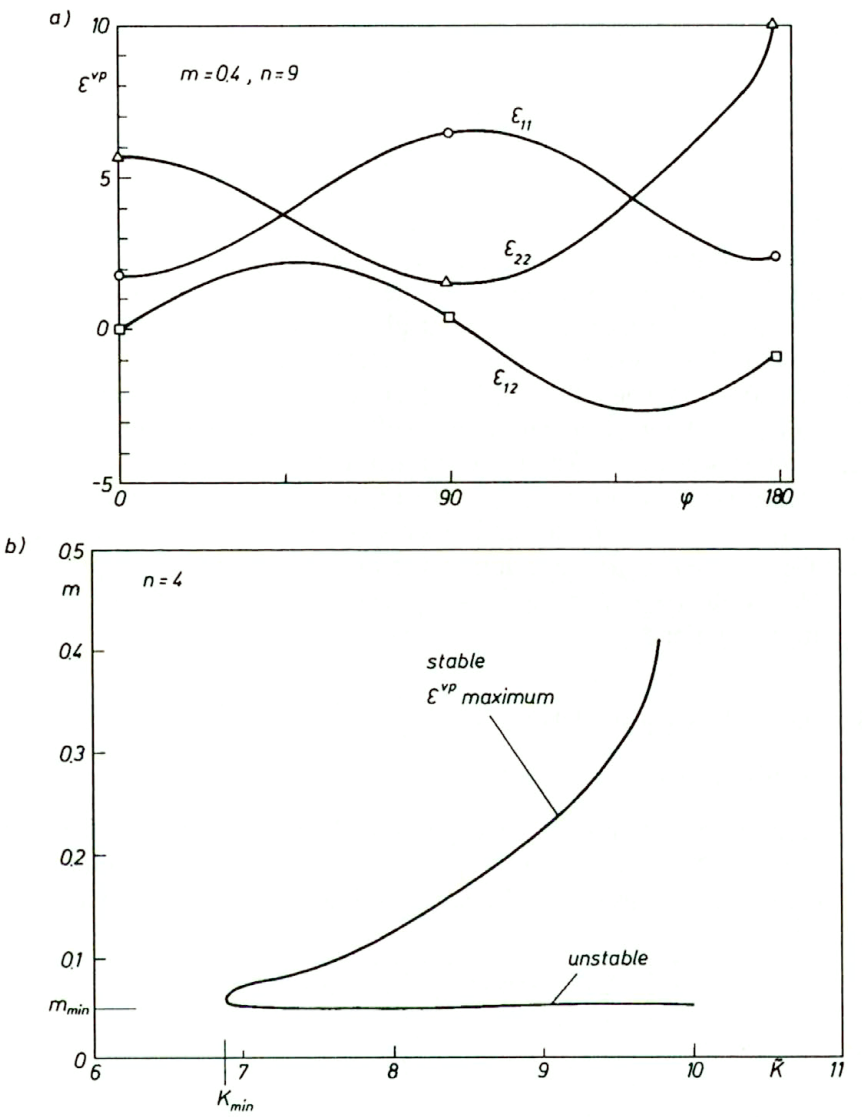

FIG. 4. a) Viscoplastic part of the strains, b) small scale yielding investigation.

Next, the viscoplastic part of the strains is computed. Using (2.4) and the ansatz

$$\varepsilon_{ij}^{vp} = \left(\frac{\eta \dot{a} k^n}{r\mu^n}\right)^{1/(n-1)} \tilde{\varepsilon}_{ij}^{vp}, \tag{2.11}$$

a system of differential equations of the form similar to (2.8) is obtained. It can

be integrated analytically [9] by

$$\tilde{\varepsilon}_{ij}^{vp} = \sin^{1/(1-n)}\varphi \int_0^{\varphi} \frac{\tilde{\sigma}_e^{n-1}\,\tilde{\sigma}'_{ij}\,d\overline{\varphi}}{\sqrt{3}^{n-1}\sin^{\frac{n-2}{n-1}}\overline{\varphi}}, \tag{2.12}$$

but it is more efficient to integrate it using the same algorithm as (2.8). The result is presented in Fig. 4 a. In analogy to quasi-static creep crack growth [6], in the case of small scale yielding a more detailed investigation is possible. Adopting the fracture criterion that the equivalent plastic strain must reach a certain level $\varepsilon_e^{vp} = \varepsilon_{cr}$ at a characteristic distance x_{cr} ahead of the crack tip, it is possible to find a relation between the applied load and the crack tip velocity, which is shown in Fig. 4 b. There is a minimum load and a minimum speed below which no crack growth will occur. The upper branch is stable in the sense that the crack will accelerate or slow down, if its velocity is higher or lower than that given for a certain load level. The lower branch is unstable, because the crack will be arrested for $m < m_{min}$ and accelerate for $m > m_{min}$ until the upper branch is reached. It should be mentioned that ε_e^{vp} will attain its maximum value, if the stable state is obtained.

3. Damage yield strip model

3.1. Constitutive equations

As noted before, Gurson's damage model [5] in modified form given by TVERGAARD and NEEDLEMAN [19, 21] is used to describe the fracture process in the second part of this study. Thus, the following approximate yield condition is used:

$$\Phi = \frac{\sigma_e^2}{\sigma_M^2} + 2q_1 f^* \cosh\left(\frac{q_2\sigma_{kk}}{2\sigma_M}\right) - \left(1 + (q_1 f^*)^2\right) = 0, \tag{3.1}$$

where

$$\begin{aligned} \sigma_e &= \left(\frac{3}{2}\sigma'_{ij}\sigma'_{ij}\right)^{1/2}, \\ \sigma'_{ij} &= \sigma_{ij} - \frac{1}{3}\sigma_{kk}\delta_{ij}, \\ f^* &= \begin{cases} f & \text{if } f \le f_c, \\ f_c + \dfrac{1/q_1 - f_c}{f_f - f_c}(f - f_c) & \text{if } f > f_c. \end{cases} \end{aligned} \tag{3.2}$$

In (3.1)–(3.2), σ_{ij} and σ'_{ij} denote the macroscopic stress tensor and its deviatoric part, respectively, σ_e is the macroscopic equivalent stress, σ_M the equivalent stress of the matrix material, f the actual and f^* the effective void volume fraction; q_1,

q_2, f_c and f_f are material parameters. Note that (3.1) is reduced to the v. Mises yield condition if the void volume fraction f vanishes.

The void volume increment is divided into an increment dependent on the growth of the existing voids and an increment dependent on the nucleation of new voids:

$$\dot{f} = \dot{f}_{\text{growth}} + \dot{f}_{\text{nucleation}}, \tag{3.3}$$

where a superimposed dot denotes partial differentiation with respect to time. In (3.3), the first term can easily be derived from the condition of plastic incompressibility of the matrix material:

$$\dot{f}_{\text{growth}} = (1 - f)\dot{\varepsilon}_{kk}^{vp}. \tag{3.4}$$

According to NEEDLEMAN and RICE [10], the nucleation increment is taken to be of the following form (only strain-controlled nucleation is considered in this study):

$$\dot{f}_{\text{nucleation}} = D\,\dot{\varepsilon}_M^{vp}, \tag{3.5}$$

where $\dot{\varepsilon}_M^{vp}$ denotes the equivalent plastic strain in the matrix material. For D, CHU and NEEDLEMAN [2] have suggested a Gaussian distribution around a certain microscopic equivalent plastic strain ε_N:

$$D = \frac{f_N}{s_N\sqrt{2\pi}}\, e^{-\frac{1}{2}\left(\frac{\varepsilon_M^{vp} - \varepsilon_N}{s_N}\right)^2}, \tag{3.6}$$

where f_N and s_N are material parameters.

As in the previous section, a Perzyna-type constitutive equation is used to describe the microscopic material behaviour:

$$\dot{\varepsilon}_M^{vp} = \frac{1}{\eta}\left(\frac{\sigma_M}{\sigma_0} - 1\right)^n. \tag{3.7}$$

In (3.7), σ_0 is the initial yield stress, n a hardening exponent and η a viscosity parameter. Introduction of the flow rule

$$\dot{\varepsilon}_{ij}^{vp} = \Lambda\frac{\partial\Phi}{\partial\sigma_{ij}} \tag{3.8}$$

and the equivalence of macroscopic and microscopic work rate

$$\sigma_{ij}\,\dot{\varepsilon}_{ij}^{vp} = (1 - f)\sigma_M\,\dot{\varepsilon}_M^{vp} \tag{3.9}$$

yields the macroscopic stress-strain rate relation:

$$\dot{\varepsilon}_{ij}^{vp} = \frac{(1 - f)M_{ij}}{\frac{\sigma_e^2}{\sigma_M^2} + \alpha\frac{\sigma_{kk}}{\sigma_M}} \cdot \frac{1}{\eta}\left(\frac{\sigma_M}{\sigma_0} - 1\right)^n, \tag{3.10}$$

where

$$M_{ij} = \frac{3}{2}\frac{\sigma'_{ij}}{\sigma_M} + \alpha\delta_{ij}\,,$$

$$\alpha = \frac{1}{2}q_1 q_2 f^* \sinh\left(\frac{q_2}{2}\frac{\sigma_{kk}}{\sigma_M}\right). \tag{3.11}$$

By introduction of a macroscopic equivalent plastic strain increment

$$\dot{\varepsilon}^{vp} = \left(\frac{2}{3}\dot{\varepsilon}^{vp'}_{ij}\,\dot{\varepsilon}^{vp'}_{ij}\right)^{1/2} \tag{3.12}$$

Eqs. (3.3) and (3.10) can be rewritten in the form

$$\dot{\varepsilon}^{vp} = \frac{1-f}{\dfrac{\sigma_e}{\sigma_M} + \alpha\dfrac{\sigma_{kk}}{\sigma_e}} \cdot \frac{1}{\eta}\left(\frac{\sigma_M}{\sigma_0} - 1\right)^n, \tag{3.13}$$

$$\dot{f} = \left(\frac{3\alpha(1-f)^2}{\dfrac{\sigma_e^2}{\sigma_M^2} + \alpha\dfrac{\sigma_{kk}}{\sigma_M}} + D(\varepsilon^{vp}_M)\right) \cdot \frac{1}{\eta}\left(\frac{\sigma_M}{\sigma_0} - 1\right)^n, \tag{3.14}$$

which is more appropriate for implementation in a yield strip model (Fig. 5).

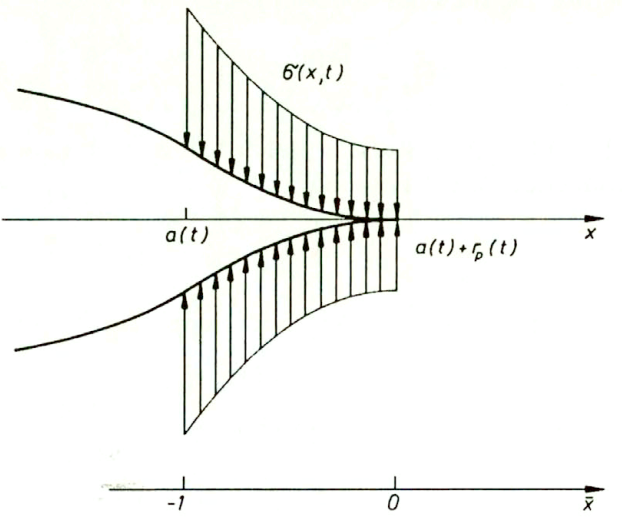

FIG. 5. Yield strip model.

3.2. Yield strip model and numerical treatment

Direct using of (3.1), (3.3) and (3.10) with the kinematic equation and the equilibrium condition or the momentum balance yields a very complicated system of equations which is difficult to solve. Therefore, a simple Dugdale - Barenblatt-type yield strip model (see Fig. 5) is employed. That means, that the crack length $a(t)$ is extended by a certain length $r_p(t)$, which is unknown as yet. Then, a stress $\sigma(x,t)$ is applied to the crack surfaces in the area of this extension. By assumption of a linear relation between crack face displacement in the yield strip area and plastic equivalent strain (using a finite yield strip width b_p)

$$\varepsilon^{vp}(x,0,t) = \frac{2v_y(x,0,t)}{b_p} \qquad \text{if } a(t) \le x < a(t) + r_p(t), \tag{3.15}$$

it becomes possible to implement the viscoplastic part of the constitutive equations (in one-dimensional form) by setting

$$\sigma(x,t) = \sigma_{22}(\varepsilon^{vp}(x,0,t)). \tag{3.16}$$

The out-of-strip area is regarded to be linear elastic. Using this procedure, the elastic-viscoplastic problem is modelled by a linear elastic problem with an extended crack and special, highly nonlinear boundary conditions.

Due to the assumption of linear elastic behaviour in the model problem, the yield strip opening displacement $\delta(x,t) = 2v_y(x,0,t)$ can be determined by superposition of the well known fundamental solutions given in the Handbook by TADA, PARIS and IRWIN [18]. It is obtained in the form

$$\delta(x,t) = 8\frac{K_{Ia}}{E^*}\sqrt{\frac{a(t)+r_p(t)-x}{2\pi}} - \frac{4}{E^*\pi}\int_{a(t)}^{a(t)+r_p(t)} \sigma(x^*)\ln\frac{\sqrt{a(t)+r_p(t)-x}+\sqrt{a(t)+r_p(t)-x^*}}{\left|\sqrt{a(t)+r_p(t)-x}-\sqrt{a(t)+r_p(t)-x^*}\right|}\,dx^*, \tag{3.17}$$

$$E^* = \begin{cases} E & \text{for plain stress,} \\ \dfrac{E}{1-\nu^2} & \text{for plain strain,} \end{cases} \tag{3.18}$$

where K_{Ia} denotes the applied stress intensity factor describing the external load, while E and ν denote Young's modulus and Poisson's ratio, respectively (Table 1).

The length r_p of the yield strip is determined from the condition, that no elastic singularity occurs at the mathematical crack tip ($x(t) = a(t) + r_p(t)$). Therefore, the total stress intensity factor must vanish:

$$K_{Ia} - \sqrt{\frac{2}{\pi}}\int_{a(t)}^{a(t)+r_p(t)} \frac{\sigma(x^*)}{\sqrt{a(t)+r_p(t)-x^*}}\,dx^* = 0. \tag{3.19}$$

Table 1. Material properties.

$E\ \left[\frac{\mathrm{N}}{\mathrm{mm}^2}\right]$	ν	$\sigma_0\ \left[\frac{\mathrm{N}}{\mathrm{mm}^2}\right]$	n	η [s]	b_p [mm]	$K_{Ia0}\ \left[\frac{\mathrm{N}}{\mathrm{mm}^{3/2}}\right]$
$2.1 \cdot 10^5$	0.3	400	6	1.0	0.1	3200
f_N	s_N	ε_N	f_c	f_f	q_1	q_2
0.06	0.1	0.3	0.15	0.25	1.5	1.0

For convenience, a dimensionless coordinate $\bar{x} = (x - a(t) - r_p(t))/r_p(t)$ (see Fig. 5) is introduced. Thus, Eqs. (3.17) and (3.19) are rewritten to the form:

$$\delta(\bar{x}) = \frac{8K_{Ia}}{E^*\sqrt{2\pi}}\sqrt{r_p}\sqrt{-\bar{x}} - \frac{4r_p}{E^*\pi}\int_{-1}^{0}\sigma(\bar{x}^*)\ln\frac{\sqrt{-\bar{x}}+\sqrt{-\bar{x}^*}}{\left|\sqrt{-\bar{x}}-\sqrt{-\bar{x}^*}\right|}\,d\bar{x}^*,$$

(3.20)

$$0 = K_{Ia} - \sqrt{\frac{2r_p}{\pi}}\int_{-1}^{0}\frac{\sigma(\bar{x}^*)}{\sqrt{-\bar{x}^*}}\,d\bar{x}^*.$$

For implementation, the material equations (3.13) and (3.14) have to be rewritten in one-dimensional form. Assuming $\sigma_{22}(\bar{x}) = \sigma(\bar{x})$ is the only non-vanishing component of the stress tensor, the following equations are obtained, definig the relation between yield strip stress $\sigma(\bar{x})$ and yield strip opening displacement $\delta(\bar{x})$:

$$\frac{\partial}{\partial\bar{x}}\delta(\bar{x}) = b_p\frac{1-f(\bar{x})}{\left(\frac{\sigma(\bar{x})}{\sigma_M(\bar{x})}+\alpha(\bar{x})\right)}\cdot\frac{1}{\eta}\left(\frac{\sigma_M(\bar{x})}{\sigma_0}-1\right)^n,$$

(3.21)

$$\frac{\partial}{\partial\bar{x}}f(\bar{x}) = \left(\frac{3\alpha(\bar{x})(1-f(\bar{x}))^2}{\frac{\sigma^2(\bar{x})}{\sigma_M^2(\bar{x})}+\alpha(\bar{x})\frac{\sigma(\bar{x})}{\sigma_M(\bar{x})}} + D(\delta(\bar{x}))\right)\cdot\frac{1}{\eta}\left(\frac{\sigma_M(\bar{x})}{\sigma_0}-1\right)^n,$$

$$0 = \frac{\sigma^2(\bar{x})}{\sigma_M^2(\bar{x})} + 2q_1 f^*(\bar{x})\cosh\left(\frac{q_2\sigma(\bar{x})}{2\sigma_M(\bar{x})}\right) - \left(1+(q_1 f^*(\bar{x}))^2\right).$$

An analytical solution of the system (3.21) is impossible, a numerical scheme must be employed. Therefore, the yield strip is discretized and the integration in Eqs. (3.20) is carried out numerically by using a summarized trapezoidal rule. A nonlinear algebraic system of equations is obtained, which is solved by a Newton-Raphson-method using parameter tracking.

3.3. Example

Numerical calculations have been carried out for the material example given in Table 1 under plane stress conditions. Four different load levels have been examined, the results are plotted in Fig. 6 a-d.

In Fig. 6 a, the yield strip stress $\sigma(\bar{x})$ is presented as a function of the coordinate $\bar{x}$. Starting from the mathematical crack tip $\bar{x} = 0$ at the right-hand side of the plot, first an area is observed, where neither hardening nor softening occurs. In this area, the yield condition is satisfied but nearly no plastic strains are

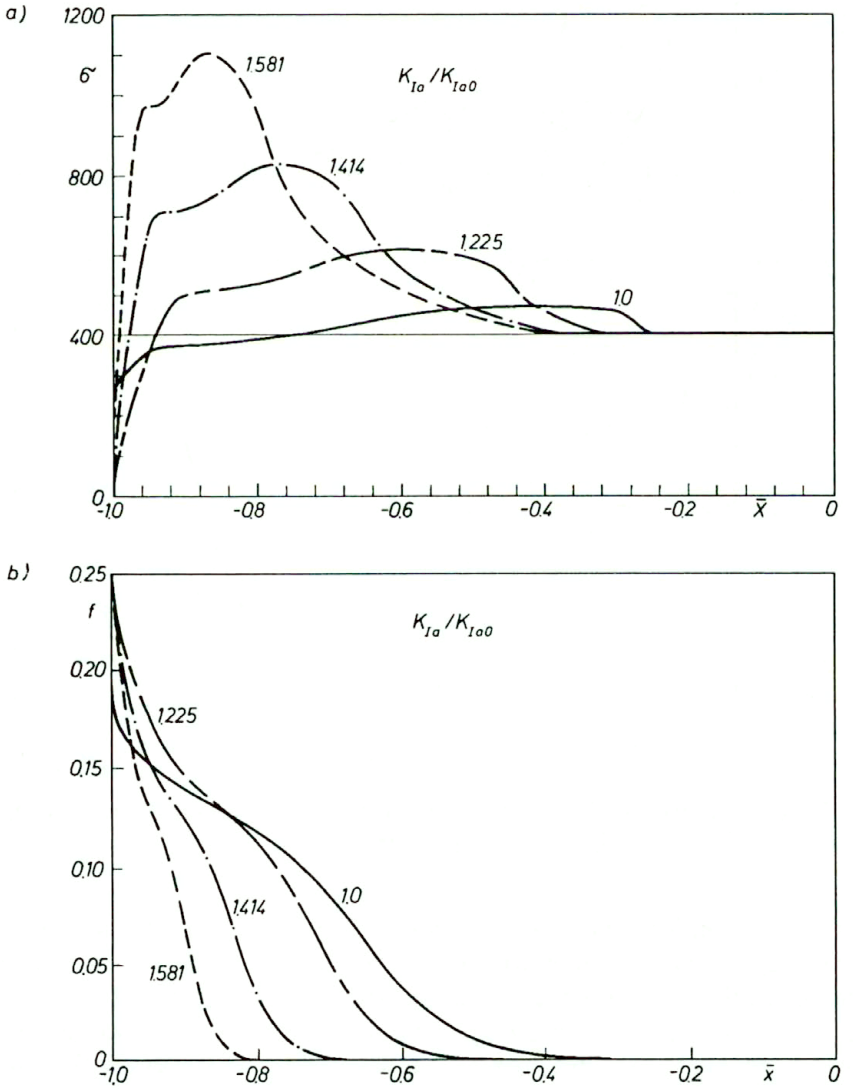

[FIG. 6 a, b]

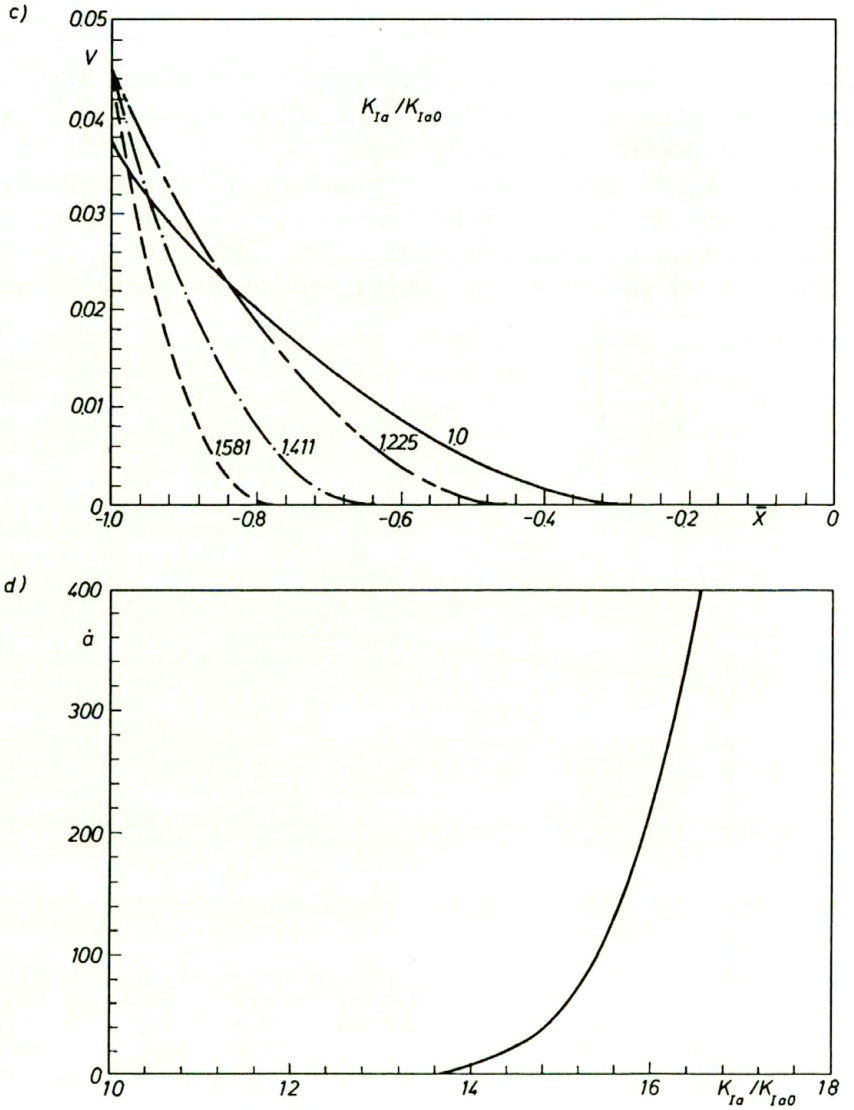

FIG. 6. Yield strip model – results; a) Yield strip stress, b) void volume fraction, c) yield strip opening displacement, d) crack tip velocity.

present. The extended crack remains perfectly closed as can be seen in Fig. 6c. If the yield strip starts to open, the yield strip stress increases due to viscoplastic hardening. On the other hand, the presence of plastic strains results in an increase of void volume fraction (see Fig. 6b). For this reason, the macroscopic yield strip stress reaches a maximum and decreases towards the physical crack tip $\bar{x} = -1$. If the void volume fraction f exceeds the value f_c, the stress gradient becomes very steep. At the crack tip, the void volume fraction f reaches the maximum value

of $f = 25\%$. At this point the stress carrying capacity of the material is totally lost. Note that this value is not reached at the lowest load level $K_{Ia} = K_{Ia0}$. At this load, the level crack propagation is impossible.

The different values of the stress maxima in Fig. 6 a can be explained by the fact, that an increasing load results in increasing crack tip velocity (see Fig. 6 d). Therefore, the strain rate is increasing with increasing load, what yields increasing viscous hardening of the material.

4. Conclusion

In the present study, fast crack propagation has been investigated. Because rate effects often cannot be neglected at high velocities, a rate-sensitive material behaviour described by a Perzyna - type constitutive equation was considered. The problem was investigated by two different models.

First, the crack tip fields were calculated by means of a multiple shooting method. A special optimization routine in conjunction with a Runge - Kutta integration led to a very stable numerical scheme to solve the field equations. Further investigations gave some results on the behaviour of a running crack. Especially it was shown that under small-scale-yielding conditions crack propagation is only possible for a certain load level that governs the crack tip velocity.

In the second part of the study, a damage model was introduced to describe the fracture process. Therefore, no external fracture criterion was needed and a direct relation between external load and crack tip velocity could be determined. To avoid the difficulties of the numerical solution of the very complicated system of constitutive equations resulting from a direct implementation of a damage model into the mechanical field equations, a damage yield strip model based on Gurson's continuum damage model has been developed. By discretization of this model, a very efficient numerical algorithm was obtained. The method was illustrated by calculating a material example.

References

1. T.C. CHANG, C.H. POPELAR and G.H. STAAB, *Creep crack growth in an elastic-creeping material*, Int. J. Frac., **33**, 31–45, 1987.
2. C.C. CHU and A. NEEDLEMAN, *Void nucleation effects in biaxially stretched sheets*, J. Engng. Mat. Tech., **102**, 249–256, 1980.
3. X. DENG and A.J. ROSAKIS, *A finite element investigation of quasi-static and dynamic asymptotic crack-tip fields in hardening elastic-plastic solids under plane stress. Part II*, Int. J. Frac., **58**, 137–156, 1992.
4. F. ERDOGAN and G.C. SIH, *On the crack extension in plates under plane loading and transverse shear*, J. Basic Engng., **85D**, 519–525, 1963.
5. A.L. GURSON, *Continuum theory of ductile rupture by void nucleation and growth. Part I. Yield criteria and flow rules for porous ductile media*, J. Engng. Mat. Tech., **99**, 2–15, 1977.
6. C.Y. HUI and H. RIEDEL, *The asymptotic stress and strain field near the tip of a growing crack under creep conditions*, Int. J. Frac., **17**, 4, 409–426, 1981.

7. C.Y. HUI and K.C. WU, *The mechanics of a constantly growing crack in an elastic power-law creeping material*, Int. J. Frac., **31**, 3–16, 1986.
8. F.Z. LI, A. NEEDLEMAN and C.F. SHIH, *Characterization of near tip stress and deformation fields in creeping solids*, Int. J. Frac., **36**, 163–186, 1988.
9. K.K. LO, *Dynamic crack-tip fields in rate-sensitive solids*, J. Mech. Phys. Solids, **31**, 4, 287–305, 1983.
10. A. NEEDLEMAN and J.R. RICE, *Limits to ductility set by plastic flow localization*, [in:] Mechanics of Sheet Metal Forming, D.P. KOISTINEN [Ed.], 237–267, Plenum Publishing, 1978.
11. F. NILSSON, P. OHLSSON, F. SJÖBERG and P. STÅHLE, *A strip-yield rate-dependent model for rapid loading conditions*, Engng. Frac. Mech., **33**, 429–436, 1989.
12. S. ÖSTLUND, *On numerical modeling and fracture criteria of dynamic elastic-viscoplastic crack growth*, Int. J. Frac., **44**, 283–299, 1990.
13. P. PERZYNA, *Fundamental problems in viscoplasticity*, Advances in Applied Mechanics, **9**, 243–377, 1966.
14. P. PERZYNA, *Constitutive modeling of dissipative solids for postcritical behavior and fracture*, J. Engng. Mat. Tech., **106**, 410–419, 1984.
15. H. RIEDEL, *Recent advances in modeling creep crack growth*, Advances in Fracture Research, **ICF 7**, 1495–1523, 1989.
16. H. STAMM and G. WALZ, *Analytical investigation of crack tip fields in viscoplastic materials*, Int. J. Frac., **64**, 135–155, 1993.
17. H. STAMM and G. WALZ, *Numerical investigation of crack tip fields in viscoplastic materials*, Int. J. Frac., **64**, 157–178, 1993.
18. H. TADA, P. PARIS and G. IRWIN, *The stress analysis of cracks handbook*, Del Research Corp. Hellertown Pa., 1973.
19. V. TVERGAARD, *Material failure by void growth to coalescence*, Advances in Applied Mechanics, **27**, 83–151, 1989.
20. V. TVERGAARD and J.W. HUTCHINSON, *The relation between crack growth resistance and fracture process parameters in elastic-plastic solids*, J. Mech. Phys. Solids, **40**, 1377–1397, 1992.
21. V. TVERGAARD and A. NEEDLEMAN, *Analysis of the cup-cone fracture in a round tensile bar*, Acta Metallurgica, **32**, 157–169, 1984.
22. Ch. ZHANG and D. GROSS, *Analysis of ductile crack growth by a simple damage model*, Transactions of the 12th International Conference on Structural Mechanics in Reactor Technology Stuttgart, 15.8.-20.8.1993, K.F. KUSSMAUL [Ed.], **B**, 363–368, 1993.

INSTITUT FÜR MECHANIK, TH DARMSTADT, GERMANY.

Received December 2, 1994.

Arch. Mech., 47, 5, pp. 915–956, Warszawa 1995

Dynamic interface crack propagation and related problems of caustics

K.P. HERRMANN and A. NOE (PADERBORN)

DYNAMIC CRACK extension of cracks running along curvilinear interfaces of brittle bimaterials subjected to mechanical crack surface loads and superimposed thermal strains acting along the ligament is considered by utilizing the linear theory of thermoelasticity. In the framework of Stroh's method, from the corresponding boundary and continuity conditions, a vectorial Hilbert problem is derived to determine vectors of generalized complex potentials. Based on a physically reasonable stress intensity vector definition, explicit integral formulae for the stress intensity vector of mechanically loaded crack surfaces and a thermally strained ligament are obtained and discussed in view of interface mechanics parameters: applied loading, interface, crack-tip velocity and curvature of the interface. In the course of an experimental determination of stress intensity factors from the experimentally recorded caustics, a measuring algorithm is proposed which does not require the crack-tip location to be known exactly.

1. Introduction

IN RECENT YEARS, compounds of materials with different material constants have turned out to be the starting point or the precondition for the development of newly designed high-tech products or high-performance processing technologies. The enumeration of various examples includes classical composite structures in spacecrafts as well as in aircrafts, electronic devices in the field of information technologies or more refined bonding processing technologies in the domain of adhesive joints and protective coatings. Essentially, the interface is often the most sensitive locus in the aforementioned compounds regarding their structural performance as well as failure behaviour. Since substantial mechanical interface characteristics of multi-phase materials are not primarily affected by the typical length scale of a structure, the mechanics of interfaces can be investigated by an intrinsic mechanical interface model, now commonly known as bimaterial. In general, during manufacturing or due to the operating conditions the interfaces are damaged and, in particular, interface cracks have been proved to be the elementary failure mechanisms in bimaterials. Nevertheless, cracks may arise inside the bulk of the phases, which are referred to as matrix cracks, or as a combination of matrix and interface cracks.

From the mechanical point of view, the formation of interface cracks and a prospective subsequent unstable propagation can be described by a set of distinct parameters of the mechanics of interfaces. Predominantly, the prescribed mechanical loading conditions and the additional influence of residual stresses due to a thermal mismatch caused by thermal loading must be taken into account. In addition, in composites the crack extension is observed, among other

phenomena, to follow curved paths along the interface. This geometrical effect, by itself, conditioned by the shape of a given structure, influences the stress fields. Finally, after the onset of unstable crack propagation, the material inertia cannot be neglected if the crack tip velocity exceeds about one half of the Rayleigh wave velocity, v_R, of the more compliant bimaterial component. In this case a non-negligible portion of the initial elastic energy is converted into the kinetic energy of the cracked body.

This explains the strong demand for the theoretical modelling of the general situation of dynamic crack extension of straight as well as curved interface cracks, in order to study the interactions of the crack-tip velocity, and of the self-stresses superimposed by mechanical crack surface loads, which originate from the applied thermal strains, and from the curvature of the interface. Restricting attention to composite structures which behave in a brittle manner and thus can be modelled as elastic bimaterials, the first basic theoretical studies of interface fracture mechanics of elastically isotropic bimaterials were published by ERDOGAN [14, 15], RICE and SIH [41] and ENGLAND [12, 13] about thirty years ago. Mathematically, these contributions were based on Muskhelishvili's method. Conceptual features of the static interface fracture mechanics, especially the importance and consequences of the peculiar oscillatory singularities have been addressed in review articles by RICE [42] and COMNINOU [7]. Moreover, noteworthy contributions are those by RÜHLE *et al.* [46] and HUTCHINSON and SUO [24]. Later on, inspired by the capabilities of Stroh's method of generalized complex potentials [48], which was algebraically structured by TING [54], the analysis of interface crack problems was successfully extended to the quasi-static and steady-state dynamic interface crack propagation between dissimilar anisotropic materials. Although LEKHNITSKII'S competitive method of generalized complex potentials [29] could also be utilized, Stroh's technique is preferred since its algebraic structure is much more refined. Concerning the quasi-static case, important research work was supplied by SUO [50], QU and BASSANI [40, 4], TING [55], HWU [27] and WU [60]. The influence of a constant cooling or heating, ΔT, or of a constant remote heat flux in the anisotropic case was investigated by ATKINSON and CLEMENTS [2], STURLA and BARBER [49] and HWU [26]. Intensive efforts dealing with the case of rapid interface crack propagation can only be encountered since a few years, apart from the basic research contribution by WILLIS [59] and the review article by ATKINSON [1]. Employing the method of Stroh, these new studies started from papers of YANG *et al.* [62] and WU [60] and were continued by DENG [9, 10], and HERRMANN and NOE [36, 37, 38]. In the latter papers, the most general situation of rapid crack extension along curvilinear interface contours subjected to mechanical and thermal loads was investigated to a certain extent. Indeed, it should be mentioned that the influence of the crack curvature was studied in an explicit manner by COTTERELL and RICE [8], GAO and CHIU [21], ENGLAND [13], and TOYA [57] for the cases of a quasi-static crack extension in a homogeneous material as well as along the interfaces of a bimaterial, and by XU and KEER [61],

LIU and ROSAKIS [30, 31] for a dynamic crack extension in a homogeneous material. The aforementioned demand for a theoretical analysis of the dynamic interface crack extension is not restricted to the determination of displacement fields, stress fields and the derived fracture mechanical parameters like mixed-mode stress intensity factors. Apparently, in view of the experimental failure analysis, by utilizing a proper experimental technique an adequate measuring algorithm has to be provided in order to extract the required experimental parameters from special patterns of the selected experimental method. In this paper, attention is focussed on the shadow-optical method of caustics. The geometric shape of the caustics is proportional to the stress field gradient and therefore the contour of a caustic can be taken as a measure for the experimental determination of stress intensity factors. For completeness and apart from the method of photoelasticity, the development of the recently presented method of coherent gradient sensing (CGS) created by TIPPUR and ROSAKIS [56] should be mentionend.

The method of caustics was developed by MANOGG [32] for a quasi-static crack propagation. Essentially, THEOCARIS [52] extended the method to mixed-mode loading cases for interface cracks. The formulation of the equations for caustics for arbitrarily curved, quasi-statically propagating interface cracks was considered by HERRMANN and NOE [22] and NOE *et al.* [35]. Even for the simplest case of a crack propagation in homogeneous materials, experimental results and simulated caustics show that the application of the static theory instead of the dynamic theory leads to essential differences in the case of higher crack tip velocities. The first attempts to apply the method of caustics to fast running cracks have been performed by ROSSMANITH [44], THEOCARIS [53], BEINERT and KALTHOFF [5]. Extensions to cases of mixed-mode loading in homogeneous materials, including the consideration of the optical anisotropy of the material, the presence of which makes the method more difficult to apply compared with the optical isotropy of the material, were carried out by NISHIOKA and KITTAKA [34]. The rapid extension of cracks situated in the interface of a linear-elastic bimaterial was reported by HERRMANN and NOE [22, 23] wherein, apart from the simulated caustics guided by the method of SANFORD and DALLY [47], a measuring algorithm for the determination of stress intensity factors from experimentally obtained caustics was presented, which at that stage did not cover all of the demands of the experimentalists and which is different from the algorithm proposed by ROSSMANITH *et al.* [45].

Apart from a revised summary of some previous results regarding the steady-state dynamic interface crack propagation, this paper contains systematic extensions of earlier results. A more comprehensive treatment of the described subject of the mechanics of interfaces was recently presented by NOE [39]. The general situation of the dynamic crack extension of straight and curved interface cracks is analysed in order to study the interactions of the crack tip velocity, self-stresses originated from thermal strains superimposed by mechanical crack surface loads and the curvature of the interface cracks. The first main objective is to present a

stress intensity vector of physical significance. From the calculated elasticity solutions for the cases of mechanical loading and thermal loading, explicit integral formulae are derived and discussed. In order to reach this goal the following three step strategy will be pursued. Firstly, the problem of the interface curvature in conjunction with a moving crack-tip will be addressed. Secondly, the problem of the motion of a crack through a dissimilar thermal displacement field will be studied. Thirdly, the solution technique of a vectorial Hilbert problem arising from the remaining elastic boundary and continuity problem will be provided. The solution vectors of the Hilbert problem are algebraically related to the mechanical fields looked for. The second main objective is to introduce a refined formalism for the simulation of caustics, to point out the significance of the associated parameters and, particularly, to present an algorithm for the determination of stress intensity factors from the experimentally gained caustics without knowing the crack-tip location.

2. Statement of the problem and thermoelastodynamic foundations

This section provides the preconditions and the mechanical methods, to obtain an at least almost time-independent mathematical model for the analysis of a dynamic crack extension in thermoelastic anisotropic dissimiliar media subjected to mechanically stressed crack surfaces, and to a constant cooling or heating, ΔT. The elimination of the time is equivalent to the transformation of an initial boundary value problem to a boundary value problem which, from the mathematical point of view, is much more easier to treat.

Figure 1 shows a bimaterial with a slightly curvilinear interface containing an interface crack running at speed $\mathbf{v}$. The crack-tip velocity, $\mathbf{v}$, is assumed to have a constant magnitude, v, but a slight variation of the orientation due to the curvature of the interface. Compared to homogeneous material, crack kinking has to be excluded since then, even for straight interface cracks, the distance between the crack tip and the interface is proportional to (vt) and, therefore, a strong time-dependence is induced. As will be shown below, the time-variations of mechanical fields are small in the sense of a first order approximation as long as the slope of the interface remains small. The vectors $\mathbf{p}$ and $\mathbf{q}$ denote the prescribed mechanical tractions on the symmetrically loaded crack surfaces and the given thermal strains along the ligament, respectively. The crack tip passes the space-fixed basis, $(\mathbf{e}_X, \mathbf{e}_Y)$, with assigned coordinates, $(X, Y) = (X_1, X_2)$, at the time $t = 0$. In addition, a running but irrotational basis, $(\mathbf{e}_x, \mathbf{e}_y)$, with associated coordinates, $(x, y) = (x_1, x_2)$, is attached to the crack tip. Moreover, the load vectors $\mathbf{p}$ and $\mathbf{q}$ are assumed to move with the crack tip basis, $(\mathbf{e}_x, \mathbf{e}_y)$, and pertubations by initial or reflected waves are avoided by studying the long-time behaviour of the crack extension and a bimaterial of infinite extension. Under these conditions the mechanical fields expressed by the coordinates (x, y) are at

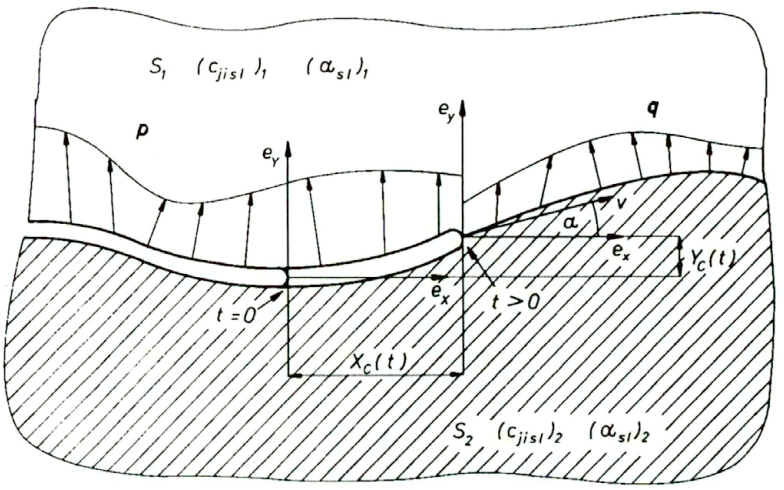

FIG. 1. Propagation of a curvilinear interface crack.

least almost time-independent; thus they are strictly time-independent for straight interface cracks. The associated boundary value problem is formulated by combining Volterra's dislocation method which was applied to quasi-static interface crack problems by BROWN and ERDOGAN [6], and Stroh's method of generalized complex potentials [48]. Volterra's method is utilized in order to handle the thermal displacements since the unbounded adjacent bimaterial components would yield a dislocation along the interface due to different tensors of thermal expansion coefficients, $(\alpha_{ij})_1$ and $(\alpha_{ij})_2$. Application of the running basis, $(\mathbf{e}_x, \mathbf{e}_y)$, requires the space-fixed total thermal displacement fields, $(u_i^{\text{th}})_1$ and $(u_i^{\text{th}})_2$, to be decomposed into parts $(u_{ic}^{\text{th}})_1$ and $(u_{ic}^{\text{th}})_2$, denoting the reference displacements associated with the moving basis, and the relative displacements $(u_{ix}^{\text{th}})_1$ and $(u_{ix}^{\text{th}})_2$. Since the reference displacements behave as rigid body displacements, no thermal stresses are generated. Henceforth and without loss of generality, $(u_{ic}^{\text{th}})_1$ and $(u_{ic}^{\text{th}})_2$ are set to zero by selecting $t = 0$. Thus Volterra's technique can be used in the sense of BROWN and ERDOGAN [6]. In the first step, the stress and displacement fields in the unbounded bimaterial parts are calculated. For a constant change of the temperature, ΔT, the thermal stresses and displacements read:

$$\Delta T = \text{const} \rightarrow \sigma_{ij}^{\text{th}} = 0, \qquad u_i^{\text{th}} = \alpha_{ij} \Delta T x_j . \tag{2.1}$$

In the second step the bimaterial parts are bounded. Since the stress vector is intrinsically continuous due to the non-existing thermal stresses, the compatibility of the displacements can only be fulfilled by adding unknown (as yet) elastic displacements. Thus, the set of transition conditions reads as follows

$$\begin{aligned} (u_i^{\text{el}} + u_i^{\text{th}})_1 &= (u_i^{\text{el}} + u_i^{\text{th}})_2 , \\ (\sigma_{ji}^{\text{el}} n_j)_1 &= (\sigma_{ji}^{\text{el}} n_j)_2 . \end{aligned} \tag{2.2}$$

The elastic displacements, u_{i1}^{el} and u_{i2}^{el}, are determined from the remaining boundary-value problem governed by the generalized Lamé-Navier equations (LNE)

$$c_{jisl}\frac{\partial^2 u_s^{el}}{\partial X_l \partial X_j} = \varrho \frac{\partial^2 u_i^{el}}{\partial t^2}, \tag{2.3}$$

where c_{jisl} and ϱ are the coefficients of the elasticity tensor and the material density, respectively. For completeness of the boundary conditions, zero stresses at infinity have been chosen. While the LNE in (2.3) formulated in the space-fixed basis, $(\mathbf{e}_X, \mathbf{e}_Y)$, are time-dependent and are partial differential equations (PDE) of hyperbolic type, the transition to the moving crack tip basis $(\mathbf{e}_x, \mathbf{e}_y)$, provides the PDE

$$c_{jisl}\frac{\partial^2 u_s^{el}}{\partial x_l \partial x_j} = \varrho v^2 \left(\cos^2(\alpha)\frac{\partial^2 u_i^{el}}{\partial x_1 \partial x_1} + 2\cos(\alpha)\sin(\alpha)\frac{\partial^2 u_i^{el}}{\partial x_1 \partial x_2} + \sin^2(\alpha)\frac{\partial^2 u_i^{el}}{\partial x_2 \partial x_2}\right), \tag{2.4}$$

which is only slightly time-dependent. Referring to Fig. 1, the angle α denotes the slope of the interface contour at the crack tip location. If crack tip positions near to the non-moving basis, $(\mathbf{e}_X, \mathbf{e}_Y)$, are considered, then for small angles, α, the time-dependence of the LNE can be neglected and they assume the form

$$C_{jisl}\frac{\partial^2 u_s^{el}}{\partial x_l \partial x_j} = 0_i, \qquad C_{jisl}(v) = (c_{jisl} - \varrho v^2 \delta_{1j}\delta_{1l}\delta_{is}). \tag{2.5}$$

This form of the Lamé-Navier equations represents a set of homogeneous PDE's of the elliptic type, the same as in the case of a straight crack extension. It must be emphasized that the elasticity tensor, C_{jisl}, varies with the crack-tip velocity, v. Since (2.5) is an elliptic PDE, a complex variable method can be invoked which is the onset for Stroh's method of generalized complex potentials. By introducing the displacement vector approach

$$\mathbf{u}_{kj}^{el} = \mathbf{a}_{kj} f_{kj}(z_{kj}), \qquad z_{kj} = x + p_{kj} y \qquad (k, j = 1, 2), \tag{2.6}$$

the solution of the LNE is reduced to the eigenvalue problem

$$(\mathbf{Q} + p_k(\mathbf{R} + \mathbf{R}^T) + p_k^2 \mathbf{T})_j \mathbf{a}_{kj} = \mathbf{0}, \tag{2.7}$$

where, according to TING'S notation [54], the matrices

$$\mathbf{A}_j = (\mathbf{a}_1, \mathbf{a}_2)_j, \qquad \mathbf{P}_j = \mathrm{diag}(p_1, p_2)_j \tag{2.8}$$

are composed of the eigenvectors and eigenvalues of the LNE. The eigenvectors and eigenvalues are complex conjugate in pairs, respectively. In a wide class

of problems it is sufficient to restrict to purely imaginary eigenvalues, $p_{kj} = i\beta_{kj}$. With this restriction isotropic bimaterials and a considerable number of orthotropic bimaterials are covered. Then, for the case of a dynamic crack propagation, the eigenvalues are functions of the crack-tip velocity, v, and the characteristic wave velocities, v_{kj}, of each of the elastic materials are given by $\beta_{kj} = \sqrt{1-(v/v_{kj})^2}$. Moreover, it should be noted that for the limiting case of degenerate eigenvalues, $p_{1j} = p_{2j} = i$, assigned to isotropic material and quasi-static crack extension ($v = 0$), those algebraic features of Stroh's method which are required for the mechanical analysis of interfaces continue to apply. Referring to Ting, the matrices $\mathbf{Q} = (C_{1is1}) = \mathbf{Q}^T$, $\mathbf{R} = (C_{1is2}) \neq \mathbf{R}^T$ and $\mathbf{T} = (C_{2is2}) = \mathbf{T}^T$ contain elements of the elasticity tensor, C_{jisl}, from (2.5). The potential vectors

$$\mathbf{f}_j(\mathbf{z}_j) = (f_1(z_1), f_2(z_2))_j^T, \qquad \mathbf{z}_j = (z_1, z_2)_j^T \tag{2.9}$$

can only be obtained from the solution of the associated special boundary value problem. The displacement vectors, $\mathbf{u}_j$, and, by the definition of Ting, the stress vectors, $\mathbf{s}_{1j}$ and $\mathbf{s}_{2j}$, composed of elements of the stress tensor, σ_{ij}, are given by the subsequent expressions:

$$\mathbf{u}_j^{\mathrm{el}} = 2\,\mathrm{Re}((\mathbf{AB}^{-1})\mathbf{Bf}(\mathbf{z}))_j, \qquad \mathbf{u}_j = \mathbf{u}_j^{\mathrm{el}} + \mathbf{u}_j^{\mathrm{th}}, \tag{2.10}$$

$$\mathbf{s}_{1j} = 2\,\mathrm{Re}(\mathbf{B}_t\mathbf{Bf}'(\mathbf{z}))_j, \quad \mathbf{B}_t = -\mathbf{BPB}^{-1} + \varrho v^2\mathbf{AB}^{-1}, \quad \mathbf{s}_{1j} = (\sigma_{11}, \sigma_{21})_j^T, \tag{2.11}$$

$$\mathbf{s}_{2j} = 2\,\mathrm{Re}(\mathbf{Bf}'(\mathbf{z}))_j, \quad \mathbf{B}_j = (\mathbf{R}^T\mathbf{A} + \mathbf{TAP})_j, \quad \mathbf{s}_{2j} = (\sigma_{12}, \sigma_{22})_j^T. \tag{2.12}$$

As a fundamental essence of Stroh's method, it is worthwhile mentioning that the matrices $\mathbf{A}$ and $\mathbf{B}$ are not independent. Stroh proved the important property of the product $(\mathbf{AB}^{-1})^T = -(\overline{\mathbf{AB}^{-1}})$ to be skew-Hermitian.

With regard to the mentioned derivation of caustics equations and the associated measuring algorithm, the stress invariants of the plane stress tensor σ_{ij}, namely the sum of the principal stresses, $I_1 = (\sigma_1 + \sigma_2)$, and the difference of the principal stresses, $I_2 = (\sigma_1 - \sigma_2)$, are formulated in the framework of Stroh's method. By introducing the principal stress vectors

$$\mathbf{s}^+ = \mathbf{s}_1 + \mathbf{Js}_2, \quad \mathbf{s}^+ = (\sigma_{11} + \sigma_{22}, 0)^T, \quad \mathbf{J} = \begin{pmatrix} 0 & 1 \\ -1 & 0 \end{pmatrix}, \quad \mathbf{J}^2 = -\mathbf{I}, \tag{2.13}$$

$$\mathbf{s}^- = \mathbf{s}_1 - \mathbf{Js}_2, \quad \mathbf{s}^- = (\sigma_{11} - \sigma_{22}, 2\sigma_{12})^T \tag{2.14}$$

and by using $\mathbf{s}_1$, (2.11), and $\mathbf{s}_2$, (2.12), the expressions

$$\mathbf{s}^+ = 2\mathrm{Re}\,(\mathbf{E}^+\mathbf{f}'(\mathbf{z})), \quad \mathbf{E}^+ = (\mathbf{JB} - \mathbf{BP} + \varrho v^2\mathbf{A}), \quad \mathbf{E}^+ = \begin{pmatrix} \mathbf{e}_1^{+T} \\ \mathbf{e}_2^{+T} \end{pmatrix}, \tag{2.15}$$

$$\mathbf{s}^- = 2\mathrm{Re}\,(\mathbf{E}^-\mathbf{f}'(\mathbf{z})), \quad \mathbf{E}^- = (-\mathbf{JB} - \mathbf{BP} + \varrho v^2\mathbf{A}), \quad \mathbf{E}^- = \begin{pmatrix} \mathbf{e}_1^{-T} \\ \mathbf{e}_2^{-T} \end{pmatrix} \tag{2.16}$$

are obtained. Taking the lengths of $\mathbf{s}^+$ and $\mathbf{s}^-$, provides the principal stress formulae

$$(\sigma_1 + \sigma_2)_j = 2\sqrt{\left[\mathrm{Re}\left(\mathbf{e}_1^{+T}\mathbf{f}'(\mathbf{z})\right)\right]^2 + \left[\mathrm{Re}\left(\mathbf{e}_2^{+T}\mathbf{f}'(\mathbf{z})\right)\right]^2_j}, \tag{2.17}$$

$$(\sigma_1 - \sigma_2)_j = 2\sqrt{\left[\mathrm{Re}\left(\mathbf{e}_1^{-T}\mathbf{f}'(\mathbf{z})\right)\right]^2 + \left[\mathrm{Re}\left(\mathbf{e}_2^{-T}\mathbf{f}'(\mathbf{z})\right)\right]^2_j}. \tag{2.18}$$

In view of the isotropic material behaviour, the vector $\mathbf{e}_1^-$ is zero and thus $\sigma_1 + \sigma_2 = 2\mathrm{Re}\left[\mathbf{e}_1^{+T}\mathbf{f}'(\mathbf{z})\right]$ holds true.

Since a slightly curvilinear interface is under investigation, according to (2.2) and Fig. 2, the transition conditions for the stresses along the interface with the

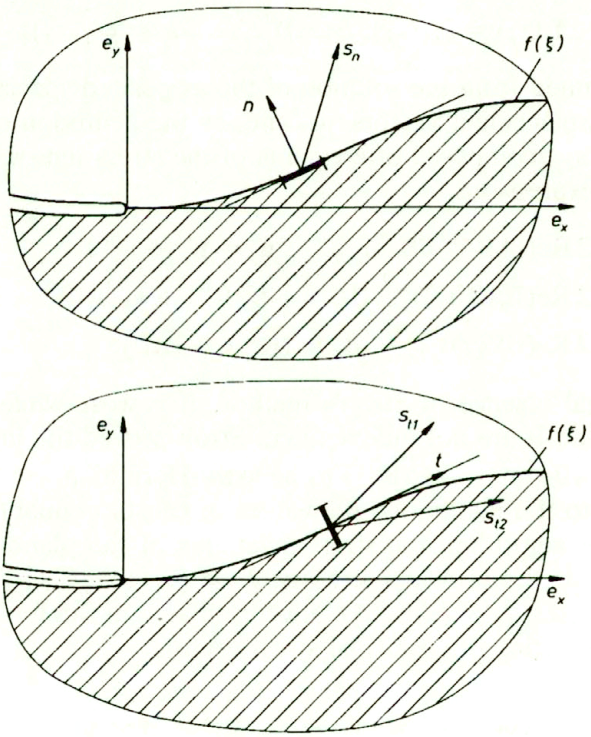

FIG. 2. Stress vectors along a curvilinear interface contour.

unit vector, $\mathbf{n}$, perpendicular to the interface contour have to be used. Therefore, the stress vectors, $\mathbf{s}_t$ and $\mathbf{s}_n$, defined by

$$\mathbf{s}_t = t_1\mathbf{s}_1 + t_2\mathbf{s}_2 \approx \mathbf{s}_1 + f'(\xi)\mathbf{s}_2\,, \qquad \mathbf{s}_t = (s_{tx}, s_{ty})^T = \mathbf{s}_t^{\mathrm{el}}\,, \tag{2.19}$$

$$\mathbf{s}_n = n_1\mathbf{s}_1 + n_2\mathbf{s}_2 \approx -f'(\xi)\mathbf{s}_1 + \mathbf{s}_2\,, \qquad \mathbf{s}_n = (s_{nx}, s_{ny})^T = \mathbf{s}_n^{\mathrm{el}} \tag{2.20}$$

are introduced where $f'(\xi)$ is the slope of the interface contour, $f(\xi)$, for the time $t = 0$, and the unit vectors $\mathbf{t}$ and $\mathbf{n}$, shown in Fig. 2, are normal vectors of the

respective planes along the interface. The formulae (2.19) and (2.20) are valid for small slopes only. The components of the vectors, $\mathbf{s}_t$ and $\mathbf{s}_n$, are coordinates of the Cartesian basis, $(\mathbf{e}_x, \mathbf{e}_y)$.

A curvi-linear interface associated with the determination of complex potentials implies the application of the conformal mapping technique. Its usage in the comparable case of an orthotropic half-space with a parabolically shaped boundary subjected to a line load dates back to LEKHNITSKIĬ [29]. As already noted by Lekhnitskiĭ, open contours can be treated much easier than the closed ones like the elliptic inclusion problems which, in the meanwhile (referring to HWU and TING [25]), have been investigated by utilizing Stroh's method. Moreover, since slightly curved interfaces are considered, a combination of the conformal mapping technique and the first-order pertubation technique can be successfully applied. This approach was also suggested by GAO [20]. On this basis, the curvilinear interface contour, L, is mapped onto the arc, L_Ω, of an auxiliary ζ-plane by the conformal mapping function

$$z = \omega(\zeta) = \zeta + if(\zeta), \qquad \zeta = \xi + i\eta, \qquad f(0) = f'(0) = f'(\infty) = 0. \tag{2.21}$$

The supplementary conditions $f(0) = f'(0) = f(\infty) = 0$ cover the afore-mentioned restriction of analysing a crack trapped running in a smooth interface with a zero slope at the location of the fixed basis, $(\mathbf{e}_X, \mathbf{e}_Y)$, as well as at infinity. If restricted to purely imaginary eigenvalues, $p_{kj} = i\beta_{kj}$, the boundary mapping in the LNE reads

$$z_{kj}(\xi) = \omega_{kj}(\xi) = \xi + i\beta_{kj} f(\xi), \qquad f(\xi) = \mathrm{Re}\,(f(\zeta_{kj})). \tag{2.22}$$

It should be pointed out that along the boundaries of the z_{kj}-planes the inequality $[z]_L \neq [z_{kj}]_L$ holds, whereas along the boundaries of the auxiliary planes, the ζ_{kj}-planes, the relation $[\zeta]_{L_\Omega} = [\zeta_{kj}]_{L_\Omega} = \xi$ is valid. Finally, instead of the potential vectors $\mathbf{f}_j(\mathbf{z}_j)$, the transformed potential vectors

$$\mathbf{f}_{\Omega j} = (f_{\Omega 1}(\zeta_1), f_{\Omega 2}(\zeta_2))_j^T \tag{2.23}$$

have to be determined. This goal, by neglecting terms of the order $O(f'^2(\xi))$, requires to provide mapping expressions for the potentials and their first derivatives in the direction of the interface. The results have the form

$$[\mathbf{f}_j(\mathbf{z}_j)]_L = [\mathbf{f}_{\Omega j}(\xi)]_{L_\Omega}, \qquad \mathbf{f}_{\Omega j}(\xi) = (f_{\Omega 1}(\xi), f_{\Omega 2}(\xi))_j^T, \tag{2.24}$$

$$[\mathbf{f}'_j(\mathbf{z}_j)]_L = (\mathbf{I} - f'(\xi)\mathbf{P}_j)[\mathbf{f}'_{\Omega j}(\xi)]_{L_\Omega}, \qquad \mathbf{P}_j = \mathrm{diag}\,(i\beta_{1j}, i\beta_{2j}). \tag{2.25}$$

Moreover, SUO's generic approach to apply the analytic continuation technique to potential vectors for the case of straight interface crack problems [50] has been used. From its extension to the case of curved interface crack problems along the

interface, the continuous stress vectors

$$\mathbf{s}_{n1}(\xi) = \mathbf{F}_{\Omega 1}(\xi)\mathbf{B}_1\mathbf{f}'^{+}_{\Omega 1}(\xi) + \mathbf{F}_{\Omega 2}(\xi)\mathbf{B}_2\mathbf{f}'^{-}_{\Omega 2}(\xi) = \mathbf{p}_{\Omega L_\Omega}(\xi), \tag{2.26}$$

$$\mathbf{s}_{n2}(\xi) = \mathbf{F}_{\Omega 1}(\xi)\mathbf{B}_1\mathbf{f}'^{+}_{\Omega 1}(\xi) + \mathbf{F}_{\Omega 2}(\xi)\mathbf{B}_2\mathbf{f}'^{-}_{\Omega 2}(\xi) = \mathbf{p}_{\Omega L_\Omega}(\xi), \tag{2.27}$$

and discontinuous stress vectors

$$\mathbf{s}_{t1}(\xi) = 2\mathrm{Re}\left[(\mathbf{B}_{t1} + f'(\xi)(\mathbf{I} + \mathbf{B}_{t1}^2))\mathbf{F}_{\Omega 1}(\xi)\mathbf{B}_1\mathbf{f}'^{+}_{\Omega 1}(\xi)\right], \tag{2.28}$$

$$\mathbf{s}_{t2}(\xi) = 2\mathrm{Re}\left[(\mathbf{B}_{t2} + f'(\xi)(\mathbf{I} + \mathbf{B}_{t2}^2))\mathbf{F}_{\Omega 2}(\xi)\mathbf{B}_2\mathbf{f}'^{-}_{\Omega 2}(\xi)\right], \tag{2.29}$$

with the matrix, $\mathbf{F}_{\Omega j}(\xi)$, and its inverse, accurate to within the first order approximation,

$$\mathbf{F}_{\Omega j}(\xi) = (\mathbf{I} - f'(\xi)\varrho v^2\mathbf{A}\mathbf{B}^{-1})_j, \qquad (\mathbf{F}_{\Omega j}(\xi))^{-1} \approx (\mathbf{I} + f'(\xi)\varrho v^2\mathbf{A}\mathbf{B}^{-1})_j \tag{2.30}$$

as well as the displacement vectors

$$\mathbf{u}(\xi) = \mathbf{u}^{\mathrm{el}}(\xi) + \mathbf{u}^{\mathrm{th}}(\xi), \qquad \mathbf{u} = (u_1, u_2)^T = (u, v)^T, \tag{2.31}$$

$$\mathbf{u}^{\mathrm{el}}(\xi) = 2\mathrm{Re}\left[(\mathbf{A}\mathbf{B}^{-1} + if'(\xi)[-i\varrho v^2(\mathbf{A}\mathbf{B}^{-1})^2])\mathbf{F}_\Omega\mathbf{B}\mathbf{f}_\Omega(\xi)\right], \tag{2.32}$$

$$\mathbf{u}^{\mathrm{th}}(\xi) = \Delta T(\alpha_{11}x(\xi), \alpha_{22}y(\xi))^T = \Delta T(\alpha_{11}\xi, \alpha_{22}f(\xi))^T \tag{2.33}$$

have been derived. The representation of the elastic displacement vector, $\mathbf{u}^{\mathrm{el}}(\xi)$, has been adapted to the further requirements. The notations $\mathbf{f}'^{+}_{\Omega 1}(\xi)$ and $\mathbf{f}'^{-}_{\Omega 2}(\xi)$ denote the limits of the unknown potential derivatives when, referring to Fig. 1, the interface contour L_Ω is approached from above and from below, respectively.

3. Vectorial Hilbert problems for a dynamically extending interface crack

By applying the stress vector formula (2.26) and the derivatives of the displacement vector formulae (2.31) to (2.33) with respect to the interface contour coordinate ξ, the transition conditions in (2.2) are converted into the vectorial Hilbert problem stated as

$$\begin{aligned} \mathbf{F}_{\Omega 1}(\xi)\mathbf{B}_1\mathbf{f}'^{+}_{\Omega 1}(\xi) + \mathbf{F}_{\Omega 2}(\xi)\mathbf{B}_2\mathbf{f}'^{-}_{\Omega 2}(\xi) &= \mathbf{p}_{\Omega L''_\Omega}(\xi), \quad \xi \in L''_\Omega, \\ \mathbf{H}_\Omega(\xi)\mathbf{F}_{\Omega 1}(\xi)\mathbf{B}_1\mathbf{f}'^{+}_{\Omega 1}(\xi) + \overline{\mathbf{H}}_\Omega(\xi)\mathbf{F}_{\Omega 2}(\xi)\mathbf{B}_2\mathbf{f}'^{-}_{\Omega 2}(\xi) &= \mathbf{q}_{\Omega L'_\Omega}(\xi), \quad \xi \in L'_\Omega. \end{aligned} \tag{3.1}$$

This Hilbert problem is a linear, inhomogeneous vectorial functional equation for the determination of the potential vectors in (2.23) which holds in the running crack tip basis, $(\mathbf{e}_x, \mathbf{e}_y)$, at the moment of time $t = 0$. It is parameterized by the coordinate, ξ, of the interface contour, L_Ω. The given vectors, $\mathbf{p}_{\Omega L''_\Omega}(\xi)$

and $\mathbf{q}_{\Omega L'_\Omega}(\xi)$, denote the respective (x, y)-coordinates of the symmetrically acting surface loads

$$\mathbf{p}_{\Omega L''_\Omega}(\xi) = (p_{nx}, p_{ny})^T_{\Omega L''_\Omega}, \tag{3.2}$$

and the mismatch of the thermal strains along the ligament is defined as follows:

$$\mathbf{q}_{\Omega L'_\Omega}(\xi) = (q_x, q_y)^T_{\Omega L'_\Omega}, \qquad \mathbf{q}_{\Omega L'_\Omega}(\xi) = \frac{d}{d\xi}(\mathbf{u}_2^{\text{th}} - \mathbf{u}_1^{\text{th}})_{\Omega L'_\Omega}. \tag{3.3}$$

The jump of the thermal strains in (3.3) may also be regarded as a prescribed density of thermal dislocations continuously distributed along the bonded part of the bimaterial interface. The non-constant coupling matrix, $\mathbf{H}_\Omega(\xi)$, whose algebraic structure determines most of the mechanical interface parameters, is defined by

$$\mathbf{H}_\Omega(\xi) = \mathbf{H} + if'(\xi)v^2\mathbf{H}_f \tag{3.4}$$

and consists of the respective skew-Hermitian matrices

$$\begin{aligned} &\mathbf{H} = -\overline{\mathbf{H}}^T, \qquad \mathbf{H} = \mathbf{A}_1\mathbf{B}_1^{-1} - \overline{\mathbf{A}}_2\overline{\mathbf{B}}_2^{-1}, \\ &\mathbf{H} = -i\mathbf{D} - \mathbf{W} = \begin{pmatrix} -iD_1 & -w_3 \\ w_3 & -iD_2 \end{pmatrix}, \end{aligned} \tag{3.5}$$

and

$$\begin{aligned} &\mathbf{H}_f = -\overline{\mathbf{H}}_f^T, \qquad \mathbf{H}_f = -i\left[\varrho_1(\mathbf{A}_1\mathbf{B}_1^{-1})^2 - \varrho_2\left(\overline{\mathbf{A}}_2\overline{\mathbf{B}}_2^{-1}\right)^2\right], \\ &\mathbf{H}_f = i\mathbf{D}_f + \mathbf{W}_f = \begin{pmatrix} iD_{f1} & w_{f3} \\ -w_{f3} & iD_{f2} \end{pmatrix}, \\ &\mathbf{H}_f = \begin{pmatrix} i\left[\varrho_1(D_1^2 + w_3^2)_1 - \varrho_2(D_1^2 + w_3^2)_2\right] & [\varrho_1(w_3(D_1 + D_2))_1 + \varrho_2(w_3(D_1 + D_2))_2] \\ -[\varrho_1(w_3(D_1 + D_2))_1 + \varrho_2(w_3(D_1 + D_2))_2] & i\left[\varrho_1(D_2^2 + w_3^2)_1 - \varrho_2(D_2^2 + w_3^2)_2\right] \end{pmatrix}, \end{aligned} \tag{3.6}$$

where the matrices $\mathbf{A}_j$ and $\mathbf{B}_j$, have been introduced in (2.8) and (2.12). In contrast to the matrices $\mathbf{H}$ and $\mathbf{H}_f$, the matrix $\mathbf{H}_\Omega(\xi)$ does not have a distinguished structure, such as the skew-Hermitian symmetry, aside from the crack tip at the coordinate $\xi = 0$. As the constant matrices, $\mathbf{H}$ and $\mathbf{H}_f$, contain material constants of both bimaterial components, they characterize the interactions of adjacent parts of different materials. The coupling matrix, $\mathbf{H}_\Omega(\xi)$, can be physically interpreted as a compliance matrix, which can be concluded from the comparison of

the stress formula and the strain formula in the Hilbert problem, respectively. In view of dynamic effects, $\det \mathbf{H}$ is proportional to the Stoneley wave velocity v_S, and $\det \mathbf{B}_j$ are proportional to the Rayleigh wave velocities v_{Rj}, related to the respective bimaterial component. The Rayleigh wave velocities v_{Rj}, are ordered by $v_{Rj} < v_{Tj} < v_{Lj}$ where v_{Tj} and v_{Lj} are the transversal and the longitudinal wave velocities, respectively. Referring to a fundamental investigation of BARNETT and LOTHE [3], the Stoneley wave velocity, v_S, and the minimum Rayleigh wave velocity, $v_{R\min}$, are related to each other by $v_{R\min} \leq v_S$, where $v_{R\min} = v_S$ holds if additional but special limitations are fulfilled. Without loss of generality, throughout this paper $v_{R\min} = v_{R1}$ has been chosen. Keeping in mind the terminology of acoustics, the matrices, $\mathbf{Y}_j = i(\mathbf{AB}^{-1})_j$ and $\mathbf{Y} = i\mathbf{H}$, are known as surface admittance matrices and interface admittance matrix, respectively.

The solution of the vectorial Hilbert problem is constructed by superimposing the problem of mechanically loaded crack surfaces, hereafter called the **p**-problem, and the case of the thermally strained ligament, hereafter called the **q**-problem. Since the Hilbert problem is a linear vectorial functional equation, it is effective to apply the methods of the linear algebra. Therefore, the solutions are gained by utilizing operations in the eigenvector planes of the **p**-problem and of the **q**-problem, respectively. The required mappings onto the eigenvector planes are provided by similarity transforms defined along the interface contour, L_Ω. For each of the problems the special mapping forms a set of two scalar Hilbert problems for a set of two scalar potentials. Referring to Muskhelishvili, the methods of the function theory are applicable. Thus, each solution is expressed by a Cauchy integral in terms of a generalized complex variable, z_{kj}. The curvature of the interface makes the Hilbert problem more difficult to solve and the structures become less transparent. However, by handling the Hilbert problems for a straight interface in the first step and, in the second step, using the results (eigenvalues, eigenvectors, potentials) as the basis to treat the case of a curved interface combined with the first order theory arguments, provides an effective strategy. This strategy leads to a simplified procedure for the determination of the potentials and to the identification of distinct algebraic quantities, which can be discussed in the framework of interface mechanics.

3.1. Mechanically loaded crack surfaces (p-problem)

The **p**-problem

$$
\begin{aligned}
\mathbf{F}_{\Omega 1}(\xi)\mathbf{B}_1\mathbf{f}'^{+}_{\Omega p1}(\xi) + \mathbf{F}_{\Omega 2}(\xi)\mathbf{B}_2\mathbf{f}'^{-}_{\Omega p2}(\xi) &= \mathbf{p}_{\Omega L''_\Omega}(\xi), \quad \xi \in L''_\Omega, \\
\mathbf{H}_\Omega(\xi)\mathbf{F}_{\Omega 1}(\xi)\mathbf{B}_1\mathbf{f}'^{+}_{\Omega p1}(\xi) + \overline{\mathbf{H}}_\Omega(\xi)\mathbf{F}_{\Omega 2}(\xi)\mathbf{B}_2\mathbf{f}'^{-}_{\Omega p2}(\xi) &= \mathbf{0}, \qquad \xi \in L'_\Omega
\end{aligned} \tag{3.7}
$$

is diagonalized by introducing the similarity transforms

$$
\begin{aligned}
\mathbf{H}_\Omega(\xi)\mathbf{F}_{\Omega 1}(\xi)\mathbf{B}_1\mathbf{f}'^{+}_{\Omega p1}(\xi) &= \mathbf{V}_{\Omega p}\mathbf{h}^{+}_{\Omega p}(\xi), \\
(-\overline{\mathbf{H}}_\Omega(\xi))\mathbf{F}_{\Omega 2}(\xi)\mathbf{B}_2\mathbf{f}'^{-}_{\Omega p2}(\xi) &= \mathbf{V}_{\Omega p}\mathbf{h}^{-}_{\Omega p}(\xi),
\end{aligned} \tag{3.8}
$$

whose selection is motivated by the physical fact that the elastic strains along the interface are continuous if thermal strains are absent. By employing this transforms, the decoupled vectorial **p**-Hilbert problem

$$\begin{aligned} \mathbf{h}^{+}_{\Omega p}(\xi) + \Lambda_{\Omega p}\mathbf{h}^{-}_{\Omega p}(\xi) &= \mathbf{p}_{\Omega\Lambda L''_{\Omega}}(\xi) = \mathbf{V}^{-1}_{\Omega p}\mathbf{H}_{\Omega}\mathbf{p}_{\Omega L''_{\Omega}}(\xi), \quad \xi \in L''_{\Omega}, \\ \mathbf{h}^{+}_{\Omega p}(\xi) - \mathbf{h}^{-}_{\Omega p}(\xi) &= \mathbf{0}, \qquad\qquad\qquad\qquad \xi \in L'_{\Omega} \end{aligned} \tag{3.9}$$

is generated if, due to the essence of the similarity transforms, the conditions

$$\Lambda_{\Omega p} = \operatorname{diag}(\lambda_{\Omega p1}, \lambda_{\Omega p2}) = \mathbf{V}^{-1}_{\Omega p}\mathbf{H}_{\Omega}(-\overline{\mathbf{H}})^{-1}_{\Omega}\mathbf{V}_{\Omega p}, \tag{3.10}$$

$$\mathbf{V}_{\Omega p} = (\mathbf{v}_{\Omega p1}, \mathbf{v}_{\Omega p2}) = EV\left(\mathbf{H}_{\Omega}(-\overline{\mathbf{H}}_{\Omega})^{-1}\right) \tag{3.11}$$

for the eigenvalues $\lambda_{\Omega pj}$, and eigenvectors $\mathbf{v}_{\Omega pj}$, of the matrix $(\mathbf{H}_{\Omega}(-\overline{\mathbf{H}}_{\Omega})^{-1})$ are fulfilled. In order to get a more detailed understanding of the interface mechanics and to extract the governed mechanical parameters directly, instead of solving the eigenvalue problem for $\lambda_{\Omega pj}$, the equivalent eigenvalue problem

$$\left[\overline{\beta}_{\Omega pj}\mathbf{I} + i\mathbf{W}\mathbf{D}^{-1} + if'(\xi)v^2(\mathbf{W}_f\mathbf{D}^{-1}\mathbf{W}\mathbf{D}^{-1} + \operatorname{adj}(\mathbf{D}_f\mathbf{D}^{-1}))\right]\mathbf{v}_{\Omega pj} = \mathbf{0} \tag{3.12}$$

is analysed. The pair of complex conjugate eigenvalues reads

$$\begin{aligned} &\beta_{\Omega p1} \equiv \beta_{\Omega} = \beta + if'(\xi)\beta_{\mathbf{H}f}, \quad \beta_{\Omega p2} = -\overline{\beta_{\Omega p1}}, \\ &\beta = \sqrt{\det(\mathbf{W}\mathbf{D}^{-1})}, \qquad \beta_{\mathbf{H}f} = -\frac{1}{2}v^2\operatorname{tr}(\mathbf{W}\mathbf{D}^{-1}\mathbf{W}_f\mathbf{D}^{-1} + \mathbf{D}_f\mathbf{D}^{-1}), \end{aligned} \tag{3.13}$$

and is related to the eigenvalues $\lambda_{\Omega pj}$, by the definition

$$\lambda_{\Omega pj} = \frac{1 + \beta_{\Omega pj}}{1 - \beta_{\Omega pj}}, \qquad \lambda_{\Omega p2} = (\overline{\lambda}_{\Omega p1})^{-1}. \tag{3.14}$$

For the pair of complex conjugate eigenvectors the formulae

$$\begin{aligned} &\mathbf{v}_{\Omega p1} = \begin{pmatrix} 1 \\ i\mu v_p \end{pmatrix}, \qquad \mathbf{v}_{\Omega p2} = \overline{\mathbf{v}}_{\Omega p1}, \qquad \mu = 1 + if'(\xi)\mu_{\mathbf{H}f}, \\ &v_p = \sqrt{\frac{D_2}{D_1}}, \qquad \mu_{\mathbf{H}f} = \frac{v^2}{2\beta}\sqrt{\frac{1}{2}\operatorname{tr}\left[\mathbf{D}^{-1}\mathbf{D}_f - \operatorname{adj}(\mathbf{D}^{-1}\mathbf{D}_f)\right]^2} \end{aligned} \tag{3.15}$$

have been obtained. The set of velocity-dependent parameters, (β, v_p), characterizes straight interfaces. The pair is augmented by the velocity-dependent parameters, $(\beta_{\mathbf{H}f}, \mu_{\mathbf{H}f})$, which is intrinsically connected to curved interfaces and to the moving basis, $(\mathbf{e}_x, \mathbf{e}_y)$. It should be noted that these elastodynamic interface parameters do not necessarily presuppose the interface to be cracked. From the

special case of the quasi-static interface crack propagation in an isotropic bimaterial, Dundurs parameters are the well-established parameters for bimaterials [11]. In this context, the real part of the eigenvalue, β, can be interpreted as a generalized second Dundurs parameter. Moreover, the complex-valued eigenvalue, β_Ω, may be denoted as a complex-valued generalized second Dundurs parameter. Each of the four interface parameters increases continuously in case when the velocity v grows.

For the sake of the further analysis it is advantageous to decompose the eigenvalues $\lambda_{\Omega pj}$ into the product

$$
\begin{aligned}
&\Lambda_{\Omega p} = \Lambda_p \Lambda_{pf}, \qquad && \Lambda_{\Omega p} = \operatorname{diag}(\lambda_{\Omega p1}, \lambda_{\Omega p2}),\\
&\Lambda_p = \operatorname{diag}(e^{-2\pi\varepsilon}, e^{2\pi\varepsilon}), \qquad && \Lambda_{pf} = \mathbf{I} e^{2i\pi\alpha_f}, \qquad \alpha_f(\xi) = f'(\xi)\alpha_{\mathbf{H}f},
\end{aligned}
\tag{3.16}
$$

leading to the definition of two additional interface parameters which are intrinsically related to cracked interfaces and, from the literature, are known as bimaterial constants. The matrices, Λ_p and Λ_{pf}, are eigenvalue matrices where Λ_p is associated with a straight interface, and Λ_{pf} corresponds to the curvature of the interface. The additional interface parameters read as follows

$$
\varepsilon = \frac{1}{2\pi} \ln\left(\frac{1-\beta}{1+\beta}\right), \qquad \varepsilon = \frac{1}{2\pi} \ln\left(\frac{1-\sqrt{\det(\mathbf{W}\mathbf{D}^{-1})}}{1+\sqrt{\det(\mathbf{W}\mathbf{D}^{-1})}}\right),
\tag{3.17}
$$

and

$$
\alpha_{\mathbf{H}f} = \frac{\beta_{\mathbf{H}f}}{\pi(1-\beta^2)}, \qquad \alpha_{\mathbf{H}f} = -\frac{1}{2\pi}\frac{v^2}{1-\beta^2}\operatorname{tr}(\mathbf{W}\mathbf{D}^{-1}\mathbf{W}_f\mathbf{D}^{-1} + \mathbf{D}_f\mathbf{D}^{-1}).
\tag{3.18}
$$

Thus, both the bimaterial constants may be physically traced back to the generalized second Dundurs parameters which in turn, from the mathematical point of view, are eigenvalue coefficients of the **p**-Hilbert problem (3.7). The classical bimaterial constant, ε, causes the peculiar and intensively discussed phenomena of oscillatory singularities and crack surface interpenetration. The additional bimaterial constant, $\alpha_{\mathbf{H}f}$, appears only if the situation of a fast interface crack extension and a non-vanishing interface curvature is simultaneously present. The bimaterial constant, $\alpha_{\mathbf{H}f}$, vanishes in the case of the crack extension in a homogeneous material, since the trace of $(\mathbf{W}\mathbf{D}^{-1}\mathbf{W}_f\mathbf{D}^{-1} + \mathbf{D}_f\mathbf{D}^{-1})$, which is also proportional to the trace of $(\mathbf{H}_f\mathbf{H}^{-1})$, vanishes identically. Similarly to the afore-introduced interface parameters, $(\beta, \beta_{\mathbf{H}f}, v_p, \mu_{\mathbf{H}f})$, the bimaterial constants increase with the growth of the crack tip velocity. The ε-value for the quasi-static case is approximately doubled if the crack tip velocity reaches 80% of the minimum Rayleigh-wave velocity, $v_{R\min} = v_1$. The value of $\alpha_{\mathbf{H}f}$ goes to infinity if $v_{R\min}$ is approached, but remains small within the first order theory if the velocity, v, is again limited to

about $v = 0.8v_{R1}$. The results of an experimentally observed interface crack propagation, reported by TIPPUR and ROSAKIS [56], state that the crack-tip velocities v are usually not higher than $v = 0.8v_{R1}$. Consequently, the presented bimaterial model based on the simplest theory of linear elasticity remains applicable. It is instructive to point out that, for the theoretical limit case of $v = v_{R1}$, the bimaterial model would totally fail since the extent of the oscillatory fields would cover the whole bimaterial and the zone of crack surface interpenetration would cover the whole length of the crack. It can be concluded that the singular stresses and strains are proportional to $r^{-1/2\pm f'(r)\alpha_{\mathrm{H}f}}$ where r denotes the distance from the crack tip [39]. By inspection of this expression for the most general case of a dynamic and curved interface crack extension, a decrease of stresses and strains is detected which depends on the distance from the crack tip. However, at the location of the crack tip itself, the order $(-1/2)$ of the singularity is preserved since $f'(0) = 0$ holds true identically and the deviation of the stress field behaviour from the $(-1/2)$-order is negligible close to the crack tip.

Now, approaching the Hilbert problem, the associated homogeneous **p**-Hilbert problem

$$\begin{aligned} \mathbf{X}^{+}_{\Omega p}(\xi) + \Lambda_{\Omega p}\mathbf{X}^{-}_{\Omega p}(\xi) &= \mathbf{0}, \qquad \xi \in L''_{\Omega}, \\ \mathbf{X}^{+}_{\Omega p}(\xi) - \mathbf{X}^{-}_{\Omega p}(\xi) &= \mathbf{0}, \qquad \xi \in L'_{\Omega} \end{aligned} \tag{3.19}$$

has to be solved for the fundamental matrix, $\mathbf{X}_{\Omega p}(\zeta_{kj})$. Guided by the first order theory approach, $\mathbf{X}_{\Omega p}(\zeta_{kj})$ is factorized into the product

$$\mathbf{X}_{\Omega p} = \mathbf{X}_p \mathbf{X}_{pf} = \operatorname{diag}(X_{p1}\, X_{pf1},\ X_{p2}\, X_{pf2}), \tag{3.20}$$

where $\mathbf{X}_p$ is associated with straight cracks and $\mathbf{X}_{pf}$ comprises the deviation due to the curvature. Substitution of (3.16) and (3.20) into (3.19) results in two independent homogeneous Hilbert problems for the determination of $\mathbf{X}_p(\zeta_{kj})$ and $\mathbf{X}_{pf}(\zeta_{kj})$, which are formally identical with (3.19). The general formulae for $\mathbf{X}_p(\zeta_{kj})$ and $\mathbf{X}_{pf}(\zeta_{kj})$ are expressed by Cauchy integrals for $\ln \mathbf{X}_p(\zeta_{kj})$ and $\ln \mathbf{X}_{pf}(\zeta_{kj})$. Moreover, since the factorization has been introduced, the evaluation of the integrals is considerably simplified. Solutions for $\mathbf{X}_{\Omega p}(\zeta_{kj})$, which fulfil the given limits

$$\Lambda_{\Omega p} = -\mathbf{X}^{+}_{\Omega p L''_{\Omega}} \left(\mathbf{X}^{-}_{\Omega p L''_{\Omega}}\right)^{-1}, \qquad \mathbf{I} = \mathbf{X}^{+}_{\Omega p L'_{\Omega}} \left(\mathbf{X}^{-}_{\Omega p L'_{\Omega}}\right)^{-1} \tag{3.21}$$

along the interface, have been evaluated for a semi-infinite interface crack along the segment $L''_{\Omega} \in [-\infty, 0]$, and for an interface crack situated along the finite segment $L''_{\Omega} \in [-a, 0]$. These solutions read

$$\mathbf{X}_{\Omega p}(\zeta_{kj}) = \operatorname{diag}\left(\zeta_{kj}^{-(1/2-\alpha_f)+i\varepsilon}, \zeta_{kj}^{-(1/2-\alpha_f)-i\varepsilon}\right) \tag{3.22}$$

for a semi-infinite interface crack, and

$$\mathbf{X}_{\Omega p}(\zeta_{kj}) = \operatorname{diag}\left(\zeta_{kj}^{-(1/2-\alpha_f)+i\varepsilon}(\zeta_{kj}+a)^{-(1/2+\alpha_f)-i\varepsilon},\ \zeta_{kj}^{-(1/2-\alpha_f)-i\varepsilon}(\zeta_{kj}+a)^{-(1/2+\alpha_f)+i\varepsilon}\right) \tag{3.23}$$

for a finite interface crack of length a. By introducing (3.21) into (3.9), the inhomogeneous **p**-Hilbert problem can be rewritten as follows:

$$\begin{aligned}
&\left[(\mathbf{X}^{+}_{\Omega p}(\xi))^{-1}\mathbf{h}^{+}_{\Omega p}(\xi)\right]_{L''_\Omega} - \left[(\mathbf{X}^{-}_{\Omega p}(\xi))^{-1}\mathbf{h}^{-}_{\Omega p}(\xi)\right]_{L''_\Omega} \\
&\qquad = \left[(\mathbf{X}^{+}_{\Omega p}(\xi))^{-1}\mathbf{p}_{\Omega\Lambda}(\xi)\right]_{L''_\Omega}, \qquad \xi \in L''_\Omega, \\
&\left[(\mathbf{X}^{+}_{\Omega p}(\xi))^{-1}\mathbf{h}^{+}_{\Omega p}(\xi)\right]_{L'_\Omega} - \left[(\mathbf{X}^{-}_{\Omega p}(\xi))^{-1}\mathbf{h}^{-}_{\Omega p}(\xi)\right]_{L'_\Omega} = \mathbf{0}, \qquad \xi \in L'_\Omega .
\end{aligned} \tag{3.24}$$

For an arbitrarily generalized complex variable, ζ_{kj}, the simplest solution for (3.24), which primarily fulfills the jump conditions (3.21), is determined by the Cauchy integral representation

$$\begin{aligned}
\mathbf{h}_{\Omega p}(\zeta_{kj}) &= \frac{1}{2\pi i}\mathbf{X}_{\Omega p}(\zeta_{kj}) \int\limits_{L''_\Omega} \left(\mathbf{X}^{+}_{\Omega p L''_\Omega}(\xi)\right)^{-1} \mathbf{p}_{\Omega\Lambda L''_\Omega}(\xi)\frac{d\xi}{\xi-\zeta_{kj}}, \\
\mathbf{h}_{\Omega p} &= (h_{\Omega p1}, h_{\Omega p2})^{T}.
\end{aligned} \tag{3.25}$$

Thereby, it is essential for an uncoupled eigenvector plane solution that a distinct element of $\mathbf{X}_{\Omega p}$ is related to a distinct potential, $\mathbf{h}_{\Omega p}$. With the exception of a single force acting on the crack surface, on account of the bimaterial constant, $\alpha_{\mathbf{H}f}$, the integrals cannot be evaluated analytically.

3.2. Thermally strained ligament (q-problem)

Apparently, the treatment of the **q**-problem is analogous to the **p**-problem and straightforward. Therefore its exposition is shortened. The **q**-problem

$$\begin{aligned}
\mathbf{F}_{\Omega 1}(\xi)\mathbf{B}_1\mathbf{f}'^{+}_{\Omega q1}(\xi) + \mathbf{F}_{\Omega 2}(\xi)\mathbf{B}_2\mathbf{f}'^{-}_{\Omega q2}(\xi) &= \mathbf{0}, \qquad \xi \in L''_\Omega, \\
\mathbf{H}_\Omega(\xi)\mathbf{F}_{\Omega 1}(\xi)\mathbf{B}_1\mathbf{f}'^{+}_{\Omega q1}(\xi) + \overline{\mathbf{H}}_\Omega(\xi)\mathbf{F}_{\Omega 2}(\xi)\mathbf{B}_2\mathbf{f}'^{-}_{\Omega q2}(\xi) &= \mathbf{q}_{\Omega L'_\Omega}(\xi), \qquad \xi \in L'_\Omega,
\end{aligned} \tag{3.26}$$

is diagonalized by introducing the similarity transforms

$$\begin{aligned}
\mathbf{F}_{\Omega 1}(\xi)\mathbf{B}_1\mathbf{f}'^{+}_{\Omega q1}(\xi) &= \mathbf{V}_{\Omega q}\mathbf{h}^{+}_{\Omega q}(\xi), \\
\mathbf{F}_{\Omega 2}(\xi)\mathbf{B}_2\mathbf{f}'^{-}_{\Omega q2}(\xi) &= -\mathbf{V}_{\Omega q}\mathbf{h}^{-}_{\Omega q}(\xi),
\end{aligned} \tag{3.27}$$

whose selection is motivated physically by the fact that the thermal strains along the interface are discontinuous. By applying these transforms the decoupled vectorial **q**-Hilbert problem

$$\begin{aligned} \mathbf{h}^{+}_{\Omega q}(\xi) - \mathbf{h}^{-}_{\Omega q}(\xi) &= \mathbf{0}, && \xi \in L''_{\Omega}, \\ \mathbf{h}^{+}_{\Omega q}(\xi) + \Lambda_{\Omega q}\mathbf{h}^{-}_{\Omega q}(\xi) &= \mathbf{q}_{\Omega \Lambda L'_{\Omega}}(\xi) = \mathbf{V}^{-1}_{\Omega q}\mathbf{H}^{-1}_{\Omega}\mathbf{q}_{\Omega L'_{\Omega}}(\xi), && \xi \in L'_{\Omega}, \end{aligned} \tag{3.28}$$

is obtained if the conditions

$$\Lambda_{\Omega q} = \operatorname{diag}(\lambda_{\Omega q1}, \lambda_{\Omega q2}) = \mathbf{V}^{-1}_{\Omega q}\mathbf{H}^{-1}_{\Omega}(-\overline{\mathbf{H}})_{\Omega}\mathbf{V}_{\Omega q}, \tag{3.29}$$

$$\mathbf{V}_{\Omega q} = (\mathbf{v}_{\Omega q1}, \mathbf{v}_{\Omega q2}) = EV(\mathbf{H}^{-1}_{\Omega}(-\overline{\mathbf{H}}_{\Omega})), \tag{3.30}$$

for the eigenvalues, $\lambda_{\Omega qj}$, and eigenvectors, $\mathbf{v}_{\Omega qj}$, of the matrix $(\mathbf{H}^{-1}_{\Omega}(-\overline{\mathbf{H}}_{\Omega}))$ are fulfilled. Instead of solving the eigenvalue problem for $\lambda_{\Omega qj}$, the fully equivalent eigenvalue problem

$$\left[\beta_{\Omega qj}\mathbf{I} + i(\mathbf{W}\mathbf{D}^{-1})^{T} - if'(\xi)v^2(\mathbf{W}\mathbf{D}^{-1}\mathbf{W}_f\mathbf{D}^{-1} + \mathbf{D}_f\mathbf{D}^{-1})^{T}\right]\mathbf{v}_{\Omega qj} = \mathbf{0} \tag{3.31}$$

is investigated. The pair of complex conjugate eigenvalues reads

$$\begin{aligned} &\beta_{\Omega q1} = -\beta - if'(\xi)\beta_{\mathbf{H}f}, \qquad \beta_{\Omega q2} = -\overline{\beta_{\Omega q1}}, \qquad \beta_{\Omega q1} = -\beta_{\Omega}, \\ &\beta = \sqrt{\det(\mathbf{W}\mathbf{D}^{-1})}, \qquad \beta_{\mathbf{H}f} = -\frac{1}{2}v^2\operatorname{tr}(\mathbf{W}\mathbf{D}^{-1}\mathbf{W}_f\mathbf{D}^{-1} + \mathbf{D}_f\mathbf{D}^{-1}). \end{aligned} \tag{3.32}$$

For the pair of complex conjugate eigenvectors the formulae

$$\begin{aligned} &\mathbf{v}_{\Omega q1} = \frac{1}{2}\begin{pmatrix} 1 \\ \dfrac{i\mu}{v_p} \end{pmatrix}, \qquad \mathbf{v}_{\Omega q2} = \overline{\mathbf{v}}_{\Omega q1}, \qquad \mu = 1 + if'(\xi)v^2\mu_f, \\ &v_p = \sqrt{\frac{D_2}{D_1}}, \qquad \mu_{\mathbf{H}f} = \frac{v^2}{2\beta}\sqrt{\frac{1}{2}\operatorname{tr}[\mathbf{D}^{-1}\mathbf{D}_f - \operatorname{adj}(\mathbf{D}^{-1}\mathbf{D}_f)]^2} \end{aligned} \tag{3.33}$$

are valid. Based on the physical reason that the selected eigenvector plane cannot affect the physical problem itself, both the similarity transforms could have been applied to the mechanical **p**-problem (and *vice versa*) to the thermal strain **q**-problem. Therefore, from a comparison of the eigenvalues for the **p**-problem and the **q**-problem, the relations

$$\begin{aligned} &\beta_{\Omega} = \beta + if'(\xi)\beta_{\mathbf{H}f}, \\ &\beta_{\Omega p1} = \beta_{\Omega}, \qquad \beta_{\Omega p2} = -\overline{\beta}_{\Omega}, \qquad \beta_{\Omega q1} = -\beta_{\Omega}, \qquad \beta_{\Omega q2} = \overline{\beta}_{\Omega} \end{aligned} \tag{3.34}$$

become obvious. It is important to recognize that the relations between the eigenvalues in the expression (3.34) are equivalent to the eigenvalue relation, $\Lambda_{\Omega p}\Lambda_{\Omega q} = \mathbf{I}$. Furthermore, by expressing the stress vector along the ligament either by the eigenvector matrix, $\mathbf{V}_{\Omega p}$, or by the eigenvector matrix, $\mathbf{V}_{\Omega q}$, it can be concluded that the eigenvectors are linked to each other by the orthogonality relation

$$\begin{aligned} &\mathbf{V}_{\Omega p}^{-1}\mathbf{H}_{\Omega} = (\mathbf{V}_{\Omega q}\mathbf{S}_{\Omega})^{-1}, \qquad \mathbf{S}_{\Omega}(\xi) = \operatorname{diag}(is_{\Omega 1}, is_{\Omega 2}), \\ &\mathbf{S}_{\Omega}(\xi) = \mathbf{S}\Lambda_{qf}^{1/2}(\xi) = \mathbf{S}e^{-i\pi\alpha_f(\xi)}, \qquad \mathbf{S} = 2i\frac{\cosh(\pi\varepsilon)}{D_1}\Lambda_q^{1/2}. \end{aligned} \tag{3.35}$$

The scaling matrix, $\mathbf{S}_{\Omega}(\xi)$, is obtained from the comparison of (3.35) and the eigenvalue problems associated with the matrices $(\mathbf{H}_{\Omega}(-\overline{\mathbf{H}}_{\Omega})^{-1})$ of the **p**-problem and $(\mathbf{H}_{\Omega}^{-1}(-\overline{\mathbf{H}}_{\Omega}))$ of the **q**-problem. Note that the matrix, **S**, is the scaling matrix for straight interfaces. It is noteworthy to emphasize that due to (3.34) and (3.35), only one eigenvalue and one eigenvector problem has to be solved explicitly. Moreover, regardless of the mechanical problem under investigation, only one set of elastodynamic interface mechanics parameters, namely $(\beta, \beta_{\mathbf{H}f}, v_p, \mu_{\mathbf{H}f})$ and, consequently, only one pair of bimaterial constants, namely $(\varepsilon, \alpha_{\mathbf{H}f})$, exists. This fact is reasonable from the viewpoint of mechanics, since $(\beta, \beta_{\mathbf{H}f}, v_p, \mu_{\mathbf{H}f})$ and $(\varepsilon, \alpha_{\mathbf{H}f})$ should characterize the material-dependent elastic coupling independent of the eigenvector planes used.

Proceeding with the **q**-Hilbert problem, the homogeneous **q**-Hilbert problem

$$\begin{aligned} &\mathbf{X}_{\Omega q}^{+}(\xi) - \mathbf{X}_{\Omega q}^{-}(\xi) = \mathbf{0}, \qquad \xi \in L_{\Omega}'', \\ &\mathbf{X}_{\Omega q}^{+}(\xi) + \Lambda_{\Omega q}\mathbf{X}_{\Omega q}^{-}(\xi) = \mathbf{0}, \qquad \xi \in L_{\Omega}'. \end{aligned} \tag{3.36}$$

has to be solved for the fundamental matrix, $\mathbf{X}_{\Omega q}(\zeta_{kj})$. Invoking the factorization of $\mathbf{X}_{\Omega q}(\zeta_{kj})$ provides the product representation

$$\mathbf{X}_{\Omega q} = \mathbf{X}_q\mathbf{X}_{qf} = \operatorname{diag}(X_{q1}X_{qf1}, X_{q2}X_{qf2}), \tag{3.37}$$

where $\mathbf{X}_q$ is associated with straight ligaments and $\mathbf{X}_{qf}$ covers the deviation due to the curvature. Solutions for $\mathbf{X}_{\Omega q}(\zeta_{kj})$, which fulfill the given limits

$$\Lambda_{\Omega q} = -\mathbf{X}_{\Omega qL_{\Omega}'}^{+}\left(\mathbf{X}_{\Omega qL_{\Omega}'}^{-}\right)^{-1}, \qquad \mathbf{I} = \mathbf{X}_{\Omega qL_{\Omega}''}^{+}\left(\mathbf{X}_{\Omega qL_{\Omega}''}^{-}\right)^{-1} \tag{3.38}$$

along the interface, have been evaluated for the cases of a semi-infinite ligament along the segment $L_{\Omega}' \in [0, \infty]$ and a ligament along the finite segment $L_{\Omega}' \in [0, b]$. The solutions read

$$\mathbf{X}_{\Omega q}(\zeta_{kj}) = \Lambda_{qf}^{1/2}(\zeta_{kj})\operatorname{diag}\left(\zeta_{kj}^{-(1/2-\alpha_f)+i\varepsilon}, \zeta_{kj}^{-(1/2-\alpha_f)-i\varepsilon}\right) \tag{3.39}$$

for a semi-infinite ligament, and

$$\mathbf{X}_{\Omega q}(\zeta_{kj}) = \operatorname{diag}\left(\zeta_{kj}^{-(1/2-\alpha_f)+i\varepsilon}(\zeta_{kj}-b)^{-(1/2+\alpha_f)-i\varepsilon},\ \zeta_{kj}^{-(1/2-\alpha_f)-i\varepsilon}(\zeta_{kj}-b)^{-(1/2+\alpha_f)+i\varepsilon}\right) \tag{3.40}$$

for a finite ligament crack of the length b. By introducing (3.38) into (3.28), the inhomogeneous **q**-Hilbert problem is reformulated as follows:

$$\begin{aligned}
&\left[(\mathbf{X}^{+}_{\Omega q}(\xi))^{-1}\mathbf{h}^{+}_{\Omega q}(\xi)\right]_{L''_\Omega} - \left[(\mathbf{X}^{-}_{\Omega q}(\xi))^{-1}\mathbf{h}^{-}_{\Omega q}(\xi)\right]_{L''_\Omega} = \mathbf{0}, && \xi \in L''_\Omega,\\
&\left[(\mathbf{X}^{+}_{\Omega q}(\xi))^{-1}\mathbf{h}^{+}_{\Omega q}(\xi)\right]_{L'_\Omega} - \left[(\mathbf{X}^{-}_{\Omega q}(\xi))^{-1}\mathbf{h}^{-}_{\Omega q}(\xi)\right]_{L'_\Omega}\\
&\qquad = \left[(\mathbf{X}^{+}_{\Omega q}(\xi))^{-1}\mathbf{q}_{\Omega\Lambda}(\xi)\right]_{L'_\Omega}, && \xi \in L'_\Omega.
\end{aligned} \tag{3.41}$$

For an arbitrarily generalized complex variable, ζ_{kj}, the simplest solution of (3.41), which primarily fulfills the jump conditions (3.39), is determined by the Cauchy integral representation

$$\begin{aligned}
\mathbf{h}_{\Omega q}(\zeta_{kj}) &= \frac{1}{2\pi i}\mathbf{X}_{\Omega q}(\zeta_{kj})\int\limits_{L'_\Omega}\left(\mathbf{X}^{+}_{\Omega q L'_\Omega}(\xi)\right)^{-1}\mathbf{q}_{\Omega\Lambda L'_\Omega}(\xi)\frac{d\xi}{\xi-\zeta_{kj}},\\
\mathbf{h}_{\Omega q} &= (h_{\Omega q1}, h_{\Omega q2})^{T}.
\end{aligned} \tag{3.42}$$

4. Stress intensity vectors for a dynamically extending interface crack

In this section, a stress intensity vector $\mathbf{K}_{R\Omega}$ definition of physical significance is introduced starting from the eigenvector planes for the **p**- and the **q**-problem, respectively. The denomination stress intensity vector is simply an adaptation of Stroh's method and will become apparent instantly. From the calculated eigenvector plane potential vectors for the cases of mechanical crack surface loading and thermal strains along the ligament, respectively, explicit integral formulae for stress intensity vectors, $\mathbf{K}_{R\Omega p}$ and $\mathbf{K}_{R\Omega q}$, are derived and discussed.

A proper eigenvector plane definition of the stress intensity vector independent of the special loading reads

$$\begin{aligned}
\mathbf{K}_{\Omega\Lambda} &= \sqrt{2\pi}\lim_{\xi\to 0}\left[(\mathbf{X}^{+}_{\Omega L'_\Omega})^{-1}(\xi)\mathbf{p}_{\Omega\Lambda L'_\Omega}(\xi)\right],\\
\mathbf{K}_{\Omega\Lambda} &= (K_{\Omega\Lambda\mathrm{II}}, K_{\Omega\Lambda\mathrm{I}})^{T},\\
\mathbf{X}^{+}_{\Omega L'_\Omega} &= \operatorname{diag}\left(\xi^{-1/2+f'\alpha_{\mathrm{II}f}+i\varepsilon}, \xi^{-1/2+f'\alpha_{\mathrm{II}f}-i\varepsilon}\right),\\
\mathbf{p}_{\Omega\Lambda L'_\Omega} &= (p_{\Omega\Lambda\mathrm{II}}, p_{\Omega\Lambda\mathrm{I}})^{T}_{L'_\Omega},
\end{aligned} \tag{4.1}$$

and formally assigns a single eigenvector plane stress vector component $p_{\Omega\Lambda j}$ to a single eigenvector plane stress intensity vector component $K_{\Omega\Lambda j}$, $(j = \mathrm{I}, \mathrm{II})$, similar to the case of cracks in a homogeneous material. However, the special interface fracture mechanics feature of the coupling of stress intensity factors and stress components is maintained in the physical plane and is only mathematically resolved. The derivation of the physical plane stress intensity vector definition is based on the physical requirement that the proportionality of any two vectors undergoing a transform must be preserved. Starting from the transformation relation of the stress vector in the physical plane and the eigenvector plane via the mappings

$$\begin{aligned}
\mathbf{p}_{\Omega p\Lambda} &= (\mathbf{V}_{\Omega p}^{-1}\mathbf{H}_{\Omega})\mathbf{p}_{\Omega p} = (\mathbf{V}_{\Omega q}\mathbf{S}_{\Omega})^{-1}\mathbf{p}_{\Omega p} \\
&\xrightarrow[\xi\to 0]{} \mathbf{p}_{\Omega p\Lambda} = (\mathbf{V}_p^{-1}\mathbf{H})\mathbf{p}_{\Omega p} = (\mathbf{V}_q\mathbf{S})^{-1}\mathbf{p}_{\Omega p}\,, \\
\mathbf{p}_{\Omega q\Lambda} &= \Lambda_{\Omega q}\mathbf{V}_{\Omega q}^{-1}\mathbf{p}_{\Omega q} = \mathbf{S}_{\Omega}\mathbf{V}_{\Omega p}^{-1}(-\overline{\mathbf{H}})_{\Omega} \\
&\xrightarrow[\xi\to 0]{} \mathbf{p}_{\Omega q\Lambda} = \Lambda_q\mathbf{V}_q^{-1}\mathbf{p}_{\Omega q} = \mathbf{S}\mathbf{V}_p^{-1}\mathbf{H}^T\mathbf{p}_{\Omega q},
\end{aligned} \tag{4.2}$$

to be applied for the coordinate $\xi = 0$, since the stress intensity vector measures the stress intensity at the location of the crack tip at $\xi = 0$, the stress intensity vector transformation laws

$$\begin{aligned}
\mathbf{K}_{\Omega p\Lambda} &= (\mathbf{V}_p^{-1}\mathbf{H})\mathbf{K}_{\Omega p} = (\mathbf{V}_q\mathbf{S})^{-1}\mathbf{K}_{\Omega p}\,, \qquad \mathbf{K}_{\Omega p} = (K_{\Omega p\mathrm{II}}, K_{\Omega p\mathrm{I}})^T\,, \\
\mathbf{K}_{\Omega q\Lambda} &= \Lambda_q\mathbf{V}_q^{-1}\mathbf{K}_{\Omega q} = \mathbf{S}\mathbf{V}_p^{-1}\mathbf{H}^T\mathbf{K}_{\Omega q}\,, \qquad \mathbf{K}_{\Omega q} = (K_{\Omega q\mathrm{II}}, K_{\Omega q\mathrm{I}})^T
\end{aligned} \tag{4.3}$$

must hold. Introducing the mapping (4.2) and (4.3) into (4.1) and omitting the respective indices p and q, determines the desired stress intensity vector definition

$$\begin{aligned}
\mathbf{K}_{\Omega} &= \sqrt{2\pi}\lim_{r\to 0}\left[\mathbf{V}_q\left(\mathbf{X}^{+}_{\Omega L'_{\Omega}}(r)\right)^{-1}\mathbf{V}_q^{-1}\mathbf{p}_{\Omega L'_{\Omega}}(r)\right], \\
\mathbf{K}_{\Omega} &= (K_{\Omega\mathrm{II}}, K_{\Omega\mathrm{I}})^T\,, \\
\mathbf{X}^{+}_{\Omega L'_{\Omega}} &= \mathrm{diag}\left(r^{-1/2+f'\alpha_{\mathbf{H}f}+i\varepsilon}, r^{-1/2+f'\alpha_{\mathbf{H}f}-i\varepsilon}\right), \\
[K_{\Omega\mathrm{II,I}}] &= \mathrm{Nmm}^{-3/2}\mathrm{mm}^{-i\varepsilon}
\end{aligned} \tag{4.4}$$

for the physical plane, where $\xi = 0$ has been replaced by r according to the standard notation of fracture mechanics. Like the stress vector components, the stress intensity factors are coordinates of the basis, $(\mathbf{e}_X, \mathbf{e}_Y)$. Apart from the intrinsic coupling of the stress vector components and the stress intensity factors, as originally recognized by RICE [42] for quasi-static interface crack extension, the stress intensity factor, $(K_{\Omega\mathrm{II}}, K_{\Omega\mathrm{I}})$, has the physically meaningless dimension $[K_{\Omega\mathrm{II,I}}] = \mathrm{Nmm}^{-3/2}\mathrm{mm}^{-i\varepsilon}$. Rice removed this physical inconsistency by relating

the ligament stresses to a characteristic length, $\hat{r}$, from which results a scaling of the stress intensity factors by the length $\hat{r}$. Transferring this scaling argument to $\mathbf{K}_\Omega$, the relation

$$\begin{aligned} \mathbf{K}_{R\Omega}(\hat{r}) &= \mathbf{V}_q \mathbf{X}_R(\hat{r}) \mathbf{V}_q^{-1} \mathbf{K}_\Omega , \\ \mathbf{X}_R &= \operatorname{diag}\left(\hat{r}^{+i\varepsilon}, \hat{r}^{-i\varepsilon}\right), \qquad [K_{R\Omega \mathrm{II,I}}] = \mathrm{Nmm}^{-3/2} \end{aligned} \tag{4.5}$$

provides the physically reasonable stress intensity vector definition

$$\mathbf{K}_{R\Omega} = \mathbf{K}_{R\Omega}(\hat{r}) = \sqrt{2\pi} \lim_{r \to 0} \left[\mathbf{V}_q \mathbf{X}_R(\hat{r}) \left(\mathbf{X}^+_{\Omega L'_\Omega}(r) \right)^{-1} \mathbf{V}_q^{-1} \mathbf{p}_{\Omega L'_\Omega}(r) \right]. \tag{4.6}$$

On account of the introduction of the length $\hat{r}$, the stress intensity factors in (4.6) are unique only if the length $\hat{r}$ is known. Since the stress intensity factors, $(K_{\Omega \mathrm{II}}, K_{\Omega \mathrm{I}})$, are associated with $r = \xi = 0$ and, consequently, are assigned to coordinates of the irrotational basis $(\mathbf{e}_X, \mathbf{e}_Y)$, due to the finite characteristic length $\hat{r}$, one would expect the $\mathbf{K}_{R\Omega}$-definition to start from normal and shear stresses along the curved interface which, of course, rotate with respect to the basis $(\mathbf{e}_X, \mathbf{e}_Y)$. However, if $\hat{r}$ remains small as compared to an overall specimen length like the crack length or the ligament length, this effect can be neglected.

Explicit formulae for the respective stress intensity vectors of the **p**-problem and the **q**-problem, denoted by $\mathbf{K}_{R\Omega p}$ and $\mathbf{K}_{R\Omega q}$ can be obtained, if the eigenvector-plane representations of the ligament stress vectors, $\mathbf{p}_{\Omega p \Lambda L'_\Omega}$ and $\mathbf{p}_{\Omega q \Lambda L'_\Omega}$, specified in

$$\begin{aligned} \mathbf{p}_{\Omega p \Lambda L'_\Omega} &= (\mathbf{V}_{\Omega p}^{-1} \mathbf{H}_\Omega) \mathbf{p}_{\Omega p L'_\Omega} , \qquad \mathbf{p}_{\Omega q \Lambda L'_\Omega} = \Lambda_{\Omega q} \mathbf{V}_{\Omega q}^{-1} \mathbf{p}_{\Omega q L'_\Omega} , \\ \mathbf{q}_{\Omega \Lambda L'_\Omega} &= (\mathbf{H}_\Omega \mathbf{V}_{\Omega q})^{-1} \mathbf{q}_{\Omega L'_\Omega} \end{aligned} \tag{4.7}$$

are replaced by means of the eigenvector plane potential vectors, $\mathbf{h}_{\Omega p}$ and $\mathbf{h}_{\Omega q}$, according to

$$\begin{aligned} (\mathbf{I} + \Lambda_{\Omega p}(\xi)) \mathbf{h}^+_{\Omega p L'_\Omega}(\xi) &= \mathbf{p}_{\Omega p \Lambda L'_\Omega}(\xi), \qquad \xi \in L'_\Omega , \\ (\mathbf{I} + \Lambda_{\Omega q}(\xi)) \mathbf{h}^+_{\Omega q L'_\Omega}(\xi) - \mathbf{q}_{\Omega \Lambda L'_\Omega}(\xi) &= \mathbf{p}_{\Omega q \Lambda L'_\Omega}(\xi), \qquad \xi \in L'_\Omega . \end{aligned} \tag{4.8}$$

By inverting (4.7), introducing the result into the stress intensity vector definition (4.6) and carefully employing some lenghty but straightforward calculations, the generic-type integral representation

$$\mathbf{K}_{R\Omega p}(\hat{r}) = -\sqrt{2/\pi} \cosh(\pi\varepsilon) \int_{L''_\Omega} \mathbf{V}_q \mathbf{X}_R(\hat{r}) \mathbf{Y}_{\Omega p}(t) \mathbf{V}_{\Omega q}^{-1}(t) \mathbf{p}_{\Omega_p L''_\Omega}(t)\, dt \tag{4.9}$$

for the **p**-problem and

$$\mathbf{K}_{R\Omega q}(\hat{r}) = \sqrt{2/\pi}\cosh^2(\pi\varepsilon)\int_{L'_\Omega}\mathbf{V}_q\mathbf{X}_R(\hat{r})\mathbf{Y}_{\Omega q}(t)\mathbf{V}^{-1}_{\Omega q}(t)\mathbf{D}^{-1}\mathbf{q}_{\Omega L'_\Omega}(t)\,dt \tag{4.10}$$

for the **q**-problem can be recovered. These generic formulae hold for crack surfaces and ligaments of finite and infinite length, only the corresponding diagonal matrices, $\mathbf{Y}_{\Omega p}$ and $\mathbf{Y}_{\Omega q}$, look different in each case. The index Ω indicates the simultaneous presence of curvature and fast crack propagation to be formally incorporated. It follows from a dimensional analysis, that the term $\mathbf{D}^{-1}\mathbf{q}_{\Omega L'_\Omega}$ in (4.10) is a stress vector, since $\mathbf{D}^{-1}$ is a compliance-like matrix and $\mathbf{q}_{\Omega L'_\Omega}$ is a strain vector. However, unlike the velocity-independent stress vector, $\mathbf{p}_{\Omega L''_\Omega}$, the vector $\mathbf{D}^{-1}\mathbf{q}_{\Omega L'_\Omega}$ is a decreasing function of the crack-tip velocity v.

For the sake of further discussions, due to the condition that the crack surface loading acts in normal and tangential direction along the interval $[-a, 0]$ and only the first order terms are taken into account, the general formula (4.9) is written out to give

$$\begin{pmatrix} K_{R\Omega p\mathrm{II}} \\ K_{R\Omega p\mathrm{I}} \end{pmatrix} = \sqrt{\frac{2}{\pi}}\cosh(\pi\varepsilon)$$

$$\times\int_0^{-a}\begin{pmatrix} \operatorname{Re} Y_p & -f'\operatorname{Re} Y_p + v_p \operatorname{Im} Y_p \\ \left(1+\frac{\mu_{\mathrm{H}f}}{v_p}\right)f'\operatorname{Re} Y_p - \frac{1}{v_p}\operatorname{Im} Y_p & \operatorname{Re} Y_p \end{pmatrix}\begin{pmatrix} p_t \\ p_n \end{pmatrix}(-dt),$$

$$Y_p = (-t)^{-1/2-f'(t)\alpha_{\mathrm{H}f}}\left(-\frac{t}{\hat{r}}\right)^{-i\varepsilon}, \quad \text{for a semi-infinite interface crack,} \tag{4.11}$$

$$Y_p = \left(\frac{-at}{a+t}\right)^{-1/2-f'(t)\alpha_{\mathrm{H}f}}\left(-\frac{t}{\hat{r}}\,\frac{a}{a+t}\right)^{-i\varepsilon}, \quad \text{for an interface crack of length } a,$$

for the stress intensity factors of the **p**-problem. The analysis of the explicit integral formula (4.11) as well as the inspection of the table in Fig. 3 leads to the conclusion that the individual influence of each of the interface fracture mechanics features of interest: mechanical loading, interface, crack-tip velocity and interface curvature, and their relations with the stress intensity factors are rather complicated. Since multi-valued relations between the mechanical features and the mechanical parameters, (p_t, p_n), $\hat{r}$, v_p, ε, f', $\mu_{\mathrm{H}f}$, $\alpha_{\mathrm{H}f}$, (denoted by bold type dots in the table) exist, it can hardly be concluded from (4.11) that certain mechanical parameters and/or their interactions dominate.

An analytical solution of (4.11) can only be obtained for a single point load which stresses the crack surface at $t = -t_\delta$. Restricting the analysis to a pure normal load, $p_n = p_{0n}\delta(t + t_\delta)$, in order to extract the essential phenomena,

$K_{R\Omega pII}$ / $K_{R\Omega pI}$	p_t / p_n	$\hat{r}$	v_p	ε	f'	μ_{Hf}	α_{Hf}
loading	•						
interface		•	•	•		•	•
velocity			•	•		•	•
curvature					•	•	•

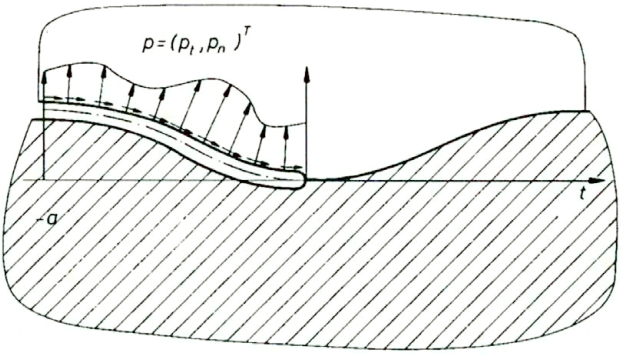

FIG. 3. Dependence of the stress intensity factors ($K_{R\Omega pII}$, $K_{R\Omega pI}$) on the parameters of interface fracture mechanics in the case of the p-problem.

the evaluation of (4.11) and the subsequent determination of the magnitude as well as the mixed-mode phase angle, defined by $K_{R\Omega p} = \sqrt{K^2_{R\Omega pI} + K^2_{R\Omega pII}}$ and $\omega_{Rp} = \arctan(K_{R\Omega pII}/K_{R\Omega pI})$, provides the following first order approximation

$$
\begin{aligned}
K_{R\Omega p} &= \sqrt{2/\pi}\,\cosh(\pi\varepsilon)p_{0n}\left(\frac{1}{t_\delta}\right)^{1/2}\left(\frac{1}{t_\delta}\right)^{\alpha_f}, \\
\alpha_f(-t_\delta) &= f'(-t_\delta)\alpha_{Hf}, \qquad (4.12) \\
\omega_{Rp} &= -\left(f'(-t_\delta) + v_p\varepsilon \ln\left(\frac{t_\delta}{\hat{r}}\right)\right).
\end{aligned}
$$

Different from the case of a straight running interface crack, the magnitude is affected by the newly introduced bimaterial constant α_{Hf}, and by the interface slope f'. The linear relation between the slope f' and the phase angle is an effect to be anticipated. This characteristic is maintained in an average manner, if the integral for $\mathbf{K}_{R\Omega p}$ in (4.11) has to be evaluated for mechanical loads stressing along the whole interval $[-a, 0]$. By inspection of the integral formula (4.11), the interface slope f' is basically a linear factor. This structure is well known from the first order analysis of COTTERELL and RICE [8] for the case of a quasi-static crack propagation in a homogeneous material. Furthermore, GAO and CHIU [21] recently investigated among other things, the quasi-static crack extension in an anisotropic homogeneous material in the first order sense. Keeping in mind that, even for an isotropic material, the dynamic case is formally equivalent to the quasi-static case for an anisotropic material, the stress intensity factor formula (4.11) is a generalization of the established results. It has to be stressed, that this paper does not deal with any time-dependent stress intensity factor formula. It treats the long-time and thus steady-state interface crack extension case, which was firstly studied by YOFFE [63] for a running Griffith crack in a homogeneous material. Therefore, the formation of the stress intensity factor as a product of a velocity-dependent and load-dependent function times a $\sqrt{t}$-function, which was

introduced and comprehensively discussed by FREUND [18, 19], is not an objective of this paper [18, 19]. To make it clear, in $\sqrt{t}$ the letter t denotes the time. The factorization problem for the general time-dependent interface crack problem is currently a completely unsolved problem, since the solution procedure of the most promising mathematical method, the vectorial Wiener-Hopf technique, is still not available. Nevertheless, as proposed by YANG *et al.* [62], a factorization, which has to incorporate the bimaterial constant ε, should exist. According to Yoffe's contribution and some extensions also confined to homogeneous material, the magnitude of the steady-state stress intensity factor is not a function of the crack-tip velocity, v. This physically unsatisfactory result can be explained by interpreting the pair of crack tips as a reversible energy converter. In this investigation, the deviations from the Yoffe problem due to an interface as well as its curvature are of interest. With regard to a qualitative understanding of the corresponding velocity dependence of the stress intensity vector $\mathbf{K}_{R\Omega p}$, its magnitude, $K_{R\Omega p}$, and its mixed-mode phase angle, ω_R, have been simulated for curvilinear interface contours up to the maximum slope of $|f'_{\max}| = 0.5$. The contours are assumed to behave as third order polynomials. The magnitude of $K_{R\Omega p}$ has been normalized with respect to the value corresponding to zero-velocity and to a straight interface. The normalization is denoted by $K_{R\Omega p0}$. The simulations have been performed in the velocity interval $[0, 0.91 v_{R1}]$. A bimaterial with the bimaterial constant $\varepsilon_0 = \varepsilon(v = 0) = 0.096$, the Rayleigh-wave velocities $v_{R1} = 988\,\text{m/s}$ and $v_{R2} = 2914\,\text{m/s}$ have been chosen. In addition, the characteristic length $\hat{r} = 1.0\,\text{mm}$ has been selected. Note that this bimaterial is strongly elastically mismatched and, as an example, corresponds to the material combination of the resin ARALDITE B and steel. From representative plots for the mixed-mode loading situation of constant magnitude, with loads $p_t = p_n = -1.0\,\text{N/mm}^2$ acting along the interval $[-a, 0]$, $a = 5.0\,\text{mm}$, and shown in Figs. 4 and 5, it is seen that, in contrast to the Yoffe case, the normalized magnitude, $(K_{R\Omega p}/K_{R\Omega p0})$, varies versus the crack-tip velocity v. However, significant changes can only be observed if the crack velocity exceeds about one half of the minimum Rayleigh-wave veloctiy, v_{R1}, and non-straight crack surfaces are additionally involved. The rapid increase of $(K_{R\Omega p}/K_{R\Omega p0})$ for velocities higher than $v = 0.8 v_{R1}$ indicates the limit of validity of the presented first order theory. One should remind that the experimentally measured crack-tip velocities are limited to about $0.8 v_{R1}$. The failure of the theory can be traced back to the tendency of the bimaterial constants to become infinite by approaching v_{R1}. Although not anticipated at the first sight, the mixed-mode phase angle ω_R varies only slightly with the crack-tip velocity as long as the first order theory remains valid. This behaviour is confirmed by the mixed-mode phase angle in (4.12). It should be noted that the loading situation $p_t = p_n$ imposed to a straight crack in a homogeneous material is associated with the mixed-mode phase angle, $\omega_R = 45°$. In addition, a phase shift proportional to the respective maximum crack surface slope, $f'_{\max}$, is not astonishing. In view of the experimental interface fracture mechanics, a velocity-independent ω_R makes

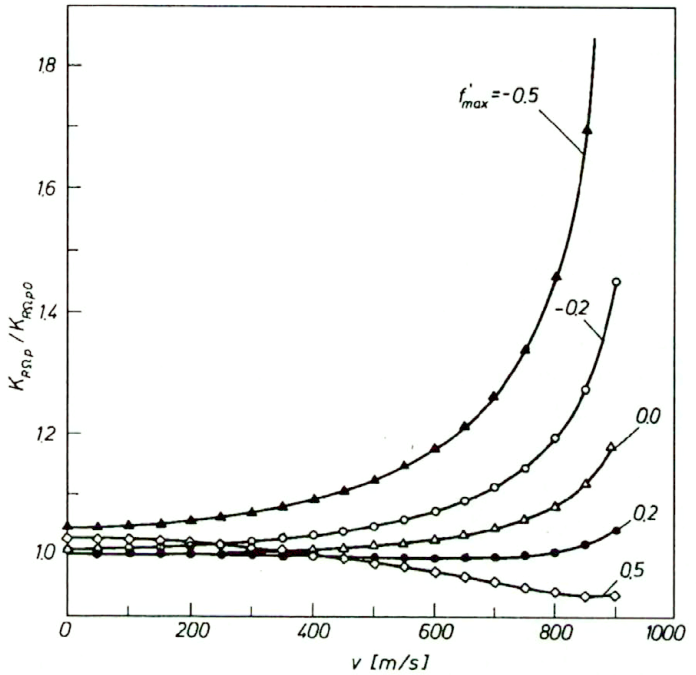

$p_t = -1.0\ \mathrm{N/mm^2}$,
$p_n = -1.0\ \mathrm{N/mm^2}$,
$q_{\Omega 0} = \Delta\alpha\Delta T = 0.0$,
$f'(t) = -4f'_{\max}[(t/5)+(t/5)^2]$,
$\varepsilon_0 = 0.096$,
$\hat{r} = 1.0$ mm.

FIG. 4. Influence of the curvature and the crack-tip velocity on the magnitude of the stress intensity vector, $\mathbf{K}_{R\Omega p}$, in case of crack surfaces under normal and shear loading.

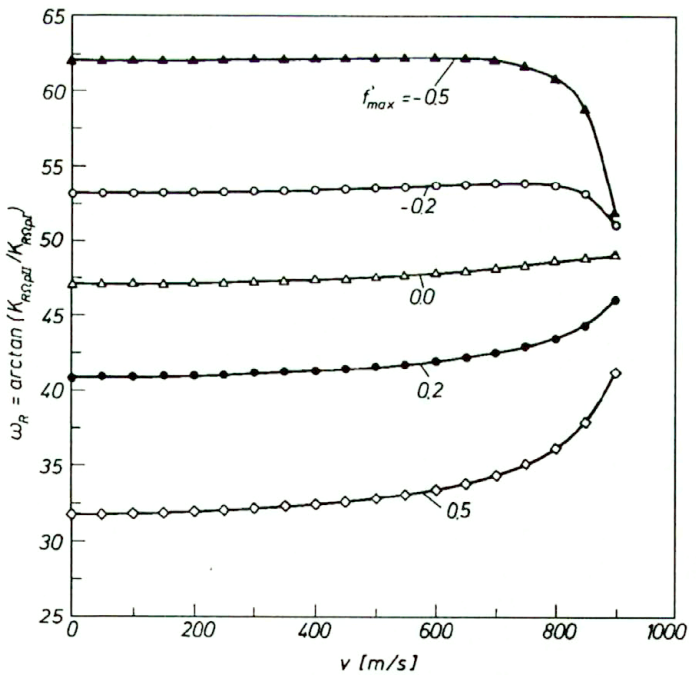

$p_t = -1.0\ \mathrm{N/mm^2}$,
$p_n = -1.0\ \mathrm{N/mm^2}$,
$q_{\Omega 0} = \Delta\alpha\Delta T = 0.0$,
$f'(t) = -4f'_{\max}[(t/5)+(t/5)^2]$,
$\varepsilon_0 = 0.096$,
$\hat{r} = 1.0$ mm.

FIG. 5. Influence of the curvature and the crack-tip velocity on the mixed-mode phase angle of the stress intensity vector, $\mathbf{K}_{R\Omega p}$, in case of crack surfaces under normal and shear loading.

possible a reduction of the experimental parameters, recorded from a running interface crack, to only one if the mixed-mode phase angle ω_R of the static case has been measured once.

For completeness note that, for a pure normal crack surface pressure, $p_n = -1.0\,\mathrm{N/mm^2}$, and for a pure shear crack surface traction, $p_t = -1.0\,\mathrm{N/mm^2}$, the characteristics of $(K_{R\Omega p}/K_{R\Omega p0})$ and ω_R do not change apart from the apparent phase shift induced by the rotation of the phase angle corresponding to the ratio (p_t/p_n).

For a more sophisticated analysis of the thermally strained ligament case, assuming that the thermal strains act along the finite interval $[0, b]$ of the length b, and neglecting second order terms, the general integral formula (4.10) transforms to the explicit expressions

$$\begin{pmatrix} K_{R\Omega q\mathrm{II}} \\ K_{R\Omega q\mathrm{I}} \end{pmatrix} = \sqrt{\frac{2}{\pi}}\cosh^2(\pi\varepsilon) \times \int_0^b \begin{pmatrix} \mathrm{Re}\, Y_q & 0 \\ f'\frac{\mu_{\mathbf{H}f}}{v_p}\mathrm{Re}\, Y_q - \frac{1}{v_p}\mathrm{Im}\, Y_q & f'\frac{1}{v_p^2}\mathrm{Re}\, Y_q \end{pmatrix} \begin{pmatrix} \Delta\alpha_{11} \\ \Delta\alpha_{22} \end{pmatrix} \frac{\Delta T}{D_1}\,dt,$$

(4.13)
$$Y_q = (t)^{-1/2-f'(t)\alpha_{\mathbf{H}f}} \left(\frac{t}{\hat{r}}\right)^{-i\varepsilon}, \qquad \text{for a semi-infinite ligament,}$$

$$Y_q = \left(\frac{bt}{b-t}\right)^{-1/2-f'(t)\alpha_{\mathbf{H}f}} \left(\frac{t}{\hat{r}}\,\frac{b}{b-t}\right)^{-i\varepsilon}, \qquad \text{for a ligament of length } b,$$

for the stress intensity factors of the **q**-problem, where $\Delta\alpha_{11} = [(\alpha_{11})_2 - (\alpha_{11})_1]$ and $\Delta\alpha_{22} = [(\alpha_{22})_2 - (\alpha_{22})_1]$ denote the difference of the thermal expansion tensor components of diagonal form, and $\Delta T = T - T_0$ denotes the applied cooling or heating relative to the reference temperature, T_0. Similar to the **p**-problem, it is recognized from (4.13) that the relations between the thermomechanical parameters, (q_x, q_y), $\hat{r}$, D_1, v_p, ε, f',$\mu_{\mathbf{H}f}$, $\alpha_{\mathbf{H}f}$, and the thermomechanical features in question: thermal loading, interface, velocity and curvature, are rather complex and by no means single-valued. This fact becomes more obvious from the inspection of the supplementary table in Fig. 6. However, note that beyond the parameters of the **p**-problem, the compliance-like constant D_1 (compare with matrix **H** (3.5)) occurs additionally. Furthermore, as the y-component of the thermal strain vector, $\mathbf{q}_{\Omega L'_\Omega} = (\Delta\alpha_{11}\Delta T,\ f'(t)\Delta\alpha_{22}\Delta T)^T = (q_x, q_y)^T$, depends on the slope of the ligament, given by the geometrical shape of the structural element under investigation, the thermal strains intrinsically cause a mixed-mode ligament stress field.

In view of outstanding dynamic aspects of the thermal strain problem, the

$K_{R\Omega q\mathrm{II}}$ / $K_{R\Omega q\mathrm{I}}$	q_x / q_y	$\hat{r}$	D_1	v_p	ε	f'	μ_{Hf}	α_{Hf}
loading	•							
interface		•	•	•	•		•	•
velocity			•	•	•		•	•
curvature	•					•	•	•

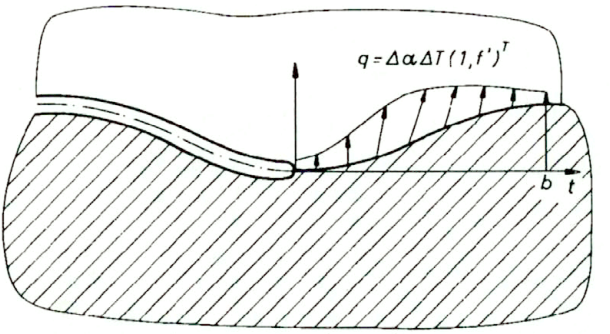

FIG. 6. Dependence of the stress intensity factors, $(K_{R\Omega q\mathrm{II}}, K_{R\Omega q\mathrm{I}})$, on the parameters of interface fracture mechanics in the case of the **q**-problem.

q-problem differs from the **p**-problem substantially by the factor

$$\begin{aligned} \frac{\cosh(\pi\varepsilon(v))(\Delta\alpha\Delta T)}{D_1(v)} &= (\Delta\alpha\Delta T)\cdot\frac{\mu_1 R_1\cosh(\pi\varepsilon)}{\tilde{D}_{11}+\tilde{D}_{12}(\mu_1 R_1)/(\mu_2 R_2)}, \\ &= (\varepsilon^{\mathrm{th}}\mu_1)\quad\cdot\qquad\Sigma(v), \\ \sigma^{\mathrm{th}}(v) &= \sigma_0^{\mathrm{th}}\quad\cdot\qquad\Sigma(v), \\ 0\le v\le v_{R1} &\rightarrow \sigma^{\mathrm{th}}(0)>\sigma^{\mathrm{th}}(v)>\sigma^{\mathrm{th}}(v_{R1})=0, \end{aligned} \tag{4.14}$$

where mechanical and thermal isotropy of the material is assumed for simplicity. From the physical point of view, the expression (4.14) states that, due to dimensional reasons, the stress-like loading in (4.13) or (4.10) splits into a constant thermal stress, $\sigma_0^{\mathrm{th}} = \varepsilon^{\mathrm{th}}\mu_1$, generated by the thermal strains, $\varepsilon^{\mathrm{th}} = \Delta\alpha\Delta T$, and the shear modulus μ_1, as well as a non-dimensional but velocity-dependent stress factor, $\Sigma(v)$, to result in a velocity-dependent thermal stress, $\sigma^{\mathrm{th}}(v)$, along the ligament. The analysis of $\Sigma(v)$ proves $\sigma^{\mathrm{th}}(v)$ to be a monotonically decreasing function of the crack-tip velocity v. This function tends to zero if the minimum Rayleigh-wave velocity v_{R1} is approached. Moreover, a monotonic decline of the $(K_{R\Omega q\mathrm{II}}, K_{R\Omega q\mathrm{I}})$-graphs versus the crack-tip velocity, v, can be detected. For the theoretical limit case of the stress intensity factors at v_{R1}, a universal statement concerning the $(K_{R\Omega q\mathrm{II}}, K_{R\Omega q\mathrm{I}})$-values is not possible. However, this velocity behaviour of $\mathbf{K}_{R\Omega q}$ is confirmed by the velocity characteristic of Nilsson's studies of a rapid crack propagation in a homogeneous material [33]. Nilsson investigated the problem of a finite strip subjected to uniform displacements at the edges and arrived at a comparable velocity influence on the stress intensity factor. Since the jump of the thermal displacement along the ligament can be interpreted as a dislocation, a comment in the framework of material science is instructive. WEERTMAN [58] studied the fast propagation of a dislocation running along the interface of dissimilar isotropic media and concluded that the stresses, σ_{2j}, decrease, if the velocity rises. He especially calculated the stresses, σ_{2j}, to be zero slightly above v_{R1}. Like in the **p**-problem, the normalized magnitude, $(K_{R\Omega q}/K_{R\Omega q0})$, and the

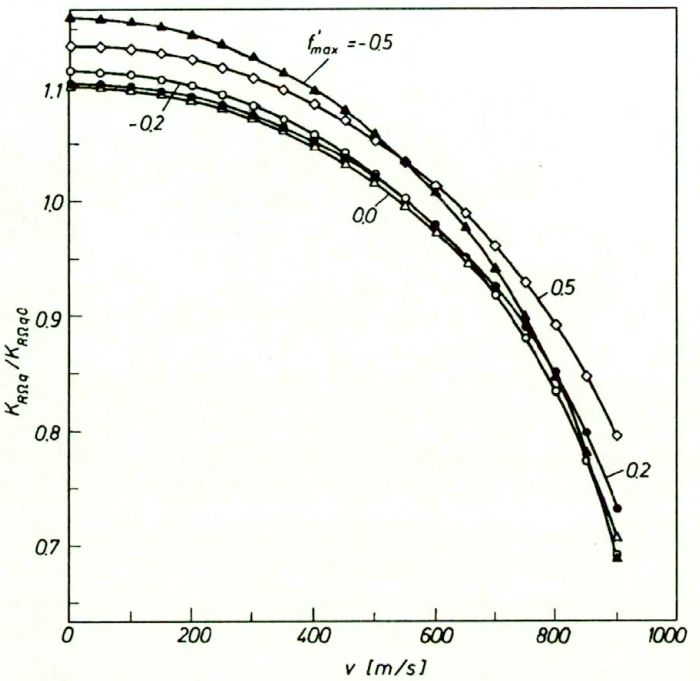

$p_t = 0.0\ \mathrm{N/mm^2}$,
$p_n = 0.0\ \mathrm{N/mm^2}$,
$q_{\Omega 0} = \Delta\alpha\Delta T = 10^{-3}$,
$f'(t) = 4f'_{\max}[(t/5)-(t/5)^2]$,
$\varepsilon_0 = 0.096$,
$\hat{r} = 1.0$ mm.

FIG. 7. Influence of the curvature and the crack-tip velocity on the magnitude of the stress intensity vector, $\mathbf{K}_{R\Omega q}$, in case of thermal strains acting along the ligament.

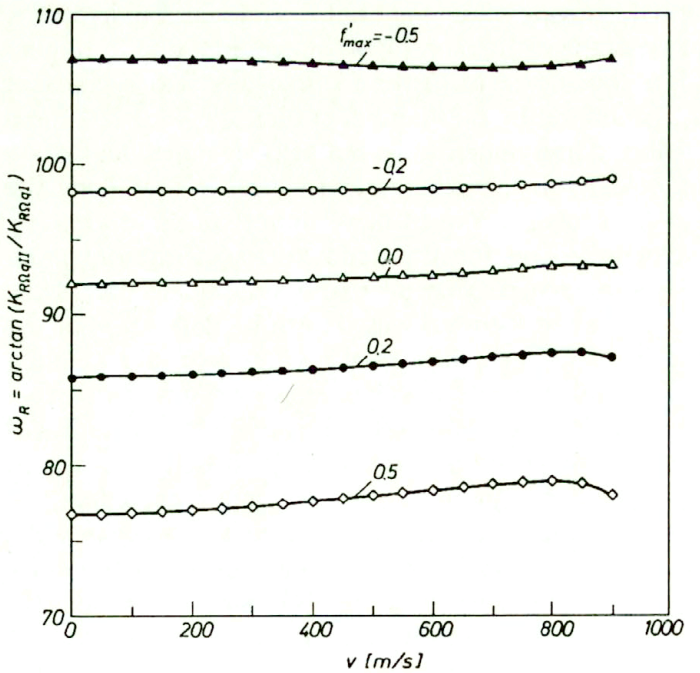

$p_t = 0.0\ \mathrm{N/mm^2}$,
$p_n = 0.0\ \mathrm{N/mm^2}$,
$q_{\Omega 0} = \Delta\alpha\Delta T = 10^{-3}$,
$f'(t) = 4f'_{\max}[(t/5)-(t/5)^2]$,
$\varepsilon_0 = 0.096$,
$\hat{r} = 1.0$ mm.

FIG. 8. Influence of the curvature and the crack-tip velocity on the mixed-mode phase angle of the stress intensity vector, $\mathbf{K}_{R\Omega q}$, in case of thermal strains acting along the ligament.

mixed-mode phase angle, $\omega_R = \arctan(K_{R\Omega q\mathrm{II}}/K_{R\Omega q\mathrm{I}})$, of the **q**-problem have been simulated to determine the velocity characteristics of $\mathbf{K}_{R\Omega q}$, where ligaments of the third order polynomials with the same limiting values of $|f'_{\max}| = 0.5$ for the maximum slope have been used. The thermal strains are selected to operate along the interval $[0, b]$ of the length, $b = 5.0\,\mathrm{mm}$. The special material constants of the **p**-problem and the characteristic length, $\hat{r} = 1.0\,\mathrm{mm}$, have been retained. The results of the simulations are shown in Figs. 7 and 8. Similarly to the **p**-problem and despite the curvature involved, almost no sensitivity to the crack-tip velocity is observed for the mixed-mode phase angle, $\omega_R = \arctan(K_{R\Omega q\mathrm{II}}/K_{R\Omega q\mathrm{I}})$. The theoretically estimated decrease of the magnitude $(K_{R\Omega q}/K_{R\Omega q0})$ versus increasing velocities becomes clearly apparent. A more detailed analysis demonstrates that the individual decrease is visibly altered by the special maximum slope of the curved ligament.

5. Determination of stress intensity factors by the method of caustics

5.1. Caustics for dynamic interface crack propagation

This section deals with the derivation of caustics equations for dynamically propagating interface cracks where the framework based on Stroh's method, which was developed before, is utilized. The curvature of the interface is excluded from the analysis. Figure 9 shows the deviation of parallel light beams, penetrating a cracked bimaterial specimen. Due to the change of the elasto-optical constants and due to the deformation of the specimen surface, induced by the stress field singularity, a shadow spot is generated in the real or the virtual reference plane. The bright limit curve of the shadow spot is called caustic. While the just described transmission principle, developed by MANOGG [32], is restricted to a transparent specimen, due to THEOCARIS [51], an opaque specimen can also be investigated by invoking the reflection principle [28]. In order to simplify the experimental set-up, the method of caustics has been extended to non-parallel light.

The mapping equation for the shadow spot is given by the expression

$$\mathbf{w}_j = m\,[\mathbf{r}_j - C_j(\nabla(\sigma_1 + \sigma_2)_j \pm \lambda_j \nabla(\sigma_1 - \sigma_2)_j)] \qquad (j = 1, 2), \tag{5.1}$$

where $C_j = (z_0 d_{\mathrm{eff}} c_j)/m$. The constants, c_j and λ_j, are the shadow optical constants and the so-called optical anisotropy constants of the bimaterial component j, respectively. The mapping scale, $m \neq 1.0$, concerns the case of non-parallel light and is determined by the experimental arrangement. The caustic can be obtained by introducing the so-called initial curve, $r = r(\phi)$, following from the solutions of the equation (5.2) into the formula (5.1)

$$J = \frac{\partial(x', y')}{\partial(x, y)} = 0, \qquad \mathbf{w} = (x', y'), \qquad \mathbf{r} = (x(r, \phi), y(r, \phi)). \tag{5.2}$$

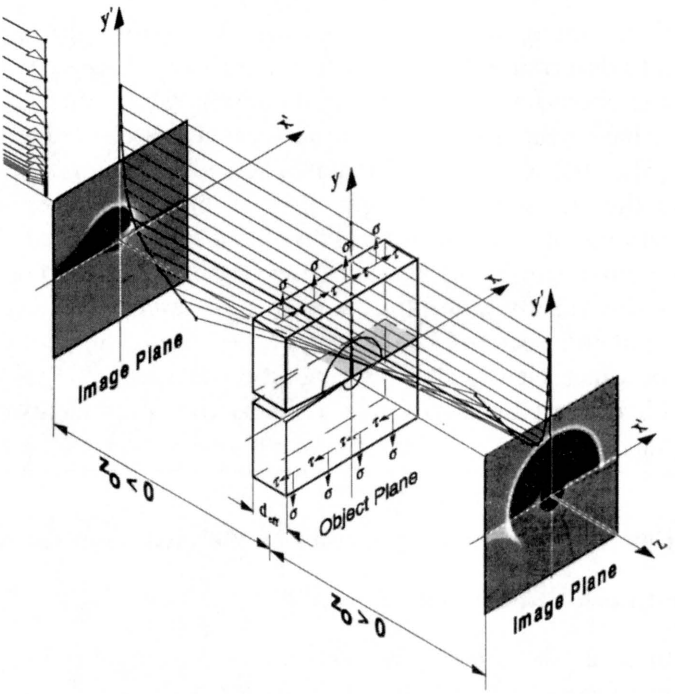

FIG. 9. Physical principle of caustics around an interface crack.

In other words, a light beam intersecting the fictitious initial curve is deflected in such a manner that it forms a point of the caustic contour. In the case of existence of optical anisotropy in both parts of the bimaterial, two shadow spots and thus two caustics, so-called double caustics, are generated, where the latter are built up from two initial curves. The caustics are no longer simply connected curves due to the discontinuity of the material constants along the interface. By applying the gradient operator to the sum and the difference of the principal stresses, referring to the equations (2.17) and (2.18), and by introducing the results into the general mapping equation (5.1), the expressions

$$\mathbf{w}_j = \mathbf{r}_j - 2C_j \left(\frac{(\operatorname{Re}(\mathbf{E}^+\mathbf{f}'(\mathbf{z})))_j^T}{|\operatorname{Re}(\mathbf{E}^+\mathbf{f}'(\mathbf{z}))|_j} \operatorname{Re} \begin{pmatrix} \mathbf{E}^+\mathbf{f}''(\mathbf{z}) \\ \mathbf{E}^+\mathbf{P}\mathbf{f}''(\mathbf{z}) \end{pmatrix}_j \pm \lambda_j \frac{(\operatorname{Re}(\mathbf{E}^-\mathbf{f}'(\mathbf{z})))_j^T}{|\operatorname{Re}(\mathbf{E}^-\mathbf{f}'(\mathbf{z}))|_j} \operatorname{Re} \begin{pmatrix} \mathbf{E}^-\mathbf{f}''(\mathbf{z}) \\ \mathbf{E}^-\mathbf{P}\mathbf{f}''(\mathbf{z}) \end{pmatrix}_j \right) \tag{5.3}$$

are obtained. Since the experimental determination of the stress intensity factors is in question, and therefore no potential vectors calculated from the special solutions of the **p**-problem and of the **q**-problem are required, the near-tip potential vectors are utilized. The near-tip potential vectors which are much easier

to handle are derived by presupposing the mechanical loads on the crack surfaces and the thermal strains along the ligament to be zero, and thereby arriving at the homogeneous vectorial Hilbert problem related to (3.1). The components of the near-tip potential vectors valid for the bimaterial part j, $(j = 1, 2)$ read

$$
\begin{aligned}
f'_{k1}(z_{k1}) &= \mathbf{i}_k^T \mathbf{B}_1^{-1} \frac{1}{\sqrt{2\pi}} \mathbf{V}_q (\mathbf{I} + \Lambda_p)^{-1} \mathbf{X}_p(z_{k1}) \mathbf{X}_R^{-1}(\hat{r}) \mathbf{V}_q^{-1} \mathbf{K}_R(\hat{r}), \\
f'_{k2}(z_{k2}) &= \mathbf{i}_k^T \mathbf{B}_2^{-1} \frac{1}{\sqrt{2\pi}} \mathbf{V}_q (\mathbf{I} + \Lambda_q)^{-1} \mathbf{X}_p(z_{k2}) \mathbf{X}_R^{-1}(\hat{r}) \mathbf{V}_q^{-1} \mathbf{K}_R(\hat{r}), \\
\mathbf{i}_1 &= (1,0)^T, \qquad \mathbf{i}_2 = (0,1)^T.
\end{aligned} \tag{5.4}
$$

Here, with the exception of the parts related to any interface curvature, the diagonal matrix $\mathbf{X}_p$ is the same as the fundamental solution of the **p**-problem in equation (3.22). In order to determine the initial curve, the functional determinant (5.2) is calculated from equation (5.3). Disregarding the index j, the reformulated result reads

$$
J = 1 + Cu(x, y) - C^2 v(x, y) = 0, \tag{5.5}
$$

where u and v are obtained from g and h by evaluating the expressions

$$
\begin{aligned}
u &= \frac{\partial h}{\partial y} - \frac{\partial g}{\partial x}, \qquad v = \frac{\partial g}{\partial x}\frac{\partial h}{\partial y} - \frac{\partial h}{\partial x}\frac{\partial g}{\partial y}, \\
g &= g_1 \pm \lambda g_2, \qquad h = h_1 \pm \lambda h_2
\end{aligned} \tag{5.6}
$$

and g and h are related to the gradients of $(\sigma_1 + \sigma_2)$ and $(\sigma_1 - \sigma_2)$ by

$$
\nabla(\sigma_1 + \sigma_2)_j = (g_1, -h_1)_j^T, \qquad \nabla(\sigma_1 - \sigma_2)_j = (g_2, -h_2)_j^T. \tag{5.7}
$$

The fundamental problem to calculate the initial curve $r = r(\phi)$ from (5.5) can be achieved only in the case of a crack situated in a homogeneous material, because otherwise the functional determinant becomes a transcendental function and the initial curve, $r = r(\phi)$, has to be calculated numerically. Especially for the case of interface cracks, it is not advantageous to write down the mapping equation in an explicit manner, since lengthy expressions arise from which almost no quantitative conclusions can be deduced. Therefore, the characteristic influences on the caustics are obtained from numerical simulations. In what follows, the stress intensity factors $(K_{RI}(\hat{r}), K_{RII}(\hat{r}))$ are denoted by (K_I, K_{II}), and the characteristic length $\hat{r} = 1.0\,\text{mm}$ is chosen for convenience. Figure 10 shows the mixed-mode caustics around an interface crack tip on both sides of the bimaterial interface, where optical isotropy of the material is considered. The jump in the caustic size is caused by the different elastic and optical material constants across the material interface. In this study, the interface crack is assumed to be situated in a bima-

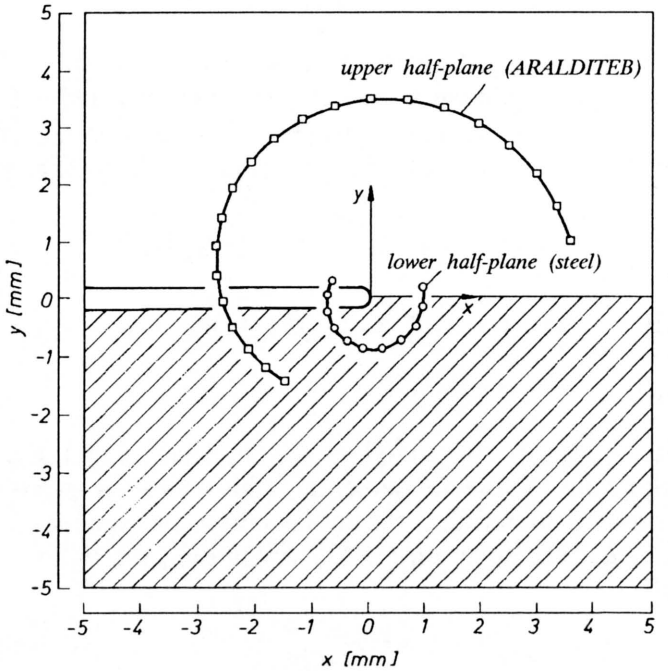

$K_{II}/K_I = 1.0,$
$\varepsilon_0 = 0.096,$
$\lambda = 0.0,$
$v/v_{R1} = 0.5.$

FIG. 10. Influence of the material inhomogeneity on the shape of mixed-mode caustics around a running interface crack tip in the case of optical isotropy of the bimaterial components.

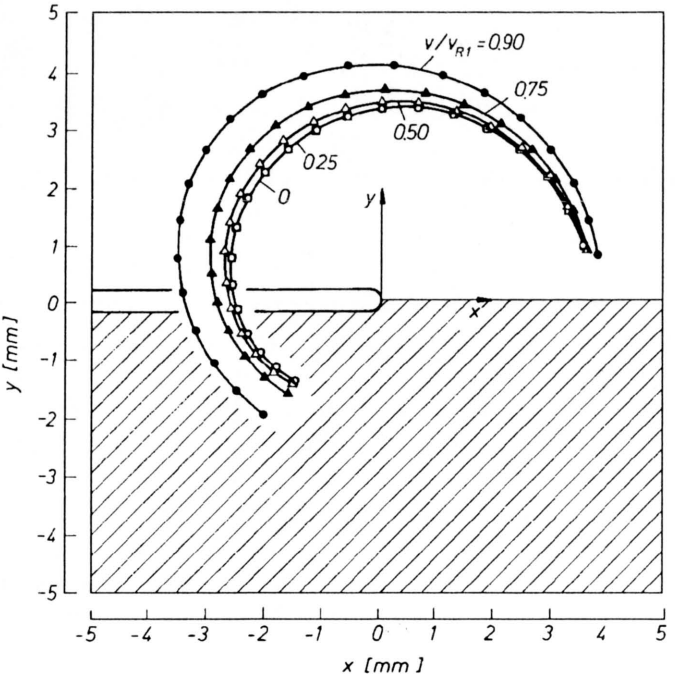

$K_{II}/K_I = 1.0,$
$\varepsilon_0 = 0.096,$
$\lambda = 0.0.$

FIG. 11. Influence of the crack tip velocity on the shape of mixed-mode caustics in the upper bimaterial component by consideration of optical isotropy of the material.

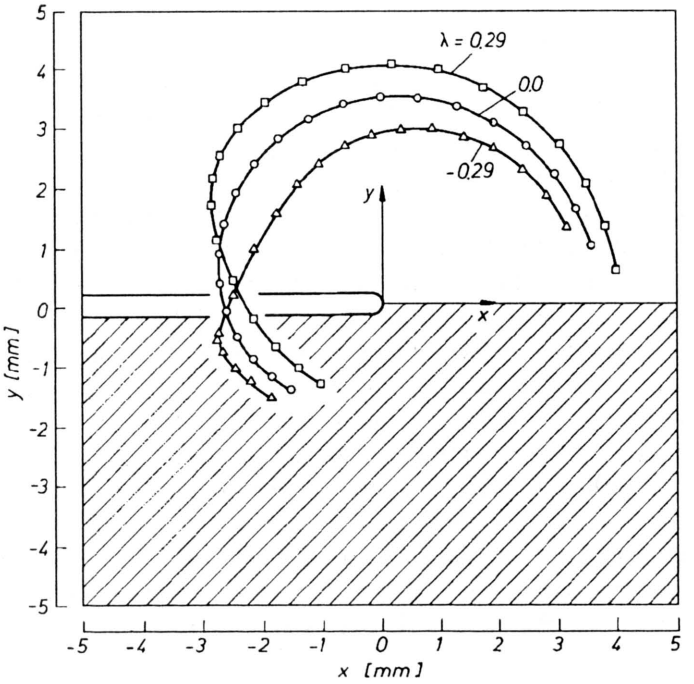

$K_{II}/K_I = 1.0,$
$\varepsilon_0 = 0.096,$
$v/v_{R1} = 0.5.$

FIG. 12. Comparison of caustics for optical isotropy and optical anisotropy of the material by consideration of the upper bimaterial component.

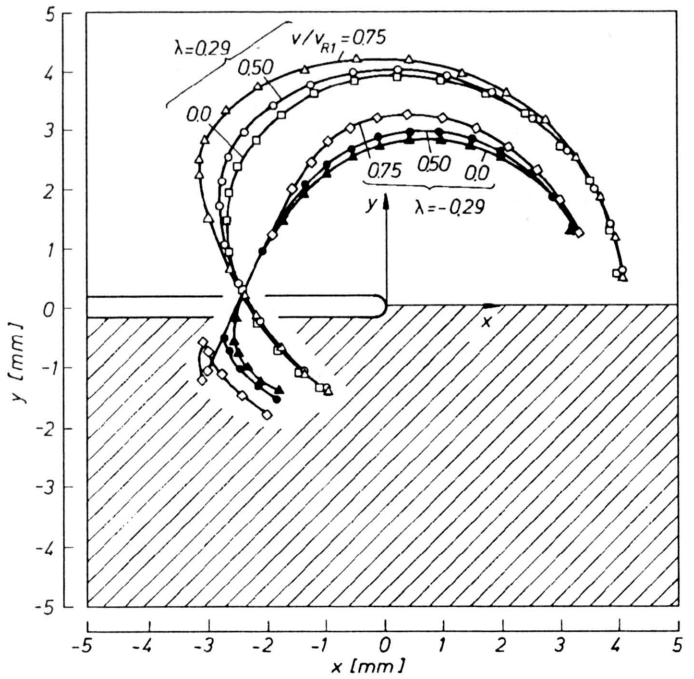

$K_{II}/K_I = 1.0,$
$\varepsilon_0 = 0.096.$

FIG. 13. Influence of the crack-tip velocity and the optical anisotropy of the material on the shape of mixed-mode caustics in the upper bimaterial component.

terial with material properties of the compound of resin ARALDITE B and steel. Figure 11 demonstrates the influence of the crack-tip velocity on the shape of the caustics obtained by considering the mixed-mode loading relations around the tip of a running interface crack where only the upper side of the bimaterial interface has been taken into account. The size of the caustics increases with increasing crack-tip velocity, this increase being significant only for crack-tip velocities of at least about one half of the minimum of the Rayleigh-wave velocity v_{R1}. This result has been confirmed by the investigations of KALTHOFF [28] and NISHIOKA and KITTAKA [34] for running cracks in a homogeneous material. In addition, it is confirmed by the conclusions inferred from the simulations of the magnitudes and the mixed-mode phase angles of the stress intensity vectors, $\mathbf{K}_{R\Omega p}$ and $\mathbf{K}_{R\Omega q}$, versus the crack-tip velocity v. A more extensive discussion concerning different mixe-mode ratios can be found in [22, 23, 39]. In Fig. 12 both parts of a double caustic are compared with the associated caustic for the case of optical isotropy. Figure 13 shows that each branch of the double caustic is influenced by the crack tip velocity, but a general comparison with Fig. 12 demonstrates that the influence of the optical anisotropy is more distinct for that chosen λ-value.

5.2. Algorithm for the determination of stress intensity factors

Basing on the caustics equations derived before, a measuring algorithm has been formulated in order to determine stress intensity factors from the experimentally obtained caustics. For a more accurate and more complete recording of the caustic geometry, the application of a digital image system has been included into the evaluation process, since the latter allows to use numerous appropriate measuring points along the caustic contour. It has to be pointed out that, in addition to the stress intensity factors, K_{I} and K_{II}, the radii r_i and the angles ϕ_i of the measuring points i in the reference plane are additional unknowns. Moreover, if the method of caustics is applied, the position of the crack tip can hardly be detected from the experimentally determined shadow spots. Thus, the previously proposed algorithm [22, 23] in which the crack tip position is assumed to be known has been improved in order to cover all demands of experimental arrangements. Regardless of any especially devised algorithm and apart from the application of the mapping equation (5.1), the algorithm must necessarily contain the functional determinant (5.2), since the latter selects the caustic as a special mapping function.

The new two-step algorithm assumes, in the first step, one crack-tip coordinate to be known and calculates pairs of stress intensity factors, $(K_{\mathrm{I}}, K_{\mathrm{II}})$, depending on the variation of the unknown crack tip coordinate. In the second step, the known and the unknown coordinates are interchanged leading to a second set of stress intensity factors, $(K_{\mathrm{I}}, K_{\mathrm{II}})$, depending on the other crack-tip coordinate variation. This procedure generates two curves in a plane spanned by K_{I} and K_{II}. The point of intersection represents the pair of the physical stress intensity factors

being in demand. For the purpose of realization of the algorithm based on one unknown crack-tip coordinate, a pair of measuring points, (P_{2i}, P_{2i-1}), is selected. Next, those components of the associated mapping equations are subtracted which eliminate the unknown crack-tip coordinate. This operation leads to a set of 3 equations. This set completed by the functional determinants belonging to the pair of measuring points provides a system of 5 nonlinear equations, reading

$$\mathbf{0} = \mathbf{f}_i(\mathbf{x}_i) = \begin{pmatrix} f_{i1} \\ f_{i2} \\ f_{i3} \\ f_{i4} \\ f_{i5} \end{pmatrix} = \begin{pmatrix} (x_{2i}'^{(\exp)} - x_{2i-1}'^{(\exp)}) - ((r\cos(\phi) - Cg)_{2i} - (r\cos(\phi) - Cg)_{2i-1}) \\ y_{2i-1}'^{(\exp)} - (r\sin(\phi) + Ch)_{2i-1} \\ y_{2i}'^{(\exp)} - (r\sin(\phi) + Ch)_{2i} \\ (1 + Cu - C^2v)_{2i-1} \\ (1 + Cu - C^2v)_{2i} \end{pmatrix} \tag{5.8}$$

for the algorithm independent of the x-coordinate of the crack tip, and

$$\mathbf{0} = \mathbf{f}_i(\mathbf{x}_i) = \begin{pmatrix} f_{i1} \\ f_{i2} \\ f_{i3} \\ f_{i4} \\ f_{i5} \end{pmatrix} = \begin{pmatrix} x_{2i-1}'^{(\exp)} - (r\cos(\phi) - Cg)_{2i-1} \\ x_{2i}'^{(\exp)} - (r\cos(\phi) - Cg)_{2i} \\ (y_{2i}'^{(\exp)} - y_{2i-1}'^{(\exp)}) - ((r\sin(\phi) + Ch)_{2i} - (r\sin(\phi) + Ch)_{2i-1}) \\ (1 + Cu - C^2v)_{2i-1} \\ (1 + Cu - C^2v)_{2i} \end{pmatrix} \tag{5.9}$$

for the algorithm independent of the y-coordinate of the crack tip, which can be solved for a set of N $(N \geq 2)$ pairs of measuring points. Provided N pairs of measuring points are given, the following system of $5N$ equations

$$\mathbf{f}^T = (\mathbf{f}_1, \cdot\cdot, \mathbf{f}_i, \cdot\cdot, \mathbf{f}_N) = \mathbf{0}^T \tag{5.10}$$

can be constructed and solved for the $(4N+2)$-vector of unknowns

$$\begin{aligned} \mathbf{x}^T &= (\mathbf{x}_K,\ \mathbf{x}_1,\ \cdot\cdot,\ \mathbf{x}_j,\ \cdot\cdot,\ \mathbf{x}_N), \\ \mathbf{x}_K^T &= (K_{\mathrm{I}}, K_{\mathrm{II}}), \qquad \mathbf{x}_j^T = (r_j, \phi_j) \qquad (j = 2i-1,\ 2i). \end{aligned} \tag{5.11}$$

By applying a series expansion, this overdetermined system of nonlinear equations can be simplified to an overdetermined system of linear equations, which can be handled by the Householder-transform technique available in any linear-algebra package. In order to find the desired solution vector for $\mathbf{f}(\mathbf{x}) = \mathbf{0}$, the series expansion

$$\mathbf{f}^{(m+1)}(\mathbf{x}^{(m+1)}) = \mathbf{f}^{(m)}(\mathbf{x}^{(m)}) + \left[\frac{\partial \mathbf{f}(\mathbf{x})}{\partial \mathbf{x}}\right]^{(m)} \Delta\mathbf{x}^{(m)}, \qquad \mathbf{A}^{(m)} = \left[\frac{\partial \mathbf{f}(\mathbf{x})}{\partial \mathbf{x}}\right]^{(m)} \tag{5.12}$$

starting from point $\mathbf{x}^{(m)}$, and truncated after the first term is found. Assuming $\mathbf{x}^{(m+1)}$ to be the solution vector of (5.10), the following system of algebraic equations

$$\mathbf{A}^{(m)}\Delta\mathbf{x}^{(m)} = -\mathbf{f}^{(m)}(\mathbf{x}^{(m)}) \tag{5.13}$$

with the $(5N, 4N + 2)$-functional matrix

$$\mathbf{A}^{(m)} = \begin{pmatrix} \dfrac{\partial \mathbf{f}_1}{\partial \mathbf{x}_K} & \dfrac{\partial \mathbf{f}_1}{\partial \mathbf{x}_1} & \dfrac{\partial \mathbf{f}_1}{\partial \mathbf{x}_2} & 0 & \dots & \dots & 0 \\ \dots & \dots & \dots & \dots & \dots & \dots & \dots \\ \dfrac{\partial \mathbf{f}_i}{\partial \mathbf{x}_K} & 0 & \dots & \dfrac{\partial \mathbf{f}_i}{\partial \mathbf{x}_{2i-1}} & \dfrac{\partial \mathbf{f}_i}{\partial \mathbf{x}_{2i}} & \dots & 0 \\ \dots & \dots & \dots & \dots & \dots & \dots & \dots \\ \dfrac{\partial \mathbf{f}_N}{\partial \mathbf{x}_K} & 0 & \dots & \dots & \dots & \dfrac{\partial \mathbf{f}_N}{\partial \mathbf{x}_{2N-1}} & \dfrac{\partial \mathbf{f}_N}{\partial \mathbf{x}_{2N}} \end{pmatrix}^{(m)} \tag{5.14}$$

is obtained. The sub-matrix formed by the partial derivatives with respect to the stress intensity vector, $\mathbf{x}_K$, reads

$$\frac{\partial \mathbf{f}_i}{\partial \mathbf{x}_K} = \begin{pmatrix} \dfrac{\partial f_{i1}}{\partial K_{\mathrm{I}}} & \dfrac{\partial f_{i2}}{\partial K_{\mathrm{I}}} & \dfrac{\partial f_{i3}}{\partial K_{\mathrm{I}}} & \dfrac{\partial f_{i4}}{\partial K_{\mathrm{I}}} & \dfrac{\partial f_{i5}}{\partial K_{\mathrm{I}}} \\ \dfrac{\partial f_{i1}}{\partial K_{\mathrm{II}}} & \dfrac{\partial f_{i2}}{\partial K_{\mathrm{II}}} & \dfrac{\partial f_{i3}}{\partial K_{\mathrm{II}}} & \dfrac{\partial f_{i4}}{\partial K_{\mathrm{II}}} & \dfrac{\partial f_{i5}}{\partial K_{\mathrm{II}}} \end{pmatrix}^T . \tag{5.15}$$

The sub-matrices resulting from the partial derivatives with respect to the space-coordinate vector, $\mathbf{x}_j$, read

$$\frac{\partial \mathbf{f}_i}{\partial \mathbf{x}_{2i-1}} = \begin{pmatrix} \dfrac{\partial f_{i1}}{\partial r_{2i-1}} & \dfrac{\partial f_{i2}}{\partial r_{2i-1}} & 0 & \dfrac{\partial f_{i4}}{\partial r_{2i-1}} & 0 \\ \dfrac{\partial f_{i1}}{\partial \phi_{2i-1}} & \dfrac{\partial f_{i2}}{\partial \phi_{2i-1}} & 0 & \dfrac{\partial f_{i4}}{\partial \phi_{2i-1}} & 0 \end{pmatrix}^T ,$$

$$\frac{\partial \mathbf{f}_i}{\partial \mathbf{x}_{2i}} = \begin{pmatrix} \dfrac{\partial f_{i1}}{\partial r_{2i}} & 0 & \dfrac{\partial f_{i3}}{\partial r_{2i}} & 0 & \dfrac{\partial f_{i5}}{\partial r_{2i}} \\ \dfrac{\partial f_{i1}}{\partial \phi_{2i}} & 0 & \dfrac{\partial f_{i3}}{\partial \phi_{2i}} & 0 & \dfrac{\partial f_{i5}}{\partial \phi_{2i}} \end{pmatrix}^T , \tag{5.16}$$

for the algorithm independent of the x-coordinate of the crack tip, and

$$\frac{\partial \mathbf{f}_i}{\partial \mathbf{x}_{2i-1}} = \begin{pmatrix} \dfrac{\partial f_{i1}}{\partial r_{2i-1}} & 0 & \dfrac{\partial f_{i3}}{\partial r_{2i-1}} & \dfrac{\partial f_{i4}}{\partial r_{2i-1}} & 0 \\ \dfrac{\partial f_{i1}}{\partial \phi_{2i-1}} & 0 & \dfrac{\partial f_{i3}}{\partial \phi_{2i-1}} & \dfrac{\partial f_{i4}}{\partial \phi_{2i-1}} & 0 \end{pmatrix}^T,$$

(5.17)

$$\frac{\partial \mathbf{f}_i}{\partial \mathbf{x}_{2i}} = \begin{pmatrix} 0 & \dfrac{\partial f_{i2}}{\partial r_{2i}} & \dfrac{\partial f_{i3}}{\partial r_{2i}} & 0 & \dfrac{\partial f_{i5}}{\partial r_{2i}} \\ 0 & \dfrac{\partial f_{i2}}{\partial \phi_{2i}} & \dfrac{\partial f_{i3}}{\partial \phi_{2i}} & 0 & \dfrac{\partial f_{i5}}{\partial \phi_{2i}} \end{pmatrix}^T,$$

for the algorithm independent of the y-coordinate of the crack tip. Since, in general, $\mathbf{f}^{(m+1)}(\mathbf{x}^{(m+1)})$ does not fulfill equation (5.12), the starting vector, $\mathbf{x}^{(m)}$, is corrected by the solution vector, $\Delta\mathbf{x}^{(m)}$, of (5.13) to give the new start vector

$$\mathbf{x}^{(m+1)} = \mathbf{x}^{(m)} + \Delta\mathbf{x}^{(m)} \tag{5.18}$$

for the next iteration step. This procedure has to be repeated as often as the truncation criterion

$$\|\Delta\mathbf{x}\|^{(m)} < \|\mathbf{x}\|^{(m)} \cdot \varepsilon \tag{5.19}$$

is satisfied for a fixed ε, where $\|\cdot\|$ denotes the L_2-norm.

The newly developed measuring algorithm was tested for quasi-static and dynamic crack extensions of straight cracks in a homogeneous material matrix as well as interface cracks, where optical isotropy as well as optical anisotropy of the material was considered. Simulated shadow spots of the most general case are shown in the Fig. 14. The tests have been performed for a crack-tip velocity v of 65 percent of the minimum Rayleigh-wave velocity, v_{R1}, in order to guarantee noticeable dynamic effects. A bimaterial with the bimaterial constant $\varepsilon_0 = \varepsilon(v = 0) = 0.067$ has been chosen. The shadow optical anisotropy constant, $\lambda = \pm 0.29$, which, for simplicity, is assumed to be the same in both bimaterial components, ensures considerable anisotropy effects. For the location of crack-tip coordinates, (x_R, y_R), an indefiniteness of $(\Delta x_R, \Delta y_R) = (0.1\,\text{mm}, 0.1\,\text{mm})$ has been presupposed. This inaccurate crack-tip position is located inside a squared interval of lateral length, 0.2 mm, centered at the real crack-tip position. Thereby, the algorithm runs throughout this two-dimensional interval. The stress intensity factors which have been calculated from a set of measuring points recorded from simulated caustics and by using the digital image system developed by FERBER and HINZ [16, 17], have been compared with the stress intensity factors $K_I = 10\,\text{Nmm}^{-3/2}$ and $K_{II} = 5\,\text{Nmm}^{-3/2}$ assumed for the associated simulations. The circles marked on the caustics contours are the used measuring points. In the

a)

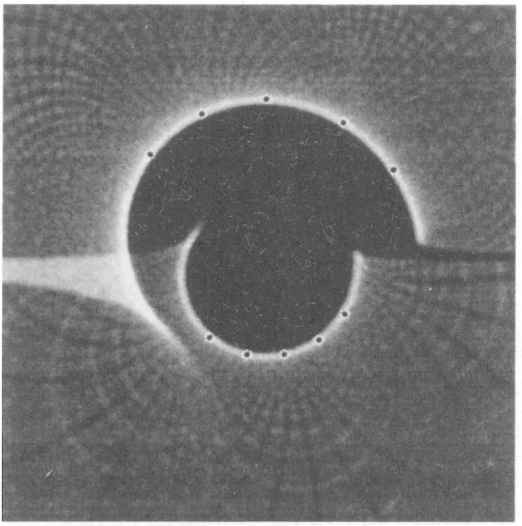

b)

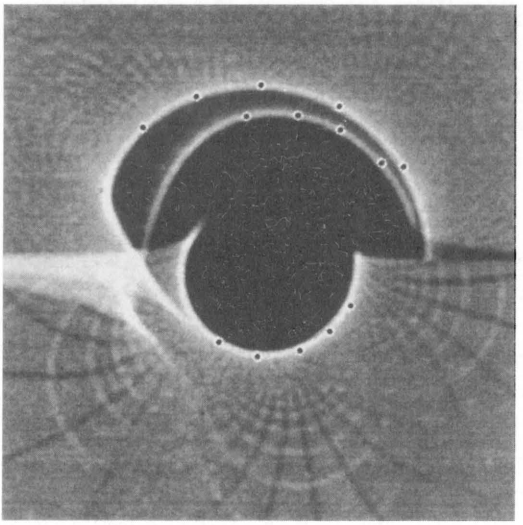

selected	calculated
$K_I = 10.0\,Nmm^{-3/2}$	$K_I = 10.0\,Nmm^{-3/2}$
$K_{II} = 5.0\,Nmm^{-3/2}$	$K_{II} = 5.3\,Nmm^{-3/2}$
$(v/v_{R1}) = 0.65, \quad \varepsilon_0 = 0.067, \quad \lambda = 0.0$	

selected	calculated
$K_I = 10.0\,Nmm^{-3/2}$	$K_I = 10.4\,Nmm^{-3/2}$
$K_{II} = 5.0\,Nmm^{-3/2}$	$K_{II} = 4.6\,Nmm^{-3/2}$
$(v/v_{R1}) = 0.65, \quad \varepsilon_0 = 0.067, \quad \lambda = \pm 0.29$	

FIG. 14. Simulated shadow spots in the case of a dynamic interface crack propagation by consideration of optical isotropy and optical anisotropy of the material; a) Optical isotropy of the material; b) Optical anisotropy of the material.

case of interface cracks the data points have been equally selected from the upper and the lower caustics. By consideration of the optical anisotropy of the material, provided the existence of two sharp caustic branches could be observed, two separate sets of measuring points were chosen, each of them being taken from the caustics related to the positive and negative parts of the optical anisotropy term in the mapping equation (5.1). For the cases when one branch of a double caustic outshines the other one, cf. Fig. 14 b, the brightest caustic branch was used for the evaluation process. Although the proposed algorithm, of course, is not so precise as the formerly presented algorithm assuming the crack-tip location to be known from the measurement, it has led to results for K_{I} and K_{II} with an average error of less than 10 percent. The obtained results are surprisingly accurate, although a relatively large system of linear equations had to be solved and a simple L_2-norm convergence criterion has been applied.

6. Summary

Dynamic crack extension of cracks running along curved interfaces of brittle bimaterials subjected to mechanical crack surface loads and superimposed thermal strains acting along the ligament was investigated. Assuming a small interface curvature, an at least almost steady-state boundary-value problem was obtained. In the framework of Stroh's complex method, from the corresponding boundary and continuity conditions a vectorial Hilbert problem was derived to determine the generalized complex potentials. The solution of the vectorial Hilbert problem was constructed by superimposing the problem of mechanically loaded crack surfaces, called **p**-problem, and of a thermally strained ligament, called **q**-problem. Since linear vectorial problems were under investigation, the solutions were constructed by utilizing the eigenvector planes of the **p**-problem and of the **q**-problem. For each of the problems, a set of two scalar Hilbert problems for a set of two scalar potentials expressed by Cauchy integrals was obtained. The curvature of the interface was handled by applying the conformal mapping technique and methods of the first order pertubation analysis. This strategy led to a considerably simplified determination of the potentials and to the identification of distinct algebraic quantities, from which the following results could be extracted. Firstly, the parameters of the eigenvalues and of the eigenvectors of the Hilbert problem must be interpreted as interface mechanics parameters reading $(\beta, v_p, \beta_{\mathrm{H}f}, \mu_{\mathrm{H}f})$. Secondly, the parameters of interface fracture mechanics are additionally influenced by two bimaterial constants, $(\varepsilon, \alpha_{\mathrm{H}f})$, which are related to $(\beta, \beta_{\mathrm{H}f})$. Based on a physically reasonable stress intensity vector definition, explicit integral formulae for the stress intensity vectors of the **p**-problem and of the **q**-problem were determined by applying the suggested eigenvector-plane approach, and by invoking Rice's scaling procedure for stress intensity factors. It was concluded that the individual influences of each of the interface frac-

ture mechanics features of interest, namely: thermomechanical loading, interface, crack-tip velocity and interface curvature, and their effects on the stress intensity factors are rather complicated, because the existence of multi-valued relations between the mechanical features and the thermomechanical parameters, (p_t, p_n), $\hat{r}$, v_p, ε, f', μ_{Hf}, α_{Hf} for the **p**-problem, and (q_x, q_y), $\hat{r}$, D_1, v_p, ε, f', μ_{Hf}, α_{Hf} for the **q**-problem, could be demonstrated. The discussion of the mixed-mode phase angles of the stress intensity vectors shows that they are almost independent of the crack-tip velocity but shifted due to the slope of the interface. In the case of the **p**-problem, the normalized magnitude of the stress intensity vector is considerably affected by the crack-tip velocity if it exceeds about one half of the minimum Rayleigh-wave velocity v_{R1}. In contrast to this, for the **q**-problem the magnitude decreases monotonically with increasing crack-tip velocity.

In determining the stress intensity factors from the experimentally recorded caustics, a measuring algorithm was proposed which theoretically yields an arbitrary number of measuring points. Moreover, it does not require the crack-tip location to be known exactly. This measuring algorithm proved to be almost as accurate as the formerly developed measuring algorithm which assumed the crack-tip position to be available.

References

1. C. ATKINSON, *Dynamic crack problems in dissimilar media*, [in:] Mechanics of Fracture 4, G.C. SIH [Ed.], Noordhoff International Publishing, Leyden, 213–248, 1977.
2. C. ATKINSON and D.L. CLEMENTS, *On some crack problems in anisotropic thermoelasticity*, Int. J. Solids Struct., **13**, 855–864, 1977.
3. D.M. BARNETT, M. LOTHE and S.D. GAVAZZA, *Considerations of the existence of interfacial (Stoneley) waves in bonded anisotropic elastic half-spaces*, Proc. R. Soc. Lond. A., **402**, 153–166, 1985.
4. J.L. BASSANI and J. QU, *Finite cracks on bimaterial and bicrystal interfaces*, J. Mech. Phys. Solids, **37**, 435–453, 1989.
5. J. BEINERT and J.F. KALTHOFF, *Experimental determination of dynamic stress intensity factors by shadow patterns*, [in:] Experimental Evaluation of Stress Concentration and Intensity Factors, G.C. SIH [Ed.], Martinus Nijhoff, The Hague, 281–330, 1981.
6. E.J. BROWN and F. ERDOGAN, *Thermal stresses in bonded materials containing cuts on the interface*, Int. J. Engng. Science, **6**, 517–529, 1968.
7. M. COMNINOU, *An overview of interface cracks*, Engng. Fracture Mech., **37**, 197–208, 1990.
8. R. COTTERELL and J.R. RICE, *Slighty curved or kinked cracks*, Int. J. Fracture, **16**, 155–175, 1980.
9. X. DENG, *Complete complex series expansions of near tip fields for steadily growing interface cracks in dissimilar isotropic materials*, Engng. Fracture Mech., **42**, 237–242, 1992.
10. X. DENG, *General crack-tip fields for stationary and steadily growing interface cracks in anisotropic bimaterials*, J. Appl. Mech., **60**, 183–189, 1993.
11. J. DUNDURS, *Edge-bonded dissimilar orthogonal elastic wedges under normal and shear loading*, J. Appl. Mech., **36**, 650–652, 1969.
12. A.H. ENGLAND, *A crack between dissimilar media*, J. Appl. Mech., **32**, 400–402, 1965.
13. A.H. ENGLAND, *An arc crack around a circular elastic inclusion*, J. Appl. Mech., **33**, 637–640, 1966.
14. F. ERDOGAN, *Stress distribution in a nonhomogeneous elastic plane with cracks*, J. Appl. Mech., **30**, 232–237, 1963.
15. F. ERDOGAN, *Stress distribution in bonded dissimilar materials with cracks*, J. Appl. Mech., **32**, 403–410, 1965.

16. F. FERBER, A. NOE, O. HINZ and K.P. HERRMANN, *Isochromatics and caustics around the tips of interface cracks observed by digital image processing*, [in:] VDI Berichte, **940**, 69–78, 1992.
17. F. FERBER, O. HINZ and K.P. HERRMANN, *Numerical and experimental modelling of crack systems in homogeneous and nonhomogeneous solids*, [in:] Computational Methods and Experimental Measurements VI, C.A. BREBBIA, G.M. CARLOMAGNO [Eds.], Elsevier Applied Science, London, **2**, 259–276, 1993.
18. L.B. FREUND, *Crack propagation in an elastic solid subjected to general loading. I. Constant rate of extension*, J. Mech. Phys. Solids, **20**, 129–140, 1972.
19. L.B. FREUND, *Dynamic fracture mechanics*, Cambridge University Press, Cambridge 1990.
20. H. GAO, *Stress analysis of holes in anisotropic elastic solids: Conformal mapping and boundary perturbation*, Q. Appl. Math., **45**, 553–572, 1992.
21. H. GAO and C. CHIU, *Slightly curved or kinked cracks in anisotropic elastic solids*, Int. J. Solids Struct., **29**, 947–972, 1992.
22. K.P. HERRMANN and A. NOE, *Analysis of quasi-static and dynamic interface crack extension by the method of caustics*, Engng. Fracture Mech., **42**, 573–588, 1992.
23. K.P HERRMANN and A. NOE, *Analysis of dynamic mixed-mode stress fields in bimaterials by the method of caustics*, Theo. Appl. Fracture Mech., **19**, 49–59, 1993.
24. J. HUTCHINSON and Z. SUO, *Mixed-mode cracking in layered media*, [in:] Advances in Applied Mechanics, J. HUTCHINSON, Th. WU [Eds.], **29**, 64–191, 1991.
25. C. HWU and T.C.T. TING, *Two-dimensional problems of the anisotropic elastic solid with an elliptic inclusion*, Q. Appl. Math., **42**, 553–572, 1989.
26. C. HWU, *Thermoelastic interface crack problems in dissimilar anisotropic media*, Int. J. Solids Struct., **29**, 2077–2090, 1992.
27. C. HWU, *Explicit solutions for collinear interface cracks*, Int. J. Solids Struct., **30**, 301–312, 1993.
28. J. KALTHOFF, *The shadow optical method of caustics*, [in:] Optical Methods in Mechanics, 3. Static and Dynamic Photoelasticity and Caustics, CISM, Udine 1984.
29. S.G. LEKHNITSKIĬ, *Elasticity theory of an anisotropic body*, Mir Publishers, Moscow 1981.
30. C. LIU and A.J. ROSAKIS, *On the higher order asymptotic analysis of a non-uniformly propagating dynamic crack along an arbitrary path*, SM Report 92-45, Graduate Aeronautical Laboratories, California Institute of Technology, 1992.
31. C. LIU, J. LAMBROS and A.J. ROSAKIS, *Highly transient crack growth in a bimaterial interface: Higher order asymptotic analysis and optical experiments*, J. Mech. Phys. Solids, **41**, 1887–1993, 1993.
32. P. MANOGG, *Anwendungen der Schattenoptik zur Untersuchung des Zerreißvorganges von Platten*, PhD Dissertation, Ernst-Mach-Institut, Freiburg 1964.
33. F. NILSSON, *Dynamic stress intensity factors for finite strip problems*, Int. J. Fracture, **8**, 403–411, 1972.
34. T. NISHIOKA and H. KITTAKA, *A theory of caustics for mixed-mode fast running cracks*, Engng. Fracture Mech., **36**, 987–998, 1990.
35. A. NOE, F. FERBER and K.P. HERRMANN, *Application of the shadow optical method of caustics for the analysis of interface crack problems in composite models*, [in:] Experimentelle Mechanik in Forschung und Praxis, 14. GESA-Symposium, VDI Berichte, **882**, 313–324, 1991.
36. A. NOE and K.P. HERRMANN, *Dynamische Ausbreitung gekrümmter Grenzflächenrisse*, ZAMM, **73**, T469–T472, 1993.
37. A. NOE and K.P. HERRMANN, *Dynamic extension of curvilinear interface cracks in self-stressed two-phase composite structures*, [in:] Continuum Models of Discrete Systems - CMDS-7, Series: Material Science Forum, **123–125**, K.-H. ANTHONY, H.J. WAGNER [Eds.], Trans Tech Publications Ltd., 531–540, Aedersmannsdorf, Switzerland 1993.
38. A. NOE and K.P. HERRMANN, *Fast interface crack propagation in thermomechanically loaded bi-materials*, [in:] Mis-Matching of Welds, Reihe: ESIS 17, K.H. SCHWALBE, M. KOCAK [Eds.], Mechanical Engineering Publications, 205–215, London 1994.
39. A. NOE, *Zur dynamischen Ausbreitung gerader und gekrümmter Grenzflächenrisse in thermomechanisch belasteten Bimaterialien. Ein Beitrag zur Grenzflächenmechanik*, PhD Dissertation, Paderborn University, 1994.
40. J. QU and J.L. BASSANI, *Cracks on bimaterial and bicrystal interfaces*, J. Mech. Phys. Solids, **37**, 417–433, 1989.
41. J.R. RICE and G.C. SIH, *Plane problems of cracks in dissimilar media*, J. Appl. Mech., **32**, 418–423, 1965.

42. J.R. RICE, *Elastic fracture mechanics concepts for interfacial cracks*, J. Appl. Mech., **55**, 98–103, 1988.
43. A.J. ROSAKIS, L. CHENG and L.B. FREUND, *On the asymptotic stress field of a non-uniformly propagating dynamic crack*, Int. J. Fracture, **50**, R39–R45, 1991.
44. H.P. ROSSMANITH, *Determination of stress intensity factors by the dynamic method of caustics for optically isotropic materials*, Ing.-Arch., **48**, 363–381, 1979.
45. H.P. ROSSMANITH, R.E. KNASMILLNER and J. ZHANG, *Ein interaktives Verfahren zur Auswertung von Kaustiken an Trennflächenrissen*, Arch. Appl. Mech., **62**, 115–122, 1992.
46. M. RÜHLE, A.G. EVANS, M.F. ASHBY and J.P. HIRTH, *Metal – ceramic interfaces*, Acta-Scripta Metallurgica, Proceedings Series Volume 4, Pergamon Press, New York 1990.
47. R.J. SANFORD and J. DALLY, *A general method for determining mixed-mode stress intensity factors from isochromatic fringe patterns*, Engng. Fracture Mech., **11**, 621–633, 1979.
48. A.N. STROH, *Steady state problems in anisotropic elasticity*, J. Math. and Phys., **41**, 77–103, 1962.
49. F.A. STURLA and J.R. BARBER, *Thermal stresses due to a plane crack in general anisotropic material*, J. Appl. Mech., **55**, 372–376, 1988.
50. Z. SUO, *Singularities, interfaces and cracks in dissimilar anisotropic media*, Proc. R. Soc. Lond. A., **427**, 331–358, 1990.
51. P.S. THEOCARIS, *Reflected shadow method for the study of constrained zones in cracked plates*, Appl. Optics, **10**, 2240–2247, 1971.
52. P.S. THEOCARIS, *Partly unbonded interfaces between dissimilar materials under normal und shear loading*, Acta Mech., **24**, 99–115, 1976.
53. P.S. THEOCARIS and N. IOAKIMIDIS, *The equation of caustics and other dynamic elasticity problems*, Engng. Fracture Mech., **12**, 613–615, 1979.
54. T.C.T. TING, *Explicit solution and invariance of the singularities at an interface crack in anisotropic composites*, Int. J. Solids Struct., **22**, 965–983, 1986.
55. T.C.T. TING, *Interface cracks in anisotropic elastic bimaterials – a decomposition principle*, Int. J. Solids Struct., **29**, 1989–2003, 1992.
56. H.V. TIPPUR and A.J. ROSAKIS, *Quasi-static and dynamic crack growth along bimaterial interfaces: a note on crack-tip field measurements using coherent gradient sensing*, Exp. Mech., **31**, 243–251, 1991.
57. M. TOYA, *A crack along the interface of a circular inclusion embedded in an infinite solid*, J. Mech. Phys. Solids, **22**, 325–348, 1974.
58. J. WEERTMAN, *Dislocations moving uniformly on the interface between isotropic media of different elastic properties*, J. Mech. Phys. Solids, **11**, 197–204, 1963.
59. J.R. WILLIS, *Fracture mechanics of interfacial cracks*, J. Mech. Phys. Solids, **19**, 353–368, 1971.
60. K.C. WU, *Explicit crack-tip fields of an extending interface crack in an anisotropic bimaterial*, Int. J. Solids Struct., **27**, 455–466, 1991.
61. Y. XU and L.M. KEER, *Non-steady state solution of a moving crack in an anisotropic solid*, Engng. Fracture Mech., **44**, 63–73, 1993.
62. W. YANG, Z. SUO and C.F. SHIH, *Mechanics of dynamic debonding*, Proc. R. Soc. Lond. A., **433**, 679–697, 1991.
63. E. YOFFE, *The moving Griffith crack*, Phil. Mag., **42**, 739–750, 1951.

LABORATORIUM FÜR TECHNISCHE MECHANIK
UNIVERSITÄT PADERBORN, GERMANY.

Received January 13, 1995.

Arch. Mech., 47, 5, pp. 957–970, Warszawa 1995

The influence of the temperature field on the propagation of cracks

S.K. KOURKOULIS and N.P. ANDRIANOPOULOS (ATHENS)

THE INFLUENCE of the temperature field, that is developed around a propagating crack, on the further crack propagation process itself is studied in the present work. The main target is to check whether the temperature field supports the experimentally observed tendency of a running crack to deviate from its initial straight path after a certain velocity limit. The study is carried out by means of the "Twin Crack" and the "Non-Steady Heat Source" models and it is proved that an intrinsic relation between the temperature field and the dynamic crack instability phenomena exists.

1. Introduction

IT IS NOWADAYS GENERALLY accepted that around the tip of a propagating crack a temperature field of significant intensity is developed. The origin of this field is found at the irreversible (plastic) processes that take place in the immediate vicinity of the crack tip, since 90% of the respective work is converted into heat, in the case of metals [1], and about 70% in the case of polymeric materials [2]. Experimentally, temperatures between 150°C and 450°C have been detected for cracks propagating in 4340 steel [3] and of the order of 3000°C for cracks propagating in glass [4]. On the other hand, various theoretical approaches of the problem have appeared, predicting temperature elevations varying in very broad limits [5, 6]. The number of works devoted to the subject that appear in the literature increases steadily, indicating an increasing interest in the subject.

The importance of studying this temperature field can be easily understood if, for example, the case of PMMA is taken into account. Really, temperatures of the order of some hundreds ° C have been reported for this material, while it is known, that a temperature increase from 20°C to 80°C causes a decrease of the yield stress to half its initial value. The same is true for the case of steel for which a temperature increase of 300°C causes a 25% reduction of its elastic modulus. It is, thus, obvious that, locally, the properties of the material are completely different than those initially assumed.

On the other hand it is proved [7] that the spatial distribution of the temperature increase around the crack tip is not uniform. It is, hence, implied that the material surrounding the crack tip is not homogeneous. Based on this observation, an effort is undertaken in the present work to check whether or not a connection exists between the branching phenomenon and the temperature field. In other words, the influence of the temperature field on further propagation of the two microcracks emanating from the mother crack-tip and forming finally the

macrobranches is studied. The main question is whether the temperature field supports the tendency of these microcracks to further deviate from their original straight path and to develop independently.

The study is carried out by engaging the "Non-Steady Heat Source" and the "Twin Crack" models which are briefly described in next sections. However, a short chronological survey of the most important works on the subject is given, first, in order to obtain a global picture of the state-of-the-art.

2. Short chronological survey

In spite of its importance, it was only in early fifties when WELLS [8] measured the temperature elevations around running cracks by using a thermocouple system, in order to estimate the amount of the emitted heat quantity. More than a decade later KAMBOUR and BARKER [9] estimated the temperature elevation around cracks propagating in PMMA by considering a rectangular layer ahead of the tip to be the heat source and gave a velocity limit above which the phenomenon is measurable. RICE and LEVY [10] used the Dugdale model to obtain the shape of the heat source and calculated the temperature rise for various crack speeds, while FULLER *et al.* [11] measured the temperature rise by using infrared detectors and thermocouples. WILLIAMS [12] estimated the heating effects at the moving crack tip by considering a simple energy balance for a circular craze at the crack tip, as a means to explain the $K_C - \dot{a}$ (critical stress intensity factor – crack velocity) function for PMMA. DÖLL [5] calculated the temperature elevations and heat outputs for fast running cracks using thermocouples and one-dimensional theory, and MARSHALL *et al.* [13] investigated the temperature effects on the fracture of PMMA by modifying the Dugdale model.

With the works of WEICHERT and SCHÖNERT [4, 6], who calculated the temperature distribution by considering a circular heat source of uniform heat distribution and also measured the temperature rise by using a very sensitive radiation thermometer, a new period begins, in which the temperature field is studied not as a secondary effect of fracture but as the main subject. Later, SHOCKEY *et al.* [14] recorded temperature maxima, very near to the running tip, with the aid of thermocouples and related these measurements with K_{ID} variations. ZIMMERMANN *et al.* [15] monitored the temperature profiles close to the running tip and gave the velocity limits for which all the energy delivered at the tip is transformed into heat. They also considered heat measurements as an alternative tool for checking the validity of dynamic fracture criteria. KUANG and ATLURI [16, 17] employed the finite element method to solve the problem and overcame the difficulties appearing by considering the heat distribution to follow an $1/r$ law instead of being constant.

DOUGLAS and MAIR [18] analyzed the Mode-III problem by using asymptotic fields, and LI *et al.* [19] solved the same problem by considering the plastic zone

around the crack tip to be the heat source. A plane strain solution was employed by SUNG and ACHENBACH [20], while MALALI [21] used a superposition principle for the heat sources to calculate the temperature rise. Also, KLEMM [22] obtained the temperature profile for cracks running in ductile materials.

In the very recent years the number of works studying the problem increases steadily. Among them, the works by KOBAYASHI *et al.* [23] who measured experimentally the heat generated around the tip using thermistors, by KUMAR *et al.* [24] who solved the Mode-I problem numerically and also studied the influence of strain rate sensitivity on the temperature rise, and finally the experimental work by ZEHNDER and ROSAKIS [3] who used noncontact infrared sensors to measure the temperature rise, are worth mentioning.

3. Theoretical preliminaries

3.1. The non-steady heat source model

The Non-Steady Heat Source (NSHS) model, introduced by THEOCARIS *et al.* [7, 25], is used in the present analysis. It cures some of the drawbacks of previous models by engaging more realistic assumptions concerning the shape of the heat source and the distribution of heat production over it. It is based on the following two hypotheses:

1. *The heat source coincides with the plastically deformed region enveloping the propagating crack tip.*

2. *The spatial heat production distribution is intimately related to the distribution of plastic work or, equivalently, to the distribution of plastic deformations.*

The second hypothesis is fulfilled by a family of functions of the following form:

$$dq(r_s, \theta_s) = \frac{h}{A}\left[\frac{2r_M^n(\theta)}{r_s^n + r_M^n} - 1\right]\cos^n\left(\frac{\theta_s}{2}\right)dA \tag{3.1}$$

covering additionally the requirements of maximum heat production at the crack tip, zero heat production at the elastic-plastic boundary and simulation of the equivalent stress variation (which is analogous to the plastic work) between these two extreme values. In this function $dq(r_s, \theta_s)$ is the elementary heat produced at the elementary area dA around point (r_s, θ_s) of the heat source (Fig. 1), A is the total area of the plastic enclave, and $r_M(\theta_s)$ is the radius of the elastic-plastic boundary along the line connecting the crack tip and the elementary heat source. In the same function h is a parameter defined by satisfying the demand that the integral of dq over the area of the heat source equals the total heat produced Q, i.e through the equation:

$$\iint_A dq(r_s, \theta_s) = Q. \tag{3.2}$$

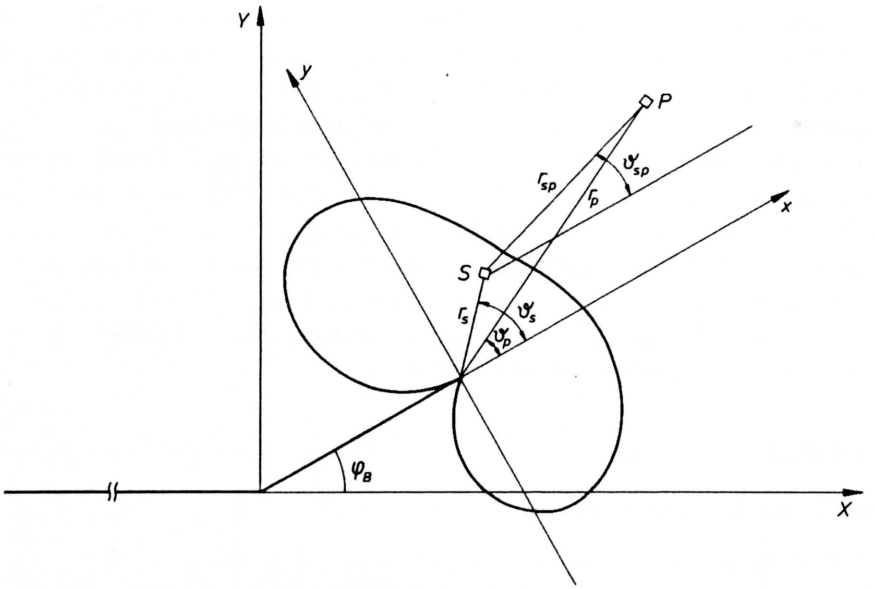

FIG. 1. The plastic envelope as heat source.

Finally, n is an arbitrary positive real number, the value of which describes the abruptness of the radial and polar variation of the heat production distribution. The exact value of this parameter depends on the constitutive equation of the material and on its thermal properties. Its influence on the final results is significant and has been analytically discussed in Ref. [7].

The heat production function being known the ROSENTHAL'S [26] solution for a moving point-heat-source is integrated over the whole area of the plastic enclave and the total temperature elevation at an arbitrary point outside the plastic enclave is obtained:

$$\Delta T(r_p, \theta_p) = \iint_A \frac{c}{2\pi K} \exp\left\{-\frac{c r_{ps} \cos\theta_{ps}}{2a}\right\} K_0\left(\frac{c r_{ps}}{2a}\right) dq(r_s, \theta_s), \tag{3.3}$$

where $\Delta T(r_p, \theta_p)$ is the temperature rise at the point $P(r_p, \theta_p)$ outside the plastic zone, c is the velocity of the crack, (r_{ps}, θ_{ps}) the coordinates of the point P in relation to the elementary point heat source $S(r_s, \theta_s)$ (Fig. 1), K and a are, respectively, the coefficients of thermal conductivity and thermal diffusivity of the material, and K_0 is the Bessel function of the second kind and zero order.

Combining Eqs. (3.1) to (3.3) the temperature rise is obtained.

3.2. The "Twin Crack" model

Based on the experimental observation that, long before macroscopical branching, the tip of the running crack is surrounded by a tuft of microcracks, from

which, at the final steps before macroscopic branching is observed, only two dominate over the others, THEOCARIS *et al.* [27] proposed the "Twin Crack" model, in an effort to explain the branching phenomenon and predict the future path of the newly formed branches. Hence, according to this model the macroscopic dynamic path instability is the final outcome of microscopic multibranching at the tip of the running crack.

The main assumptions of the "Twin Crack" model are as follows:

1. *The propagating crack is better described as a running cloud of microcracks rather than as a single point.*

2. *At the final steps two of these microcracks* ($0B$ *and* $0C$ *in* Fig. 2) *dominate over the others, exactly the ones which form the final macrobranches.*

3. *Each macroscopic fracture criterion is applied in the vicinity of two mutually influenced microbranches instead around a single mathematical tip.*

4. *The future path of each microbranch* ($\theta_{pr}^{B,C}$) *depends both on macroscopic factors, like stress level and crack velocity, and microscopic ones, like local structure irregularities and local abrupt changes of the material properties. The dynamic instability phenomena are, thus, confronted as doubly faced, with both deterministic and stochastic parts.*

5. *The stochastic part is assumed to be represented by the initial orientations* φ_i ($i = B, C$) *of the two microbranches and also their initial length ratio* $r = b/c$ (Fig. 2).

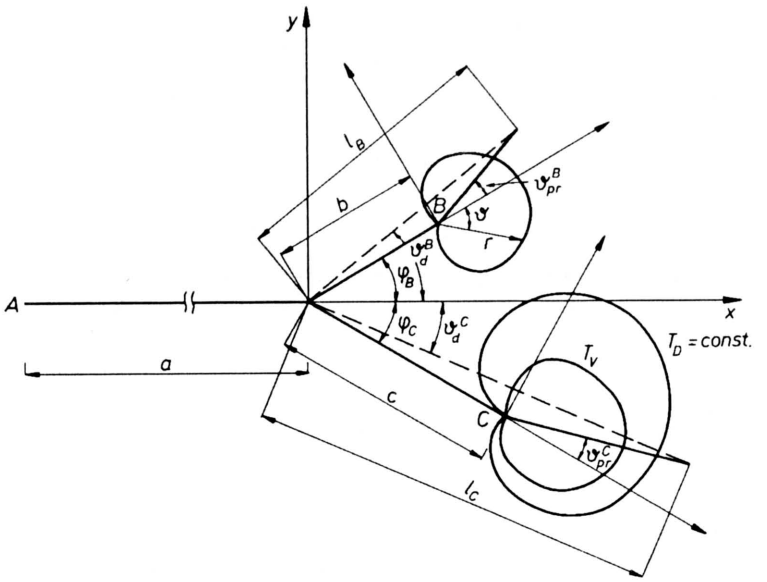

FIG. 2. The geometry of the prebranched crack configuration.

Selecting, thus, a suitable fracture criterion and knowing the dynamic stress field distribution and its intensity (the respective dynamic stress intensity factors (SIFs)), the future path of each microbranch can be predicted.

It has been proved [28] that the "Twin Crack" model constitutes a very flexible tool and, depending on the values of φ_i and the lengths' ratio of the microbranches, all types of macroscopically observed dynamic crack path and crack velocity instabilities (branching, kinking, curving, arrest and reinitiation) can be satisfactorily predicted by it. Also, in spite of the arbitrariness of the values of the stochastic factors, the predictions of the model are not random, but they form rather narrow prediction bands, in close agreement with experimental results.

4. Application and results

4.1. Description of the procedure

A crack $0A$ (Fig. 2) propagating with constant velocity c in thin sheets of PMMA under plane stress conditions is considered in the present study. Tip 0 becomes suddenly stationary and two branches $0B$ and $0C$ of lengths b and c appear and start propagating towards initial directions φ_i $(i = B, C)$ with velocities equal to c.

The dynamic stress field distribution around tips B and C is given by the FREUND and CLIFTON solution [29]:

$$\sigma_{ij} = \frac{K_{\mathrm{I}}^D}{\sqrt{2\pi r}} \Gamma_{ij}^{\mathrm{I}}(\theta, c, c_1, c_2) + \frac{K_{\mathrm{II}}^D}{\sqrt{2\pi r}} \Gamma_{ij}^{\mathrm{II}}(\theta, c, c_1, c_2) + 0(1), \tag{4.1}$$

where (r, θ) are the polar coordinates in relation to a system centered at the tip of the running crack, Γ_{ij}^{λ} $(i, j = 1, 2$ and $\lambda = \mathrm{I}, \mathrm{II})$ are analytic functions of the angle θ, the crack velocity c and the dilatational and distortional stress waves velocities c_1, c_2, respectively.

The Mode I and II dynamic SIFs, K_{λ}^D $(\lambda = \mathrm{I}, \mathrm{II})$ are obtained by adopting the technique described by KOSTROV [30], according to which the dynamic SIFs are given as functions of their respective stationary value, K_{λ}^S and a correction factor k_{λ}, which depends on the velocities of the crack and the stress waves:

$$K_{\lambda}^D(t) = K_{\lambda}^S k_{\lambda}^{\mu}(c), \qquad k_{\lambda}^{\mu} = S\left(-\frac{1}{c}\right)\left[1 - \left(\frac{c}{c_r}\right)\right] \Big/ \left[1 - \left(\frac{c}{c_{\mu}}\right)\right]^{1/2}, \tag{4.2}$$

$$\lambda = \mathrm{I}, \mathrm{II}, \qquad \mu = 1, 2,$$

where c_r is the velocity of the Rayleigh stress waves and S is a holomorphic function of crack velocity, which can be calculated numerically.

Concerning the static SIFs around the crack tips in the configuration of Fig. 2, the technique developed by THEOCARIS [31] is adopted, based on a system of three complex singular integral equations, according to the DATSHYSHIN and SAVRUK [32] method, which is solved numerically.

Combining Eqs. (4.1)–(4.2) with a suitable yield criterion, the radius, $r_M(\theta)$, of the elastic-plastic envelope can be obtained. In the present work the von Mises criterion is selected and thus the following expression for $r_M(\theta)$ is obtained:

$$r_M(\theta) = a_1 f_1^2(\theta) + a_2 f_2^2(\theta) + a_3 f_1(\theta) f_2(\theta) + a_4 [f_3(\theta) - f_4(\theta)]^2 \tag{4.3}$$

in relation to a polar system (r, θ) located at the running tip. In this equation, $f_i(\theta)$ $(i = 1, 4)$ are functions of c, c_1 and c_2, and a_i $(i = 1, 4)$ are constants. Their analytic expressions can be found in Ref. [7].

Introducing the expression for $r_M(\theta)$ into Eq. (3.3), combining with Eqs. (3.1)–(3.2) and with the further assumption that $n = 1$, i.e. adopting a $1/r$ distribution for q in the plastic zone, we obtain the following expression for the temperature rise at a point P in the vicinity of tips B and C:

$$\Delta T(r_p, \theta_p) = \iint_A \frac{Qc \dfrac{r_M - r_s}{r_M + r_s} \cos(\theta_s/2)}{2\pi K(3 - 4\ln 2) \displaystyle\int_0^n r_M^2 \cos(\theta_s/2)} \times \exp\left\{-\frac{cr_{ps}\cos\theta_{ps}}{2a}\right\} \mathcal{K}_0\left(\frac{cr_{ps}}{2a}\right) dA. \tag{4.4}$$

Solving numerically the above equation with the aid of a suitable code developed for this purpose, the temperature elevation at any point P can be obtained. The code proved to be stable and accurate [7] and the maximum error, for the present application, was estimated to be less than 2% in all cases.

4.2. Results and discussion

The procedure described in previous section was applied for the case of PMMA with $K = 0.193\,\mathrm{Wm^{-1}\,^\circ C}$, and $a = 9.46 \times 10^{-5}\mathrm{m^2 s^{-1}}$. Thin plates of PMMA were subjected to dynamic loading causing propagation of a preexisting crack of initial length $2a = 0.10\,\mathrm{m}$ under Mode-I plane stress conditions, with constant velocity c. Suddenly two microbranches $0B$ and $0C$ of equal lengths (b, c) and inclinations φ_i $(i = B, C)$ appear, propagating with the same velocity c. Three characteristic values for c were selected, equal, respectively, to $0.35c_2$, $0.50c_2$ and $0.65c_2$.

Concerning the values of the total heat quantity Q produced during crack propagation, use was made of the results obtained by KOBAYASHI *et al.* [23]. For the externally applied load, a reasonable value equal to $0.2\sigma_0$, where σ_0 is the yield stress of the material, was assumed.

In Figs. 3–5 the reduced, over the initial temperature, polar distribution, $T^* = T^*(\theta_p)$, of the temperature elevation is plotted for the three characteristic crack velocities. The inclinations φ_B and φ_C of the two microbranches are assumed to be equal, since in this case the total amount of heat can be distributed

symmetrically to the two microbranches. Seven different values for the initial angle inclination are selected, namely $\varphi = \varphi_B = -\varphi_C = 5°$, 10°, 15°, 20°, 30°, 40° and 50°.

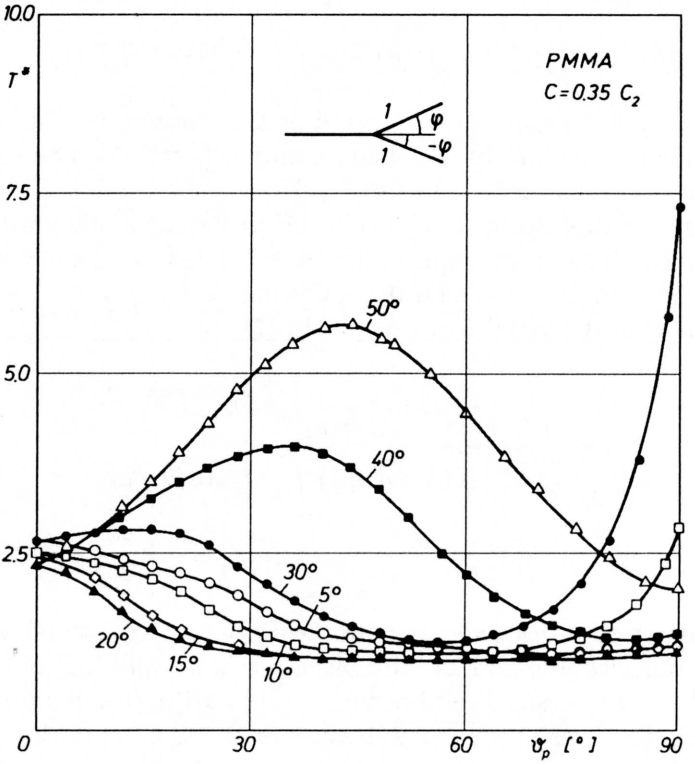

FIG. 3. Polar distribution of temperature elevations around tip B for $c = 0.35c_2$, for various branch inclinations.

From these figures it can be seen that the distribution of the temperature rise around tips B and C is neither monotonous nor self-similar for the various inclination angles. In fact, concerning the initial inclinations of the microbranches, two cases can be distinguished, i.e. angles φ below the limit of 20° and angles φ above this limit. Obviously this limiting value is connected to the local minimum value of the dilatational strain energy density distribution separating its two local maxima [27].

For the first crack velocity (Fig. 3), i.e. $c = 0.35c_2$, the $T^* = T^*(\theta_p)$ distribution decreases steadily for φ values in the first group ($\varphi \leq 20°$) and then this tendency is reversed and the values of T^* start increasing as angle φ increases. Concerning its θ_p-dependence, the T^* distribution shows a monotonously decreasing behaviour with a minimum value for angles θ_p between 50° and 60°, depending on the specific value of angle φ, for the first group of angles φ ($\varphi \leq 20°$). For angles $\varphi > 20°$ this tendency is reversed and a maximum value, whose magnitude and position strongly depends on the φ-value, is observed.

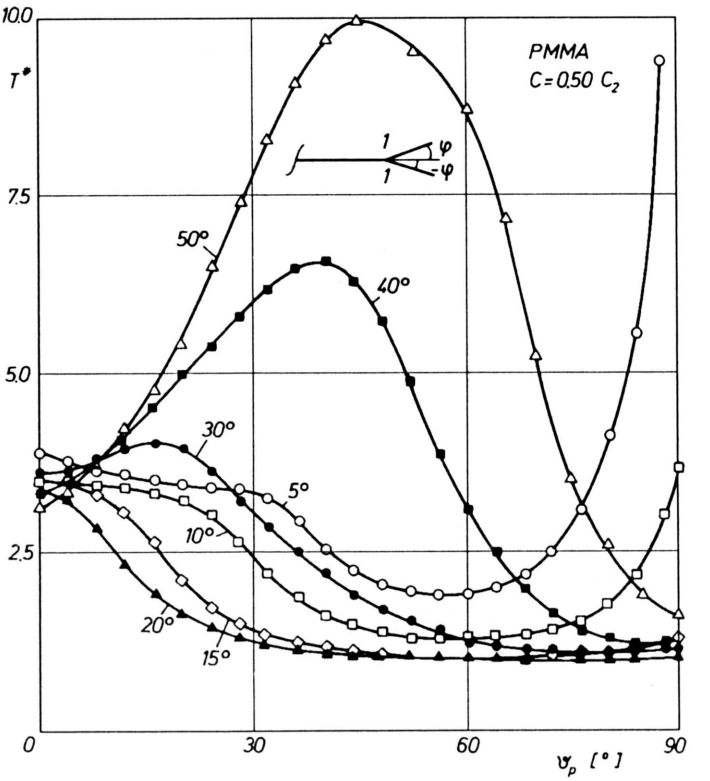

FIG. 4. Polar distribution of temperature elevations around tip B for $c = 0.50c_2$, for various branch inclinations.

For the second crack velocity ($c = 0.50c_2$) (Fig. 4) the situation is almost similar and only the absolute magnitudes of the temperature elevations are significantly higher, almost up to 25%. Things are, however, dramatically changed for the third characteristic crack velocity, $c = 0.65c_2$ (Fig. 5). From $\varphi = 5°$, a local maximum already appears, whose absolute value decreases with increasing φ-values and, at the same moment, it is removed towards lower θ_p-values, until it disappears. Then, for $\varphi > 30°$ it appears again, weakly in the beginning, and it increases steadily moving towards higher θ_p-values.

Since it is known from many sources (see for example Ref. [33]), that for the case of PMMA, the most possible crack velocity for branching to be observed is about $0.6c_2$, it is reasonable to connect these dramatic changes of the temperature rise for velocities higher than $0.50c_2$ with the branching phenomenon.

For this purpose it is recalled, that applying the T-criterion of failure [34] according to the "Twin Crack" model and for symmetric prebranching conditions [27], it is predicted that the most favourable initial direction φ is about 7°, independently from crack propagation velocity, giving angles of further branch propagation, $\theta_{pr}^{B} = \theta_{pr}^{C}$, between 16° and 35°. It can be concluded, according to

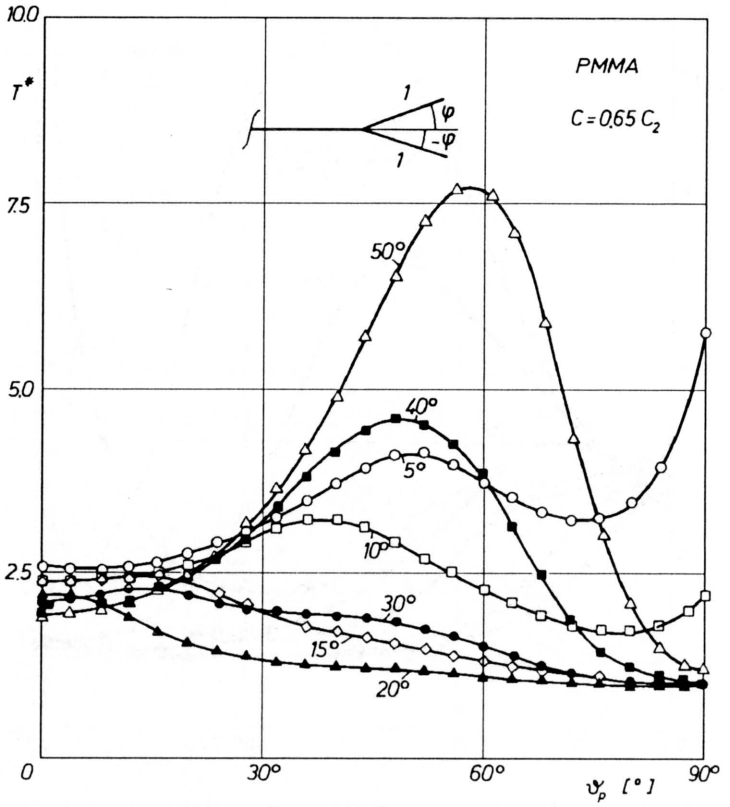

FIG. 5. Polar distribution of temperature elevations around tip B for $c = 0.65c_2$, for various branch inclinations.

the previously described behaviour of temperature fields and Fig. 6, where the T^* distribution is drawn for the three characteristic velocities and $\varphi = 7°$, that for crack velocities lower than $0.50c_2$ the branching tendency is suppressed by the decreasing temperature field, in the whole range (16° – 35°) of θ_p-angles. On the contrary, for higher crack velocities this tendency is supported by the increasing temperature field, for the same θ_p-angles, since the material appeares to be weaker due to higher crack temperatures.

Finally, in Fig. 7 the first attempt is described to take into account the influence of a slight asymmetry of the initial lengths of the micro-branches. In this figure the polar temperature elevation distribution is plotted for the case with $b/c = 1.00/0.75$, for a φ value equal to 15° and crack velocity equal to $0.5c_2$. Considerable differences in the absolute values of temperatures around the two tips are observed. However, this phenomenon demands further investigation in close relation to the assumption of equal velocity of the two microbranches of the "Twin Crack" model, which seems rather inadequate for the case of asymmetric prebranching conditions.

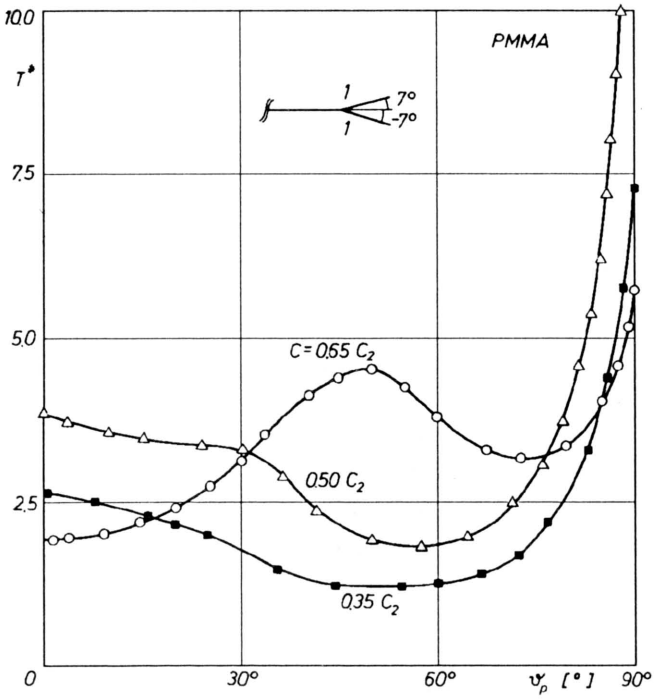

FIG. 6. The influence of crack velocity on the temperature elevations, for $\varphi_B = \varphi_C = 7°$.

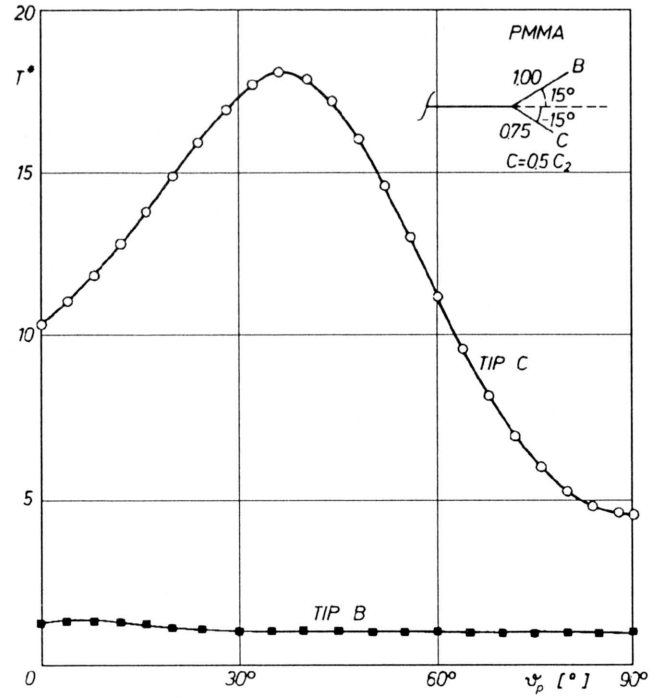

FIG. 7. Polar distribution of temperature elevations for tips B, C in case of slightly asymmetric branch lengths ($b/c = 0.75$) and $\varphi_B = -\varphi_C = 15°$.

5. Conclusions

In the present work the temperature distribution around microscopically prebranched propagating cracks was studied. The main conclusion is that the temperature field around a running crack tip interacts with the crack path instability phenomena. Also, it is indicated that the temperature field and its influence on the mechanical and thermal properties of the material cannot be ignored. Indeed, maximum temperatures up to 180°C detected in a very narrow zone outside the plastic envelope cannot be ignored in case of temperature-sensitive materials like PMMA, in spite of the narrowness of this zone (temperature gradient about $1.5 \times 10^8\,°\mathrm{C\,m^{-1}}$ [7]) indicating insignificant temperature elevations just a few microns away from the plastic envelope.

A complete solution of the problem is not yet available. Hence, this study should be only considered as a first step towards the understanding of the complicated procedure connecting the temperature field and the dynamic crack instability phenomena, since a number of questions remain still open. For example, in the theoretical domain, the exact shape of the heat source, compatible with a fully dynamic elastic-plastic solution of the respective stress field and the exact spatial distribution of the produced heat are needed. Also, the variation of the mechanical and thermal properties of the studied materials with temperature should be taken into account, since an initial study of this problem [35] made for a different material (steel) indicated that a reduction of the estimated temperature elevations of the order of 25% is observed. Significant difficulties, of course, exist also in the experimental study of the problem. For example, the extremely small dimensions of the area in which temperature elevation is measurable compared to the dimensions of the measuring equipment and sensors, in combination with the fact that the trajectory of any dynamically propagating crack cannot be accurately predefined is the most serious difficulty. Also, the slowness of most experimental devices for application in truly dynamic phenomena causes significant difficulties.

Finally, the influence of initial asymmetry of the prebranched configuration should be subject of further study, since initial indications exist that other instability phenomena, apart from branching, could be better understood through a combined approach including the temperature field influence on the whole procedure.

6. Acknowledgements

This work was partly presented at EUROMECH 326 colloquium on *Experiment and Macroscopic Theory in Crack Propagation*, held in Kielce, Poland on September 25-28, 1994.

References

1. G.I. TAYLOR and H. QUINNEY, *Mechanics of solids*, The Scientific Papers of Sir Geoffrey Ingram Taylor, **1**, 310–323, Cambridge University Press, Cambridge 1958.
2. R. ENGELTER and F.H. MÜLLER, *Thermische Effekte bei Mechanisher Deformation, insbesondere von Hochpolymeren*, Kolloid-Z, **157**, 89–111, 1958.
3. A.T. ZEHNDER and A.J. ROSAKIS, *On the temperature distribution at the vicinity of dynamically propagating cracks in 4340 steel*, J. Mech. Phys. Solids, **39**, 3, 385–415, 1991.
4. R. WEICHERT and K. SCHÖNERT, *Heat generation at the tip of a moving crack*, J. Mech. Phys. Solids, **26**, 151–161, 1978.
5. W. DÖLL, *An experimental study of the heat generated in the plastic region of a running crack in different polymeric materials*, Engng. Fract. Mech., **5**, 259–268, 1973.
6. R. WEICHERT and K. SCHÖNERT, *On the temperature rise at the tip of a fast running crack*, J. Mech. Phys. Solids, **22**, 127–133, 1974.
7. P.S. THEOCARIS, S.K. KOURKOULIS and N.P. ANDRIANOPOULOS, *The von Mises plastically deformed enclave as heat source for running cracks*, Int. J. Solids and Structures, **29**, 2, 187–196, 1992.
8. A.A. WELLS, *The mechanics of notch brittle fracture*, Welding Res., **7**, 34–56.
9. R.P. KAMBOUR and R.E. BARKER, *Mechanisms of fracture in glassy polymers. IV*, J. Polymer Science: A-2, **4**, 359–363, 1966.
10. J.R. RICE and N. LEVY, *Physics of strength and plasticity*, M.I.T. Press, Cambridge, Massachusetts, 277, 1969.
11. K.N.G. FULLER, P.G. FOX and J.E. FIELD, *Proceedings of Royal Society*, **A341**, 537, London 1975.
12. J.G. WILLIAMS, *Visco-Elastic and thermal effects on crack growth in PMMA*, Int. J. Fract. Mech., **8**, 4, 393–401, 1972.
13. G.P. MARSHALL, L.H. COUTTS and J.G. MARSHALL, *Temperature effects in the fracture of PMMA*, J. Mat. Sci., **9**, 1409–1419, 1974.
14. D.A. SHOCKEY, J.F. KALTHOFF, W. KLEMM and S. WINKLER, *Simultaneous measurements of stress intensity and toughness for fast-running cracks in steel*, Exp. Mech., **40**, 140–145, 1983.
15. C. ZIMMERMANN, W. KLEMM and K. SCHÖNERT, *Dynamic energy release rate and fracture heat in PMMA and a high strength steel*, Engng. Fract. Mech., **20**, 5/6, 772–782, 1984.
16. Z.B. KUANG and S.N. ATLURI, J. Appl. Mech, **52**, 274–280, 1985.
17. S.N. ATLURI and Z.B. KUANG, Appl. Math. Mech., **7**, 383, 1986.
18. A.S. DOUGLAS and H.U. MAIR, Scripta Metallurgica, **21**, 479–484, 1985.
19. Z.L. LI, J.L. YANG and H. LEE, *Temperature fields near a running crack tip*, Engng. Fract. Mech., **30**, 6, 791–799, 1988.
20. J.C. SUNG and J.D. ACHENBACH, J. Thermal Stresses, **10**, 243, 1987.
21. P.N. MALALI, *Thermal fields generated by dynamic Mode III fracture in ductile materials*, M.S. Thesis, The J. Hopkins University, Baltimore 1988.
22. W. KLEMM, Proc. ASME JSME Int. Pressure and Piping Conf., Honolulu, Hawai 1989.
23. A. KOBAYASHI, N. OHTANI and M. GOROG, *Heat generation during fracture*, Int. Conf. Mech. Prop. Mat. at high Rates of Strain, 31–36, Oxford 1989.
24. R.K. KUMAR, R. NARASIMHAN and O. PRABHAKAR, *Temperature rise in a viscoplastic material during dynamic crack growth*, Int. J. Fracture, **48**, 23–40, 1991.
25. N.P. ANDRIANOPOULOS and S.K. KOURKOULIS, *Crack propagation in a temperature-dependent material*, 3rd Nat. Conf. on Mechanics, Athens 1992.
26. D. ROSENTHAL, *The theory of moving sources of heat and its application to metal treatment*, Trans. ASME, **68**, 849–866, 1946.
27. P.S. THEOCARIS, N.P. ANDRIANOPOULOS and S.K. KOURKOULIS, *Crack branching: A "Twin-crack" model based on macroscopic energy fracture criteria*, Engng. Fract. Mech., **34**, 5/6, 1097–1107, 1989.
28. N.P. ANDRIANOPOULOS and S.K. KOURKOULIS, *Dynamic crack instability – The "Twin-crack" model*, Euromech 326, Kielce, Poland, 1994.
29. L.B. FREUND and R.J. CLIFTON, *On the uniqueness of plane elastodynamic solutions for running cracks*, J. Elasticity, **4**, 293–299, 1974.

30. B.V. KOSTROV, *On the crack propagation of cracks with variable velocity*, Int. J. Fracture, **11**, 47–56, 1975.
31. P.S. THEOCARIS, *Asymmetric branching of cracks*, J. Appl. Mech., **44**, 611–618, 1977.
32. A.P. DATSHYSHIN and M.P. SAVRUK, *A system of arbitrary oriented cracks in elastic solids*, J. Appl. Math. Mech. (PMM), **37**, 306–313, 1973.
33. P.S. THEOCARIS, N.P. ANDRIANOPOULOS and S.K. KOURKOULIS, *Brittle curving and branching under high dynamic loading*, Int. J. Pres. Ves. and Piping, **46**, 149–166, 1991.
34. P.S. THEOCARIS and N.P. ANDRIANOPOULOS, *The Griffith–Orowan fracture theory revisited: The T-criterion*, Int. J. Mech. Sci., **27**, 783–801, 1985.
35. N.P. ANDRIANOPOULOS and S.K. KOURKOULIS, *Can the influence of varying mechanical and thermal properties on temperature fields around running cracks be ignored?*, Int. J. Fracture, **65**, R17–R20, 1994.

NATIONAL TECHNICAL UNIVERSITY OF ATHENS
DEPARTMENT OF ENGINEERING SCIENCE, ATHENS, GREECE.

Received January 13, 1995.

Arch. Mech., 47, 5, pp. 971–984, Warszawa 1995

Dynamic fracture under pressure and shear

J. LU, A. DHUMNE and K. RAVI-CHANDAR (HOUSTON)

POLYCARBONATE EXHIBITS transitions in the failure mechanisms and modes, as a function of the rate of loading and the constraint placed on the crack. In this paper, the recently discovered transition from brittle to ductile mode with increased loading rate is examined by the method of photoelasticity. The evolution of the dynamic stress field as a function of time and rate of loading is examined both near the intial crack tip and the growing shear band/crack tip.

1. Introduction

BROBERG [1] showed that if the in-plane compression is sufficiently large, the only available path for the crack extension might be along the direction of maximum shear and that while experimentally difficult, "Mode II growth should be obtained for virtually all materials"; the reasoning behind this is that any micro-cracks that are formed ahead of the crack will be closed by the compressive stresses. Recently, KALTHOFF [2] experimenting with a high strength steel, showed that some combinations of pressure and shear loading of a crack resulted in a transition from a brittle to a ductile mechanism of crack growth as the rate of loading was increased; this is thought to be due to the large compressive stresses parallel and normal to the crack, that are introduced by the asymmetric impact loading arrangement, which inhibit brittle fracture. However, since the stresses are still quite large in the impact loading, a shear failure occurred. KALTHOFF [2] suggested, through *post-mortem* examinations of the failure surface, that an adiabatic shear band had formed prior to the shear fracture. ROSAKIS *et al.* [3] have observed similar shear banding in steels.

Recently, we observed a similar transition from ductile-to-brittle-to-ductile failure in polycarbonate [4], a thermoplastic polymer capable of sustaining large inelastic deformations. Using an asymmetrically impacted, single edge-notched specimen which is slightly different from the loading arrangement used by KALTHOFF [2] in his investigations on the high strength steel, and varying the rate of impact loading, it was found that at low rates of loading the failure was ductile with a transition to a brittle Mode-I cracking at higher speeds of impact; finally, at very high impact speeds, again a ductile shear banding/cracking along with shear strain localization was observed. The dissimilarities in the microstructure of the two materials and the micromechanisms of deformation and fracture are readily apparent – the high strength steel with a polycrystalline grain structure and with deformation and fracture mechanisms such as dislocation motion, grain boundary sliding, cleavage, and intergranular fracture and the polycarbonate with an amorphous, entangled macromolecular structure and with deformation and

failure mechanisms such as crazing, molecular disentanglement, molecular segmental rotation, chain scission etc. However, the macroscopic manifestations of deformation and failure, if characterized in terms of the observed deformation localization and failure mode transitions, appear to be identical [4]. In this paper the extent of similarity in the macroscopic deformation and dynamic failure behavior is examined. LEE and FREUND [5] analysed the corresponding elastodynamic problem for a stationary crack and found that the crack experiences both a compression and shear, at least for a short duration after initial impact; MASON *et al.* [4] showed through experiments that at long times from impact, a Mode I loading developed. The finite length and diameter of the projectile make the actual loading to become significantly different from the idealized loading assumed by Lee and Freund.

2. Experiment

The specimen geometry and loading are shown in Fig. 1. The specimen material was polycarbonate; the choice of polycarbonate was motivated by its ductile response under some loading conditions and by its suitability in dynamic photoelastic investigations. A 12.7 mm deep crack was machined into a 100 mm wide $\times$ 400 mm long $\times$ 5 mm thick specimen with a mill cutter of 0.3 mm thickness; the root of this machined crack was scribed with a sharp razor blade to simulate a sharp crack tip. The dynamic asymmetric impact loading was obtained by

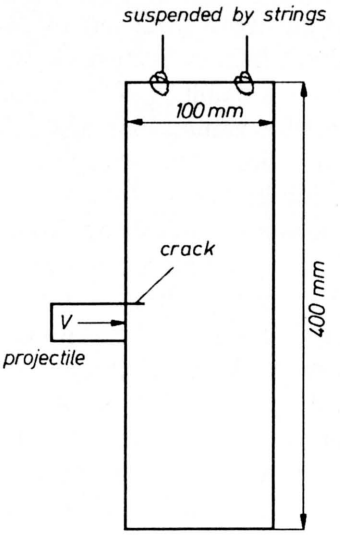

FIG. 1. Specimen geometry for the asymmetric impact loading experiment.

launching a polycarbonate projectile (50 mm diameter, 100 mm long), at speeds in the range of 25 to 60 m/s from the barrel of an air-gun. The air-gun consists of a reservoir, a solenoid valve and a 1.5 m long barrel, with a maximum pressure

capacity of 90 psi. The speed of the projectile was measured by the interruption of a laser beam placed across the path of the projectile.

The stress field information was acquired through the methods of photoelasticity and caustics, and recorded on film using a high speed camera capable of making 100,000 frames per second (fps). The high speed camera, built in-house, was a continuous access rotating mirror camera. Shuttering or framing is achieved solely by pulsing the laser light source with a pulse time of 15 ns, short enough to freeze the motion of the crack. The camera was triggered by detecting the projectile just prior to impact on the specimen, and at the rate of 100,000 fps the crack motion was followed until the crack moves out of the field of view, usually for about 200 μs.The application of the method of photoelasticity and caustics is rather well established in dynamic fracture investigations and hence the techniques will not be described here at all.

The impact velocity was varied in the range of 25 to 60 m/s. Also, since the air-gun was at some distance away from the specimen in order to allow for our speed measurement system, aiming for the projectile impact to occur just below the crack line was not easy; in different experiments, the projectile impact was always at some level below the crack line which varied from about 3 mm to 25 mm; this actually becomes another way of varying the rate of loading as well as the ratio of the shear to compressive loading. These variations in the loading lead to interesting transitions in the mechanisms and modes of fracture and we discuss these transitions in the next two sections. The transitions in polycarbonate bear a very strong resemblance to failure mode transitions in ductile metals, even though the microstructures of the materials as well as the micromechanisms of deformation and fracture are very different.

3. Fracture under asymmetric impact

Polycarbonate is a thermoplastic polymer with a molecular structure that consists of a bisphenol *A* component and a carbonate component; the bisphenolic component gives a high glass transition temperature of about 150°C, while the carbonate component provides a high rotational mobility resulting in a capacity to shear yield. Thus, at room temperature at low to moderate loading rate, polycarbonate exhibits ductile fracture behavior; as the loading rate is increased, a ductile to brittle fracture transition occurs [7], which is similar to such transitions observed in metals. In the present series of experiments using the asymmetric impact of the edge cracked plate, in addition to this ductile to brittle transition, at higher rates of loading a brittle to ductile transition with increasing loading rates was observed, similar to the observations of KALTHOFF [2]. It must be observed that, as the loading rate was increased, the crack tip constraint could not be maintained at the same level due to the nature of the biaxial loading wave that is generated by the impact.

Depending on the velocity of impact, the time for the initiation of crack growth and the mechanism governing the mode of crack growth changed. Figure 2 provides a summary of the various impact velocity ranges and the corresponding crack behavior; in each range, the crack surface is also shown. Corresponding to each of these velocity ranges, the high speed photographs are shown in Figs. 3–6. At this stage, we will interpret the high speed photographs qualitatively with respect to the stress field parameters, since the region near the crack tip is obscured by a pseudo-schlieren ([1]) effect. Note that the pseudo-schlieren appears only in the photoelastic pictures, where the camera is focussed on the specimen plane and not in the caustics, which are recorded on a screen plane at some distance away from the specimen and hence do not contain the light rays from a small region near the crack tip.

At slow impact speeds (less than 28 m/s), the magnitude and the rate of loading on the specimen are small, and the amplitude of the stress wave loading is not sufficient to cause initiation of the crack. In fact, the material exhibits a ductile response in this loading regime and a large plastic zone is formed near the crack tip; Fig. 3 shows a selected sequence of dynamic photoelastic pictures. From the frame labelled 0 μs it is clear that impact has already occurred some distance below the crack line, and that the loading wave front is just beginning to enter the field of view of the camera. After 20 μs, the wave front has arrived at the crack tip and the beginning of the scattering event is evident. However, it takes another 20 μs before the crack tip isochromatic fringes resemble the typical pattern associated with a Mode II square root singular stress field. The stress state changes quickly as the wave loading continues; further frames in the figure indicate that at 80 μs and 110 μs after impact, the isochromatics are suggestive of a Mode I type loading. At about 200 μs, the isochromatic fringes indicate the disappearance of the usual square-root singular crack tip stress field. The large fringe density indicates a large shear gradient near the crack tip; the crack does not initiate even after very long time from impact (~ 500 μs). Post-mortem examination of the specimen revealed that the crack tip had significant plastic deformation.

As the impact speed is increased to the range between 29 m/s to 32 m/s, crack initiation occurs, but only upon the arrival of stress waves reflected from the boundaries of the specimen, which provide additional loading to the crack tip. Figure 4 shows a selected sequence of dynamic photoelastic pictures from this experiment. The initial impact event was not captured by the high speed camera due to a trigger problem and hence we are unable to precisely indicate the time for initiation; however, it is possible to infer from the frames that were recorded that the initiation occurred at least 800 μs after impact, and that many wave reflections had occurred from the boundaries of the specimen before crack initiation. The pseudo-schlieren effect blocks out the near-tip isochromatic fringes and hence

([1]) The diameter of the rotating mirror of the high speed camera is about 13 mm and therefore light rays that deviate to large angles are effectively cut off from the film; thus the mirror plays a role similar to a knife edge in a schlieren set-up and these rays do not reach the film plane.

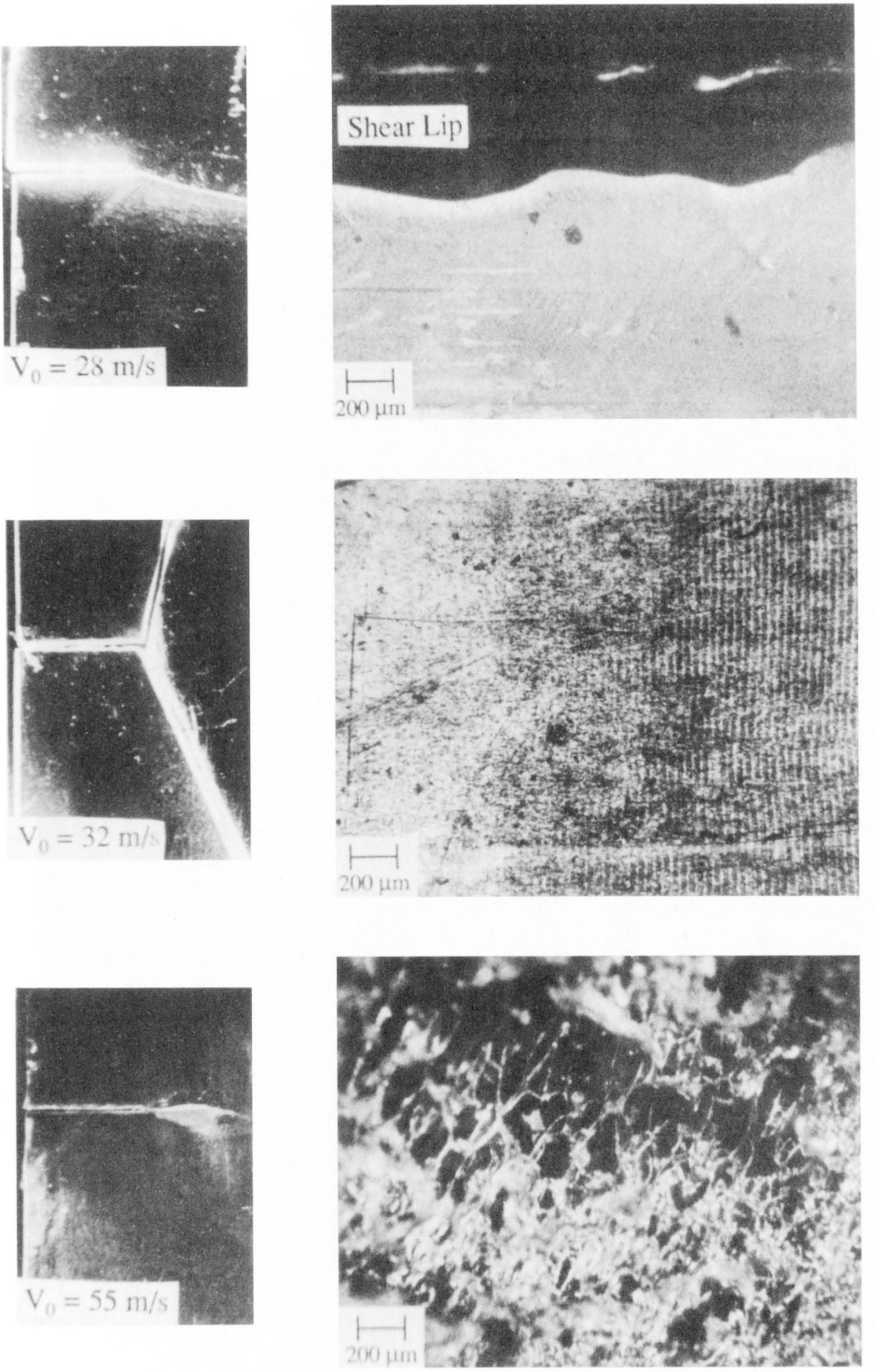

FIG. 2. Summary of crack growth behavior in polycarbonate; specimen geometry and fracture surface morphologies are shown.

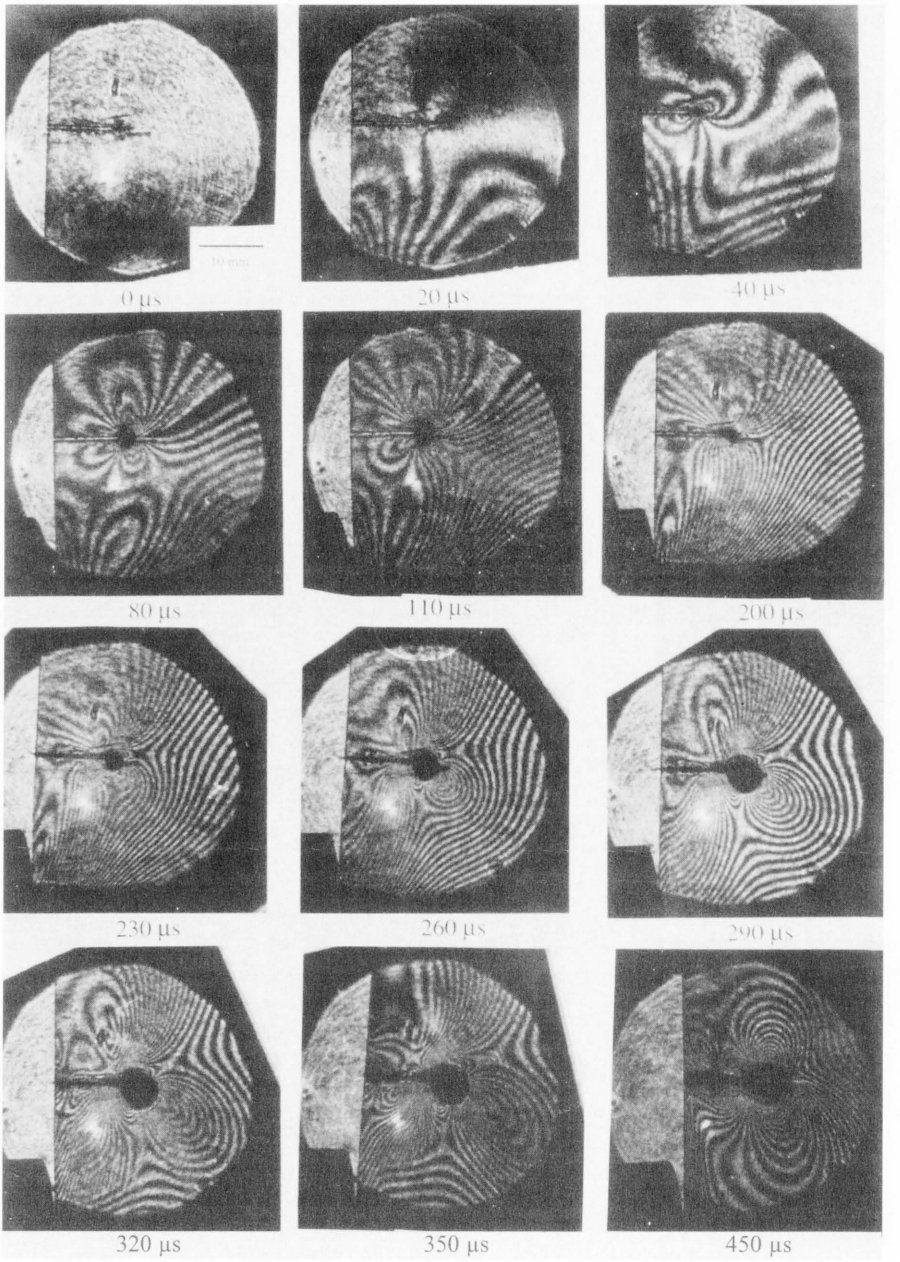

FIG. 3. Selected sequence of high speed photographs showing isochromatic fringe patterns; impact speed = 25 m/s.

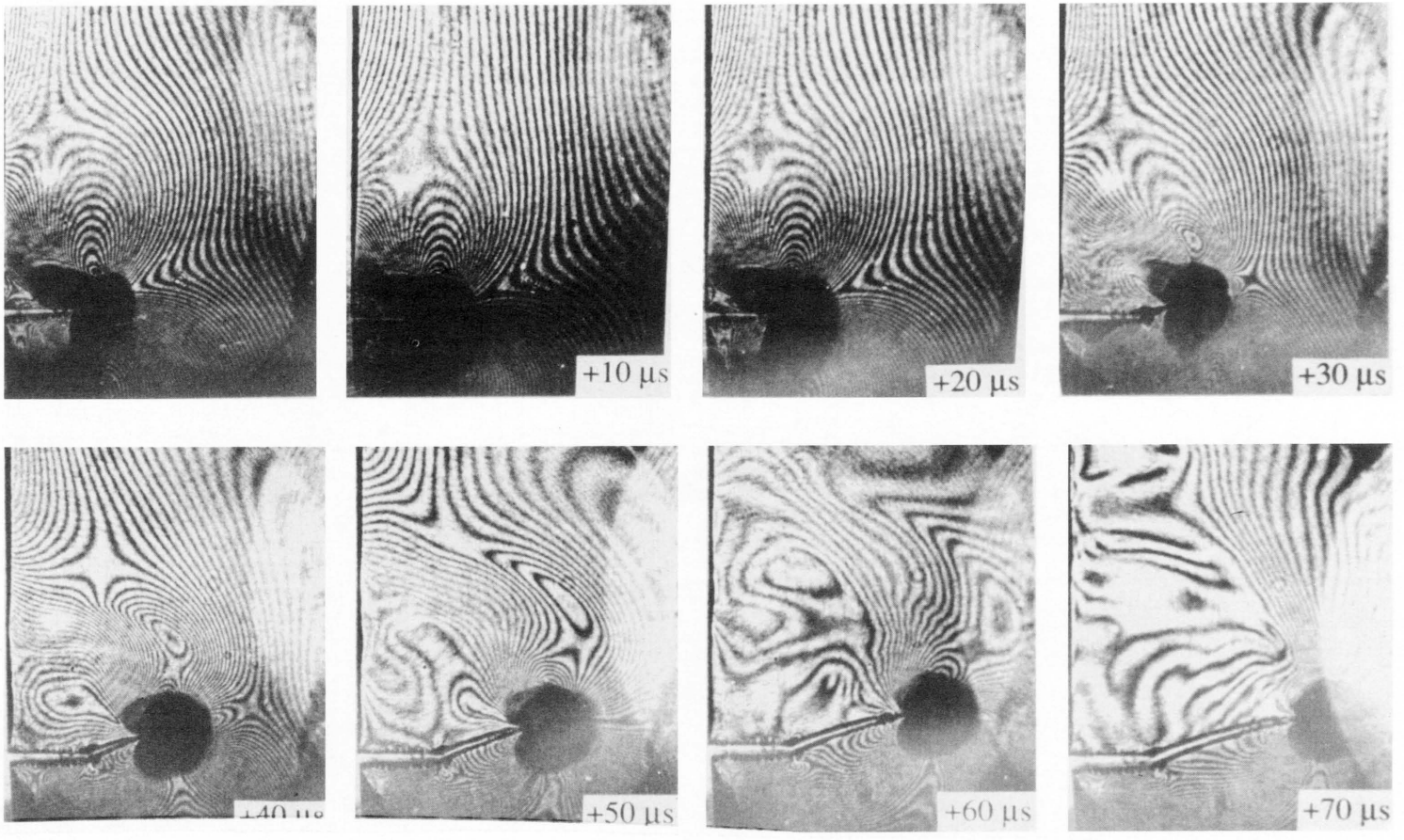

FIG. 4. Selected sequence of high speed photographs showing isochromatic fringe patterns; impact speed = 28 m/s.

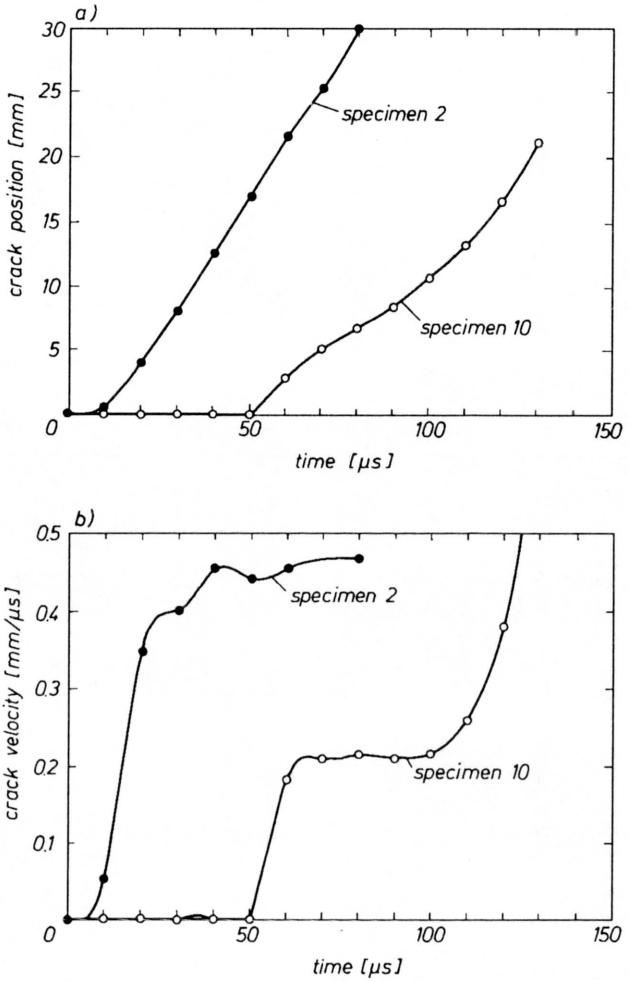

FIG. 5. a) Crack position variation with time corresponding to Figs. 4 and 6. b) Crack velocity variation with time from Figs. 4 and 6.

we are unable to get a quantitative estimate of the stress intensity factor along the crack path. The crack tip state is a mixed mode loading state and thus the crack propagates along a curved path, with a initial kink angle of about 22°. The crack position variation with time is shown in Fig. 5a (labelled Specimen 2), where the distance along the path of the curved crack is indicated; the corresponding velocity variation is indicated in Fig. 5b. Clearly the crack accelerates quickly to about 450 m/s, which is one half of the Rayleigh wave speed in the material. The fracture surface, shown in Fig. 2a indicates a mirror-type, rather featureless flat fracture in the middle of the plate and a shear lip towards the outer edge of the plate. While the shear lips are very similar to observations in the quasi-static fracture in metallic materials, the mirror-like fracture surface is quite unusual

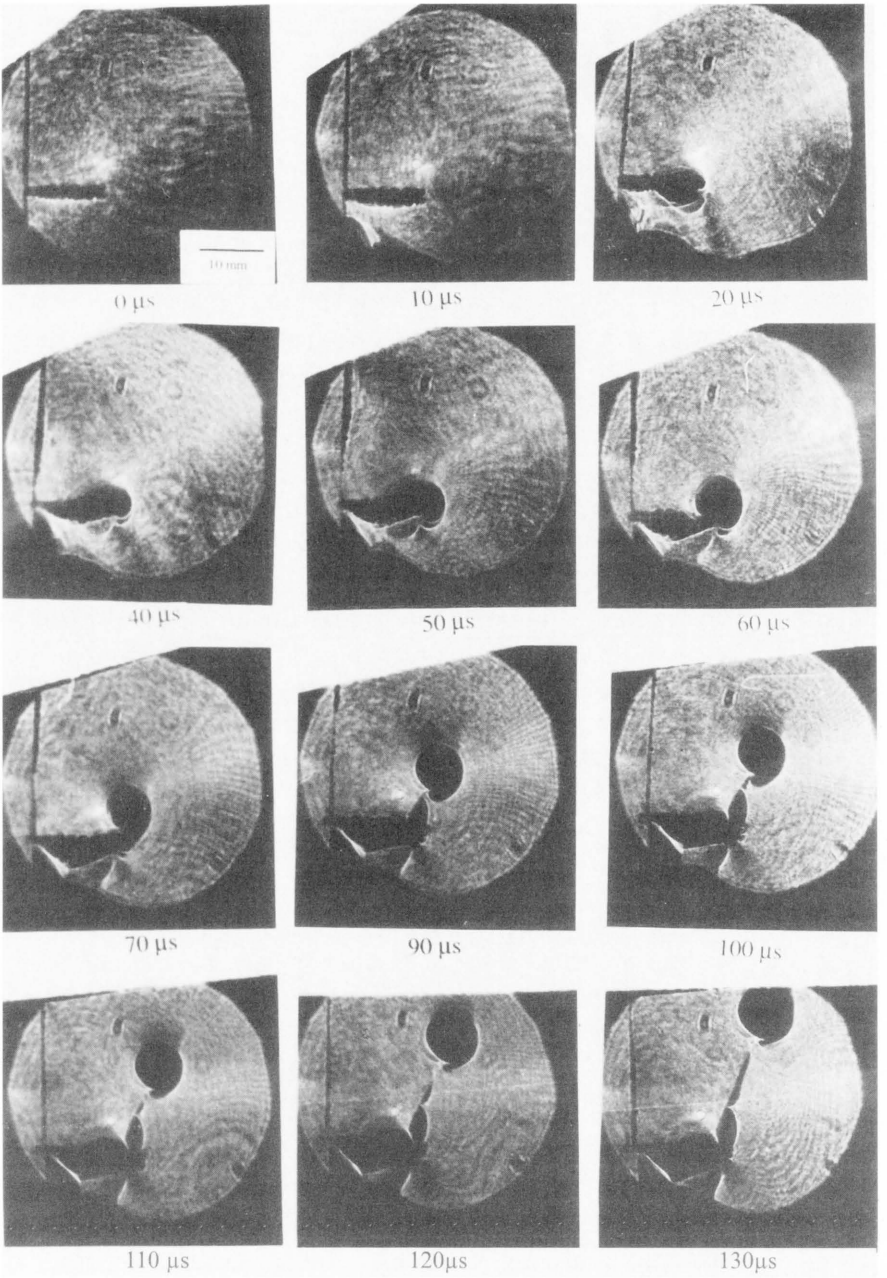

FIG. 6. Selected sequence of high speed photographs showing shadowoptical caustic patterns; impact speed = 32 m/s.

in polycarbonate. The shear lips are rather small, about 400 μm on either side, compared to a plate thickness of about 6.3 mm.

As the impact velocity is increased above 32 m/s, crack initiation occurs prior to the arrival of waves reflected from the far boundaries and we have an experimental realization of the infinite geometry configuration illustrated in Fig. 1; Fig. 2b shows a post mortem picture of the crack path and the fracture surface. Figure 6 shows a selected sequence of high speed photographs from this experiment. These high speed photographs were taken under a shadowgraph arrangement of the optics and hence caustics are seen in these figures instead of isochromatics; the size and shape of the caustics can be interpreted in terms of the crack tip stress intensity facors, but here we interpret them only qualitatively. During the first 50 μs, the build-up of the crack tip loading is evident from the increasing size of the caustic; the shape of this caustic indicates the presence of both a shearing component and a compressive component, as can be expected from the loading arrangement. Crack initiation occurs at about 50 μs after the initial impact and the symmetry of the shape of the caustic about the new crack direction at 60 μs indicates that the crack had initiated along the direction of the local Mode-I. The crack kinks from the initial direction at an angle of about 68°; several repeated experiments in this impact velocity range indicated very little change in the crack kink direction. The following frames suggest that the crack propagated nearly along a straight line, with the caustic pattern suggesting a mixed-mode loading. The crack position variation with time is shown in Fig. 5a (Specimen 10); the corresponding velocities are shown in Fig. 5b. The crack accelerates quickly to a velocity of around 220 m/s and propagates at a constant speed until the arrival of the waves reflected from the far boundary at about 100 μs, when the additional loading induces an acceleration of the crack. The slow speed of the crack, compared to the speed in Specimen 2 is puzzling, considering that the impact energy is higher; however, the high impact speed is also associated with a larger compressive loading parallel to the initial crack, and thus the kinked crack could experience crack surface friction leading to smaller speeds. An examination of the fracture surface indicates periodic striations, with a spacing of 36 μm; however, these striations are not visible all along the crack path as can be seen from Fig. 2. The mechanisms of formation of these striations is not clear yet, although there is some speculation that sequential formation and breakdown of crazes might lead to such striations [8].

A more dramatic change in the mode and mechanism of crack initiation and growth occurs as the impact speed is increased above 50 m/s. Figure 7 shows a selected sequence of high speed photographs corresponding to the specimen shown in Fig. 2c; the projectile impact speed was 55 m/s. Even though the impact speed was higher, the crack did not propagate along the direction of local Mode I (about 68° from the crack line as indicated from the previous experiment), but instead a shear band/crack grew from the crack tip along the original crack line. The first frame that was captured by the high speed camera occurred about

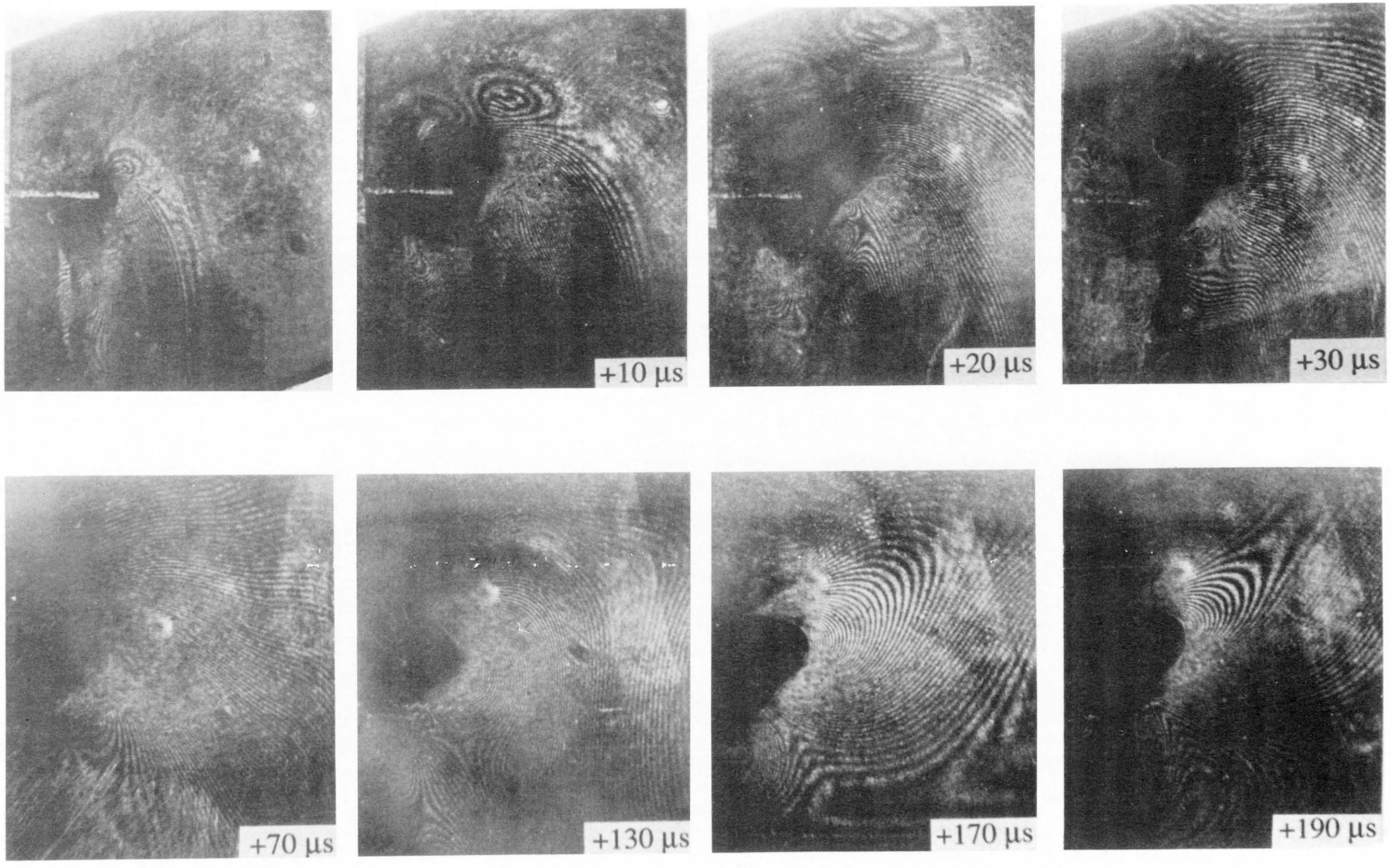

FIG. 7. Selected sequence of high speed photographs showing isochromatic fringe patterns; impact speed = 55 m/s.

30 μs after impact; subsequent frames were 10 μs apart. The high intensity of the loading is indicated by the large number of isochromatic fringes that can be seen in these photographs; each isochromatic fringe order corresponds to a shear stress difference of about 1.1 MPa; the largest measured shear stresses are of the order of 100 MPa. During the first 30 to 40 μs after the stress wave encounter with the crack tip, the machined crack faces can be observed to close; also, in the frames +20 μs and +30 μs isochromatic fringe lobes characteristic of a crack tip field can be seen to appear. Furthermore, the isochromatic fringes are very closely spaced, compared to the isochromatic fringes in Figs. 3 and 4, indicating that the shear stress gradients along the crack line are quite large. The large intensity of the crack tip deformations exacerbate the pseudo-schlieren effect and at increasing times, the crack tip region is not clearly visible. Therefore, the exact time and evolution of the shear band/crack as it initiates from the crack tip are not resolvable, but from the photographs at later times, particularly at +170 μs and +190 μs, and from the sudden drop in the shear stress gradient one might surmise that the shear band/crack had begun propagation around this time; the unloading waves from this initiation event decreases the shear stresses ahead, as can be seen from the decrease in the fringe density at later times. Figure 2c shows the fracture surface of this specimen; the surface is distinctly different from other fracture surfaces, presenting a dull apearance to the eye and at high magnifications showing indications of ductile type of fracture, with dimples and stretched ligaments visible on the fracture surface.

4. Conclusion

In summary, polycarbonate presents a wide array of ductile and brittle failure mechanisms; under suitable external loading arrangements, such as in the asymmetric impact experiment, transitions between a ductile fracture mode, a brittle fracture mode and shear banding/cracking are observed. Such transitions have been observed in metallic materials by KALTHOFF [2] and ROSAKIS *et al.* [3], but the present results suggest that such transitions could also be possible in nonmetallic materials. In order to explore the material dependence further, these asymmetric impact experiments were performed in polymethylmethacrylate (PMMA); in the range of impact speeds from about 20 to 60 m/s, only brittle fracture was observed. However, a rather curious observation is shown in Fig. 8, where a selected sequence of high speed photographs from a PMMA specimen is shown; the impact speed was 32 m/s and the photographs were taken using a shadowgraph set-up, resulting in caustics. The projectile impact occurred about 15 mm below the crack line and hence the projectile itself is not seen in the photographs. Two observations from this figure are worth noting. First, the crack kinks at an angle of 90°; this is quite unexpected, since an analysis of the state of stress near the crack tip indicates that the crack should kink at an angle of

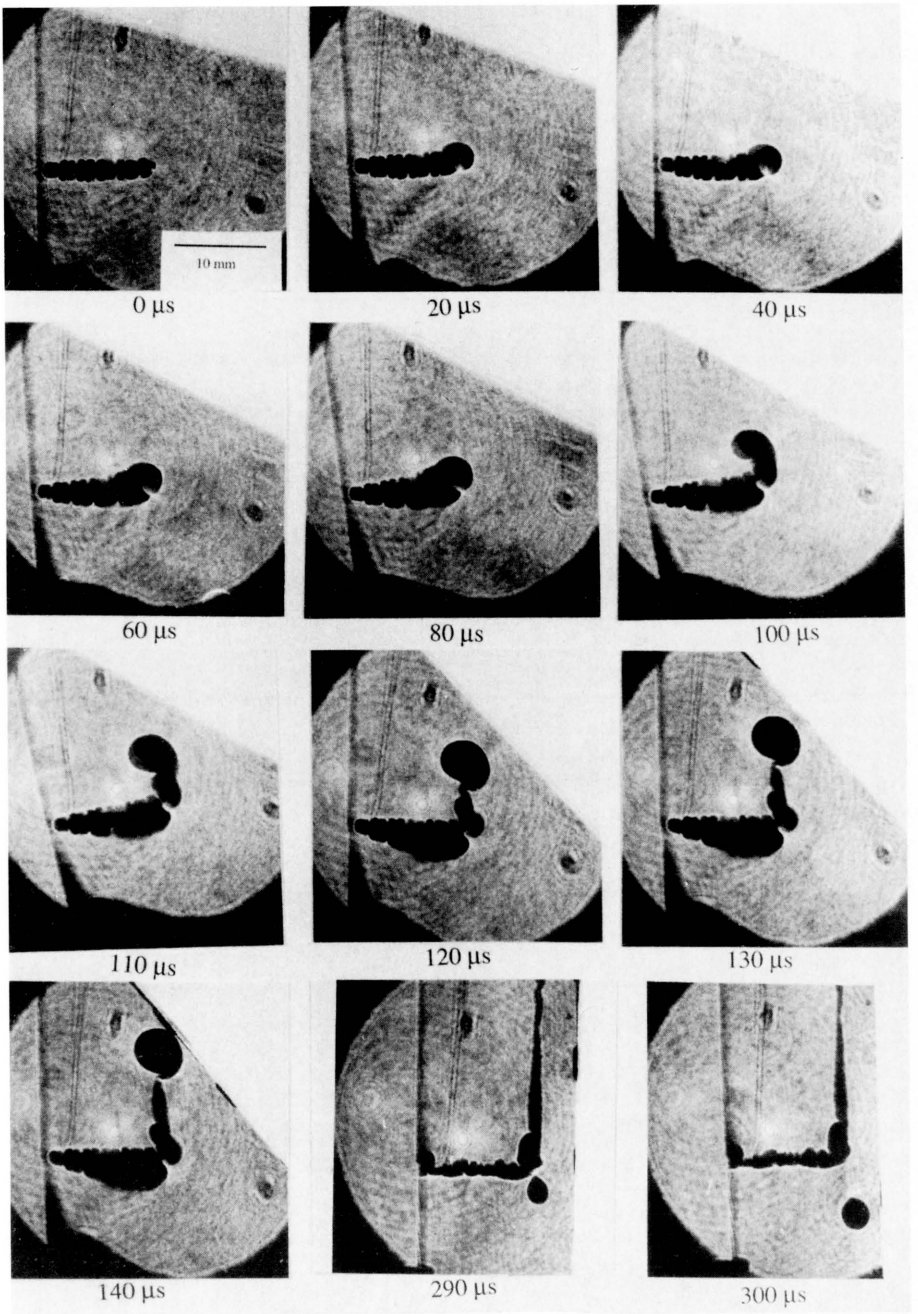

FIG. 8. Selected sequence of high speed photographs showing shadowoptical caustic patterns in PMMA; impact speed = 32 m/s.

about 70° for pure Mode II, and at smaller angles for combined Mode II and compression normal to the crack. Secondly, the crack speed is very low – about 200 m/s – compared to the Rayleigh wave speed of the material, about 1200 m/s; Mode I cracks typically grow at about 600 m/s in PMMA. The shadowgraphs in Fig. 8 suggest that the crack faces are in contact, and perhaps the contact pressure and and crack surface friction play a role in dictating both the large kinking angle and the low crack speeds.

References

1. B. BROBERG, *On crack paths*, [in:] Proc. of the NSF-ARO Workshop on Dynamic Fracture, W.G. KNAUSS, K. RAVI-CHANDAR and A.J. ROSAKIS [Eds.], 140–155, 1983.
2. J.F. KALTHOFF, *Shadow optical analysis of dynamic shear fracture*, Optical Enging., **27**, 835–840, 1988.
3. A.J. ROSAKIS *et al.*, presented at the 31st Annual Meeting of the Society for Engineering Science, 1994.
4. K. RAVI-CHANDAR, *On the failure mode transitions in polycarbonate under dynamic mixed-mode loading*, Intern. J. Solids and Structures, **32**, 925–938, 1995.
5. Y.J. LEE and L.B. FREUND, *Fracture initiation due to asymmetric impact loading of an edge cracked plate*, J.Àppl. Mech., **57**, 104–111, 1990.
6. J.J. MASON, J. LAMBROS and A.J. ROSAKIS, *The use of a coherent gradient sensor in dynamic mixed-mode fracture mechanics experiments*, J. Mech. and Physics of Solids, **40**, 641–661, 1988.
7. M. PARVIN and J.G. WILLIAMS, *Ductile-brittle fracture transitions in polycarbonate*, Intern. J. Fracture, **11**, 963–972, 1975.
8. P.D. WASHABAUGH and W.G. KNAUSS, *Nonsteady periodic behavior in dynamic fracture of PMMA*, Intern. J. Fracture, **59**, 187–197, 1993.

DEPARTMENT OF MECHANICAL ENGINEERING
UNIVERSITY OF HOUSTON, HOUSTON, USA.

Received February 17, 1995.

Arch. Mech., 47, 5, pp. 985–1001, Warszawa 1995

Controversies in dynamic fracture mechanics

A. NEIMITZ (KIELCE)

IN THE ARTICLE the discrepancies between theory and experiment in the fast crack growth phenomenon will be shortly reviewed. The main features of this phenomenon will be listed according to the experimental observations. The sources of those discrepancies will be suggested. The crack growth equations will be characterized and discussed from the point of view of equilibrium and nonequilibrium thermodynamics. The recently introduced crack growth equation will be presented and discussed along with the computer simulation of the crack growth process.

1. Introduction

ACCORDING TO CARL POPPER (philosopher), the theory can not be verified by experiment. The experiment may only show that the theory is wrong. One can prove the theorem but not the theory. Therefore if we want to compare the theory with experiment, we should seek for discrepancies between them. Thus, the main purpose of this presentation is to point out the experimental facts that contradict widely accepted theories within the field of the fast crack growth. This will be done in the first part of the paper. Next, the most important features of the fast crack growth phenomenon will be listed including recent observations. The theory must reflect these features as well as it must introduce parameters that are measurable and are connected with boundary conditions, since only the theory sets up what is observed experimentally. Finally, the origins of the discrepancies between theory and experiment will be discussed and certain recent theoretical results that much better reflect the basic features of experiment than the theories based on equilibrium, non-dissipative thermodynamics, will be presented.

2. Discrepancies between theory and experiment

• The best known argument against the existing theories based on the linear theory of elasticity and assumption that effective fracture energy is not dependent on the crack tip speed is the observation that the limit crack velocity is much lower than the Rayleigh or shear wave speeds. Such a velocity limit is predicted by the theory. Usually, we observe speeds less than half of those values. However if one assumes that the effective surface energy is a function of crack tip velocity and the crack growth equation is in the form:

$$G_i^d[a, \sigma_a, v] = G_{iC}^d[v] \equiv \dot{\gamma}[v], \qquad i = \mathrm{I}, \mathrm{II}, \mathrm{III} \tag{1}$$

or

$$K_I^d[a\sigma_a, v] = K_{IC}^d[v], \tag{2}$$

where G_i^d is dynamic energy release rate (DERR), K_I^d is dynamic stress intensity factor (DSIF), v is crack tip speed, the material functions K_{IC}^d and G_{IC}^d are geometry-dependent and from the practical point of view become useless.

- Another important discrepancy between the theory and experiment is that experiments show the lack of the unique dependence between the crack tip speed and Dynamic Stress Intensity Factor (DWIN). It was shown by KALTHOFF *et al.* [5], RAVI-CHANDAR *et al.* [13] and FINEBERG *et al.* [1], among others. Such a dependence is predicted by the theory.
- According to the theory, the stress field in front of the crack tip and the energy flux to the crack tip are not functions of the crack tip acceleration. In the experiment the acceleration/deceleration are observed and the change of the crack tip speed does not follow the SIF-velocity relations. Quite recently, new results by FREUND and ROSAKIS [3] as well as MARDER [8] introduce the acceleration to the equations for the stress distribution in front of the crack tip.
- There are other features of the fast crack growth that are either not predictable (as periodic oscillations) or not predictable correctly (the crack branching process).

3. Features of the fast crack growth process

Thus, because the existing theories were so many times questioned by experiment, they should be changed or at least corrected. To have a predictive power, the theory must reflect the basic features of the process observed. What are those features? Let us repeat the most important ones:

a. Just after the moment of the fast crack growth initiation (that is often preceded by subcritical, stable crack growth), the crack tip accelerates rapidly (the acceleration is of the order of $10^6 - 10^8$ m/s) to a certain critical velocity, usually less than $0.5c_R$. This velocity, say, mean velocity does not change considerably over almost all the period of cracking. In most of the experimental works this velocity was constant. However, FINEBERG and coworkers [1] reported increasing mean velocity, although with a modest acceleration. During this first stage of propagation the fracture surface remains smooth and is usually called the mirror surface.

b. According to the FINEBERG *et al.* [1], the critical velocity at which the acceleration decays is independent of the specimen geometry, specimen thickness, applied stress, surrounding ambient atmosphere and acceleration of the crack tip. It is a very important feature, although other authors do not confirm it in all aspects. E.g. KALTHOFF [5] observed that the mean maximum velocity was dependent on the external loading level. TAKAHASHI and ARAKAWA [19] reported the

influence of the specimen geometry on the maximum crack tip speed. However, more experiments are necessary to verify the above controversies; one thing remains unquestionable: when the critical velocity is reached, the crack propagation reflects features of the dissipative, nonlinear dynamic problem. This conclusion is supported by the observation that the fracture surface changes from mirror to mist, and the mist region is characterized by coherent oscillations with a particular wavelength that is increasing, as well as surface amplitude, together with the mean crack tip speed. In contrast, the frequencies of oscillations are constant.

c. With increasing crack tip velocity, the oscillations become more chaotic and fracture process enters the third stage with a hackled fracture surface. The oscillations registered on the fracture surfaces are accompanied by dramatic oscillations of the crack tip velocities.

Three-stage fast crack propagations in the form of mirror, mist and hackle surfaces were observed in the amorphous materials by several authors. Sharp oscillations of the crack tip velocity were observed by FINEBERG *et al.* [1] only because of high resolution in their experimental techniques.

d. It should also be mentioned that experiments performed by RAVI-CHANDAR *et al.* [13], ROSAKIS *et al.* [16], TAKAHASHI and ARAKAWA [19] show that the stress field in front of the crack moving with high velocity is not dominated by a one-term approximation of the asymptotic expansion that is represented by a well known Dynamic Stress Intensity Factor.

All experimental facts that were discussed so far are not described and predicted by the theory. These facts, along with the earlier mentioned discrepancies between the theory and experiment allow us to postulate that the existing theory should be changed or at least corrected to take into account transient and nonlinear effects.

4. New theoretical results

Recent years brought several theoretical results that, being not the theory, have yet sketched a path along which the theory should go. These results can be classified within two groups of problems. The first one, certainly better known, concerns the structure of the mechanical fields in front of the moving cracks. The second one, equally important, concerns the structure of the crack growth equations. Now, both of them will be discussed with the emphasis put on the equations of the crack evolution.

4.1. Stress field in front of the moving crack

FREUND and ROSAKIS [3], stimulated by experimental results, derived the formula for stress distribution in front of the crack tip in the form of asymptotic expansion with several terms relatively well defined. It turns out that the higher

order terms contain an important information concerning the transient stages of the crack growth. The structure of this formula is as follows:

$$\sigma_{11} + \sigma_{22} \sim r_d^{-1/2} f_1 \left[v(t), \Theta, K_1^d(t) \right] + r_d^0 f_2 \left[v(t), A_1(t) \right] + r_d^{1/2} f_3 \left[v(t), \dot{v}(t), K_1^d(t) \dot{K}_{\mathrm{I}}^{d}(t), \Theta \right] + 0(r_d^1), \tag{3}$$

where

$$r_d = x_1^2 + \left[1 - \frac{v^2(t)}{c_d^2} \right] x_2^2, \tag{4}$$

c_d is a speed of dilatation wave.

The role of the third term in the transient stage of the crack growth seems to be very important, in particular at the beginning of propagation. LIU and coworkers [7] compared the third term of the above expansion with the equivalent term of the expansion of the Broberg problem. It turned out that the third term was singular with respect to time. The Freund and Rosakis analysis requires deeper and more extended studies in order to determine unknown coefficients. As far, they were determined with the help of caustics by LIU and coworkers [7]. It follows from this analysis that DSIF becomes a function of the crack tip acceleration through the caustics diameter. It should also be mentioned that MARDER [8] derived formulas for DSIF and ERR that are functions of crack tip acceleration at almost the same time as FREUND and ROSAKIS [3]. He used a simplified procedure postulating that elastic potentials are functions of acceleration. The result of Freund and Rosakis is probably a milestone in a fast crack growth analysis, although the three-term approximation of the stress field creates a serious problems in definition of the appropriate parameter or parameters that can be used in the crack growth equation formulation.

4.2. Crack growth equations

The crack growth equation is absolutely necessary to select a particular motion from the class of all dynamically admissible ones. The proper formulation of this equation creates a very serious problems even for the one term approximation of the stress field. Let us discuss this problem in more details.

The most of the known crack growth equations are dynamic equivalents of the Griffith's energy criterion and Irwin's relationship between global quantity – the energy release rate and the local quantity – the stress intensity factor. The ingenious idea proposed by Griffith was extended to the nonlinear materials and to the fast crack growth. The structure of all crack growth equations used can be written in one general form:

$$X(\sigma_a, a, \text{geometry}, v) = X_C \quad \bigvee = X_C(v), \tag{5}$$

where

$$X = \begin{array}{ll} K_i^d & \text{dynamic stress intensity factor,} \\ G_i^d & \text{dynamic energy release rate,} \\ \delta_i^d & \text{crack tip opening displacement,} \\ \varepsilon_{x=xc} & \text{strain in front of the crack,} \\ T^* & \text{Atluri, Nishioka, Nakagaki integral,} \\ J_{\mathrm{I}}^d & \text{dynamic version of } J \text{ integral.} \end{array}$$

However, the concept of the energy release rate is the main one from which other quantities can be derived directly or indirectly, provided that the stress field is characterized by one term singular approximation.

Classical derivation of the relation:

$$G^d(\sigma_a, a, v) = G_C^d(v) \equiv 2\dot{\gamma}\,, \tag{6}$$

where $\dot{\gamma}$ is effective surface energy, follows from the first law of thermodynamics. It was done first by KOSTROV and NIKITIN [6] and later by FREUND [2]. In the final stage of derivation the contour integral is shrunk to zero and this procedure requires that it should be path-independent. It is true for steady state motion and in this case G^d represents energy flux directly into the crack tip. For the non-steady motion the integral is only asymptotically path-independent as was shown by FREUND [2] and NILSON [12]. In addition to this limitations, certain thermodynamical quantities that were used during derivation may not be well defined in the case that is far away from the equilibrium state. In general, the above equation characterizes situation which is close to the equilibrium and represents the non-dissipative processes. It was shown by RICE in [15], who derived the following equation:

$$\dot{S}_i = (G - 2\dot{\gamma})v\,, \tag{7}$$

where $\dot{S}_i$ denotes the rate of the internal entropy production. If the process is reversible, non-dissipative, $\dot{S}_i = 0$ and we obtain the structure of our equation of motion. Since, according to the second low of thermodynamics,

$$\dot{S}_i \geq 0\,, \tag{8}$$

the above equation is in fact the lower limit for the all crack growth processes

$$(G - 2\dot{\gamma}) \geq 0. \tag{9}$$

The above relations were derived for *isothermal, reversible and quasi-static* processes, utilizing the Helmholz free energy definition. These assumptions are really very strong. The isothermal conditions are acceptable for subcritical crack growth but by no means for fast crack growth. The processes of the crack growth in real materials are undoubtedly irreversible processes (with the exception reported for

mica where the partial reversibility was observed). Thus the product $\dot{\gamma} v$ represents the consumption of the irreversible energy. In thermodynamics the irreversibility is usually identified with the entropy production, thus in general the entropy should be associated with the new surface and the Rice's equation could be written in another form. The Rice's equation is in fact a typical equation of the thermodynamics of linear dissipative processes if we identify $(G - 2\dot{\gamma})$ as a thermodynamical force and v as a flux. Close to the equilibrium, the Onsager's relations are valid and the crack velocity can be computed from the relation:

$$v = L(G - 2\dot{\gamma}), \tag{10}$$

where L is a phenomenological coefficient with all properties defined by Onsager. The subcritical (stable) crack growth is an example of the linear dissipative process being very close to the state of equilibrium. For this situation both the free energy and entropy are potentials and extremes of these functions determine the attractor state. The theorem of minimum entropy production tells us that in the domain where the Onsager's relations are valid, it means in the linear domain, the system evolves into steady, stationary state (under given boundary conditions). The steady state, which is an attractor state must be a nonequilibrium state in which dissipative processes take place with the non-zero speeds. For this state also entropy becomes independent of time, thus

$$dS = 0 \quad \rightarrow \quad dS_e = -dS_i\,, \tag{11}$$

where S is total entropy of the system, S_e is reversible part of the entropy.

In the steady state the entropy of the system steadily increases. The theorem of the minimum entropy production tells us more. In this particular state the entropy production is as small as possible under the given boundary conditions. In this situation the equilibrium state becomes possible as soon as the boundary conditions allow the entropy production to vanish. In other words the system becomes passive. These properties reflect the properties of the subcritical crack growth which usually is considered as a sequence of the equilibrium states, where the time is not an independent variable and enters equations only as a parameter. The subcritical crack growth is arrested immediately after the external loading is reduced.

However, our interest in this paper is not in the subcritical crack growth but in the fast crack growth that is, by no means, the process which is close to the equilibrium.

Many of the experiments performed indicate that the fast crack growth is a strongly nonlinear, dissipative process, which takes place far from the equilibrium state. Its features including oscillations with increasing amplitude and chaotic behavior locate this process within the so-called deterministic chaos. The definition of the deterministic chaos was proposed by mathematicians during the conference organized by Royal Society in London in 1986 and is as follows: "Stochastic behavior taking place within deterministic system".

The thermodynamics of the nonlinear, nonequilibrium, dynamic systems does not provide us with precise tools to solve particular problems. As far there is no proof available concerning the theorem of the minimum entropy production for cases where fluxes are not linear functions of thermodynamical forces. It is also known that far away from the equilibrium, the system must evolve towards a certain steady state, but this state can not be characterized by a properly selected potential. If we do not know the potential, we can not say anything about stability of states to which the system evolves. If we can not define the minimum of the potential, the oscillations are not controlled by the second law of thermodynamics. For such a systems, according to Prigogine: "Stability does not follow from the general laws of physics". Thus, fluctuations that arise may not vanish, they can considerably increase leading to a chaotic behavior. These features are clearly observed during the fast crack growth and are visualized by mirror, mist and hackle surfaces as well as branching process.

From the discussion presented follows that the crack growth equation for the fast crack growth can not be derived (at the moment) rigorously from the laws of classical and nonequilibrium thermodynamics. But such an equation is absolutely necessary to analyze the process of the crack growth. It must be postulated. The postulates must be based on the analysis of experimental results. They do not have to follow from the constitutive equations or the classical laws of mechanics. The intuition will play here an important role. However, the equation should be written utilizing measurable and well defined quantities.

Experiments provide us with a certain information that should be the frame for the postulated form of equation. Experiments and requirements that any theory should have a predictive power suggest the following conditions which the crack growth equation should satisfy:

a. In general, the equation should be valid for both subcritical and fast crack growth.

b. It should be able to predict (describe) both the stage of rapid acceleration and propagation with a relatively constant mean velocity.

c. It should be able to predict oscillations and instabilities (it should be a nonlinear differential equation).

d. It should predict the limit crack tip speed for a given material, specimen geometry, and boundary conditions (so-called attractor state).

e. It should contain well defined and measurable quantities.

The starting point for the further discussion is the Rice's equation (7) that can be rewritten in the form:

$$\dot{S}_i + \dot{S}_i^{FS} (\equiv 2\dot{\gamma} v) = Gv, \tag{12}$$

where $\dot{S}_i^{FS}$ is entropy production rate associated with a fracture surface.

At the moment we forget about all uncertainties concerning the derivation of the above equation that arise when it is applied to the nonequilibirum process.

In this case if one knew the proper definition of the entropy production, the above equation would become the expected crack growth equation. However, in general, the definition of the S_i becomes a formidable task. Dissipation during the fast crack growth may have a variety of forms:

- dislocations creation and propagation,
- voids nucleation and growth,
- other microstructural mechanisms,
- roughness of the fracture surface,
- crack branching,
- crack velocity oscillations,
- other (?).

Thus, to solve a problem one should choose those mechanisms or mechanism that would probably dominate during the crack propagation. In the further discussion the results of the following works will be utilized: A. NEIMITZ [9], A. NEIMITZ [10], A. NEIMITZ, Z. LIS [11], L.I. SLEPYAN [17], L.I. SLEPYAN [18], H. GAO [4].

In [17] SLEPYAN formulated the principle of maximum energy dissipation in the form:

$$N = vG(v) \quad \rightarrow \quad \max_v N \quad (G \geq 2\gamma). \tag{13}$$

The same principle was proposed by GAO [4].

Physically it means that if N is the energy flux into the crack tip and this energy is dissipated there, the criterion of the maximum energy dissipated with respect to the crack tip speed gives the maximum possible crack tip velocity

$$\frac{\partial N}{\partial v} = 0 \quad \rightarrow \quad v_{\max}. \tag{14}$$

One could associate the dissipation of energy with the entropy production and the maximum of this quantity would define the attractor state to which the system evolves.

Slepyan obtained the following possible maximum crack tip velocities:

Mode I $v_{\max} = 0.517 c_R$ for $\nu = 0.3$,

Mode II $v_{\max} = 0.638 c_R$ for $\nu = 0.3$,

Mode III $v_{\max} = 0.618 c_T$.

In [18] SLEPYAN extended his principle. He defined the excess of the energy flux M:

$$M = (G - 2\dot{\gamma})v, \tag{15}$$

which is in fact the Rice's equation with $\dot{S}_i$ replaced by M. According to the principle of the maximum energy dissipation, the crack can propagate with the maximum speed according to the equation:

$$\frac{\partial M}{\partial v} = 0 \quad \rightarrow \quad \frac{\partial N}{\partial v} = 2\dot{\gamma} \tag{16}$$

and it can be demonstrated graphically in the form shown in Fig. 1, where v_n is an actual maximum crack tip speed.

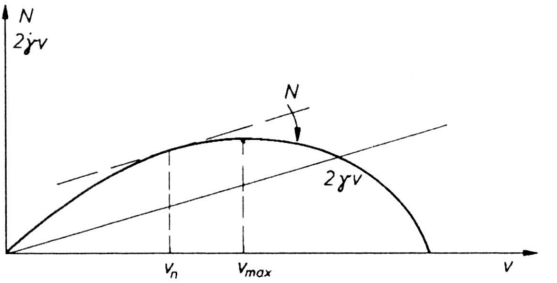

FIG. 1. Energy dissipation as a function of the crack growth speed.

According to the definition of the quantities entering the above principle, the equation obtained is not a crack growth equation. It defines the attractor state to which the system evolves.

In 1990 the equation similar to that introduced by Rice was proposed by Neimitz as a crack growth equation. In this case the entropy production rate was replaced by the energy flux, and the flux of dissipated energy was absorbed by the whole plastic or process zone, not only by the crack tip. The computations were performed for the strip yield zone model of the crack. The Mode III was analyzed.

The strip yield zone was allowed to change the size during propagation. The energy flux was computed in the form:

$$\dot{\Gamma}_{\mathrm{III}} = \beta c_T \frac{K_{\mathrm{III}}^2}{2\mu}\left(\frac{1-\beta}{1+\beta}\right)^{1/2} \qquad \text{for } \beta_T = \beta_L = \beta, \tag{17}$$

where $\beta_T = v_T/c_T$, $\beta_L = v_L/c_T$, v_L and v_T are velocities of the leading and trailing edges, respectively, K_{III} is the instantaneous static SIF, c_T is the shear wave speed

$$\dot{\Gamma}_{\mathrm{III}} = \beta_T c_T \frac{K_{\mathrm{III}}^2}{2\mu}\left(\frac{1-\beta_T}{1+\beta_L}\right)^{1/2}\left\{2-\left(\frac{1+\beta_T}{1+\beta_L}\right)^{1/2}+\frac{2(\beta_L-\beta_T)}{3\beta_T}\right. \tag{18}$$
$$\left.+\left(\frac{\beta_T-\beta_L}{\beta_T}\right)^{1/2}\left(\frac{1+\beta_L}{\beta_T}\right)^{1/2}\ln\left[\frac{(1+\beta_T)^{1/2}+(\beta_T-\beta_L)^{1/2}}{(1+\beta_L)^{1/2}}\right]\right\}$$

for $\beta_T > \beta_L$,

$$\dot{\Gamma}_{\mathrm{III}} = \beta_T c_T \frac{K_{\mathrm{III}}^2}{2\mu}\left(\frac{1-\beta_T}{1+\beta_L}\right)^{1/2}\left\{2-\left(\frac{1+\beta_T}{1+\beta_L}\right)^{1/2}+\frac{2(\beta_L-\beta_T)}{3\beta_T}\right. \tag{19}$$
$$\left.+\left(\frac{\beta_L-\beta_T}{\beta_T}\right)^{1/2}\left(\frac{1+\beta_L}{\beta_T}\right)^{1/2}\operatorname{arctg}\left(\frac{\beta_L-\beta_T}{1+\beta_T}\right)^{1/2}\right\}$$

for $\beta_L > \beta_T$.

The right-hand side of the above equations can be written as:

$$\beta_T c_T \Xi^d_{\mathrm{III}}(a, \sigma_a, v_T, v_L) \tag{20}$$

and Ξ^d_{III} can be called the energy release rate, but released within the whole plastic zone. In the next step the crack growth kinetics was assumed in the form shown in the Fig. 2.

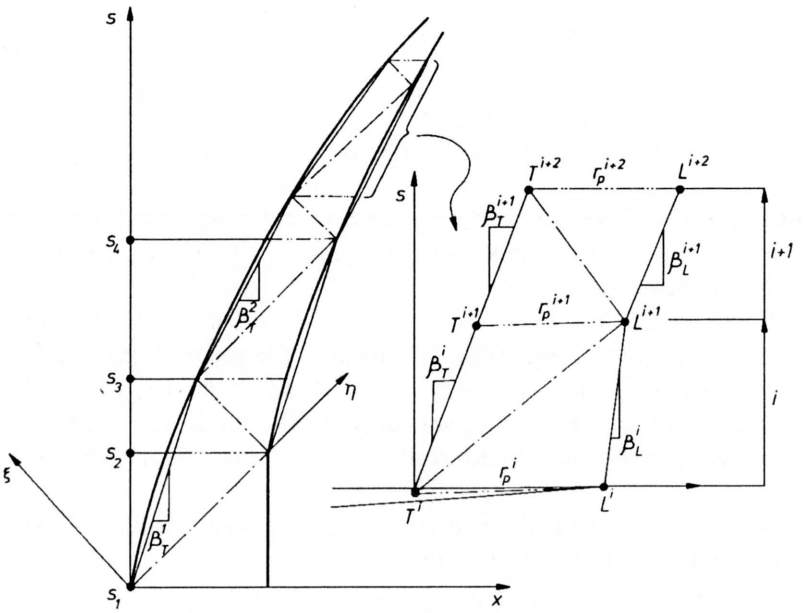

FIG. 2. The scheme of the crack growth kinetics, $s = c_T t$.

The smooth trajectories of both the leading and trailing edges were approximated by a piece-wise linear functions. Such an approximation was not arbitrary but included the interaction of both edges. The leading edge is allowed to change the speed after it obtains the information (with a speed of the sound) transmitted from the trailing edge. It generally follows the velocity of the leading edge. The trailing edge changes the velocity when it obtains the information from the leading edge and the new velocity must satisfy the crack growth equation. What is the shape of this equation? We assume that the whole energy that is transmitted to the plastic zone is dissipated there. Thus,

$$\Xi^d_{\mathrm{III}}(a, \sigma_a, v_T, v_L) = \dot{\Gamma}, \tag{21}$$

where $\dot{\Gamma}$ can be considered as a net power per unit thickness dissipated within the plastic zone and the energy of a new unit surface is also taken into account. In such formulation the quantity Γ is not only a material property but includes also the geometry of the specimen through the size of the plastic zone. If the energy

dissipated Γ is assumed to be a function of the crack tip speed (v_T) and this function is expanded into series around the steady-state $((v_T)_{ss})$, the net power can be rewritten and the crack growth equation assumes the following form:

$$\Xi^d_{\mathrm{III}} = \dot{\Gamma}^{\,d}_{\mathrm{III}C}(v_T)\Big|_{ss} + m(t)\frac{dv_T}{dt} + v_T\frac{dm(t)}{dt}, \tag{22}$$

where (with a good will) m can be called an "equivalent mass" (the units are mass unit over meter).

The above equation can be rewritten in the form:

$$v_T\left[\Xi^d_{\mathrm{III}} - \dot{\Gamma}^{\,d}_{\mathrm{III}C}(v)\Big|_{ss}\right] = v_T\left[m(t)\frac{dv_T}{dt} + v_T\frac{dm(t)}{dt}\right] \tag{23}$$

or to make it more familiar,

$$v_T\left[\Xi^d_{\mathrm{III}} - \dot{\Gamma}^{\,d}_{\mathrm{III}C}\Big|_{ss}\right] = v_T M\,. \tag{24}$$

For a steady state crack growth when $\beta_T = \beta_L = \beta$ the equation reduces to the classical form of equation and $\Xi = G$.

This equation was tested numerically using the earlier shown formula for Ξ^d_{III} and the crack growth kinetics model. The equivalent mass was taken to be proportional to the product ϱr_p^2, where r_p is the length of the strip yield zone and ϱ is material density, and it was assumed to be constant. In the Appendix several examples of the computer simulation were shown. One may notice that the analysis based on the proposed crack growth equation gives the qualitative picture of the fast crack growth, that is quite similar to those observed experimentally. One feature is not observed within this model – the oscillations of the crack tip velocity. However, the oscillations may appear if the viscous dissipation is introduced into this model.

In general, the above equation can have another form if dissipation is associated with other mechanism, e.g. void nucleation and growth.

Appendix

As a result of the computer simulation, more than 100 examples of the fast crack growth histories have been obtained. A few of them are shown in this Appendix. In the left-hand side of the upper part of each figure the shape of the function $\Gamma^d_{\mathrm{III}}(v)_{ss}$ is presented, in the centre the assumed external loading history is shown. Lower part of each figure shows the crack edges (leading and trailing) trajectories (a), plot of the crack edges velocities vs. time (b), plot of the length of the crack vs. time (c), plot of the plastic zone length vs. time (d).

In each figure the characteristic stage of the crack acceleration is observed. When certain critical velocity is reached, one can observe relatively constant crack

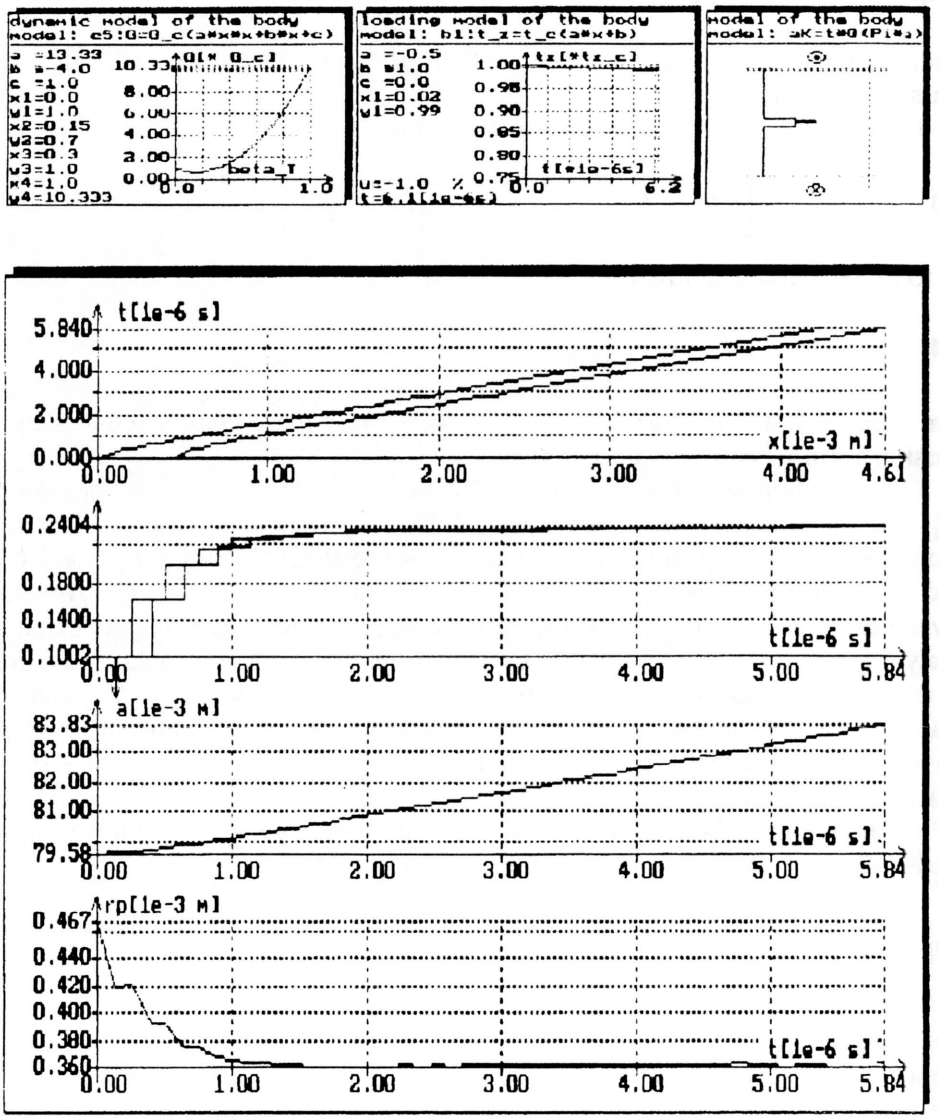

Fig. A.1

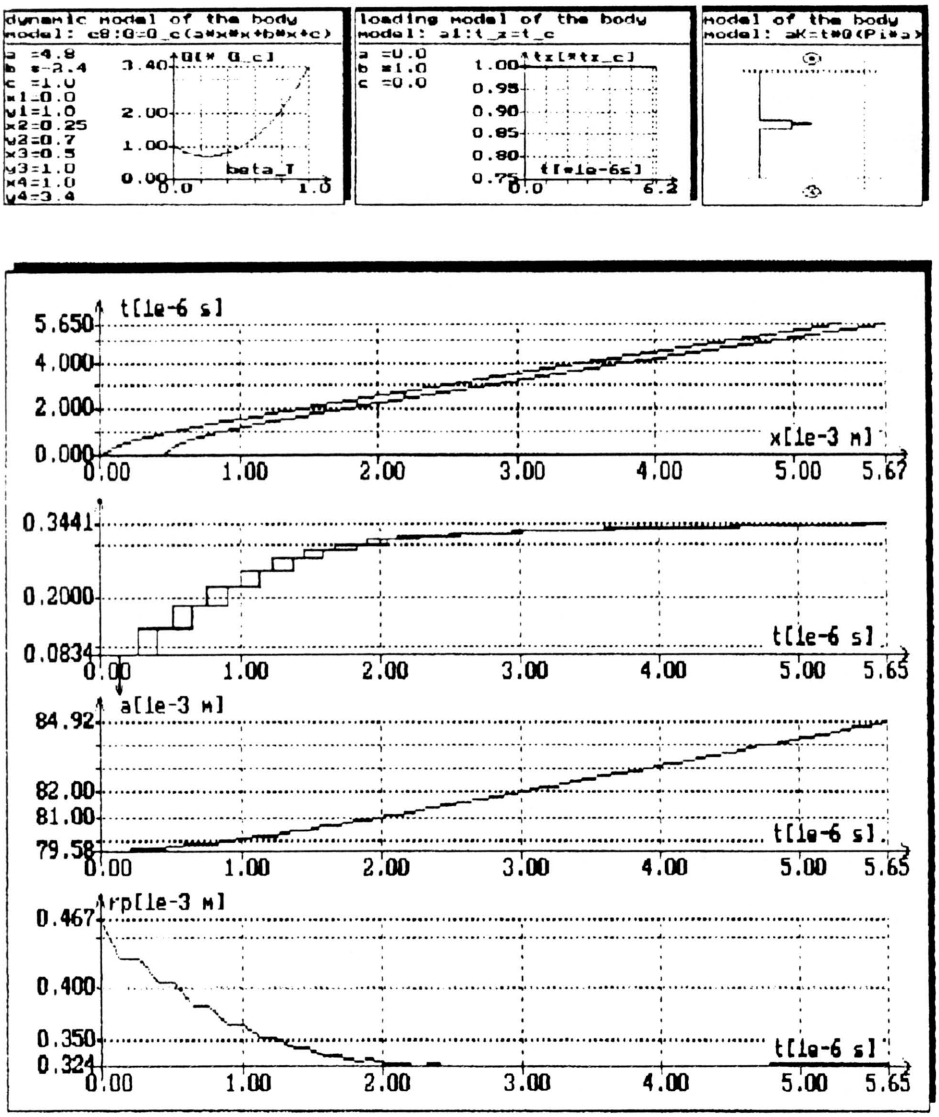

Fig. A.2

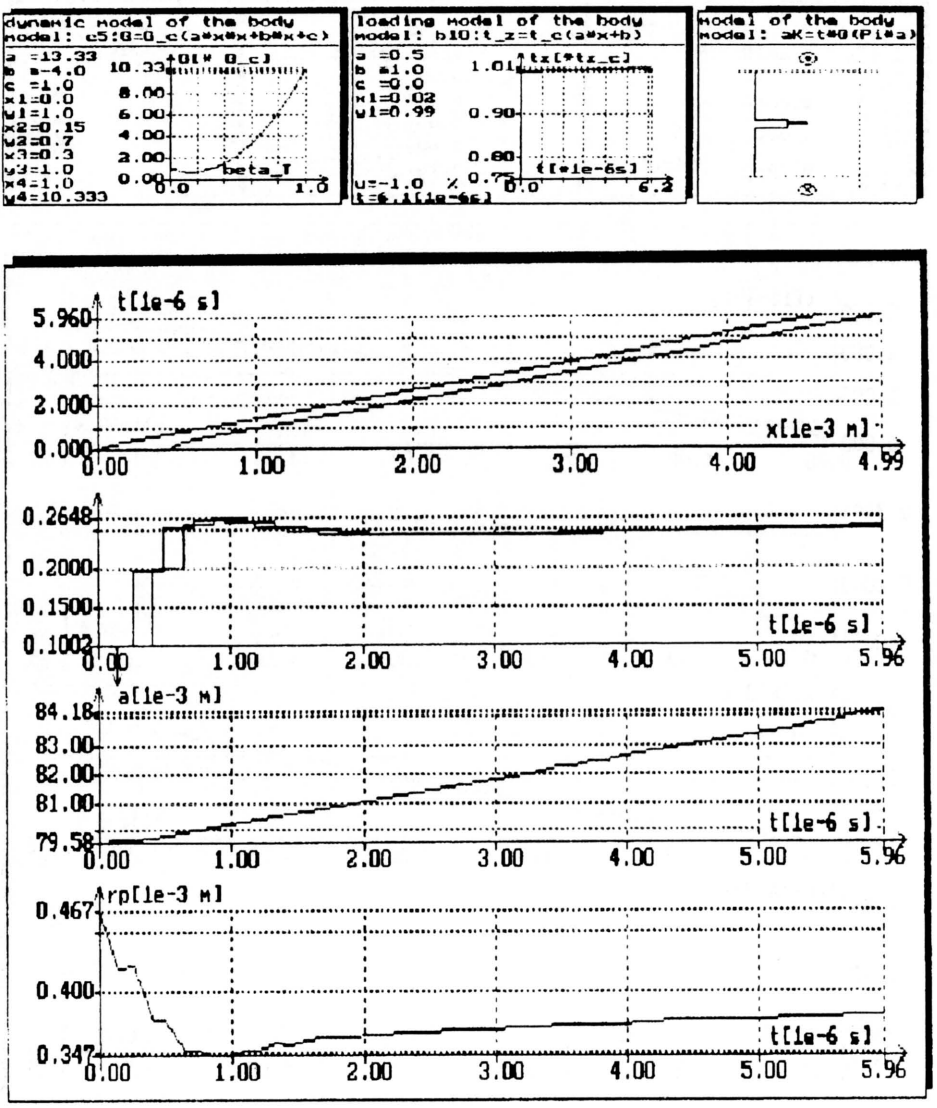

Fig. A.3

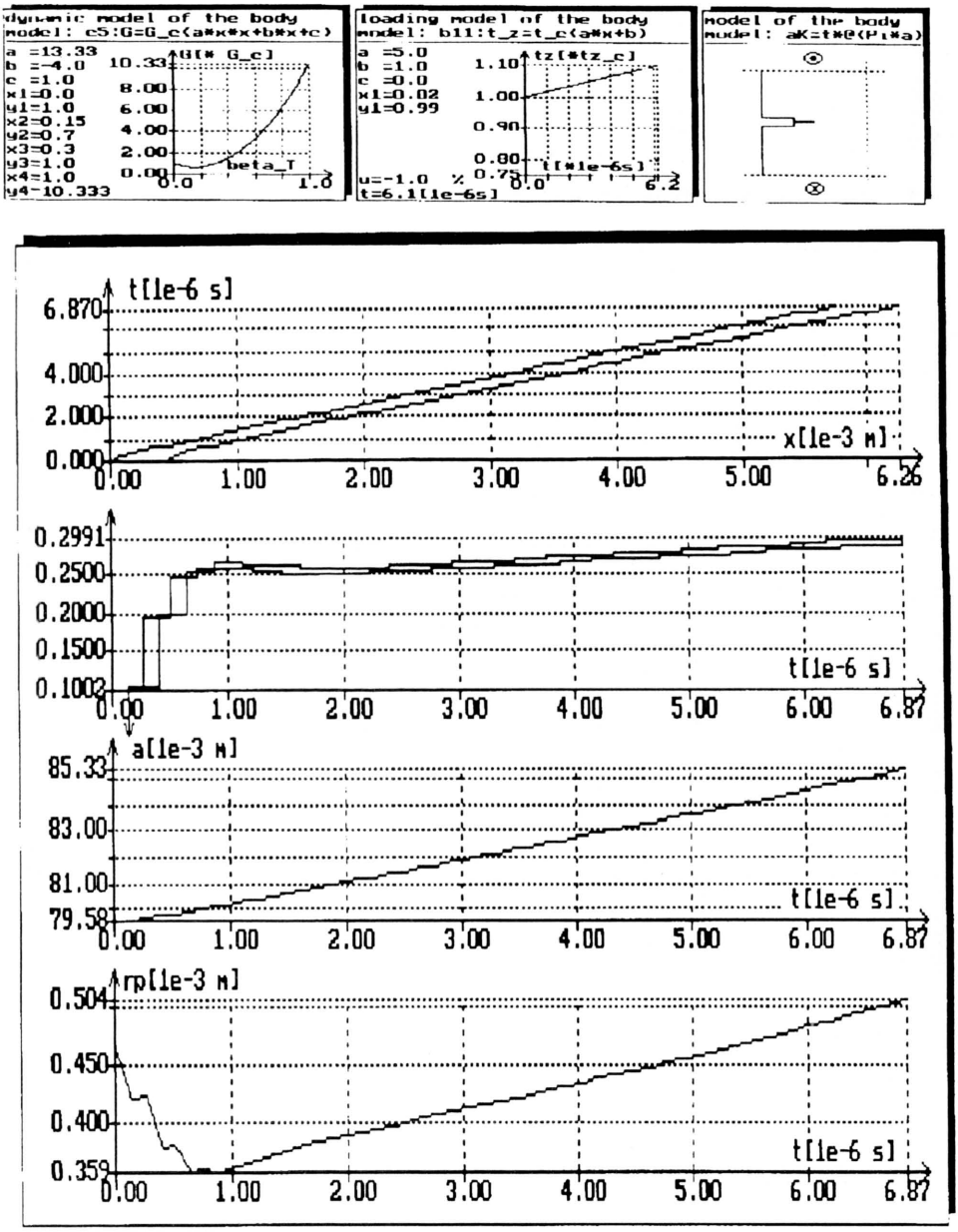

Fig. A.4

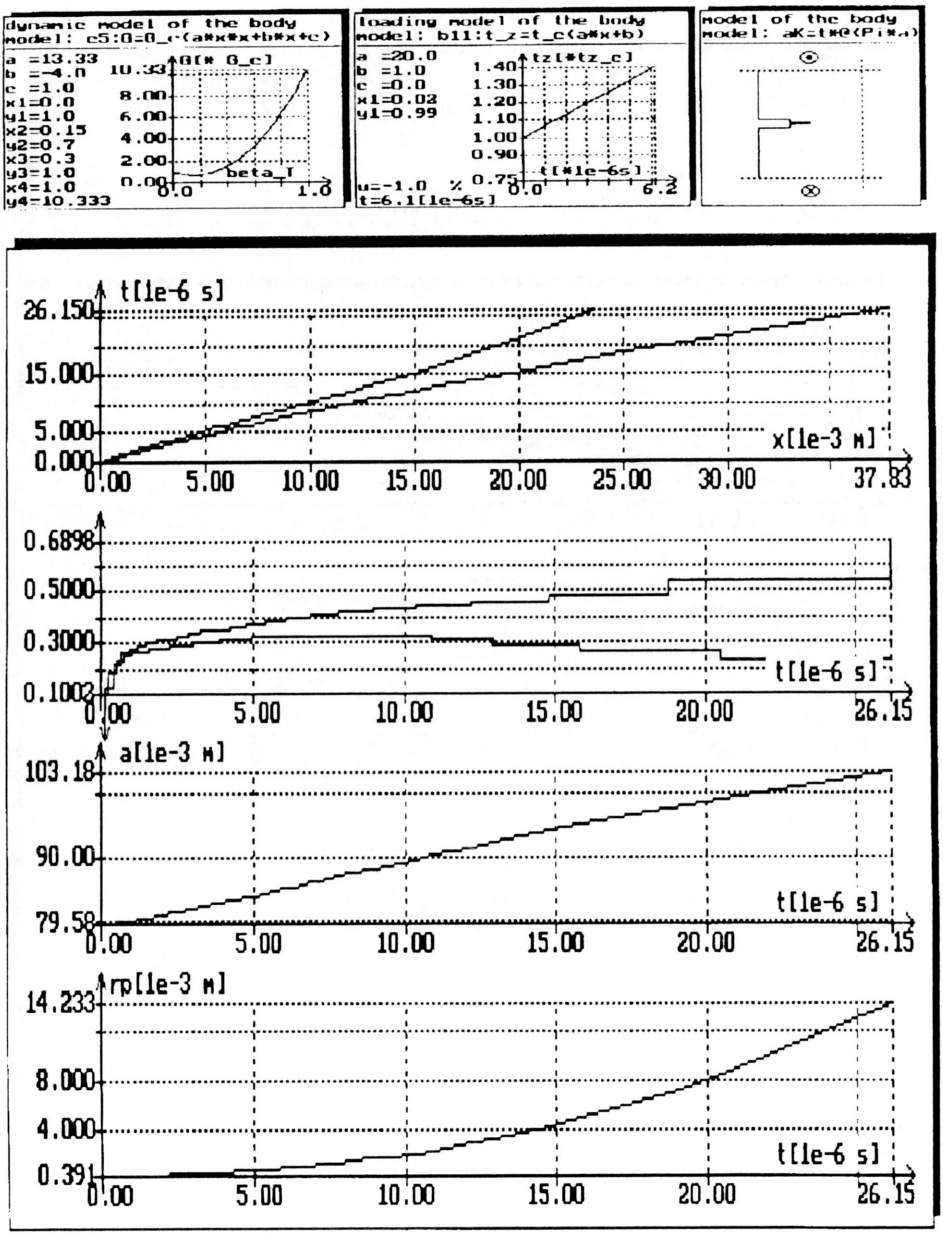

Fig. A.5

tip speed (with a modest acceleration). This velocity is not strongly dependent on the specimen loading history. It can be seen by comparing the succeeding figures. However, if the external loading is sharply increasing while the crack is growing, the tendency to the crack arrest is observed due to the rapid enlargement of the plastic zone. All those features are in agreement with experiment.

References

1. J. FINEBERG, S.P. GROSS, M. MARDER and H.L. SWINNEY, *Instability in the propagation of fast cracks*, Physical Review B, **45**, 10, pp. 5146–5154, 1992.
2. L.B. FREUND, *Energy flux into the tip of an extending crack in an elastic solid*, J. Elasticity, **2**, pp. 341–349, 1972.
3. L.B. FREUND and A.J. ROSAKIS, *The structure of the near-tip field during transient elastodynamic crack growth*, J. Mech. Phys. Solids, **40**, pp. 699–719, 1992.
4. H. GAO, *Surface roughening and branching instabilities in dynamic fracture*, J. Mech. Phys. Solids, **41**, pp. 457–486, 1993.
5. J.F. KALTHOFF, J. BEINERT and S. WINKLER, *Measurements of dynamic stress intensity factors for fast running and arresting cracks in double-cantilever-beam specimens*, [in:] Fast Fracture and Crack Arrest, G.T. HAHN, M.F. KANNINEN [Eds.], American Society for Testing and Materials, Philadelphia, pp. 161–176, 1977.
6. B.V. KOSTROV and L.V. NIKITIN, *Some general problems of mechanics of brittle fracture*, Arch. Mech., **22**, pp. 749–776, 1970.
7. C. LIU, A. ROSAKIS and L.B. FREUND, *The interpretation of optical caustics in the presence of dynamic non-uniform crack-tip motion histories: a study based on a higher order transient crack-tip expansion*, Intern. J. Solids and Structures, **30**, pp. 875–897, 1993.
8. M. MARDER, *New dynamical equation for cracks*, Physical Review Letters, **66**, pp. 2484–2487, 1991.
9. A. NEIMITZ, *On fast crack growth in elastic and elastic-plastic materials. Part I. Mechanic fields ahead of fast moving D-P crack*, pp. 1119–1124; *Part II. Equations of crack motion*, pp. 1125–1130, [in:] Proceedings of ECF 8, Torino, D. FIRRAO [Ed.], EMAS, 1990.
10. A. NEIMITZ, *Analysis of the crack motion with varying velocity according to the Dugdale-Panasyuk model*, Engng. Fracture Mech., **39**, pp. 329–338, 1991.
11. A. NEIMITZ and Z. LIS, *Simulation of fast Dugdale crack motion with varying velocity*, Proc. of the Conference "Dynamic Failure of Materials", P. ROSSMANITH [Ed.], Elsevier, pp. 362–377, 1991.
12. F. NILSSON, *Dynamic fracture theory*, Lectures in CISM, Udine, Italy.
13. K. RAVI-CHANDAR and W.G. KNAUSS, *An experimental investigation into dynamic fracture. I. Crack initiation and arrest*, Intern. J. Fracture, **25**, pp. 247–262, 1984.
14. K. RAVI-CHANDAR and W.G. KNAUSS, *An experimental investigation into dynamic fracture. II. Microstructural aspects*, Intern. J. Fracture, **26**, pp. 65–80, 1984.
15. J.R. RICE, *Thermodynamics of the quasi-static growth of Griffith cracks*, J. Mech. Phys. Solids, **26**, pp. 61–78, 1978.
16. A.J. ROSAKIS, S. KRISHNASWAMY and G. RAVI-CHANDRAN, *On the reliability of experimental measurements in dynamic fracture*, Proc. of the Conference "Materials at high rates of strain", IOP Publishing Ltd., pp. 1–13, 1989.
17. L.I. SLEPYAN, *Maximum dissipation power criteria in crack dynamics* [in Russian], Rep. Acad. Sci. USSR, **324**, 1, pp. 69–72, 1991.
18. L.I. SLEPYAN, *Principle of maximum energy dissipation rate in crack dynamics*, J. Mech. Phys. Solids, **41**, pp. 1019–1033, 1993.
19. K. TAKAHASHI and K. ARAKAWA *Dependence of crack acceleration on the dynamic stress-intensity factor in polymers*, Experimental Mechanics, **27**, pp. 195–200, 1987.

KIELCE UNIVERSITY OF TECHNOLOGY, POLAND.

Received January 13, 1995.

Arch. Mech., 47, 5, pp. 1003–1009, Warszawa 1995

Terminal velocity of rapid crack propagation

M. WATANABE (HIGASHI-HIROSHIMA)

ASSUMING THAT A CRACK "sees" the nonlinear Young's modulus, E^{NL}, the velocity of a crack during rapid crack propagation (RCP) is obtained by the improved Mott's analysis. When the inequality, $E/E^{NL} \gg 1$, is satisfied, the theory predicts the constant speed of RCP, provided the Young's modulus changes from E at $t = 0$ to E^{NL} for $t > +0$. The results are in qualitative agreement with the published experiments.

1. Introduction

ALTHOUGH MUCH WORK has been done on rapid crack propagation (RCP) for many years, the mechanisms that govern the dynamics of cracks are not well understood. One of the obvious controversions between theory and experiment in the RCP is that cracks do not attain the terminal velocity (or the limiting velocity) predicted by the linear elastic theory [1]. We will elucidate the difficulties associated with the terminal velocity of a crack referring to the most recent experimental works on RCP, and try to explain their results qualitatively.

STROH [2] argued that the terminal velocity can be found from the crack length dependence of various energies, U_S, U_K and U_D associated with RCP, where U_S is the elastic component of stored energy and U_K – the kinetic energy of a crack. U_D is the sum of all the irreversible energies such as surface energy, plastic work and viscous dissipation. All the energies except U_D are proportional to the square of the length of a crack, a^2, while U_D is proportional to the crack length, a, when the fracture surface is smooth. Thus the dissipative energy may be neglected for large values of a and the propagation of a crack becomes the motion of surface disturbance in nondissipative medium. Such a motion is known to propagate at the velocity c_R of the Rayleigh wave. Thus the terminal velocity of a crack is found to be the Rayleigh wave speed.

Let us derive the velocity, v, of a crack by the improved Mott's analysis [3, 4] based on the presentation given by ERDOGAN [5]. We consider propagation of a centrally located through crack in an infinite elastic plate subjected to a time-indpendent uniaxial tension perpendicular to the plane of the crack. The energy balance equation of a crack is

$$\frac{dU_{\text{ext}}}{dt} = \frac{dU_S}{dt} + \frac{dU_K}{dt} + \frac{dU_D}{dt}, \tag{1.1}$$

where t is time. These energies and the crack resistance, R, are defined as

$$U_{\text{ext}} - U_S = \frac{\pi\sigma^2 a^2}{E}, \qquad U_K = \frac{\kappa\varrho a^2 v^2 \sigma^2}{2E^2}, \qquad R = \frac{\partial U_D}{\partial a}, \tag{1.2}$$

where the quantity E is Young's modulus and σ is the applied stress. ϱ is the mass density of the plate and κ is a constant. The crack resistance R is set to be

$$R = G_{Ic}, \qquad G_{Ic} = \frac{2\pi\sigma^2 a_0}{E}, \tag{1.3}$$

where G_{Ic} is Griffith's critical energy release rate for the growth of a crack and a_0 is the initial crack length. Notice here that the crack length dependence of various energies can be easily seen from Eqs. (1.2) and (1.3), which are identical to that discussed above.

Substituting Eq. (1.2) into Eq. (1.1), and then integrating Eq. (1.1) from $t = 0$ to $t = t$, we find

$$v = \sqrt{\frac{2\pi E}{\kappa\varrho}}\left(1 - \frac{a_0}{a}\right). \tag{1.4}$$

The terminal velocity of a crack becomes identical to the Rayleigh wave speed if the constant κ is so chosen that

$$\sqrt{\frac{2\pi E}{\kappa\varrho}} = c_R. \tag{1.5}$$

Thus Eq. (1.4) can be written as

$$v = c_R\left(1 - \frac{a_0}{a}\right). \tag{1.6}$$

Derivation of Eq. (1.6) is based on the idealized modeling of RCP, in which the crack resistance, R, is assumed to be a constant. The crack resistance corresponds to the fracture surface roughness, which is known to exhibit a characteristic sequence of pattern called "mirror, mist and hackle", as a crack proceeds. Recent experiments using thin plate of Polymethylmethacrylate (PMMA) [6, 7, 8] and glass [9] reveal that the transition from smooth to rough fracture surface is triggered by the instability associated with RCP, which is observed when the velocity of a crack exceeds the critical velocity, v_c. When the velocity is larger than the critical one, it oscillates. This oscillation is found to be strongly correlated with fracture surface roughness. Although the terminal velocity of a crack is of the order of $0.6c_R$, the average velocity of a crack is compared with Eq. (1.6) [7, 8].

We are not interested in clarifying how the fracture surface becomes rough, but we are interested in the terminal velocity of a crack when the fracture surface becomes rough. For this purpose we can consider the case $v_c \to 0$ without loss of generality, and the crack resistance can be written as

$$R = G_{Ic} + R' \cdot (a - a_0), \qquad R' = \frac{\partial R}{\partial a} \quad \text{at} \quad a = a_0. \tag{1.7}$$

The crack resistance is a function of the velocity of a crack rather than the crack length since the material properties are, in general, rate-dependent. In this sense Eq. (1.7) is not realistic and we will not be able to find the correct terminal velocity if the velocity dependence of the crack resistance affects its value [10, 11]. However, Eq. (1.7) combined with Eqs. (1.1), (1.2) and (1.5) at least gives the answer to the question related to the argument of STROH [2]. The question is, how the terminal velocity, which is the Rayleigh wave speed, is modified if the dissipated energy U_D associated with RCP is proportional to a^2, which is a similar crack length dependence to that of U_K and U_S. Such crack length dependence of R defined in Eq. (1.7) can be seen in Fig. 12 of Ref. [8] provided that the crack resistance is proportional to fracture surface amplitude.

Substituting Eq. (1.2) and (1.7) into Eq. (1.1) and then integrating over time, we find [12]

$$v = \sqrt{1 - \frac{R' \cdot a_0}{G_{Ic}}}\, c_R \left(1 - \frac{a_0}{a}\right), \tag{1.8}$$

where Eq. (1.5) was used. Equation (1.8) can be compared with the observed average velocity of a crack. Making use of the experimental result [7, 8] where the terminal velocity is of the order of $0.6c_R$, we find the value of the quantity $(1 - R' \cdot a_0/G_{Ic}) \equiv 0.36$.

In Sec. 2 we will discuss the cases when the velocity of a crack remains constant, while the fracture surface is smooth in one case [13], and rough in the other [14]. Section 3 is devoted to discussion.

2. Constant crack velocity during RCP

Terminal velocity of RCP is ordinarily defined as the velocity of a crack when its length approaches infinity in the limit ($a \to \infty$). Recent refined experiments [13, 14] seem to destroy the concept of the terminal velocity since the velocity of a crack remains constant during RCP. The authors of these experiments proposed two different ideas on RCP by comparing their results with the following equation of motion of dynamically propagating Mode I crack in the infinite elastic plate [1]

$$\left(1 - \frac{v}{c_R}\right) G^* = \gamma_d, \tag{2.1}$$

where the quantity G^* in Eq. (2.1) is the "static" energy release rate and γ_d is the effective surface energy. Equation (2.1) is the energy balance equation based on the elastodynamic solution for arbitrarily moving crack. Since G^* increases approximately linearly with increasing crack length, a, the quantity $(1 - v/c_R)$ must gradually decrease towards zero when γ_d is a constant. Thus the velocity of a crack approaches Rayleigh wave speed according to Eq. (2.1). If the equation $\gamma_d = G_{Ic}$ is substituted into Eq. (2.1), the velocity of a crack becomes essentially identical to Eq. (1.6), as remarked by FEINBERG *et al.* [7, 8].

2.1. Experiment by IVANKOVIC and WILLIAMS [13]

These authors performed an experiment using single edge notch tensile (SENT) specimens made of PMMA and polycarbonate (PC). Remarkably constant crack speeds were observed with smooth fracture surface and higher crack speeds corresponded to the higher preload. The two-dimensional finite element simulation was performed to calculate the crack resistance R, which was equal to the energy release rate. The basic equation for this numerical analysis was the macroscopic energy balance equation (1.1) with the appropriate boundary conditions and experimentally measured crack speed. They found that the numerical simulation of the constant speed RCPs generated highly scattered crack resistance data with respect to the crack speed, and also very large variations of the crack resistance with the length of a crack. These numerical results did not correspond to the observed smooth fracture surface appearance. These discrepancies indicate that the conventional analysis of the energy balance equation (1.1) can not be used to explain the experimental results. They tried to overcome these difficulties by exploring the concept that the anomalies arise from large local strains around the rapidly moving crack tip, resulting in the crack "seeing" a low local modulus, which was proposed and studied by BROBERG [15, 16] as a local low modulus strip model of RCP. The numerical analysis of this model applied to RCP is performed by determining the width and nonlinear Young's modulus of the strip from the measured strain histories near the crack tip. They found that the local strip modulus analysis resolved the difficulties discussed above.

We now use the concept that a crack "sees" a local low modulus to derive the velocity of a crack. We denote the value of Young's modulus at time $t = 0$ and $t = t$ by E and E^{NL}, respectively. Since the observed fracture surface is smooth, we use the crack resistance expressed by Eq. (1.3) and take the similar procedure in deriving the velocity of a crack shown in Eq. (1.4), and then use Eq. (1.5). The velocity of a crack is found to be

$$v = c_R \frac{E^{\mathrm{NL}}}{E} \sqrt{\left(1 - \frac{a_0}{a}\right)^2 + \left(\frac{E}{E^{\mathrm{NL}}} - 1\right)}. \tag{2.2}$$

If the condition

$$\frac{E}{E^{\mathrm{NL}}} \gg 1 \tag{2.3}$$

is satisfied, Eq. (2.2) can be written as

$$v = c_R \sqrt{\frac{E^{\mathrm{NL}}}{E}}, \tag{2.4}$$

which is the Rayleigh wave speed in the medium with the Young's modulus E^{NL}. Equation (2.4) predicts a constant velocity of RCP provided the Young's modulus

changes from E at $t = 0$ to E^{NL} for $t > +0$. The infinitesimal time, $+0$, could be the time resolution of the experiment. The observed maximum speed of RCP in PMMA was 420 m/s, which is of the order of $0.4c_R$. Substituting this value into Eq. (2.4), we find $E/E^{NL} \approx 6$, which satisfies the inequality shown in Eq. (2.3).

2.2. Experiment of RAVI-CHANDAR and KNAUSS [14]

These authors performed a series of experiments on RCP [14, 17]. The terminal velocity of a crack was discussed in the third of a series of four papers. They observed that the velocity of a crack remains constant during RCP. Discussion of the results obtained was based on the energy balance equation (2.1), which was rewritten in terms of the stress intensity factor, K, in the following form:

$$\frac{E}{K^2} = \frac{1 - v/c_R}{\gamma_d(v)}, \tag{2.5}$$

where the velocity dependence of the effective surface energy is explicitly written. According to their observation [14, 17] the velocity of a crack remains constant in spite of considerable changes (factors on the order of 2) in the stress intensity factor, and fracture surface shows a characteristic sequence of "mirror, mist and hackle", accordingly. We quote their argument, which is based on Eq. (2.5). "If γ_d is allowed to be a function of crack velocity, it creates a contradiction in explaining the constancy of crack velocity. The reasons for the existence of a terminal velocity lower than the Rayleigh wave speed has to be explained then in a different way." The authors suggested that a microcrack formation reduces the terminal crack tip speed. This interpretation was that RCP in an amorphous, brittle solids was associated with multiple flaws or microcracks preceding the main crack and these multiple cracks coalesced to form the main crack. Thus it takes time for waves to travel back and forth between the individual microfractures in order to coordinate them into forming the major crack. Then the terminal velocity of RCP could be substantially smaller than the Rayleigh wave speed.

This microcrack interpretation of RCP sounds reasonable; however, it is very hard to make this idea quantitative because such microcrack interactions are not usually accounted for in elasticity models of RCP. Therefore, we assume that the crack "sees" nonlinear Young's modulus through multiple microcracks generated at the tip of a crack. In other words, we consider that RCP may be governed by such microscopic processes as microcrack interactions generated at the tip of a crack, but in some respects it behaves like a macroscopic property of the material, which is characterized by nonlinear Young's modulus, E^{NL}. This observation suggests that a detailed analysis of the interaction between microcracks is not necessary, at least not until the point when branching occurs.

Distinguishing Young's modulus at $t = 0$ and $t = t$ as E and E^{NL}, respectively, and then using Eq. (1.7), the velocity of a crack can be easily obtained from

Eqs. (1.1) and (1.2) as

$$v = c_R \frac{E^{NL}}{E} \sqrt{\left(1 - \frac{R' \cdot a_0}{G_{Ic}}\right)\left(1 - \frac{a_0}{a}\right)^2 + \left(\frac{E}{E^{NL}} - 1\right)}, \tag{2.6}$$

where Eq. (1.5) is used. Equation (2.6) has a form which combines two Eqs. (1.8) and (2.2). It indicates that the effect of nonlinear Young's modulus on the velocity of a crack is more dominant than Eq. (2.2), because the value of the quantity $(1 - R' \cdot a_0/G_{Ic})$ is smaller than unity since the fracture surface is rough in this case. If the condition expressed by Eq. (2.3) is satisfied, we again obtain the constant velocity of a crack expressed by Eq. (2.4). Substituting the observed terminal velocity of a crack, $0.46c_R$, into Eq. (2.4), we find $E/E^{NL} \approx 4.7$ for the experiment of RAVI-CHANDAR and KNAUSS [14].

3. Discussion

Since the experiment of PAXON and LUCAS [18] in 1973 it is known that the effective surface energy γ_d increases very sharply as the terminal velocity (or the maximum crack speed) is approached . The dynamic crack instability observed by FEINBERG *et al.* [7, 8] could be the mechanism of this sharp increase in γ_d. In this experiment the strong correlation between the oscillation of the velocity of a crack and fracture surface roughness was emphasized. It is known, however, that the increased fracture surface roughness accounts only for a minor part of the energy dissipation at fracture [5, 10]. The greater part of this increased consumption of energy by the crack is dissipated as heat, and the temperature rise at the tip of a crack in RCP for PMMA was measured [19, 20]. In the present work the effect of this temperature rise on the properties of material is taken into account as the nonlinear Young's modulus, E^{NL}, while the fracture surface roughness is expressed by the crack resistance R, although the treatment is phenomenological in nature.

Let us consider how the crack "sees" nonlinear Young's modulus at the tip of a crack. The region around the rapidly propagating crack tip is characterized by large strains, high strain rates and high temperature. Unfortunately, neither of these nor the parameters which may describe the response of the materials under such conditions were known. The experimental results that the velocity of a crack in RCP remains constant suggest that the material properties at the tip of a crack can be macroscopically characterized by a one of nonlinear Young's modulus since RCP is in a steady state. In this argument we have disregarded the possible spatial dependence of this modulus. If it is possible to use a single nonlinear Young's modulus and if such treatment as distinguishing the Young's modulus at $t = 0$ and $t = t$ as discussed is allowed, the velocity of a crack shown in Eqs. (2.2) and (2.6) could be meaningful. Considering the difficulty asssociated with RCP, it is worthwhile to regard the results shown in Eq. (1.8), (2.2) and (2.6)

as a working hypothesis since these results are in qualitative agreement with the corresponding experiments discussed. The validity of these results, however, has to be proved by more rigorous treatment.

References

1. L.B. FREUND, *Dynamic fracture mechanics*, Cambridge Univ. Press, 1990.
2. A.N. STROH, *A simple model of a propagating crack*, J. Mech. Phys. of Solids, **8**, 119–122, 1960.
3. N.F. MOTT, *Fracture of metals: Some theoretical consideration*, Engng., **165**, 16–18, 1948.
4. J.P. BERRY, *Some kinematic considerations of the Griffith's criterion for fracture*, J. Mech. Phys. of Solids, **8**, 194–206, 1960.
5. F. ERDOGAN, *Crack propagation theories*, **2**, 497–590, [in:] Fracture, H. LIEBOWITZ [Ed.], Academic Press, N.Y. 1968.
6. K. TAKAHASHI, K. MATSUSHIGE, Y. SAKURADA and T. MAEDA, Bull. Res. Inst. Appl., Mech. Kyushu Univ., No. 57, 285–300, 1982 [in Japanese].
7. J. FINEBERG, S.P. GROSS, M. MARDER and H.L. SWINNEY, *Instability in dynamic fracture*, Phys. Rev. Lett., **67**, 457–460, 1991.
8. J. FINEBERG, S.P. GROSS, M. MARDER and H.L. SWINNEY, *Instability in the propagation of fast cracks*, Phys. Rev., **B45**, 5146–5154, 1992.
9. S.P. GROSS, J. FINEBERG, M. MARDER, W.D.McCORMICK and H.L. SWINNEY, *Acoustic emission from rapidly moving cracks*, Phys. Rev. Lett., **71**, 3162–3165, 1993.
10. L.R.F. ROSE, *Recent theoretical and experimental results on fast brittle fracture*, Int. J. Fract., **12**, 799–813, 1976.
11. M. WATANABE, *Phenomenological equations of a dynamic fracture*, Phys. Lett., **A179**, 41–44, 1993.
12. M. WATANABE, *Dynamic crack propagation and surface roughness*, [in:] Impact and Dynamic Fracture of Polymers and Composites, ESIS 19, J.G. WILLIAMS and A. PAVAN [Eds.], Mech. Engng. Pub., London, 147–153, 1995.
13. A. IVANKOVIC and J.G. WILLIAMS, *A local modulus analysis of rapid crack propagation in polymers*, Int. J. Fracture, **64**, 251–268, 1993.
14. K. RAVI-CHANDAR and W.G. KNAUSS, *An experimental investigation into dynamic fracture III. On steady state crack propagation and crack branching*, Int. J. Fract., **26**, 141–154, 1984.
15. K.B. BROBERG, *On dynamic crack propagation in elastic-plastic media*, Proc. of Int. Conf. on Dynamic Crack Propagation, Nordhoff Int. Pub., Leyden, 461–499, 1973.
16. K.B. BROBERG, *On effects of plastic flow at fast crack growth*, ASTM STP, **627**, 243, 1977.
17. K. RAVI-CHANDAR and W.G. KNAUSS, *An experimental inveastigation into dynamic fracture. I. Crack initiation and arrest*, Int. J. Fract., **25**, 247–262, *II. Microstructural aspects*, **26**, 65–80, *IV. On the interaction of stress waves with propagating cracks*, **26**, 189–200, 1984.
18. T.L. PAXON and R.A. LUCAS, *An exprimental investigation of velocity charactristics of a fixed boundary fracture model*, 415–426 [in:] Dynamic Crack Propagation, G.C. SIH [Ed.], Nordhoff, Leyden 1973.
19. W. DOLL, *An experimental study of the heat generated in the plastic region of a running crack in different polymeric materials*, Engng. Fract. Mech., **5**, 259–268, 1973.
20. K.N.G. FULLER, P.G. FOX and J.E. FIELD, *The temperature rise at the tip of fast-moving crack in glassy polymers*, Proc. of the Roy. Soc. London, **A341**, 537–557, 1975.

KINKI UNIVERSITY
FACULTY OF ENGINEERING, TAKAYA, HIGASHI-HIROSHIMA, JAPAN.

Received January 13, 1995.

DIRECTIONS FOR THE AUTHORS

The journal *ARCHIVES OF MECHANICS (ARCHIWUM MECHANIKI STOSOWANEJ)* deals with the printing of original papers which should not appear in any other periodicals.

As a rule, the volume of a paper should not exceed 40 000 typographic signs, that is about 20 type-written pages, format: 210 × 297 mm, leaded. The papers should be submitted in two copies. They must be set in accordance with the norms established by the Editorial Office. Special importance is attached to the following directions:

1. The title of the paper should be as short as possible.

2. The text should be preceded by a brief introduction; it is also desirable that a list of notations used in the paper should be given.

3. The formula number consists of two figures: the first represents the section number and the other the formula number in that section. Thus the division into subsections does not influence the numbering of formulae. Only such formulae should be numbered to which the author refers throughout the paper, and also the resulting formulae. The formula number should be written on the left-hand side of the formula; round brackets are necessary to avoid any misunderstanding. For instance, if the author refers to the third formula of the set (2.1), a subscript should be added to denote the formula, viz. $(2.1)_3$.

4. All the notations should be written very distincly. Special care must be taken to write small and capital letters as precisely as possible. Semi-bold type should be underlined in black pencil. Explanations should be given on the margin of the manuscript in case of special type face.

5. It has been established to denote vectors by semi-bold type. Trigonometric functions are denoted by sin, cos, tg and ctg, inverse functions – by arc sin, arc cos, arc tg and arc ctg; hyperbolic functions are denoted by sh, ch, th and cth, inverse functions – by Arsh, Arch, Arth and Arcth.

6. Figures in square brackets denote reference titles. Items appearing in the reference list should include the initials of the first name of the author and his surname, also the full title of the paper (in the language of the original paper); moreover;

a) In the case of books, the publisher's name, the place and year of publication should be given, e.g.,
5. S. Ziemba, *Vibration analysis*, PWN, Warszawa 1970;

b) In the case of a periodical, the full title of the periodical, consecutive volume number, current issue number, pp. from ... to ..., year of publication should be mentioned; the annual volume number must be marked in black pencil so as to distinguish it from the current issue number, e.g.,
6. M. Sokołowski, *A thermoelastic problem for a strip with discontinuous boundary conditions*, Arch. Mech., **13**, 3, 337–354, 1961.

7. The authors should enclose a summary of the paper. The volume of the summary is to be about 100 words.

8. The authors are kindly requested to enclose the figures prepared on diskettes (format PCX, BitMap or PostScript).

Upon receipt of the paper, the Editorial Office forwards it to the reviewer. His opinion is the basis for the Editorial Committee to determine whether the paper can be accepted for publication or not.

The printing of the paper completed, the author receives 25 copies of reprints free of charge. The authors wishing to get more copies should advise the Editorial Office accordingly, not later than the date of obtaining the galley proofs.

The papers submitted for publication in the journal should be written in English. No royalty is paid to the authors.

Please send us, in addition to the typescript, the same text prepared on a diskette (floppy disk) 3 1/2″ or 5 1/4″ as an ASCII file, in Dos or Unix format.

EDITORIAL COMMITTEE
ARCHIVES OF MECHANICS
(ARCHIWUM MECHANIKI STOSOWANEJ)

INSTITUTE OF FUNDAMENTAL TECHNOLOGICAL RESEARCH
is publishing the following periodicals:

ARCHIVES OF MECHANICS — bimonthly (in English)

ARCHIVES OF ACOUSTICS — quarterly (in English)

ARCHIVES OF CIVIL ENGINEERING — quarterly (in English)

ENGINEERING TRANSACTION — quarterly (in English)

COMPUTER ASSISTED MECHANICS AND ENGINEERING SCIENCES — quarterly (in English)

JOURNAL OF TECHNICAL PHYSICS — quarterly (in English)

Subscription orders for all the magazines published in Poland available trought the local press distributors or directly trought the *Foreign Enterprise ARS POLONA*, Krakowskie Przedmieście 7, 00-068 Warszawa, Poland and trought the Editorial Office.

Address of the Editorial Office:

Institute of Fundamental Technological Research,
Świętokrzyska 21, p. 508,
00-049 WARSZAWA, Poland.